Understanding the molecular mechanisms and modifiers underlying *CRB1*-linked retinal degenerations

Dissertation

zur Erlangung des Grades eines

Doktors der Naturwissenschaften

der Mathematisch-Naturwissenschaftlichen Fakultät

und

der Medizinischen Fakultät

der Eberhard-Karls-Universität Tübingen

vorgelegt

von

Isabel Felicitas Stehle

aus Wesel, Deutschland

2024

Tag der mündlichen Prüfung: 29.05.2024

Dekan der Math.-Nat. Fakultät: Prof. Dr. Thilo Stehle

Dekan der Medizinischen Fakultät: Prof. Dr. Bernd Pichler

1. Berichterstatter: Prof. Dr. Marius Ueffing

2. Berichterstatter: PD Dr. Christian Johannes Gloeckner

Prüfungskommission: Prof. Dr. Marius Ueffing

Prof. Dr. Melanie Philipp

Prof. Dr. Bernd Wissinger

PD Dr. Christian Johannes Gloeckner

Erklärung / Declaration:

Ich erkläre, dass ich die zur Promotion eingereichte Arbeit mit dem Titel:

„Understanding the molecular mechanisms and modifiers underlying *CRB1*-linked retinal degenerations “

selbständig verfasst, nur die angegebenen Quellen und Hilfsmittel benutzt und wörtlich oder inhaltlich übernommene Stellen als solche gekennzeichnet habe. Ich versichere an Eides statt, dass diese Angaben wahr sind und dass ich nichts verschwiegen habe. Mir ist bekannt, dass die falsche Abgabe einer Versicherung an Eides statt mit Freiheitsstrafe bis zu drei Jahren oder mit Geldstrafe bestraft wird.

*I hereby declare that I have produced the work entitled “*Understanding the molecular mechanisms and modifiers underlying *CRB1*-linked retinal degenerations*”, submitted for the award of a doctorate, on my own (without external help), have used only the sources and aids indicated and have marked passages included from other works, whether verbatim or in content, as such. I swear upon oath that these statements are true and that I have not concealed anything. I am aware that making a false declaration under oath is punishable by a term of imprisonment of up to three years or by a fine.*

Tübingen, den ....

Datum / Date Unterschrift /Signature

Für meine Eltern

Table of contents

Table of contents I
Statement of contributions V
List of figures VI
List of tables VIII
Abbreviations IX
Summary XII
Zusammenfassung XV
1. Introduction 1
1.1 The vertebrate retina 1
1.1.1 Photoreceptor cells 3
1.1.2 Phototransduction and the visual cycle 4
1.1.3 Müller Glia cells 5
1.2 Inherited retinal diseases caused by mutations in *Crumbs homologue 1* 6
1.2.1 Crumbs homologue 1 7
1.2.1.1 CRB1 isoforms and localisation in the human retina 7
1.2.1.2 The two other members of the human Crumbs family: CRB2 and CRB3 8
1.2.1.3 The crumbs complex and its function: Insights from different models 9
1.2.1.4 CRB1 mutations are predominantly located in the extracellular domain 11
1.2.2 CRB1-associated retinal degenerations are clinically heterogeneous 12
1.2.3 Siblings with identical homozygous CRB1 C948Y mutation but with different severity of symptoms 14
2. Aim of the study 15
3. Material and Methods 17
3.1 Material 17
3.1.1 Consumables 17
3.1.2 Chemicals and reagents 17
3.1.3 Buffer and solutions 19
3.1.3.1 Bacteria culture 19
3.1.3.2 Cell culture and retinal explant culture 19
3.1.3.3 Western blot analysis 19
3.1.3.4 Proteomics 20
3.1.4 Kits 21
3.1.5 Enzymes 21
3.1.6 Bacteria 22
3.1.7 Human cell lines 22
3.1.8 Primer 22
3.1.8.1 Gateway cloning 22
3.1.8.2 Site-directed mutagenesis (SDM) 23
3.1.8.3 RT-qPCR primer 24
3.1.8.4 Sequencing 24
3.1.8.5 Other (*CRB1* Splicing, *GUCA1B* variant) 25
3.1.8.6 *CRB1* siRNA duplex oligonucleotide sequence 25
3.1.9 Commercially available primary antibodies and dyes 25

3.1.10 Commercially available secondary antibodies 26
3.1.11 Plasmids....26
3.1.12 Software 26
3.1.13 Online Tools....27
3.1.14 Instruments and tools 27

3.2 Methods....28

3.2.1 Ethic agreement 28
3.2.2 Cell culture of cell lines 28

3.2.2.1 Maintenance of cell lines 28
3.2.2.2 Passaging of cell lines 28
3.2.2.3 Thawing of cell lines 29
3.2.2.4 Freezing of cell lines....29

3.2.3 iPSC culture and generation of iPSC-derived retinal organoids 29
3.2.4 Cloning 29

3.2.4.1 Gateway® cloning 29
3.2.4.2 Agarose gel electrophoresis 31
3.2.4.3 Site directed mutagenesis 31
3.2.4.4 Transformation of chemically competent bacteria 32
3.2.4.5 Plasmid DNA purification from chemically competent bacteria....32

3.2.5 Immunofluorescence microscopy....32
3.2.6 Porcine retina pull- down approach....33

3.2.6.1 Pig retina lysate preparation 33
3.2.6.2 Cell seeding and transfection using polyethylenimine....33
3.2.6.3 Cell lysis and Bradford assay....33
3.2.6.4 FLAG-immunoprecipitation and porcine retinal pull-down 34
3.2.6.5 Protein precipitation and tryptic digest 34
3.2.6.6 Stop-and-go extraction tips for desalting and clean up....35
3.2.6.7 Mass spectrometry 35

3.2.7 Data analysis....36
3.2.8 Full proteome analysis of iPSC-derived retinal organoids 36

3.2.8.1 Lysis of iPSC-derived retinal organoids and digest 36
3.2.8.2 Mass spectrometry using data-independent acquisition....37
3.2.8.3 MS/MS date analysis using data-independent acquisition 37

3.2.9 Co-immunoprecipitation....38
3.2.10 Western blot analysis....38

3.2.10.1 Sodium-dodecylsulfate-polyacrylamide gel electrophoresis 38
3.2.10.2 Immunoblotting 38

3.2.11 Whole Genome Sequencing and variant analysis....39
3.2.12 RNA isolation....39
3.2.13 Genomic DNA removal from RNA samples....40
3.2.14 cDNA synthesis 40
3.2.15 Real-time quantitative polymerase chain reaction....40
3.2.16 CRB1 splicing analysis 41

3.2.16.1 Polymerase chain reaction using DreamTaq Polymerase 41
3.2.16.2 Purification of DNA from PCR products for Sanger sequencing 41
3.2.16.3 Agarose gel extraction for Sanger sequencing....41
3.2.16.4 PJET PCR cloning of PCR amplicons....42
3.2.16.5 Colony PCR....42

3.2.17 Porcine retina explant culture and reverse magnetofection....42

3.2.18 Production of monoclonal antibodies for CRB1 43

3.2.18.1 Screening of hybridoma clones by western blot analysis 43
3.2.18.2 Validation of clones by immunofluorescence microscopy 43

4. Results 45

4.1 Reduced CRB1 C948Y protein levels and OLM localisation in patient ROs 45
4.2 Molecular mechanism underlying CRB1 protein reduction by *CRB1* c.2843G>A;p.C948Y mutation 47

4.2.1 CRB1 C948Y did not influence BIP levels in patient RO 47
4.2.2 *CRB1* c.2843G>A led to a partially misspliced *CRB1* transcript 47
4.2.3 CRB1 C948Y mildly affected CRB1-CRB1 homophilic interaction 49

4.2.3.1 CRB1 homomer formation was mediated by the extracellular domain 49
4.2.3.2 *CRB1* missense mutations mildly influenced CRB1-CRB1 homomer formation 51
4.2.3.3 Loss of a single EGF domain did not disrupt CRB1-CRB1 interaction 52

4.3 Retinal pull-down approach of CRB1 revealed new interactors of the crumbs complex in the retina 53

4.3.1 CRB1 was exclusively expressed in the neuroretina 54
4.3.2 Porcine retinal pull-down approach of human canonical CRB1-FLAG WT revealed novel interactors of the crumbs complex 56
4.3.3 Protein-protein interactions were highly overlapping between N- and C-terminal FLAG-tagged CRB1 62
4.3.4 Majority of retinal interactors of canonical CRB1 WT were maintained in CRB1 C948Y MT 63
4.3.5 Porcine retinal pull-down using the CRB1 extracellular isoform revealed new potential extracellular interactors 64
4.3.6 Porcine retinal pull-down showed no significant differences in the retinal interactors of WT and C948Y CRB1 extracellular domain 70

4.4 Investigation of CRB1 and the regulation of the actin cytoskeleton 71

4.4.1 CRB1 localised closely to F-actin and various actin regulators in control RO 71
4.4.2 F-actin intensity was significantly reduced in patient A and patient B RO 73
4.4.3 Full-proteome analysis revealed downregulation of actin-based processes in CRB1 patients 74

4.5 Identification of candidate modifiers of disease severity between CRB1 patient brothers 77

4.5.1 Full-proteome analysis of patient RO revealed differentially abundant biological processes 78
4.5.2 Potential candidate modifiers identified by short-read WGS 81

4.5.2.1 Potentially harmful candidates of disease severity identified in the more affected patient A 83
4.5.2.2 Potentially protective candidates of disease severity identified in the less affected patient B 84

4.5.3 Both patients had an heterozygous variant of unknown significance in *GUCA1B* c.560G>A;p.S187N 86

4.6 Investigation of the molecular mechanism underlying CRB2 as a potential modifier in CRB1-linked retinal degenerations 87

4.6.1 Human CRB1 and CRB2, but not CRB3, adhered homo- and heterotypically 87
4.6.2 CRB2 pulled-down endogenous CRB1 from retinal tissue 88

4.6.3 Retinal protein-protein interaction network of CRB1 and CRB2 were highly overlapping 90
4.6.4 Missense mutations in the CRB1 extracellular domain only mildly influenced CRB1-CRB2 interaction *in vitro* 93
4.7 Establishment of a porcine retinal explant system to screen for candidate modifiers in CRB1-linked retinal degenerations 94
4.7.1 Expression of CRB1 was variable in different regions of the pig retina and different eyes 95
4.7.2 Preliminary knockdown experiments of *CRB1* in porcine retina explants by reverse magnetofection 96
4.7.3 Generation of monoclonal antibodies against human and porcine CRB1 and CRB2 97
5. Discussion 100
5.1 Human CRB1 and CRB2 formed homo- and heteromeric complexes at the OLM 101
5.2 Function of the CRB-CRB interaction and the role of the extracellular domain 102
5.3 CRB1 protein levels were reduced in homozygous CRB1 C948Y mutation 105
5.4 The CRB1 retinal protein-protein interaction network provides novel insights on the retinal Crumbs complex 106
5.5 Novel candidate modifiers of disease severity in *CRB1*-linked retinal degenerations 109
5.6 The role of CRB2 in modulating CRB1-linked retinal degenerations 111
6. References 115
7. Acknowledgements 127
8. Appendix 128

Statement of contributions

This dissertation is part of a joint DFG-funded SPP2127 project between the group of Prof. Marius Ueffing (Institute for Ophthalmic Research, University Clinics Tuebingen) and Prof. Stefan Liebau (Institute of Neuroanatomy & Developmental Biology, University of Tuebingen). As part of this collaboration, Dr. Kevin Achberger and Virginia Cora from the Institute of Neuroanatomy & Developmental Biology, University of Tuebingen cultured and provided patient and control iPSC-derived retinal organoids and unstained cryosections. I used these unprocessed samples as starting material for the full-proteomic analysis of the retinal organoids (Chapter 4.4.3 and Chapter 4.5.1), the analysis of CRB1 expression and splicing (Chapter 4.1 and Chapter 4.2) and the validation of the CRB1 interactome (Chapter 4.4 and Chapter 4.5).

For the whole-genome sequencing, which is described in Chapter 4.5.2, the isolation of DNA from blood samples was performed by Dr. Susanne Kohl and Eva Weber (Institute for Ophthalmic Research, University Clinics Tuebingen). The short-read whole genome sequencing and primary analysis was performed by the Core Facility for Medical Genetics and Applied Genomics cATG/NCCT (University of Tuebingen).

The generation of monoclonal antibodies against human and porcine CRB1 and CRB2, was performed in collaboration with the Core Facility Monoclonal Antibodies at the Helmholtz Centre Munich including antigen immunisation and fusion, multiplex-high throughput screening, titre assessment and sub-cloning. I validated the obtained supernatants by western blot and immunofluorescence microscopy on iPSC-derived RO (Chapter 4.7.3). Sylvia Bolz and Selina Kugler (Institute for Ophthalmic Research, University Clinics Tuebingen) validated the clones by immunofluorescence microscopy using the porcine retinal sections (Figure 42 C+D).

In addition, a manuscript entitled “Human CRB1 and CRB2 form homo- and heteromeric protein complexes in the retina” is published at Life Science Alliance [1]. The method sections 3.2.6; 3.2.7, 3.2.9 and 3.2.10, the results chapter 4.6 and the Appendix 26, 27 and 28 of this dissertation including the figures and legends are taken and adapted from the manuscript. I performed all the experiments, analysis and wrote the initial version of the above mentioned sections. In addition, I wrote the initial version of the introduction and discussion of the manuscript. All authors provided feedback on the initial manuscript draft.

All of the other data in this thesis has been collected and analysed by myself.

List of figures

Figure 1| The vertebrate retina is a complex, multilayered tissue 1
Figure 2| Structure and light-induced signalling cascade of rod and cone photoreceptors 3
Figure 3| Isoforms and localisation of the Crumbs protein family members in the retina 7
Figure 4| CRB organises a large intracellular protein scaffold through the conserved intracellular domain 10
Figure 5| The majority of CRB1 patient mutations are located in the larger extracellular domain 12
Figure 6| CRB1 patient RO showed a significant reduction in CRB1 protein levels and localisation 46
Figure 7| CRB1 p.C948Y did not influence BIP levels in patient iPSC-derived RO 47
Figure 8| CRB1 c.2843G>A partially led in part to a misspliced CRB1 transcript 48
Figure 9| CRB1-CRB1 homotypic interaction was dependent on the large extracellular domain 50
Figure 10| A panel of CRB1 missense mutations mildly influenced CRB1-CRB1 homophilic interactions 52
Figure 11| EGF domain 15, 17, 18 and 19 were not solely essential for CRB1-CRB1 interaction 53
Figure 12| CRB1 and CRB2 were highly expressed in iPSC-derived retinal organoids 55
Figure 13| Porcine CRB1 localised at the OLM and was high expressed in the porcine retina 56
Figure 14| Significantly enriched proteins after stringent SDS washing of canonical CRB1-FLAG without porcine retinal lysate incubation 57
Figure 15| Significantly highly abundant proteins in CRB1-FLAG SDS washed samples included known crumbs complex members 58
Figure 16| Incubation of canonical CRB1-FLAG with porcine retina resulted in significant enrichment of known and novel interactors 60
Figure 17| Retinal protein-protein interaction network of canonical CRB1 showed high abundance of proteins linked to the actin cytoskeleton 61
Figure 18| Crumbs complex members MPP5 and PATJ were specifically identified with the N-terminal tagged CRB1 construct 63
Figure 19| Retinal interactors of canonical WT CRB1 were preserved in the C948Y mutant 64
Figure 20| Without incubation with porcine retinal lysate, interactors of the CRB1 extracellular isoform were linked to processes involving or associated with the actin cytoskeleton 66
Figure 21| Retinal interactors of the CRB1 extracellular isoform and the canonical isoform were involved in similar biological processes 68
Figure 22| Protein-protein interaction network of the CRB1 extracellular isoform revealed new candidate interactors of the extracellular domain 69
Figure 23| No significant loss or gain of protein-protein interactions was identified in CRB1 extracellular WT and C948Y mutant 71

Figure 24| CRB1 localised together with F-actin, GSN, DBN1 and ARHGAP21 at the base of the segment-like protrusion in control iPSC-derived RO....72

Figure 25| RO of patient A and patient B showed a significant reduction in F-actin intensity at the OLM....74

Figure 26| Full proteome analysis showed reduced CRB1 and partially increased Crumbs complex members abundance in patient RO compared to control....75

Figure 27| CRB1 patient RO showed high abundance of phototransduction proteins and decreased abundance of actin-associated proteins....77

Figure 28| Proteins linked to actin filament, cell-matrix adhesion, growth cone, lysosomes and endosomes were significantly reduced in patient iPSC-derived RO....78

Figure 29| Patients RO show differences in pathways related to UPR, phototransduction and cilia....80

Figure 30| Lower abundant proteins in patient A RO are linked to cilia, synapse, light detection and signalling....81

Figure 31| Patient A and patient B RO showed difference in the abundance of proteins linked to cilia, phototransduction, UPR and signalling....82

Figure 32| Potential candidate modifiers were mildly reduced in patient A RO lysate compared to patient B....83

Figure 33| Protective candidates in patient B included the crumbs complex member CRB2....85

Figure 34| Both patients carried a heterozygous variant of unknown significance in *GUCA1B* c.560G>A;p.S187N encoding GCAP2....86

Figure 35| Human canonical CRB1 and CRB2 interacted homo- and heterotypically....88

Figure 36| CRB2 pulled-down endogenous CRB1 from retinal tissue....89

Figure 37| Retinal protein-protein interaction linked CRB2 to actin cytoskeleton and vesicular transport....90

Figure 38| CRB2 protein-protein retinal interaction network included proteins involved in signalling, lipid metabolism, cytoskeleton, cilia and ion transport....92

Figure 39| CRB1 missense mutations tested did not or mildly alter CRB1-CRB2 interaction....93

Figure 40| Expression of CRB1 varied in different regions of the porcine retina....95

Figure 41| Preliminary data on CRB1 silencing in porcine retina explants....96

Figure 42| CRB1C 25G2 and CRB1B 27A5 detect CRB1 using western blot and immunofluorescence microscopy....99

Figure 43| Multimodal approach to investigate disease mechanism and candidate modifiers in two siblings with early-onset RP....100

List of tables

Table 1| Primers used for Gateway Cloning 22
Table 2| Primers used for site-directed mutagenesis 23
Table 3| Primers used for RT-qPCR 24
Table 4| Primers used for sequencing 24
Table 5| Primers used for *CRB1* splicing analysis and *GUCA1B* amplification 25
Table 6| Overview of sequences of siRNAs 25
Table 7| Overview of primary antibody and fluorescent dyes 25
Table 8| Overview of the commercially available secondary antibodies 26
Table 9| Pipetting scheme for PCR amplification of *CRB1* and CRB3 with attB1 and attB2 overhang primers 30
Table 10| PCR program for *CRB1* amplification with attB1 and attB2 overhang primers 30
Table 11| PCR program for *CRB3* amplification with attB1 and attB2 overhang primers 30
Table 12| Pipetting scheme for PCR amplification of *CRB2* with attB1 and attB2 overhang primers 30
Table 13| PCR program for *CRB2* amplification with attB1 and attB2 overhang primers 30
Table 14| PCR protocol used for Phusion polymerase 31
Table 15| PCR program for Phusion polymerase 31
Table 16| BSA dilution series performed to assess protein concentration by Bradford assay 34
Table 17| BioRad program for RT-qPCR analysis 40
Table 18| DreamTaq PCR protocol for splicing analysis 41
Table 19| PCR program for Dream Taq DNA Polymerase 41
Table 20| Potentially harmful candidate modifiers identified in patient A 83
Table 21| Potential protective candidates in patient B include CRB2 84
Table 22| Overview of the antigen peptides used for monoclonal antibody production 97

Abbreviations

ABC	Ammonium bicarbonate
ACN	Acetonitrile
AIPL1	Aryl hydrocarbon receptor interacting protein like 1
APKC	Atypical protein kinase C
APS	Ammonium persulfate
ARHGEF	Rho guanine nucleotide exchange factor
BIP	Binding immunoglobulin protein
BP	Biological process
Ca^{2+}	Calcium
CC	Cellular component
cDNA	complementary deoxyribonucleic acid
cGMP	cyclic guanosine monophosphate
Co-IP	Co-immunoprecipitation
CRB	Crumbs
CRB1	Crumbs homologue 1
CRB2	Crumbs homologue 2
CRB3	Crumbs homologue 3
C-term	C-terminal
CX3CR1	CX3C motif chemokine receptor 1
CYGB	Cytoglobin
DDA	Data-dependent acquisition
DIA	Data-independent acquisition
dNTP	Deoxynucleotide triphosphate
EPB41L5	Erythrocyte Membrane Protein Band 4.1 Like 5
ERAD	Endoplasmic-reticulum-associated protein degradation
ERG	Electroretinogram
FERM	Protein 4.1, ezrin, radixin, moesin
GCAP	Guanylate cyclase-activating protein
GCL	Ganglion cell layer
GPCR	G protein-coupled receptor
GSN	Gelsolin
HAc	Acetic acid
HEK	Human embryonic kidney
HPRT	Hypoxanthine-guanine phosphoribosyltransferase
IAA	2-iodacetamide
IB	Immunoblot
ILM	Inner limiting membrane

INL	Inner nuclear layer
IP	Immunoprecipitation
IPL	Inner plexiform layer
IPSC	Induced pluripotent stem cell
IRD	Inherited retinal degenerations
IS	Inner segment
JAK	Janus kinase
KO	Knock-out
LB	Lysogeny broth
LCA	Leber congenital amaurosis
LC-MS/MS	Liquid chromatography–tandem mass spectrometry
MPP5	Membrane palmitoylated protein 5
MS/MS	Tandem mass spectrometry
MT	Mutant
NaCl	Sodium Chloride
N-term	N-terminal
OLM	Outer limiting membrane
ONL	Outer nuclear layer
OS	Outer segment
PALS1	Protein associated with Lin-7
PCA	Principle component analysis
PDE	Phosphodiesterase
PDZ	PSD-95/Dlg-A/ZO-1
PEI	Polyethylenimine
PI	Phosphoinositide
PI2/3	Phosphatase Inhibitor Cocktail 2/3
PIC	Protease Inhibitor Cocktail
PPI	Protein-protein interaction
PVDF	Polyvinylidene difluoride
RO	Retinal organoid
ROI	Region of Interest
RP	Retinitis pigmentosa
RPE	Retinal pigment epithelium
SDM	Site-directed mutagenesis
Sdt	Stardust
siRNA	small interfering RNA
StageTips	Stop-and-go extraction tips
TBS	Tris-buffered saline

TBST	Tris-buffered saline Tween
TFA	Trifluoroacetic acid
UPR	Unfolded protein response
w/v	Weight per volume
WGS	Whole genome sequencing
ZO	Zonula occludens

Summary

Vision is one of the most important senses that allows us to perceive the environment [2, 3]. The first steps of vision involve photoreceptors, which are highly specialised neuroepithelial cells in our retina [4, 5]. Therefore, photoreceptor dysfunction leading to visual impairment, significantly reduces the quality of life and personal independence [3, 5]. Inherited retinal degenerations (IRD) are among the leading causes of blindness in people under the age of 45 years [6]. Bi-allelic mutations in *Crumbs homologue 1 (CRB1)* are responsible for 10 % of all cases of Leber congenital amaurosis (LCA), the most severe form of IRD, and 6.5 % of the Retinitis pigmentosa (RP) conditions [7-10]. There is currently no treatment available to stop vision loss in these patients [20, 185].

Canonical CRB1 is a transmembrane protein that comprises an extracellular domain of a signal peptide, 19 EGF-like domains and three Laminin A globular (G)-like domains [8, 11, 12]. The extracellular domain is fused to an intracellular domain containing a Protein 4.1, ezrin, radixin, moesin (FERM) domain and a PSD-95/Dlg-A/ZO-1 (PDZ) motif [8, 11]. In human foetal retina and human induced pluripotent stem cell (iPSC)-derived retinal organoids (RO), CRB1 localises to the outer limiting membrane (OLM) in the subapical region of photoreceptors and Müller glia cells [13-16]. In human, CRB1 belongs to the Crumbs protein family along with CRB2 and CRB3, the latter of which lacks the extracellular domain [16-18]. Based on the protein-protein interactions (PPI) of the conserved intracellular domain, Crumbs proteins have been identified as key regulators of cell polarity, migration, asymmetric cell division and cell junctions [16, 19, 20]. In contrast, the function of the extracellular domain, where most of the patient mutations are located, is poorly described and hinders a better understanding of the disease mechanism [8]. In addition, *CRB1*-linked IRD are characterised by an enormous clinical heterogeneity suggesting the existence of additional modifiers of disease severity [21]. Identification of these modifiers may provide new insights for therapeutic strategies.

The aim of this study was to identify the molecular mechanisms and potential modifiers underlying *CRB1*-associated IRD. To achieve this goal, two siblings, who were diagnosed with early-onset RP due to a homozygous *CRB1* c.2843G>A;p.C948Y mutation, were studied as a proof-of-concept [22]. Interestingly, while one of the siblings (referred to as patient A) was blind, the other sibling (referred to as patient B) was significantly less affected and had residual visual capacity [22]. Previously, Dr. Achberger (group of Prof Liebau, University of Tuebingen) had generated and characterised iPSC-derived RO of both patients [22]. Using calcium (Ca^{2+})-imaging, Dr. Achberger and colleagues observed different responses to light stimulation in RO from patient A and patient B compared to the control, which to some extent reflected the clinical history [22].

In the first chapter of this study, CRB1 protein levels were investigated in RO of patient A and patient B using western blot and immunofluorescence microscopy. The results showed a significant reduction in total CRB1 protein and localisation to the OLM in RO of both patients compared to the control. No significant difference in CRB1 levels was found between RO of patient A and patient B suggesting that the variation in disease severity cannot be explained by a difference in CRB1 level. To investigate the molecular mechanism underlying the reduction of CRB1 protein in patient RO, the effect of c.2843G>A on *CRB1* splicing was examined using cDNA from patient and control RO. The c.2843G residue represents the first base of exon 9. Endpoint PCR analysis revealed that in several *CRB1* transcripts, carrying the c.2843G>A mutation, exon 9 was skipped, resulting in a frameshift and a premature stop codon in exon 10. While missplicing remains a possible explanation for reduced CRB1 levels, studies in *Drosophila (Drosophila melanogaster)* have suggested a role of the extracellular domain in stable membrane localisation of CRB1 [23]. Data obtained in this study showed that human CRB1-CRB1 homomeric complexes are formed through the extracellular domain. With approximately 20 %, the C948Y missense mutation slightly impaired CRB1-CRB1 interaction *in vitro*. Collectively, this chapter revealed that CRB1 protein levels are reduced in both patient RO indicating that any process requiring the full-length CRB1 protein may be affected.

In the next chapter, the retinal CRB1 interactome was investigated using a porcine retinal pull-down approach followed by mass spectrometry to gain further insight into the function of CRB1. In addition to the previously described intracellular interactors, novel members of the retinal CRB1 complex were identified, which are regulators of the actin cytoskeleton (e.g. GSN, ARHGAP21 and DBN1), vesicular trafficking and lipid metabolism. In addition, SFRP2, a regulator of WNT signalling, and LTBP1, involved in TGF-ß signalling, were identified as potential interactors of the CRB1 extracellular domain. Furthermore, the data showed no significant loss of PPI upon introduction of the C948Y mutation.

Given the high abundance of actin regulators in the CRB1 interactome and the importance of the actin cytoskeleton in photoreceptor cells, the localisation of F-actin and CRB1 was further investigated by immunofluorescence microscopy. In control RO, CRB1 and the actin regulators, GSN, DBN1 and ARHGAP21, localised together with F-actin at the OLM. Preliminary data revealed a significant reduction in F-actin intensity at the OLM in patient A and patient B RO compared to control. This reduction was significantly higher in RO of patient B compared to patient A. In addition, full-proteome analysis by mass spectrometry was performed using lysates of control and patient RO. Data indicated significantly lower level of, among others, members of the ARP2/3 complex, growth cone and cell-matrix adhesion proteins in patient A and patient B RO compared to control. Taken together, these data suggest that CRB1 may directly or indirectly affect the actin cytoskeleton and actin-based processes in RO.

In the next chapter, the molecular differences between the two patients were investigated and potential candidate modifiers were defined. Interestingly, RO of patient A displayed a significantly lower abundance of proteins involved in synaptic signalling and light detection compared to RO of patient B, reflecting to some extent the difference in light sensitivity observed by Dr. Achberger and colleagues [22]. To define candidate modifiers, whole genome sequencing (WGS) was performed. One of the potential protective candidate modifiers identified was CRB2, a member of the CRB protein family. CRB2 was slightly but significantly more abundant in RO of patient B compared to RO of patient A and the control. In addition, a heterozygous single nucleotide variant upstream of the *CRB2* gene (chr9: 123351196 G>T) gene was identified in patient B by WGS. Taken together, the data described in this chapter provided novel protective and harmful candidate modulators of disease severity in CRB1-associated IRD.

Next, the relationship between CRB1 and CRB2 was further investigated as several studies highlight the modulatory and rescue ability of CRB2 in CRB1-associated IRD [15, 24, 25]. The results obtained show that CRB1 and CRB2 form homo- and heteromeric complexes. Furthermore, human CRB2 was able to pull-down endogenous CRB1 from porcine retinal lysates. In addition, the retinal PPI network of CRB2 revealed a high overlap with that of CRB1, suggesting that CRB1 and CRB2 may be involved in similar cellular processes. Nevertheless, the patient's missense mutation in CRB1 only mildly influenced the CRB1-CRB2 interaction.

The final chapter explored the potential of porcine retinal explants as a less time-consuming, costly and material-restrictive model to investigate the identified candidate modifiers [272]. Results from preliminary experiments showed that CRB1 expression varies in different regions of the porcine retina and that *CRB1* mRNA expression can be reduced by applying small interfering RNA (siRNA) mediated silencing using reverse magnetofection. In addition, a monoclonal antibody against human and porcine CRB1 was generated in together with the Core Facility Monoclonal Antibodies (Helmholtz Centre, Munich) allowing to further investigate the corroborative function of CRB1 function and the potential modifiers in a porcine explant culture system in the future.

Zusammenfassung

Die Sehkraft ist einer unserer wichtigsten Sinne, die wir für die Wahrnehmung unserer Umwelt benötigen [2, 3]. Am Vorgang des Sehens sind initial spezialisierte Neuroepithelzellen in unserer Netzhaut beteiligt [4, 5]. Funktionsstörungen dieser so genannten Photorezeptoren führen zu einem eingeschränkten Sehvermögen, welches die Lebensqualität und die persönliche Unabhängigkeit stark beeinträchtigt [3, 5]. Zu den Hauptursachen für den Verlust des Sehvermögens gehören, bis zu einem Alter von 45 Jahren, erblich bedingte Netzhautdegenerationen [6]. Genmutationen in Crumbs homolog 1 (CRB1) sind für 10 % aller Fälle von Lebersche kongenitale Amaurose (LCA), der schwersten Form von erblichen Netzhauterkrankungen, und für 6,5 % aller Retinitis pigmentosa (RP) Erkrankungen verantwortlich [7-9]. Für diese Patienten gibt es derzeit keine Behandlungsmöglichkeit, die den Verlust des Sehvermögens aufhalten kann [20, 185].

CRB1 ist ein Transmembranprotein mit einer extrazellulären Domäne, die aus einem Signalpeptid, 19 epidermalen Wachstumsfaktor-ähnlichen Domänen und drei Laminin A-ähnlichen Domänen besteht [8, 11]. Der extrazelluläre Teil des CRB1-Proteins ist über eine Transmembrandomäne mit einer intrazellulären FERM- und einer PDZ-Domäne verbunden [8, 11]. In der humanen embryonalen Netzhaut und in humanen Netzhautorganoiden, die aus induzierten pluripotenten Stammzellen differenziert wurden, befindet sich CRB1 an der äußeren Begrenzungsmembran in Photorezeptoren und in Müller-Gliazellen [13-15]. Im Menschen gehört CRB1 zusammen mit CRB2 und CRB3, welches als einziges keine extrazelluläre Domäne besitzt, zur Familie der Crumbs-Proteine [16-18]. Die konservierte intrazelluläre Domäne der Crumbs-Proteine bindet an zahlreiche Proteine und reguliert so die Zellpolarität, Migration, asymmetrische Zellteilung und Zellverbindungen [16, 19, 20]. Im Gegensatz hierzu ist über die Funktion der extrazellulären Domäne des CRB1 Proteins, in der sich die meisten Patientenmutationen befinden, wenig bekannt [8]. Ein weiteres Merkmal der CRB1-bedingten Netzhautdegenerationen ist das heterogene klinische Krankheitsbild, weshalb zusätzliche Faktoren vermutet werden, die die Ausprägung der Symptome beeinflussen [21]. Die Identifizierung dieser Einflussfaktoren und ein besseres Verständnis der zugrundeliegenden Erkrankungsmechanismen können daher zu neuen Therapieansätzen führen.

Das Ziel dieser Arbeit war es, neue Erkenntnisse über die molekularen Erkrankungsmechanismen CRB1-bedingter Netzhautdegenerationen zu gewinnen und mögliche Faktoren zu identifizieren, die die Schwere des Krankheitsverlaufs beeinflussen. Hierfür wurde der Fall zweier Geschwistern untersucht, die aufgrund einer homozygoten CRB1-Mutation c.2843G>A;p.C948Y an RP erkrankt sind [22]. Interessanterweise ist einer der Patienten (Patient A) bereits vollständig erblindet, wohingegen der andere Patient (Patient B)

einen milderen Verlauf mit verbleibender Sehkraft zeigt [22]. Im Vorfeld dieser Arbeit, hat Dr. Achberger (Arbeitsgruppe Prof. Liebau, Universität Tübingen) mit Hilfe von induzierten pluripotenten Stammzellen Netzhautorganoide von beiden Patienten und Kontrollpersonen differenziert und charakterisiert [22]. Mittels Kalzium-Imaging konnte nachgewiesen werden, dass die Netzhautorganoide der beiden Patienten eine unterschiedliche Lichtsensitivität aufweisen, die mit der klinischen Symptomatik korreliert [22].

Im ersten Kapitel dieser Arbeit wurde zunächst der Einfluss der c.2843G>A;p.C948Y Mutation auf die CRB1 Proteinmenge untersucht. Mittels Western Blot und Immunfluoreszenzmikroskopie, konnte gezeigt werden, dass die Netzhautorganoide beider Patienten im Vergleich zu Kontrollen sowohl eine signifikant geringere Gesamtmenge an CRB1-Protein aufweisen, als auch weniger CRB1 an der äußeren Begrenzungsmembran lokalisiert war. Es wurde jedoch kein signifikanter Unterschied in der Menge an CRB1 zwischen den Patienten gefunden. Somit konnte gezeigt werden, dass die Menge des CRB1-Proteins in den Netzhautorganoiden nicht mit der Schwere der Symptome der Patienten korreliert. Im nächsten Schritt wurde die Ursache des Proteinverlustes untersucht. Da c.2843G>A die erste Base von Exon 9 (NM_201253.3) betrifft, wurde das Spleißen von *CRB1* mit Hilfe von generierter cDNA aus Patienten- und Kontroll-Netzhautorganoiden mittels PCR analysiert. Die Ergebnisse haben ergeben, dass Exon 9 in einem Teil der CRB1 Transkripte mit c.2843G>A Mutation fehlt, was zu einem Frameshift mit vorzeitigem Stop-Codon in Exon 10 führt. Neben dem Spleißen wurde der Einfluss der C948Y Mutation auf die Bindungsfähigkeit von CRB1 an andere CRB1 Proteine analysiert. Die Ergebnisse zeigten, dass CRB1-Proteine über die extrazelluläre Domäne aneinanderbinden können und, dass die Interaktion im Falle der C948Y Mutation *in vitro* geringfügig, um ca. 20 %, beeinträchtigt ist. Zusammenfassend konnte gezeigt werden, dass die Menge des CRB1 Proteins in den Netzhautorganoiden der beiden Patienten mit homozygoter CRB1 c.2843G>A;p.C948Y Mutation stark reduziert und somit Prozesse, die abhängig sind von der Menge und Lokalisation von CRB1 sind, in den Patienten beeinträchtigt waren.

Um die Funktionen von CRB1 in der Netzhaut zu untersuchen, wurde im nächsten Kapitel ein Pull-Down-Verfahren aus der Schweinenetzhaut mit anschließender Massenspektrometrie durchgeführt. Neben den bereits beschriebenen Interaktoren wurden Proteine mit Funktionen im Aktinzytoskelett (GSN, DBN1 und ARHGAP21), im vesikulären Transport und im Lipidstoffwechsel als neue mögliche Bindungspartner des retinalen CRB1-Komplexes identifiziert. Die extrazellulären Proteine SFRP2, ein Regulator des WNT-Signalweges und LTBP1, eine Komponente des TGF-ß-Signalweges wurden als potentielle Bindungspartner der extrazellulären Domäne gefunden. Darüber hinaus ergaben die Ergebnisse keinen signifikanten Verlust eines CRB1-Bindungspartners im Falle der C948Y-Mutation.

Aufgrund der Vielzahl der in der CRB1-Interaktom-Analyse identifizierten Aktinregulatoren und der essentiellen Rolle des Aktinzytoskeletts in Photorezeptoren wurde die Beziehung zwischen Aktin und CRB1 mittels Immunfluoreszenzmikroskopie weiter untersucht. Die Ergebnisse zeigten, dass CRB1 zusammen mit den Aktin-Regulatoren GSN, DBN1 und ARHGAP21 sowie F-Aktin an der äußeren Begrenzungsmembran in Netzhautorganoiden von Kontrollpersonen lokalisiert ist. Außerdem wurde in den Netzhautorganoiden der beiden Patienten signifikant weniger F-Aktin an der äußeren Begrenzungsmembran gefunden als in den Netzhautorganoiden der Kontrollpersonen. Zudem, schien F-Aktin in den Netzhautorganoiden von Patient B im Vergleich zu Patient A stärker reduziert zu sein. Neben der Immunfluoreszenzmikroskopie, wurde eine Proteomeanalyse der Lysate von Kontrollpersonen- und Patienten-Netzhautorganoiden mittels Massenspektrometrie durchgeführt. Die Ergebnisse zeigten, unter anderem, eine signifikante Reduktion der Proteine des ARP2/3-Komplexes und der Zell-Matrix-Adhäsion in den Netzhautorganoiden beider Patienten im Vergleich zu Kontrollpersonen. Insgesamt deuten die Ergebnisse auf eine mögliche direkte oder indirekte Rolle von CRB1 bei der Regulation des Aktinzytoskeletts hin.

Im nächsten Kapitel wurden die molekularen Unterschiede und möglichen Faktoren, die den Schweregrad des Krankheitsverlaufs beeinflussen, mit Hilfe der Proteomeanalyse von Netzhautorganoidlysaten, Genomsequenzierung und der CRB1 Interaktomdaten identifiziert. Es wurde gezeigt, dass Netzhautorganoide von Patienten A im Vergleich zu Netzhautorganoiden des Patienten B eine signifikant geringere Menge an Proteinen für die Phototransduktion und die Signalübertragung an der Synapse aufweisen. Außerdem, wurde CRB2 als einer der möglichen Einflussfaktoren für den unterschiedlichen Krankheitsverlauf der beiden Patienten identifiziert. Netzhautorganoidlysate des weniger stark betroffenen Patienten B enthielten signifikant mehr CRB2 im Vergleich zu denen des Patienten A und der Kontrollpersonen. Zudem wurde eine heterozygote einzelne Nucleotid Variante vor dem CRB2-Gen (chr9: 123351196 G>T) des Patienten B gefunden.

Das CRB2-Protein wurde bereits in Studien an Mäusen und humanen Netzhautorganoiden als möglicher Einflussfaktor auf den Schweregrad von CRB1-bedingten Netzhautdegenerationen diskutiert [15, 24, 25]. Jedoch ist die molekulare Wechselwirkung von CRB1 und CRB2 nicht bekannt und wurde im nächsten Kapitel weiter untersucht. Es wurde gezeigt, dass CRB1 und CRB2 homo- und heteromere Komplexe bilden. Außerdem konnte endogenes CRB1 aus der Schweinenetzhaut mit humanem CRB2 angereichert werden. Darüber hinaus zeigte das Interaktom von CRB2 eine starke Überlappung mit dem von CRB1, was darauf hindeutet, dass CRB1 und CRB2 an ähnlichen zellulären Prozessen beteiligt sein könnten. Allerdings wirkten sich Patienten Missense-Mutationen in CRB1 nur geringfügig auf die Interaktion zwischen CRB1 und CRB2 aus.

Um die gefundenen Kandidaten mit Einfluss auf die Erkankungsausprägung weiter zu untersuchen, bieten Kulturen explantierter Schweinenetzhaut aufgrund des geringeren Zeitaufwandes, der geringeren Kosten und der höheren Materialverfügbarkeit eine vielversprechende Ergänzung zu Netzhautorganoiden [272]. Erste Ergebnisse dieser Arbeit ergaben, dass verschiedene Regionen der Schweineretina eine unterschiedlich hohe Expression von CRB1 aufweisen, die mittels reverser Magnetofektion einer *CRB1* siRNA reduziert werden kann. Darüber hinaus wurde in Zusammenarbeit mit der Core Facility für monoklonaler Antikörper am Helmholtz Zentrum München ein entsprechender Antikörper gegen das humane und porcine CRB1 generiert, der weitere Untersuchungen zur Funktion von CRB1 und potenziellen Einflussfaktoren ermöglicht.

1. Introduction

1.1 The vertebrate retina

Vision is one of the five commonly understood human senses, which allows us to contact and navigate in our environment [2, 26]. As it makes approximately 80 % of the sensory input that we perceive, impairment or loss of vision substantially reduces the quality of life and personal independence and can impair mental health, mobility, social contact and increase fall-related injuries [2, 3, 27].

Vision begins when photons enter our camera-type eye and are focused through the cornea and the lens onto the retina (**Figure 1**) [5]. The retina is a multilayer tissue that

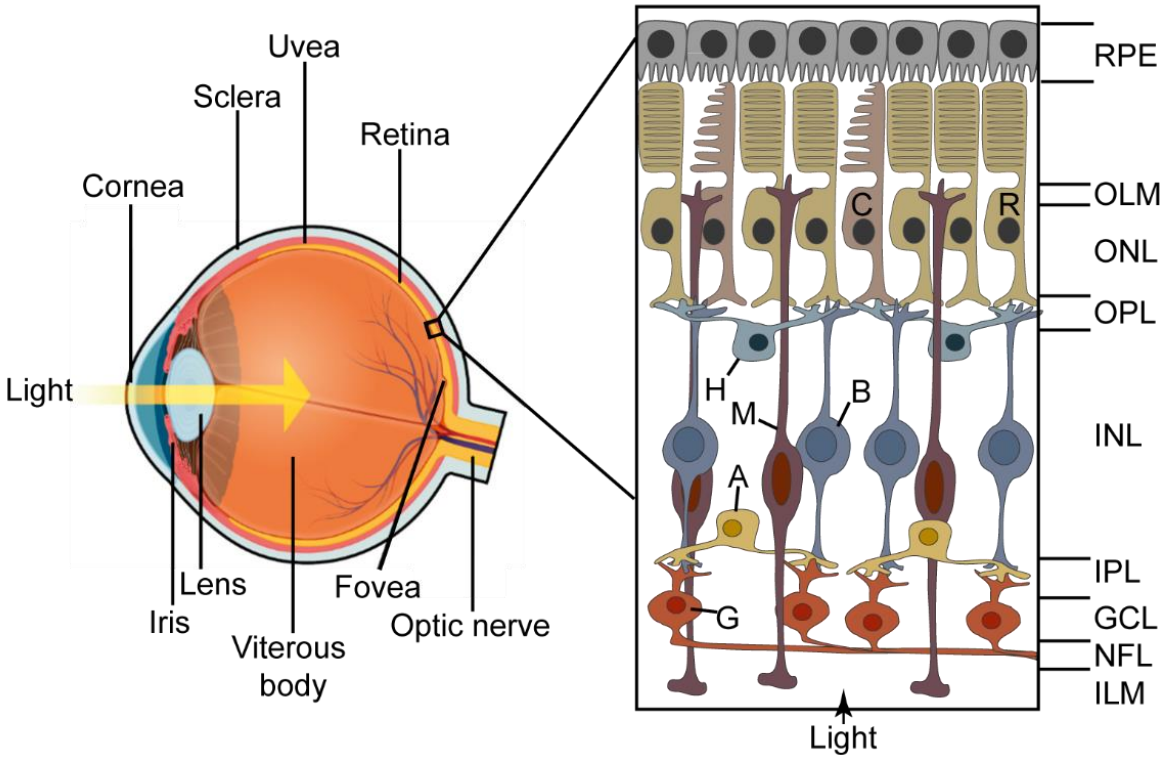

Figure 1| The vertebrate retina is a complex, multilayered tissue
Left panel depicts an illustration of a cross-section through the human eye. Light enters through the cornea and the lens to the retina. Right panel depicts the different layers of the human retina. RPE=retinal pigment epithelium, OLM= outer limiting membrane, ONL= outer nuclear layer, OPL=outer plexiform layer, INL= inner nuclear layer, IPL= inner plexiform layer, GCL= ganglion cell layer, NFL= nerve fibre layer, ILM= internal limiting membrane, C= cone, R= rod, B= bipolar cell, H= horizontal cell, M=Müller glia cell, A= amacrine cell, G= ganglion cell. Adapted from Ptito *et al.* and Gigoryan *et al.* [33, 267]

perceives and converts the incoming light signal into an electrical signal, which is eventually transferred to the brain [4, 5]. The retina, as part of the central nervous system, consists of neurons and glia cells and is also termed the 'window to the brain' [5, 28]. Five neuronal cell types (retinal ganglion cells, bipolar cells, horizontal cell, amacrine cells, photoreceptors) and one major glial cell type, termed Müller glia cell, are generated from common retinal progenitor cells [5]. In addition, two other types of glia cells, astrocytes and microglia, migrate from other

origins to the developing retina [29-31]. All retinal cell types are organised into multiple cell layers [5, 29].

The innermost layer, termed internal limiting membrane (ILM), contains the Müller Glia cell end feet, and forms a basement barrier between the vitreous cavity and the retina [5, 32, 33]. The nerve fibre layer is located above the ILM and contains the long axons of the ganglion cells [5, 32, 33]. At the optic disc, those axons leave the retina to form the optic nerve, which transmits signals to the corresponding brain regions [5, 33]. The third layer comprises the cell bodies of the ganglion cells and is termed the ganglion cell layer [5, 33]. The fourth innermost layer, the inner plexiform layer, contains the synapses formed between presynaptic terminal endings of bipolar cells and postsynaptic endings of amacrine and ganglion cells [5, 33]. The cell bodies of the bipolar cells, the Müller glia cells, the horizontal and amacrine cells form the fifth layer, the inner nuclear layer (INL) [5, 33]. The next layer, termed the outer plexiform layer contains the synapses formed between photoreceptors, bipolar cells, and horizontal cells [5, 33]. Above, the photoreceptor nuclei form the next layer, which is called the outer nuclear layer (ONL) [5, 33]. The eighth layer, comprises adherens junctions and tight junctions formed between Müller glia cells and photoreceptors, termed the outer limiting membrane (OLM) [5, 33]. The OLM separates the photoreceptor cell nuclei from the light-sensitive segments [5, 33]. The layer of the retinal pigment epithelium (RPE) is characterised by a high number of melanosomes and melanin granules and forms the outermost layer of the retina [5, 33]. The RPE is connected to the outer segments (OS) of the photoreceptor at the apical site and the Bruch’s membrane on the basal site [34]. The RPE has an important role in the visual cycle, phagocytosis of photoreceptor OS, barrier, substance transport and protection from light damage and oxidative stress [34-37].

The retinal layers are connected by two main pathways, the vertical and the horizontal pathway [33]. The vertical pathway starts with the capturing of a photon by the photoreceptor, which will be converted and sent as a chemical signal through the release of the excitatory neurotransmitter glutamate to the bipolar cells [33]. There are multiple types of bipolar cells in the humans, which are generally categorised into ON and OFF types [33]. They provide the first layer of encoding visual information depending on the light intensity received by the photoreceptor cells [33]. Bipolar cells signal to ganglion cells, which further process the signal and send it to the brain [33]. The horizontal pathway comprises amacrine cells or horizontal cells, which are laterally connected and modulate the signalling between bipolar and ganglion cells, or photoreceptor and bipolar cells, respectively [33, 38]. In this way, motion, photoreceptor convergence, visual contrast and contextual modulation are regulated [33, 39].

1.1.1 Photoreceptor cells

Photoreceptors are involved in the first step of the phototransduction cascade [5]. Based on their expression of the light-detecting opsin photopigments, their morphology and spectral sensitivity, they are classified into two main types, rods and cones [5]. While rods, which are sensitive to a single photon, function for low light vision and motion detection (scotopic vision), cones are required for high acuity and colour vison during the day (photopic vision) [5, 40, 41]. Cones are further classified based on the wavelength sensitivity of their expressed opsin. Three types of cones are present in the human retina, which either express a short-wavelength sensitive opsin (maximum absorbance 420 nm; S/blue cones), a medium-wavelength sensitive opsin (maximum absorbance 534 nm, M/green cones) or a long-wavelength sensitive opsin (maximum absorbance 564 nm; L/red cones) [5, 42]. Rods express rhodopsin, which has absorption maxima of 498 nm in human [5, 42]. The sensitivity of opsin and rhodopsin is caused by differences in the amino acid sequence, which influence the interaction with the light-sensitive chromophore, the vitamin A derivative 11-*cis* retinal [5].

Both rods and cones share a highly specialised and unique morphology of an elongated OS, a connecting cilium, a mitochondria-rich inner segment (IS), a nucleus-containing cell body and a synaptic terminal [5, 43] (**Figure 2 A**). The OS is a highly modified primary cilium [5, 44].

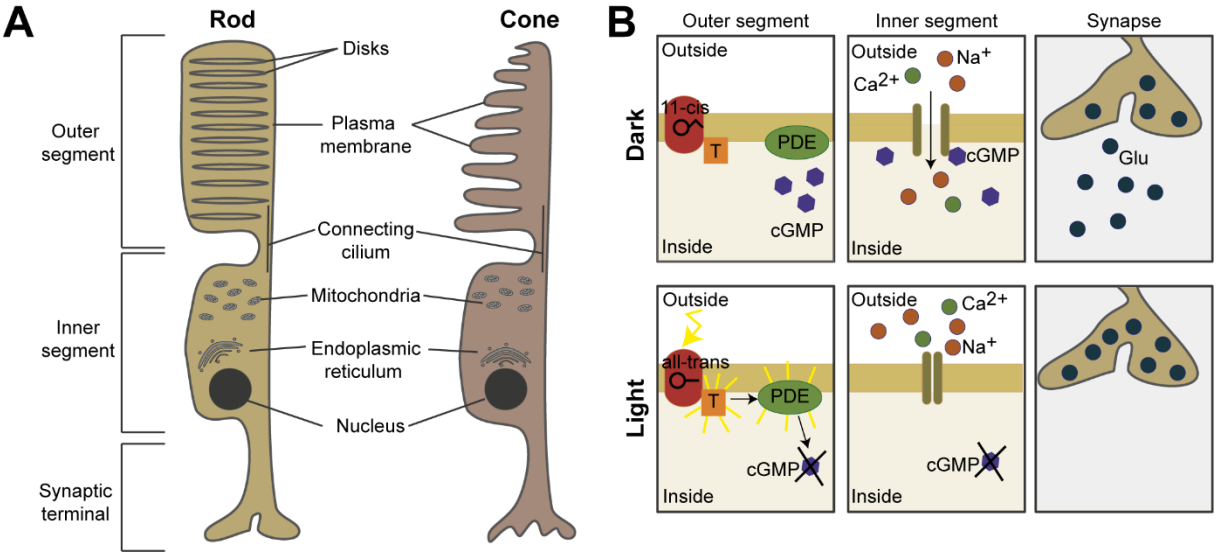

Figure 2| Structure and light-induced signalling cascade of rod and cone photoreceptors
(A) Illustration of the specialised morphology of rod (left panel) and cone (right panel) photoreceptors. Both share a large OS containing the photopigment, which is connected through the connecting cilium to the IS and the synaptic terminal. Adapted from Hussey *et al.* [5] **(B)** Representation of the phototransduction cascade. In the dark (top panel), 11-*cis* retinal is attached to rhodopsin in the OS disc membrane. Transducin (T) and phosphodiesterase (PDE) are inactive leading to high cGMP levels and the opening of the cGMP-gated cation channels. The influx of Ca^{2+} and Na^{+} leads to depolarisation of the photoreceptor and the release of glutamate (Glu) at the synapse. In light conditions (lower panel), 11-*cis* retinal isomerises to all-trans retinal and detaches from rhodopsin, which in turn activates Transducin. Activated transducin activates PDE, leading to a decrease in cGMP levels and closure of the cGMP gated cation channels. The photoreceptor hyperpolarises leading to loss of Glu release at the synapse. Adapted from Klapper *et al.* [268]

The long and cylindrical rod OS contains ‘discs’, which are individual and parallel membrane compartments sealed-off from the plasma membrane [44, 45]. Those discs and the plasma membrane contain rhodopsin [5, 46]. In contrast, the conical-shaped OS of cones has multiple ‘sacs’ that evaginate from the plasma membrane and contain opsin [44, 47].

The photoreceptor OS is constantly generated near the ciliary neck at the base of the OS, where the photopigment gets incorporated into the new membranes [44, 48]. Simultaneously, the OS tip is phagocytosed by the RPE ensuring a constant length of the OS [44]. The connecting cilium resembles the ciliary transition zone and provides the bridge between the OS and the IS, where *de novo* biosynthesis of all OS proteins occurs [49-51]. The connecting cilium contains an axoneme with a 9+0 arrangement of tubulin doublets, which is linked to the plasma membrane by Y-shaped linker structures and connected through the basal body to the IS [43, 52]. The basal body consists of a nine-triplet microtubule, that acts as an organizing center and nucleation site for the growth of the axoneme [43, 50]. The base of the cilia is further attached to the cell by a fibrous cytoskeletal structure, the ciliary rootlet [53, 54]. Besides the OS, which requires constant transport of proteins from the IS, the synapse at the base of the photoreceptor is also dependent on constant transport of proteins from the IS emphasising the importance of vesicular sorting and transport in the photoreceptor [49, 50].

1.1.2 Phototransduction and the visual cycle

The first step of phototransduction occurs in the OS, where the photon is captured by the chromophore, 11-*cis* retinal, which is covalently attached to rhodopsin [55-58] (**Figure 2 B**). Next, 11-*cis* retinal isomerises to all-*trans* retinal leading to a conformational change and activation of the attached rhodopsin [55-59]. Rhodopsin is a G-protein coupled receptor (GPCR), which upon activation, interacts with the GDP-bound form of transducin [55-58]. Subsequently, GDP on the α-subunit of transducin is replaced by GTP through rhodopsin leading to the dissociation of the GTP-bound α-subunit from rhodopsin and the β- and γ-subunits of transducin [55-58]. The GTP-bound α-subunit binds to the inhibitory γ-subunit cyclic guanosine monophosphate (cGMP) PDE or PDE6 [55-58]. Consequently, the activity of the PDE catalytic subunits (αβ in rods, αα in cones) increases, leading to a reduction of the second messenger cGMP [55-58]. In turn, low cGMP levels result in closure of the cGMP-gated Na^+ and Ca^{2+} channels, which cause membrane hyperpolarisation and reduced glutamate release at the photoreceptor synapse [55-58].

To maintain vision sensitivity, various regulators contribute to reverting the phototransduction cascade. For instance, a low intracellular Ca^{2+} level activates guanylate cyclases through the guanylate cyclase-activating proteins (GCAP) [60]. The activated guanylate cyclases then synthesise cGMP to restore cGMP levels [60]. Moreover, to prevent further activation of transducin, rhodopsin is phosphorylated by rhodopsin kinase and bound

by arrestin [43, 61-63]. Subsequently, phosphorylated rhodopsin loses all-*trans*-retinal [43, 61]. All-*trans*-retinal is reconverted into 11-*cis*-retinal in the retinoid or visual cycle, which involves multiple enzymatic reactions in photoreceptors and RPE cells [64]. Upon dissociation from the activated opsin, all-*trans*-retinal is converted into all-*trans*-retinol by all-*trans*-retinol dehydrogenase 8 [64]. Next, all-*trans*-retinol is transferred from the photoreceptor OS to the RPE [64]. In a series of further enzymatic conversions in the RPE, 11-*cis*-retinal is regenerated, which is transported back to the photoreceptor OS [64].

1.1.3 Müller Glia cells

With their apical and basal processes, Müller glia cells cover the entire neuroretina from the ILM to the OLM allowing the contact with all neuronal cell types and synapses [65, 66]. Müller glia cells support synapse development, neuronal survival, retinal structure and organisation [29]. Illustrating this point, impairment of Müller glia development in various knock-out (KO) models resulted in a lack of retinal lamination and ectopic neural rosette formation [67-69]. Furthermore, Müller glia cells secrete trophic factors important for the viability of neurons such as vascular endothelial growth factor (VEGF) and neuritogenesis including interleukin-6 [29, 70-72]. At the same time, Müller glia cells supply neurons with neurotransmitter precursors and recycle neurotransmitters such as glutamate, preventing glutamate-induced neurotoxicity and improving the spatial resolution [65, 73-78]. Due to their direct contact with endothelial cells, Müller glia cells contribute to the formation of the blood-retinal barrier, regulate retinal vasculature development and exchange molecules, including nutrients and metabolic waste products between neurons and retinal vessels [29, 65, 66, 71]. In addition, Müller glia cells control the extracellular pH, water, and ion balance, which influence the signal-to-noise ratio during synaptic transmission [29, 65, 66]. For cones, Müller glia cells contribute, besides the RPE, to the assembly, phagocytosis and chromophore recycling [79]. A recent study has demonstrated that Müller glia cells guide light to the photoreceptors and protect them from mechanical stress [65, 80].

In the mature retina, Müller glia cells seem to harbour stem cell-like characteristics and regenerative properties [65, 81]. Upon pathological stimuli, Müller glia cells undergo a transition from quiescence to a process termed reactive gliosis, during which they change morphology, dedifferentiate and migrate [82]. Unlike other species, mammalian Müller glia cells are unable to differentiate into neurons *in vivo* and the multipotency and proliferation of adult human Müller glia cells have only been shown in *vitro* [81, 82]. However, during gliosis, activated Müller glia cells increase the density of intermediate filaments and secrete neuroprotective factors [83]. Although these responses are protective, chronic activation of Müller glia cells results in neuronal cell death and glia scar formation leading to neuronal degeneration as commonly seen in inherited retinal degenerations (IRD) [83].

1.2 Inherited retinal diseases caused by mutations in *Crumbs homologue 1*

IRD are a group of genetic diseases that range from progressive loss of vision to complete blindness from birth to late middle age [84]. Monogenic IRD affect approximately 1 in 2000 individuals [85]. IRD are further categorized based on the photoreceptor subtype that is primarily affected [84]. Rod-Cone dystrophies, for example retinitis pigmentosa (RP) and Leber congenital amaurosis (LCA), initially cause rod degeneration followed by cone degeneration [84]. This is in contrast to macular, cone and cone-rod dystrophies, which initially impair cones and later rods [84]. Several IRD have additional systemic symptoms such as for Usher syndrome (hearing impairment); Bardet Biedl syndrome (obesity, renal dysfunction, polydactyly) and Joubert syndrome (cerebellar hypoplasia) [84]. IRD are genotypically and phenotypically heterogeneous, meaning that mutations in the same gene can cause different types of IRD while similar phenotypes can be caused by mutations in different genes [84, 86].

Up to date, 270 genes have been associated with IRD, amongst them *Crumbs homologue 1* (*CRB1*), in which bi-allelic mutations are linked to multiple forms of IRD [7, 84]. Mutations in *CRB1* are linked to 10 % of all cases of LCA and severe early-onset retinal dystrophy [7]. LCA is the earliest and most severe form of IRD, affecting individuals at birth or within the first six months of life [7]. LCA is further characterised by nystagmus and the absence of photopic and scotopic responses in electroretinogram (ERG) measurements [8, 9]. ERG is an electrodiagnostic test, in which skin electrodes are applied to the lower lid and the response upon flash, pattern and flicker stimuli indicates the function of retinal cell types [84]. Furthermore, *CRB1* mutations account for 6.5% of RP cases [7, 8]. Compared to LCA, RP is generally considered to be a milder form because the onset of visual impairment is not congenital but occurs in the first decade or later in life [8]. RP symptoms initially start with night blindness alongside with reduced photopic responses and attenuated scotopic responses by ERG leading to complete blindness in the fourth decade of life [9]. Apart from RP and LCA, *CRB1* mutations have also been described in cases of cone-rod dystrophies, foveal retinoschisis, macular dystrophy and fenestrated slit maculopathy [7].

CRB1-linked IRD typically display nummular pigment clumping at the level of the RPE with yellow and white spots and an abnormal layered and thickened retina in optical coherence tomography, an ultrasound-like technique that allows analysis of the retinal thickness, segmentation and retinal layers [84]. Furthermore, *CRB1* mutations are associated with preserved para-arteriolar RPE, in which RPE degenerates throughout the entire retina except for the RPE adjacted to retinal arterioles [8]. Patients with *CRB1* mutations may also present with Coats-like vasculopathy, in which abnormally permeable blood vessels cause exudation, retinal detachment and neovascular glaucoma [8]. Additional nanophthalmos, hyperopia, a

narrow anterior chamber, optic disc drusen and keratoconus have been reported in *CRB1* patients [7, 8].

1.2.1 Crumbs homologue 1

1.2.1.1 CRB1 isoforms and localisation in the human retina

The large type I transmembrane protein Crumbs (CRB) was initially described in the apical membrane of *Drosophila (Drosophila melanogaster)* epithelial cells, where its loss resulted in a dotted (crumbs-like) instead of a continuous presentation of the ectoderm-derived cuticle [87, 88]. In 1999, IRDs were linked to mutations in the human homologue *crumbs homologue 1* (*CRB1)* on chromosome 1q31.3 [11]. The canonical isoform of CRB1 (also referred to as CRB1-A, CRB1 full-length, CRB1 prototypic isoform) consists of a large extracellular domain with an N-terminal (N-term) signal peptide, 19 epidermal growth factor (EGF)-like domains and three laminin A globular (G)-like domains [1, 8] (**Figure 3 A**). This extracellular domain is

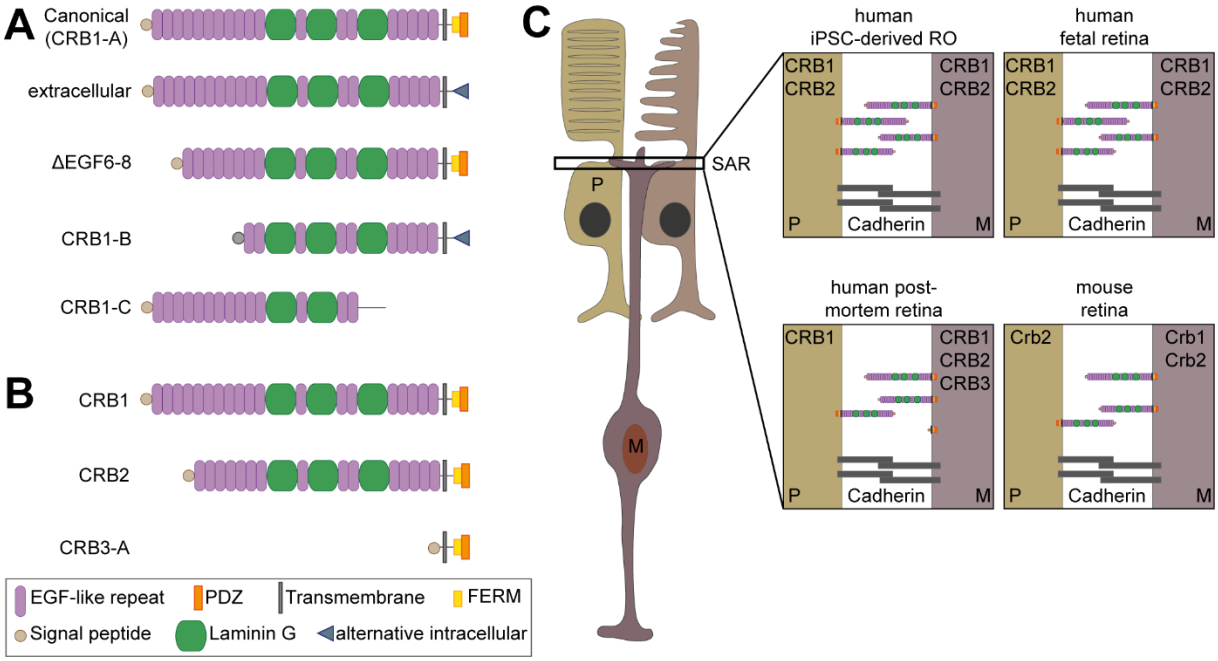

Figure 3| Isoforms and localisation of the Crumbs protein family members in the retina
(A) Graphical representation of the isoforms described for CRB1 in the retina. Initially, the canonical CRB1, the CRB1 extracellular, which lacks the intracellular FERM and PDZ domain, but contains an alternative C-terminal (C-term) part and an isoform that lacks EGF6-8 were described [11, 15, 89]. In 2020, Ray *et al.* identified CRB1-B and CRB1-C as the most abundant retinal isoforms together with CRB1-A [91]. Colours represent predicted protein domains. **(B)** Depiction of the structure of the human CRB protein family members. Colours represent protein domains. **(C)** Localisation of CRB1/Crb1, CRB2/Crb2 and CRB3 in human iPSC-derived RO, human fetal retina, human post-mortem retina and mouse retina above the adherens junctions in the subapical region of the OLM. P=Photoreceptor, M= Müller glia cell, SAR= subapical region. This figure is taken and modified from Quinn *et al.* and Boon *et al.* [16, 20]

connected through a single pass transmembrane domain to 37 amino acid intracellular domain, which contains a protein 4.1, ezrin, radixin, moesin (FERM) domain and a C-terminal (C-term) PSD-95/Dlg-A/ZO-1 (PDZ) binding motif [1, 8, 89, 90].

Besides the canonical isoform, other *CRB1* isoforms have been identified [16]. Initially, a truncated *CRB1* isoform (also known as CRB1 extracellular or potentially secreted) has been validated in the human retina, which contains an alternative exon 11 [89]. The consequence of this alternative exon 11 remains disputed. In one study, this alternative exon 11 was reported to lack the transmembrane and intracellular domain and might be secreted, while others predicted it encodes a transmembrane and a 22 amino acid intracellular domain [11, 15, 89]. Furthermore, an isoform that lacks exon 3 and 4 leading to an in-frame deletion of EGF 6-8 has been validated in the human retina [15]. In 2020, Ray *et al.* described a novel CRB1 isoform termed CRB1-B, as the most dominant isoform in the human retina [91]. This isoform has an alternative 5' promotor resulting in a similar but shorter extracellular domain compared to canonical CRB1 [91]. In contrast, the intracellular domain of CRB1-B is different from the canonical form and similar to the previously identified extracellular isoform [89, 91]. While canonical CRB1 was detected as the second-highest expressed isoform, an isoform termed CRB1-C was identified as the third most abundant form by Ray *et al.* [91]. This CRB1-C isoform lacks parts of the C-terminal extracellular, transmembrane, and intracellular domain of the canonical CRB1 protein [91].

In the human retina CRB1 has been detected in the subapical region above the adherens junctions at the OLM in both photoreceptor cells and Müller glia cells in second-trimester fetal human retina, post-mortem human retina, and human iPSC-derived retinal organoids (RO) [1, 13-15]. Furthermore, while canonical CRB1 was mainly localized in the apical protrusions of Müller glia cells at the OLM, CRB1-B was detected in rod and cone photoreceptors with high expression in the IS and OS [91]. Function and contribution of the different CRB1 isoforms to the development of *CRB1*-linked IRD provide a current burning issue especially for the field of *CRB1* gene editing and therapeutic replacement strategies [185].

1.2.1.2 The two other members of the human Crumbs family: CRB2 and CRB3

In contrast to *Drosophila*, which only has one Crumbs protein, human CRB1 is a member of the CRB protein family along with Crumbs homologue 2 (CRB2) and Crumbs homologue 3 (CRB3) [16] (**Figure 3 B**). Similar to CRB1, CRB2 has an intracellular FERM and PDZ domain and a large extracellular domain, which lacks 4 EGF domains compared to CRB1 [16]. Unlike CRB1, which is almost exclusively expressed in the retina, CRB2 is abundant in multiple epithelial-derived tissues including the brain and the kidney [20]. Given this expression, the 37 patients with bi-allelic *CRB2* mutations, that have been described up to date, display syndromic symptoms covering a range of severe prenatal abnormalities to postnatal isolated renal abnormalities with very few cases of IRD [92, 93]. In the human retina, CRB2, similar to CRB1, localises to the subapical region of photoreceptors and Müller glia cells in human iPSC-derived RO and second-trimester human foetal retina [13-16, 94] (**Figure 3 C**). Additionally, only CRB2

and not CRB1 was shown to be present in human foetal retina during the first trimester [14]. In post-mortem human retina, CRB2 has been detected in the subapical region of Müller glia cells and in the vesicles in the photoreceptor IS but not in the subapical region [15, 95]. Besides in the neuroretina, CRB2 is highly abundant in the RPE [96].

Notably, the cellular localization of CRB1 and CRB2 further varies among species. Illustrating this point, in the mouse retina, Crb2 is located in the subapical region of both Müller glia cells and photoreceptors, while canonical Crb1 is solely present in Müller glia cells [12, 97-99]. Crb1-B was further present in the OS in mice [91]. In zebrafish *(Danio rerio)*, two CRB2 orthologues exist, crb2a (ome) and crb2b, which localise to the subapical region of all photoreceptors and Müller glia cells or the subapical region of cones, respectively [100, 101]. Furthermore, zebrafish crb1 is expressed only in cones and not in rods, and does not localise to the subapical region but the OS [100]. Together these variations emphasise the importance of a human-based research model to understand the molecular mechanism underlying CRB1-linked IRD.

The third member of the human Crumbs protein family is CRB3, for which two main isoforms are described, both lacking the extracellular domain [17, 102] (**Figure 3 B**). Instead, the transmembrane domain is fused to the conserved intracellular domain containing a FERM and a PDZ domain for the CRB3-A isoform or to a FERM and a cysteine-leucine-proline-isoleucine (CLPI) domain for the CRB3-B isoform [17, 102]. Levels of CRB3 are associated with tumourigenesis [103, 104]. In human post-mortem retina, CRB3-A was detected in the subapical region of Müller glia cells and the photoreceptor IS [15, 95] (**Figure 3 C**). However, neither in the human foetal retina nor in iPSC-derived RO, has the localisation of CRB3 been published.

1.2.1.3 The crumbs complex and its function: Insights from different models

The CRB intracellular domain is not only conserved within the human Crumbs protein family but also between species and organises a large protein scaffold [19]. Through the -ERLI motif in the PDZ domain CRB interacts with membrane palmitoylated protein 5 (MPP5), which is also known as protein associated with Lin-7 (PALS1) [19, 99] (**Figure 4**).

In mice, small interfering RNA (siRNA)-mediated downregulation of *Mpp5* in Müller glia cells disturbs Crb1 and Crb2 localisation at the OLM indicating that Mpp5 is important for CRB localisation [97]. Besides the loss of Crb in the subapical region, Mpp5 depletion in conditional KO mice also impair RPE structure and retinal layering [105]. The orthologues of MPP5 are Stardust (Sdt) in *Drosophila* and nagie oko (Nok) in zebrafish [106, 107, 114]. The depletion of Sdt in *Drosophila* causes shortening of the stalk membrane and abnormal rhabdomere formation [108-110]. In zebrafish, loss of the Nok causes abnormal retinal layering without affecting cell type specification [111, 112].

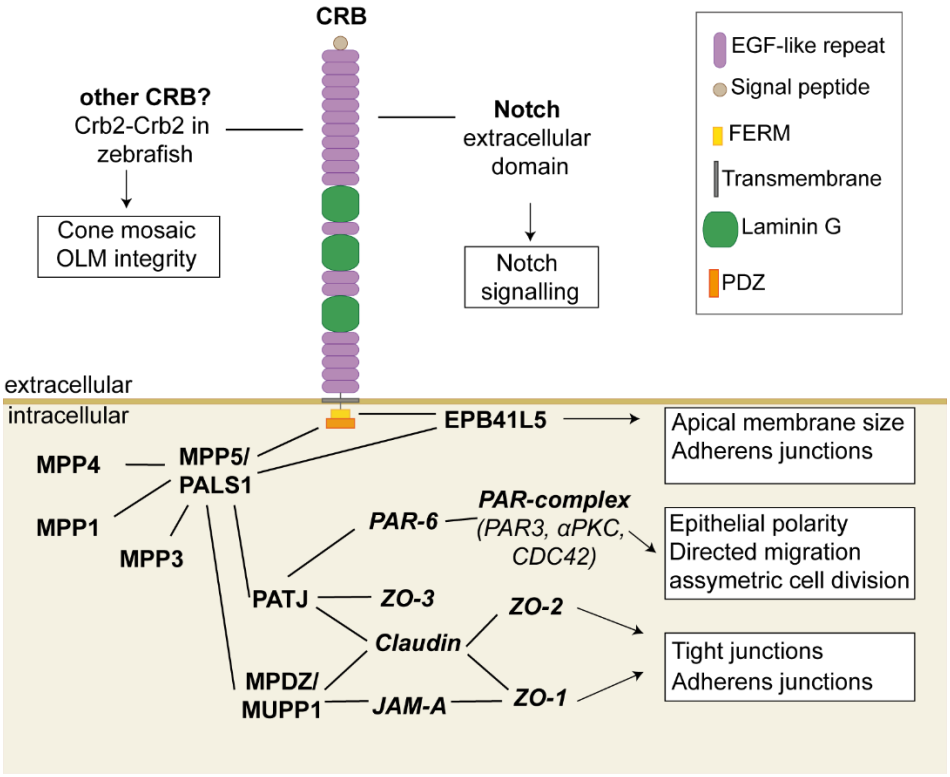

Figure 4| CRB organises a large intracellular protein scaffold through the conserved intracellular domain Illustration of the interactions and functions that have been described for CRB in different species. Bold and italics depict interactions that have been shown in the retina and polarised cells, respectively. Modified after Gosens *et al.* [19].

Besides MPP5, CRB also directly interacts with erythrocyte membrane protein band 4.1 like 5 (EPB41L5) through the GTY motif of the FERM domain [113]. The orthologues of EPB41L5 are Yurt in *Drosophila* and Yurt/Mosaic eyes-like 1 (Ymo1) in zebrafish, respectively [114, 115]. In zebrafish, a direct interaction of Nok and Ymo1 was demonstrated [114, 115]. Loss of Nok and Yurt increases apical membrane size in both zebrafish and *Drosophila*, respectively, hence providing negative feedback to CRB apical membrane formation activity [115-117]. Unlike in zebrafish and *Drosophila*, Crb localises normally in the absence of Epb41l5 in mice and its function in the mammalian retina is poorly investigated [118].

Beyond this core direct interaction of CRB, MPP5 can recruit MPP3, MPP1 and MPP4 to the core crumbs complex [119-121]. Conditional loss of *Mpp3* in mice causes early onset retinal degeneration together with a significant reduction of Mpp5 at the subapical region indicating that Mpp3 is important for Mpp5 localization [122]. In contrast, loss of *Mpp4* in mice does not impair CRB complex localisation and only rarely induces photoreceptor delocalization [123, 124]. Additionally, MPP5 can recruit multiple PDZ domain protein 1 (MUPP1/MPDZ) and protein associated with tight junctions (PATJ) [125, 126]. PATJ also binds to zonula occludens-3 (ZO-3) and claudin [127]. MPDZ interacts through claudin and junctional adhesion molecule -A (JAM-A) with ZO-1 and ZO-2 linking the Crumbs complex to tight and adherens junctions [128]. Furthermore, in *Drosophila* Patj protects against photoreceptor degeneration and is

important for the positioning of adherens junctions in photoreceptors [129, 130]. PATJ additionally binds partitioning defective-6 homologue (PAR-6), which recruits the PAR complex consisting of PAR3, atypical protein kinase C (aPKC) and cell division control 42 (CDC42) [131-136]. Through this interaction, CRB regulates apical-basal polarity and cell adhesion [20, 136].

1.2.1.4 CRB1 mutations are predominantly located in the extracellular domain

In contrast to the various interactions that have been demonstrated for the conserved CRB intracellular domain, binding partners of the extracellular domain are poorly defined [170]. In addition, its functional relevance remains a subject of debate and is most likely context-dependent [170]. On the one hand, overexpression of the intracellular domain, but not the extracellular domain, of Crumbs is able to rescue the cuticle polarity phenotype in *Drosophila* comparably to the full-length Crumbs [137]. Similarly, Crb mutants (MT) that lead to a truncated protein lacking parts of the intracellular domain present a similar apical-basal polarity phenotype as loss of the whole *Crb* locus [90, 138]. Furthermore, the introduction of *Crb3* mRNA improved the apical-basal polarity and the formation of retinal architecture in a *crb2a* (also called ome) MT zebrafish [1, 101].

On the other hand, several lines of evidence indicate that the extracellular domain is not unimportant for CRB1 function, but plays a key role in intercellular adhesion, Notch signalling and membrane localisation [23, 139-141]. For instance, intercellular homo- and heterophilic interaction of the Crb2a and Crb2b extracellular domains is critical for maintaining OLM integrity and the cone mosaic in zebrafish [139, 140]. Further studies in zebrafish have shown that the intracellular domain of Crb2a induces the apical distribution of adherens junction components, however it is only through the interactions of the Crb2a extracellular domain that adherens junctions accumulate to form the OLM [142]. Furthermore, in the *Drosophila* follicle cell epithelium, overexpression of the intracellular domain leads to endocytosis of the endogenous Crb, whereas overexpression of the Crb extracellular domain localises to the apical membrane similarly to endogenous Crb [1, 23, 143]. These data suggest a self-recruitment mechanism of Crb to the apical membrane involving homophilic interaction of the extracellular domain in *cis* or *trans* [23, 143, 144, 170]. Furthermore, the Crb extracellular domain bound to the membrane was important for rhabdomere elongation and the length of the stalk, which is the homologue of the IS [116, 145]. In addition, Das *et al.* generated a fosmid based expression of the entire *Crb* locus expressing either the membrane bound extracellular or intracellular domain in a *Crb* MT *Drosophila* background [146]. Their results revealed that the intracellular domain is sufficient to restore apical-basal polarity, whereas the extracellular domain is required to fully rescue the morphogenesis of the neurogenic ectoderm and ventral epidermis as it ensures apical localisation of Crb and Notch and junction stabilisation [146].

Further studies have shown that the extracellular domain of Crb directly interacts with the extracellular domain of Notch in *Drosophila*, zebrafish, and human iPSC-derived RO, preventing Notch endocytosis, and regulating Notch through the γ-secretase complex activity [141, 147, 148]. Consequently, reduction of CRB leads to impaired Notch receptor localisation in iPSC-derived RO and *Drosophila* [141, 147, 149].

Finally, up to date more than 450 pathogenic variants have been identified in *CRB1* [155]. While the majority comprises missense or nonsense single nucleotide variants (SNV) with approximately 73 %, splice variants (6 %) and insertion/deletion (21 %) have also been reported [155]. The common variant is the p.C948Y in EGF14, which is responsible for almost a quarter of the *CRB1*-linked IRD [8]. Interestingly, the majority of pathogenic *CRB1* variants are located in the large extracellular domain, possibly also due to its size [8] (**Figure 5**).

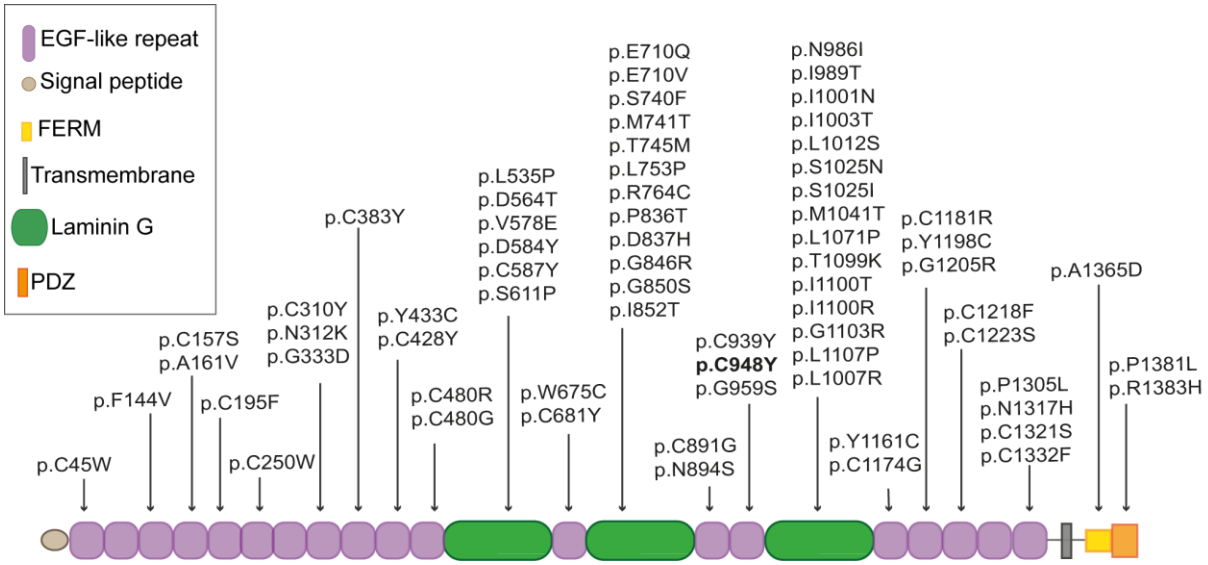

Figure 5| The majority of CRB1 patient mutations are located in the larger extracellular domain
Illustration of missense mutations identified in patients together with their position in the canonical CRB1 isoform. The most frequent mutation C948Y is depicted in bold. Colours represent predicted protein domains. Based on Bujakowska *et al.* [8]

Overall, these data emphasise the importance of further investigating the role of the extracellular domain and identifying binding partners, which may contribute to a better understanding of the disease mechanisms underlying CRB1-linked IRD.

1.2.2 CRB1-associated retinal degenerations are clinically heterogeneous

Besides the elusive role of the extracellular domain, CRB1-linked IRD are characterised by an enormous clinical heterogeneity, which hampers the development and evaluation of the efficacy of treatment strategies [21]. Numerous attempts have been made to identify genotype-phenotype correlations for CRB1 patients [7, 8, 12, 16, 150-153, 155]. Overall, *CRB1* null mutations, leading to a premature stop codon, are more common in patients with the more severe LCA diagnosis compared to those with an RP diagnosis [8]. Furthermore, the *CRB1*

c.498_506del variant is associated with macular dystrophy, indicating that this in-frame deletion is associated with a milder, mostly late-onset and macular-restricted phenotype without peripheral vision loss or night blindness [151, 154]. Moreover, Mairot *et al.* showed that mutations affecting only affect the canonical CRB1 isoform but not CRB1-B can also cause severe early-onset IRD, indicating that the affected CRB1 isoform may not correlate with the disease severity [155]. In addition, different phenotypes concerning the protein abundance, localisation and retinal degeneration have been reported following the introduction of various missense mutations in *Crb* in *Drosophila* suggesting potential mutation-specific effects [156].

Nonetheless, given that substantial variation in the disease onset and severity even among patients with the same *CRB1* mutation, the presence of additional modifiers is assumable. In humans, only aryl hydrocarbon receptor interacting protein like 1 (*AIPL1)*, a photoreceptor co-chaperone involved in the assembly of PDE6, has been identified as a potential modifier in a patient with a causal homozygous *CRB1* mutation [157, 158]. In the *Crb1* rd8 mouse model, multiple genes have been shown to modulate the retinal phenotype. The *Crb1* rd8 mouse model is one of the twelve mouse models that have been generated and has a naturally occurring single base deletion in exon 9 that results in a truncated Crb1 protein [20]. It shows disruption of the OLM, retinal folds and photoreceptor displacement leading to degeneration mainly in the inferior part of the retina [159]. Mutations in Janus kinase 3 (*Jak3*), depletion of cytoglobin (*Cygb*) or depletion of CX3C motif chemokine receptor 1 (*Cx3cr1*), alone did not cause any retinal phenotype or early onset retinal degeneration, each of which amplifies the retinal phenotype when combined with the *Crb1* rd8 mutation [160-162]. Furthermore, heterozygous loss of methylene tetrahydrofolate reductase (*Mthfr*), Rho guanine nucleotide exchange factor (*Arhgef)12* and protein kinase Cı (*Pkcl*) has been shown to accelerate the onset and the severity observed of retinal degeneration in the *Crb1* rd8 mouse model [163, 164]. In addition, the *Crb1* rd8 mutation enhances the age-related macular degeneration and choroidal neovascularisation phenotype in the nuclear factor E2-related factor 2 (*Nrf2*) KO mouse model [165].

Interestingly, multiple lines of evidence suggest CRB2 as a potential modulator in CRB1-linked IRD [15, 24, 166]. In mice, loss of both *Crb2* and *Crb1* causes a more severe retinal phenotype than single loss [15, 24, 166]. Furthermore, supplementation of CRB2/Crb2 can improve histological and transcriptional phenotypes observed in *CRB1* patient iPSC-derived RO, *CRB1* KO RO and a *Crb1* MT mouse model [94, 95, 167, 168]. However, as the identified modifiers are not associated to a common pathway, the identification of additional modifiers is required [164].

1.2.3 Siblings with identical homozygous CRB1 C948Y mutation but with different severity of symptoms

The presence of potential modifiers is particularly evident in relatives, where the same *CRB1* mutation is associated with a different manifestation of the disease [22]. Given the common genetic background of close relatives, studies involving siblings are promising to identify potential genetic modulators. Previously, Dr. Achberger (group of Prof. Liebau, University of Tuebingen) generated and characterised iPSC-derived RO from two early onset RP patients carrying the same homozygous c.2843G>A;C948Y mutation in *CRB1* [22]. Interestingly, these patients were siblings, but with a different severity of disease [22]. While one of the siblings (referred to as patient A) was blind and thus displayed a severe phenotype, the other sibling (referred to as patient B) was less affected and showed symptoms of advanced RP with residual vision [22]. IPSC-derived RO of these two patients displayed no difference in the morphology, number of retinal progenitor cells, proliferation, abundance of neuronal cell types, synapse, photoreceptor cell formation compared to control iPSC-derived RO [22]. However, RO from both patients showed decreased levels of apoptotic cells in the photoreceptor layer, decreased levels of Müller glia marker, increased levels of Cdc42 and altered mRNA gene expression of *Notch*, *mTOR* and *WNT* genes compared to control RO [22]. Furthermore, Dr. Achberger and colleagues used Ca^{2+} imaging to assess the light sensitivity of control and patient RO [22]. Control RO showed an increase in Ca^{2+} spiking cells upon light stimulation [22]. In contrast, the RO of the more affected patient A showed a high number of Ca^{2+} spiking cells independent of light [22]. The RO of the less affected patient B exhibited an increase in the number of Ca^{2+} spiking cells upon light stimulation, but to a lesser extent compared to the control [22]. As these dissimilarities reflect to some extent the difference in the phenotype seen between the patients, iPSC-derived RO provide a promising tool for further investigation of disease modifiers and disease mechanisms [22].

2. Aim of the study

Bi-allelic mutations in *CRB1* are a major cause of IRD, including RP and the more severe form LCA [8, 169]. *CRB1* encodes a single-type transmembrane protein with a large extracellular domain fused to a short intracellular domain [11, 12, 89]. Studies in various animal models have demonstrated that Crumbs proteins organise a large intracellular protein network that is required to regulate apical membrane size and cell polarity [19]. Despite the strong conservation of the intracellular domain, species-specific differences in the number of Crumbs orthologues and their cellular localisation have been described emphasising the requirement for human-based models [14, 15, 20, 95]. In addition, the functions and protein-protein interactions (PPI) of the large extracellular domain, where the majority of patient mutations are located, are insufficiently investigated [170]. Furthermore, potential modulators of the disease severity in patients with causal *CRB1* mutations are poorly described [157, 163, 164]. This high genetic and phenotypic heterogeneity provides is a major barrier to disease stratification and the definition of robust endpoints in clinical evaluation [21]. Consequently, no treatment is currently available to preserve vision in these patients [20, 185].

The overall aim of this project was to investigate the molecular mechanisms and potential modulating factors underlying *CRB1*-linked IRD. To achieve this goal, two siblings (patient A and patient B) carrying the same homozygous *CRB1* c.2843G>A;p.C948Y mutation, but with a substantial difference in the disease severity, were investigated in a proof-of-concept study. Previously, Dr. Achberger (Group of Prof. Liebau, University of Tuebingen) and colleagues generated iPSC-derived retinal organoids (RO) from both patients and controls and described different responses to light using Ca^{2+} imaging [22]. As siblings, the two patients share most of their genetic background and are highly valuable for identifying potential modifiers. For this project, modifiers were defined as harmful or protective genetic variants that could potentially accelerate the disease severity in patient A or reduce the progression of blindness in patient B, respectively.

The first objective was to investigate the protein abundance and localisation of CRB1 in the iPSC-derived RO. For this purpose, western blot and immunofluorescence microscopy were performed using in iPSC-derived RO and controls. This provided new insights into whether the protein level of CRB1 could correlate with the disease severity.

The second aim targeted towards the identification of the retinal PPI network of CRB1 using a porcine retinal pull-down approach combined with mass spectrometry. For this the canonical as well as the extracellular CRB1 isoform were used to determine the retinal PPI network of CRB1 wildtype (WT) together with novel candidate interactors of the extracellular domain. In a next step, the consequences of the C948Y mutation on the retinal CRB1 WT interactome were investigated. Finally, the localisation of interesting candidate interactors of

CRB1 and CRB1 was verified by immunofluorescence microscopy in iPSC-derived RO. Taken together, these data not only offered novel insights into the molecular functions of CRB1, but also provided candidate modifiers, as each of the CRB1 interactors may influence the disease phenotype.

The third objective was to investigate the cellular consequences of the CRB1 C948Y mutation based on the identified CRB1 interactors using patient and control iPSC-derived RO. For this purpose, immunofluorescence microscopy was executed to assess the localisation and expression of the interactors in patient and control iPSC-derived RO. Furthermore, proteomic analysis of patient and control iPSC-derived RO lysates was performed using mass spectrometry combined with data-independent acquisition (DIA) to identify biological processes and pathways that are significantly up- or downregulated in both patient iPSC-derived RO compared to control. Together with the CRB1 interactome, these data contributed to get access to the molecular mechanism underlying CRB1-linked IRD.

The fourth aim was to identify potential harmful and protective modifiers, that enhance the clinical phenotype in patient A or protecting patient B from progressive vision loss, respectively. For this purpose, full proteomic analysis of patient iPSC-derived RO was performed using mass spectrometry and DIA to identify differentially abundant pathways and processes between patient A and patient B iPSC-derived RO. Furthermore, whole genome sequencing (WGS) was performed to identify different genetic variants between the two brothers. Together, with the proteomic and interatomic data, candidate protective and harmful modulators were defined. Overall, these data provided valuable insights into the differences and potential candidates underlying the variable severity of symptoms in the two brothers, serving as a pilot proof-of concept study.

The final objective was to investigate the identified modulating candidate(s) regarding their interplay to CRB1. Therefore, the retinal PPI network of the modifying candidate(s) was investigated using affinity proteomics and co-immunoprecipitation (co-IP). Furthermore, a porcine retinal explants system was established to allow future large-scale screening for potential modifying candidates in CRB1-linked IRD. Overall, these data contributed to elucidate the role of the potential modifying candidates in the context of CRB1-linked IRD.

3. Material and Methods

3.1 Material

3.1.1 Consumables

96 Well Lightcycler® Plate	Sarstedt
Adhesive qPCR Seal	Sarstedt
Biopsy punch 6,0 mm	PFM Medical
Cell Chip™	Tecan Group
Cell Scraper	Sarstedt
Colour coded insert, mixed	Sarstedt
Cryo Tubes 1.8 mL	NUNC, Sarstedt
Cultube sterile culture tubes	Simport
Disposal Bags	Carl Roth
Eppendorf CombiTips	Eppendorf
Falcon 15ml Polypropylene Round-Bottom Tube	Corning
Feather Disposable Scalpel	Socorex
Filter tips 10, 20, 100, 200, 1000	Biozym, Nerbe Plus
Gel Loading Tips 0.5-200 µl,	VWR
Gilson TowerPack D10, D200, D1000 tips	Gilson
Gloves Nitrile XS, S	ABENA
Hybond-P Polyvinylidene difluoride (PVDF) Transfer membrane	GE Healthcare
Microscope slides 26 x76 mm	R. Langenbrinck GmbH
Multiply® -µStrip 8-strip	Sarstedt
Multiply®-Pro cup 0.2 ml	Sarstedt
Parafilm®	Bemis Company
Pasteur Capillary Pipettes 230 mm	VWR
Peha-soft® nitrile Guard XS	Paul Hartmann
Petridish 90 x 14.2 mm	VWR
Pipette tips 1-10/1-200/101-1000 µl	Sarstedt
PP Insert with bottom spring 0.20 mL	Sigma Aldrich
PP Reaction Tube 15 mL	Sarstedt
PP Reaction Tubes 50 mL	Sarstedt
Receiver Columns 35 µm	Macherey-Nagel
Safe-Lock Tubes 0.5 mL, 1.5 mL, 2 mL	Eppendorf
Serological pipet 2 mL, 5 mL, 10 mL, 25 mL, 50 mL	Corning, Sarstedt
Stop-and-go extraction (Stage) Tips C-18	Thermo Fisher Scientific
Super PAP Pen Liquid Blocker	Science Services
TC-Inserts 6-Well PET 0.4 µM, TP	Sarstedt
Tissue Culture Plates with 6 wells	VWR, Sarstedt, Nunc
Tissue dishes 10 cm, 14 cm	Thermo Fisher Scientific
Whatman® paper 3MM	Carl Roth

3.1.2 Chemicals and reagents

1,4-Dithiothreitol (DTT)	Merck
2-Iodacetamide (IAA)	Merck
Acetonitrile (ACN; Chromasolve®)	Sigma-Aldrich
Acrylamide/Bis Solution 37.5:1 (30% w/v, 2.6% C)	Serva
Agar-Agar	Carl-Roth
Agarose	Lonza
Ammonium bicarbonate (ABC)	Sigma-Aldrich
Ammonium Persulfate (APS)	Sigma Aldrich
Ampicillin sodium salt	Carl-Roth
Anti-FLAG® M2 Agarose Beads	Sigma-Aldrich
B-27™ Supplement (50X), serum free	Thermo Fisher Scientific

Bovine Serum Albumin	Carl Roth
Bromophenol Blue	Sigma Aldrich
Chloramphenicol	Carl-Roth
Chloroform	Merck
Deoxynucleotide triphosphate (dNTP) Solution (10 mM)	New England Biolabs
Diamidino-Phenylindole (DAPI)	Sigma Aldrich
Dimethylsulfoxide (DMSO) 100 %	Carl Roth
DNA Loading Dye (6x)	Thermo Fisher Scientific
dNTP Mix (10 mM)	Thermo Fisher Scientific
dNTPS 10 mM (RT-qPCR)	Promega
Dream Taq Green Buffer (10x)	Thermo Fisher Scientific
Dulbecco's Modified Eagle Medium (DMEM) high glucose	Sigma Aldrich, Carl Roth
Dulbecco's Phosphate Buffered Saline without CaCl2 and MgCl2	Thermo Fisher Scientific
Ethidium Bromide	AppliChem
Ethanol	VWR
Fetal Bovine Serum (FBS)	Sigma Aldrich
Fetal Bovine Serum Superior	Sigma Aldrich
FLAG-Peptide	Sigma Aldrich
Fluoromount-G®	SouthernBiotech
Gene Ruler 1 kb Plus	Thermo Fisher Scientific
Glacial Acetic Acid (HAc), p.a.	Merck
GlutaMAX™-I (100x)	Gibco
Glycerol	Carl Roth
Glycine	Carl Roth
HPLC H_2O	VWR
Hydrochloric Acid (HCL) 32%	Merck
Isopropanol	Honeywell
Kanamycin Sulfate	Carl-Roth
Methanol	Honeywell
Milk powder, dry, non-fat	Carl Roth
Millipore H_2O	Merck Millipore
M-MLV Reverse Transcriptase 5x Buffer	Promega
N2 supplement (100X)	Thermo Fisher Scientific
N,N,N',N'-tetramethylethylene-diamine (TEMED)	Merck
Neurobasal medium (1x)	Gibco
Nonidet P40 (NP40)	Roche Holding
Normal Goat Serum	Merck
Nuclease free H_2O	Promega, IDT DNA
PageRuler™ Prestained Protein Ladder (170 kDa)	Thermo Fisher Scientific
Penicillin/Streptomycin (P/S)	Thermo Fisher Scientific
PeqGold TriFast	PeQLab
Phosphatase Inhibitor Cocktail 2 (PI2)	Sigma-Aldrich
Phosphatase Inhibitor Cocktail 3 (PI3)	Sigma-Aldrich
Phusion GC Buffer (5x)	Thermo Fisher Scientific
Phusion HF Buffer (5x)	Thermo Fisher Scientific
Polyethylenimine (PEI)	PolySciences
ProSieve QuadColor Protein Marker	Biozym
Protease Inhibitor Complex Complete (PIC)	Roche
Random Primers	Promega
RapiGest™ SF Surfactant	Waters Corporation
Super optimal broth with glucose Medium	Invitrogen
Sodium Chloride (NaCl)	Merck
Sodium dodecylsulfate (SDS) (dust-free pellets >98%)	Sigma Aldrich
Sso Advanced Universal SYBR® Green Supermix	Bio-Rad
Trifluoracetic Acid (TFA, 100 %)	Fluka
Tris(hydroxymethyl) Aminomethane (TRIZMA)	Sigma Aldrich

Tris ultrapure	Sigma Aldrich
Triton® X-100	Sigma Aldrich
Tryptone/Peptone from Casein	Carl Roth
Tween®20	Sigma Aldrich
Yeast Extract	Carl Roth
β-Mercaptoethanol	Sigma Aldrich

3.1.3 Buffer and solutions

3.1.3.1 Bacteria culture

Lysogeny broth (LB) medium	1 % (w/v) Tryptone/ Petone from Casein 170 mM NaCl 0.5 % (w/v) Yeast-Extract In deionised H_2O, pH 7
LB-Agar	LB medium 1.5 % Agar-Agar
Antibiotics for LB-medium and LB-agar	100 µg/mL Ampicillin 100 µg/mL Chloramphenicol 50 µg/mL Kanamycin

3.1.3.2 Cell culture and retinal explant culture

Growth media (mammalian cell)	Dulbecco's Modified Eagle Medium 10 % FBS 0.5 % Penicillin/ Streptomycin
Starvation media (mammalian cell)	Dulbecco's Modified Eagle Medium
Cryo-media	FBS 10 % DMSO
PEI transfection	1 mg/ml Polyethylenimine in NaCl solution pH 7.8
NaCl solution	150 mM NaCl In deionised H_2O pH 5.5 with HCl
Neurobasal complete media (explants)	Neurobasal media 2 % B-27™ Supplement 1 % N2 supplement 1 % Penicillin/ Streptomycin 0.4 % GlutaMAX™-I

3.1.3.3 Western blot analysis

Laemmli buffer (5 x)	250 mM Tris-HCL, pH 6.8 50 % Glycerol 5 % SDS 0.05 % (w/v) bromophenol blue dye 500 mM β-Mercaptoethanol In deionised H_2O

Running buffer (10 x)	250 mM Tris 2 M Glycine 1 % (w/v) SDS In deionised H_2O
Running buffer (1 x)	10 % 10x Running buffer In deionised H_2O
Transfer buffer (10 x)	1.92 M Glycine 250 mM Tris In deionised H_2O
Transfer buffer (1 x)	10 % 10x Transfer buffer 20 % Methanol In deionised H_2O
Blocking solution	5 % milk or BSA In Tris-buffered saline Tween (TBST)
TBST	30 mM Tris (Trizma base) 0.15 M NaCl 0.1 % Tween In deionised H_2O pH 7.4

3.1.3.4 Proteomics

Lysis buffer	0.5 % Nonident P40 1 % PI2 1 % PI3 2 % PIC In 1x (Tris-buffered saline)
Washing buffer	0.1 % Nonident P40 1 % PI2 1 % PI3 In 1x TBS
TBS (10 x)	300 mM Tris ultrapure 1.5 mM NaCl In deionised H_2O pH 7.4
TBS (1 x)	10 % 10x TBS In deionised H_2O
SDS solution 0.01 %	0.01 % SDS In 1x TBS
FLAG-peptide	5 mg/mL in TBS
Tris buffer	1 M Tris In deionised H_2O pH 8

Glycine buffer	200 mM Glycine In deionised H_2O pH 2.5
Trypsin solution	0.5 µg/µL Trypsin NB Sequencing Grade In 50 mM HAc
IAA solution	300 mM IAA In HPLC H_2O
Dithiothreitol (DTT) solution	100 mM 1,4-Dithiothreitol In HPLC H_2O
RapiGest™	1 vial RapiGest™ SF Surfactant 50 µL HPLC H_2O
ABC solution	50 mM ABC Solution In HPLC H_2O
80 % ACN/5 % TFA solution	5 % TFA In 80 % ACN solution
50 % ACN/5 % TFA solution	5 % TFA In 50 % ACN solution
H_2O/5 % TFA solution	5 % TFA In HPLC H_2O

3.1.4 Kits

Bio-Rad Protein Assay Kit	Bio-Rad, USA
Pierce™ ECL Plus Western Blotting Substrate	Thermo Fisher Scientific
Pierce™ ECL Western Blotting Substrate	Thermo Fisher Scientific
EZ-PCR™ Mycoplasma Detection Kit	Sartorius
Monarch® Plasmid Miniprep Kit	New England Biolabs
PureYield™ Plasmid Midiprep Kit	Promega
PeqGold Cycle -Pure Kit	VWR
QIAquick® PCR Purification Kit	Carl Roth
XPMag Explant Transfection Reagent Kit	OZBiosciences
GeneJet Gel Extraction Kit	Thermo Fisher Scientific
Gateway® BP ClonaseTM II Enzyme Mix Kit	Thermo Fisher Scientific
Gateway® LR ClonaseTM II Enzyme Mix Kit	Thermo Fisher Scientific
CloneJET PCR cloning Kit	Thermo Fisher Scientific

3.1.5 Enzymes

DpnI Restriction enzyme	New England Biolabs
Dream Taq DNA Polymerase 5 U/µl	Thermo Fisher Scientific
M-MLV polymerase	Promega
Phusion High Fidelity polymerase	Thermo Fisher Scientific
Trypsin NB sequencing grade, modified from porcine pancreas	Serva Electrophoresis
DNAseI recombinant, RNAse free	Roche Diagnostics
Trypsin-EDTA (0.05 %)	Thermo Fisher Scientific

3.1.6 Bacteria

E. coli - Library Efficiency® DH5α Competent Cells	Invitrogen
E. coli - NEB® Stable Competent	New England Biolabs
E. coli - One Shot® ccdB Survival™ ® Competent Cells	Invitrogen

3.1.7 Human cell lines

ARPE19 (CRL-2302)	American Type Culture Collection
Human embryonic kidney (HEK)293T (CRL-3216)	American Type Culture Collection
hTERT-RPE1 (CRL-4000)	American Type Culture Collection
HELA	Gift from C.Piccoli, International Agency for Research on Cancer, Lyon, France
SH-SY5Y (CRL-2266)	American Type Culture Collection

3.1.8 Primer

All primers were purchased from Integrated DNA Technologies (IDT) and dissolved in nuclease-free H_2O.

3.1.8.1 Gateway cloning

Table 1| Primers used for Gateway Cloning

Target		Primer sequence 5'-3'
CRB1 canonical (C-term tag) NM_202153	Forward	**AAAAAGCAGGCTTCACC**ATGGCACTTAAGAACATTAACTAC
CRB1 canonical (C-term tag) NM_202153	Reverse	**AGAAAGCTGGGTG**AATCAGTCTCTCCATTGCA
CRB1 canonical (N-term tag) NM_202153	Forward	**AAAAAGCAGGCTTC**GCACTTAAGAACATTAACTACCTT
CRB1 canonical (N-term tag) NM_202153	Reverse	**AGAAAGCTGGGTG**CTAAATCAGTCTCTCCATTGCA
CRB2 (C-term tag) NM_173689	Forward	**AAAAAGCAGGCTTCACC**ATGGCGCTGGCCAGGCCT
CRB2 (C-term tag) NM_173689	Reverse	**AGAAAGCTGGGTG**GATGAGTCTCTCCTCCGGTGGC
CRB3 (C-term tag) NM_139161.5	Forward	**AAAAAGCAGGCTTCACC**ATGGCGAACCCCGGGCTG
CRB3 (C-terml tag) NM_139161.5	Reverse	**AGAAAGCTGGGTG**GATGAGCCGCTCTTCCGGCG
CRB1Δextra (N-term tag)	Forward	**AAAAAGCAGGCTTCACC**ATTGGCTCAGTGACTGTC
CRB1Δextra (N-term tag)	Reverse	**GGGGACCACTTTGTACAAGAAAGCTGGGTG**CTAAATCAGTCTCTCCATTGCA
CRB1ΔEGF1-14 (N-term tag)	Forward	**GGGGACAAGTTTGTACAAAAAAGCAGGCTTC**CAGTTAAATGTCTGCAACTCC
CRB1ΔEGF1-14 (N-term tag)	Reverse	**GGGGACCACTTTGTACAAGAAAGCTGGGTG**CTAAATCAGTCTCTCCATTGCA

CRB1ΔEGF1-11 (N-term tag)	Forward	**GGGGACAAGTTTGTACAAAAAAGCAGGCTTC**GCAACCACACTTTCATTTGA
CRB1ΔEGF1-11 (N-term tag)	Reverse	**GGGGACCACTTTGTACAAGAAAGCTGGGTG**CTAAATCAGTCTCTCCATTGCA
GFP (C-term tag)	Forward	**AAAAAGCAGGCTTCACC**ATGGTGAGCAAGGGCGAGGAG
GFP (C-term tag)	Reverse	**AAGAAAGCTGGGTGCTT**GTACAGCTCGTCCATGC
CRB1-extracellular ENST00000638467.1 (C-term tag)	Forward	**AAAAAGCAGGCTTCACC**ATGGCACTTAAGAACATTAACTAC
CRB1-extracellular ENST00000638467.1 (C-term tag)	Reverse	**AAGAAAGCTGGGTG**ATAATCTTCCTGTTCA
Adapter attB1	Forward	GGGGACAAGTTTGTACAAAAAAGCAGGCT
Adapter attB2	Reverse	GGGGACCACTTTGTACAAGAAAGCTGGGT

3.1.8.2 Site-directed mutagenesis (SDM)

Table 2| Primers used for site-directed mutagenesis

Target		Primer sequence 5'-3'
CRB1 p.C948Y	Forward	GGATTTGAATATATTGCAAATGCTG
CRB1 p.C948Y	Reverse	TGCAATATATTCAAATCCTTGAAGC
CRB1 p.C480R	Forward	GTCCCTGTATGAAATCGCAACCACA
CRB1 p.C480R	Reverse	GCGATTTCATACAGGGACCCGGTGT
CRB1 p.C681Y	Forward	GCCAACCTTATCAAAGCAGAGGAC
CRB1 p.C681Y	Reverse	TGCTTTGATAAGGTTGGCTTTCACA
CRB1 p.G1103R	Forward	TAGAAATCAGAGGCATTTATCTCTC
CRB1 p.G1103R	Reverse	AAATGCCTCTGATTTCTATTGTACT
CRB1 p.Y1161C	Forward	TATAGCTCTTGTCATTGCTCCTGT
CRB1 p.Y1161C	Reverse	GCAATGACAAGAGCTATAGATGTC
CRB1 p.C1174G	Forward	GGGAAACACGGTGAACTCAACATCG
CRB1 p.C1174G	Reverse	GAGTTCACCGTGTTTCCCTGACCAT
CRB1 p.C1181R	Forward	TCGATGAACGCTTTTCAAACCCCT
CRB1 p.C1181R	Reverse	TTGAAAAGCGTTCATCGATGTTGA
CRB1 p.N1317H	Forward	GACTTACTCCACAAATTCCAGTGC
CRB1 p.N1317H	Reverse	GAATTTGTGGAGTAAGTCCTGGCA
CRB1 p.C1321S	Forward	ATTCCAGTACCTCTGTGATGTTGCC
CRB1 p.C1321S	Reverse	TCACAGAGGTACTGGAATTTGTTGA
CRB1 ΔEGF15	Forward	GCTGTTTGCTCAACATCGATGAATG
CRB1 ΔEGF15	Reverse	ATGTTGAGCAAACAGCCAGTGACCA
CRB1 ΔEGF17	Forward	GTGAAGTGCAGAGCAGATTACCCTC
CRB1 ΔEGF17	Reverse	TCTGCTCTGCACTTCACAGTTCACAC
CRB1 ΔEGF18	Forward	GCAGATTAAAGGACATTGATGAGTG
CRB1 ΔEGF18	Reverse	ATGTCCTTTAATCTGCTCTGTCTGC
CRB1 ΔEGF19	Forward	GTGAAAAGGTGGACTTGGCAGATGA
CRB1 ΔEGF19	Reverse	AAGTCCACCTTTTCACACCATTCTC

3.1.8.3 RT-qPCR primer

Table 3| Primers used for RT-qPCR

Target		Primer sequence 5'-3'
Porcine *CRB1* exon 6/7	Forward	GGATTTGAATATATTGCAAATGCTG
Porcine *CRB1* exon 6/7	Reverse	ATATCCCAGGGCGTCATCTT
Porcine *CRB1* exon 9/10	Forward	CAGTGACGACAAGGGCTATT
Porcine *CRB1* exon 9/10	Reverse	TTTCTCTTTCCCGCAGACG
Porcine *GAPDH*	Forward	CCAGAACATCATCCCTGCTT
Porcine *GAPDH*	Reverse	GTCCTCAGTGTAGCCCAGGA
Porcine *HPRT*	Forward	GGACTTGAATCATGTTTGTG [171]
Porcine *HPRT*	Reverse	CAGATGTTTCCAAACTCAAC [171]
Human *CRB1* exon 2/5	Forward	TCTGTCCCCACAATTATTCTGGATA [15]
Human *CRB1* exon 2/5	Reverse	TCTCTGAGGACAGCTCCACACAT [15]
Human *CRB1* exon 4/5	Forward	GCCTCTTTGTTGGTCAAAACCTT [15]
Human *CRB1* exon 4/5	Reverse	GTGTATCCAGGCCAGCAGTGA [15]
Human *CRB1* exon 11/12	Forward	CCTCTGTGATGTTGCCTTTGC [15]
Human *CRB1* exon 11/12	Reverse	GTGGTGAAAATGTCGGAGATCAA [15]
Human *CRB2* exon 8/9	Forward	CAGGACCTGCGACTCGAT [15]
Human *CRB2* exon 8/9	Reverse	ACCATTGAAACAGGGGTCAG [15]
Human *CRB2* exon 12/13	Forward	TCTGCAATGCCAGATTCTCCGG [15]
Human *CRB2* exon 12/13	Reverse	CGGTGGCACCTTGAGGACACTGTC [15]
Human *CRB3* exon 4/5	Forward	GACCACTTCTGCAAATGAGAATAGC [15]
Human *CRB3* exon 4/5	Reverse	AGAAGACCACGATGATAGCAGTGAT [15]
Human *GAPDH*	Forward	GCAAATTCCATGGCACCGT
Human *GAPDH*	Reverse	GCCCCACTTGATTTTGGAGG

3.1.8.4 Sequencing

Table 4| Primers used for sequencing

Target	Primer sequence 5'-3'
*CRB1*_206-229	TGGAGAAGCAAGGGTCTTTCATGT
*CRB1*_1-24	ATGGCACTTAAGAACATTAACTAC
*CRB1*_396-417	TGTCTGCATCTGCCCTGCTGGA
*CRB1*_898-921	ACCTTGATGCCTCTTTGTTGGTCA
*CRB1*_1427-1448	CCGGGTCCCTGTGTGAAATCGC
*CRB1*_1898-1919	TGCCATCCACACCTTCGTTTGT
*CRB1*_2415-2446	TGAACTGTATCAGTCTTCACAAAACC
*CRB1*_3135-3156	GTCCCAGACCTCCAGGTGGCAA
*CRB1*_3667-3688	TGTGCAAATGGAGCCACCTGCA
*CRB1*_4162-4182	GGGCTCCCGAGTGGAAATGTGG
*CRB2*_93-112	GCTCTGAAGGCACCGTCCCA
*CRB2*_1-20	ATGGCGCTGGCCAGGCCTGG
*CRB2*_244-265	TGTGTGCCCCAGGGTCCAGATC
*CRB2*_774-795	CGAGGTGGACGAGGACGAGTGT
*CRB2*_1262-1283	GTTACGTCTGCCACTGCCCACC
*CRB2*_1761-1782	CCACCTCCTGCTGCCTGAGGAT
*CRB2*_2187-2208	GATGCTCAGCTTCGGGCCTGAC
*CRB2*_3275-3296	AAGCCCACGTCGACCCCTGTCA
*CRB2*_2920-2939	CTGCTGTGGCTGGATGGTGC
*CRB3*_1-18	ATGGCGAACCCCGGGCTG
*CRB3*_353-372	CTAGATGGGCAGGCAGCCCT
*CRB3*_239-258	TGCGGAAGCTTCGGGAGAAG

*CRB3*_239-259	CTTCTCCCGAAGCTTCCGCA
CMV promotor forward	CGCAAATGGGCGGTAGGCGTG
pcDNA reverse	GGCAACTAGAAGGCACAGTC

3.1.8.5 Other (*CRB1* Splicing, *GUCA1B* variant)

Table 5| Primers used for *CRB1* splicing analysis and *GUCA1B* amplification

Target		Primer sequence 5'-3'
CRB1 exon 8	Forward	GCCAGCCGGTGCTTCAAGGATT
CRB1 exon 9	Reverse	GGTCACTTCGTGCCATGTGCCA
CRB1 exon 8	Forward	TTCAGTGGTGTGGATTCAGC
CRB1 exon 10	Reverse	GCAGTTGCCTCCATTGTAGC
GAPDH	Forward	GCAAATTCCATGGCACCGT
GAPDH	Reverse	GCCCCACTTGATTTTGGAGG
GUCA1B	Forward	GTGGGGAGAGAGCTGGCTTGGA
GUCA1B	Reverse	ACCCTCACCCCTCAGTTGGCTC

3.1.8.6 *CRB1* siRNA duplex oligonucleotide sequence

All DsiRNA were purchased from IDT and dissolved in nuclease-free H_2O.

Table 6| Overview of sequences of siRNAs

Target		Sequence 5'-3'
*CRB1*_1	Sense	CAGUGGCAUUCAUCUCUCUUACUTT
*CRB1*_1	Antisense	AAAGUAAGAGAGAUGAAUGCCACUGAU
*CRB1*_2	Sense	CAAGAAUUUUUCAAAAGACAACAGT
*CRB1*_2	Antisense	ACUGUUGUCUUUUGAAAAAUUCUUGCA
*CRB1*_3	Sense	AUGUGAGGAUGGUACUGACAAUUAC
*CRB1*_3	Antisense	GUAAUUGUCAGUACCAUCCUCACAUGU
Negative control DsiRNA		IDT Catalogue number 51-01-14-03

3.1.9 Commercially available primary antibodies and dyes

Table 7| Overview of primary antibody and fluorescent dyes

Antigen	Species	Dilution WB	Dilution IF	Company	Product number
CRB1	Mouse	1:250	1:200	Abnova	H00023418-A01
CRB1	Rabbit	1:1000		Thermo Fisher Scientific	PA5-34491
CRB1	Rabbit	1:500		Sigma-Aldrich	HPA061250
CRB1	Mouse	1:1000		Merck	MABN1572
Recoverin	Rabbit		1:2000	Millipore	AB5585
Phalloidin-488			1:100	Santa Cruz	SC-363791
GSN1	Rabbit		1:50	Proteintech	11644-2-AP
DBN1	Rabbit		1:50	Proteintech	25770-1-AP
ARHGAP21	Rabbit		1:50	Proteintech	22183-1-AP
BIP	Rabbit	1:1000		Cell Signaling	3177
GAPDH	Rabbit	1:10000		Cell Signaling	D16H11
HA	Rabbit	1:2500		Cell Signaling	3724

HA	Rabbit	1:1000	Sigma-Aldrich	H6908
FLAG-HRP	Mouse	1:2500	Sigma-Aldrich	A8592
ß-Actin	Mouse	1:1000	Sigma-Aldrich	A5441

3.1.10 Commercially available secondary antibodies

Table 8| Overview of the commercially available secondary antibodies

Antigen	Species	Dilution	Label	Company
Anti-mouse	goat	1:7500	HRP	Jackson ImmunoReseach
Anti-rabbit	goat	1:7500	HRP	Jackson ImmunoReseach
Anti-mouse	goat	1:350	Alexa Fluor 488 nm	Thermo Fisher Scientific
Anti-mouse	goat	1:350	Alexa Fluor 568 nm	Thermo Fisher Scientific
Anti-mouse	goat	1:350	Alexa Fluor 647 nm	Thermo Fisher Scientific
Anti-rabbit	goat	1:350	Alexa Fluor 488 nm	Thermo Fisher Scientific
Anti-rabbit	goat	1:350	Alexa Fluor 568 nm	Thermo Fisher Scientific
Anti-rabbit	goat	1:350	Alexa Fluor 647 nm	Thermo Fisher Scientific

3.1.11 Plasmids

- pDONR201, Invitrogen
- pDEST (pcDNA 3.0) with a C-term HA tag, gift from R.Roepman, Radboud University, Nijmegen
- pDEST (pcDNA 3.0) with a N-term or C-term doublet Strep-tag II and a FLAG tag as described in [172].
- pDEST (pcDNA 3.0) with a N-term doublet Strep-tag II and a HA as described in [172]. The FLAG tag was replaced by an HA tag.
- pJET1.2/blunt Cloning vector, Thermo Fisher Scientific
- CRB1 in pcDNA3, gift from Prof. Masaki Nishimura (Molecular Neuroscience Research Center, Shiga University, Japan)
- CRB2 in pcDNA3, gift from Prof. Masaki Nishimura (Molecular Neuroscience Research Center, Shiga University, Japan)
- CRB3 in pcDNA3, gift from Prof. Masaki Nishimura (Molecular Neuroscience Research Center, Shiga University, Japan)

3.1.12 Software

- Adobe Illustrator CS5.1 — Adobe System Inc.
- CFX Maestro 1.1, version 4.1.2433.1219 — Bio-Rad Laboratories
- Cytoscape, version 3.9.1 — Cytoscape Consortium
- DIA-NN 1.8.1 — [173]
- E.A.S.Y. Win32 — Herolab
- EndNote Web — Thomson Reuters
- FIJI (ImageJ) 1.53q — Wayne Rasband, NIH
- Graphpad Prism 5.01 — GraphPad Software Inc.
- Image Lab™, version 6.0.1 — Bio-Rad Laboratories
- Integrative Genomics Viewer, version 2.12.3 — UC San Diego [174]
- Jalview version 2.11.3.2 [175] — University of Dundee
- Mascot version 1.6.1.0 — Matrix Science
- Maxquant 2.0.1.0 — MPI of Biochemistry
- Microsoft Office Professional Plaus 2016 — Microsoft Corporation
- Perseus version 1.6.15.0, 1.6.5.0 — MPI of Biochemistry

• Scaffold version 3.0, 4.0, 5.0	Proteome Software Inc
• SparkControl 2.2	Tecan Group
• ZEN (blue edition) 2.6	Carl Zeiss Microscopy

3.1.13 Online Tools

• Benchling	https://www.benchling.com/
• Clustal Omega	https://www.ebi.ac.uk/Tools/msa/clustalo/
• Ensembl	https://www.ensembl.org/index.html
• Human Protein Atlas	https://www.proteinatlas.org/
• MaxEntScan	http://hollywood.mit.edu/burgelab/maxent
• Morpheus Heatmap	https://software.broadinstitute.org/morpheus/
• NCBI PubMed	https://pubmed.ncbi.nlm.nih.gov/
• NNSPLICE, 0.9 version	https://www.fruitfly.org/seq_tools/splice.html
• Reactome	https://reactome.org/
• Sequencing	https://srvweb.microsynth.ch/ https://www.eurofins.de/
• ShinyGO version 0.77	http://bioinformatics.sdstate.edu/go/
• SpliceAI	https://spliceailookup.broadinstitute.org/
• String	https://string-db.org/
• Uniprot	https://www.uniprot.org/

3.1.14 Instruments and tools

• Acclaim PepMap RSLC C18	MPI of Biochemistry
• Acclaim PepMap100 C18	Thermo Fisher Scientific
• Agarose gel chamber	Bio-Rad Laboratories
• Agarose gel comb	Bio-Rad Laboratories
• BioRad T100™ Thermal Cycler	Bio-Rad Laboratories
• BioRad T100™ Thermal Cycler	Bio-Rad Laboratories
• Brand® Accu-jet® Pipetboy	Sigma-Aldrich
• Centrifuge 5415 R	Eppendorf
• Chemi Imager Fusion FX	Vilber
• Dissection set	ClinicCare Medizin Producte
• Drigalski spatula	Carl-Roth
• Drying Oven Cabinet UM 200	Memmert
• Duran® baffled flask	DWK Life Sciences
• Ecotron Incubation Shaker	Infors HT
• FIBERLite® F15-8x50C	Thermo Fisher Scientific
• Filter system	Millipore Filterunit Express Plus
• Gel Documentation System	Herolab GmbH
• Graduated measuring glass	Duran
• HERACell 150i CO2 Incubator	Thermo Fisher Scientific
• Heraeus Fresco 17 Centrifuge	Thermo Fisher Scientific
• Heraeus Multifuge X3R Centrifuge	Thermo Fisher Scientific
• Heraguard™ ECO Clean Bench Floor Stands	Thermo Fisher Scientific
• Immunofluorescent staining chamber	University Clinics Tuebingen
• Laboport® Mini Vacuum Pump	KNF Neuberger, Inc.
• Laboratory bottles, 50-2000 ml	Duran
• Magnetic plate	OZBiosciences
• Mini Trans-Blot® Electrophoretic Transfer Cell	Bio-Rad Laboratories
• Mini-PROTEAN II Multiscreen Apparatus	Bio-Rad Laboratories

- Mini-PROTEAN® Comb — Bio-Rad Laboratories
- Mini-PROTEAN® Short Plates — Bio-Rad Laboratories
- Mini-PROTEAN® Spacer Plates — Bio-Rad Laboratories
- Mini-PROTEAN® Tetra-Cell — Bio-Rad Laboratories
- MiniStar Centrifuge — VWR
- MSC-Advantage — Thermo Fisher Scientific
- MWG Biotech Inc Primus 25 Thermal cycler — Cole-Parmer
- NanoDrop 1000 Spectrophotometer — PeqLab
- NeoLab Intelli-Mixer — NeoLab
- Orbitrap Fusion™ Tribrid — Thermo Fisher Scientific
- Pipetman classic P10, P20, P200, P1000 — Gilson
- PowerPac™ Basic — Bio-Rad Laboratories
- PrimoVert microscope — Carl Zeiss Microscopy GmbH
- Savant RVT400 Refrigerated Vapor Trap — Thermo Fisher Scientific
- Savant SPD111V SpeedVac Concentrator — Thermo Fisher Scientific
- Staining jar according to Coplin — VWR
- Swivel Roller RM5F — Paul Marienfeld
- Systec Autoclave DX-150, DX-23 — Systec
- Tecan Spark 10M Luminescence Reader — Tecan Group
- Ultimate3000 Nano-RSLC systems — Thermo Fisher Scientific
- Vortex-Genie 2 — Scientific Industries
- VWB 18 Water bath — VWR
- Zeiss Axio Imager Z1 ApoTome Microscope — Carl Zeiss Microscopy GmbH Methods
- µPAC™ nano column (50 cm, C18) — Thermo Fisher Scientific
- µPAC™ trapping column — Thermo Fisher Scientific

3.2 Methods

3.2.1 Ethic agreement

This study was performed upon informed written consent in accordance with the guidelines and approved by the local ethics committee (project number 552/21BO2).

3.2.2 Cell culture of cell lines

3.2.2.1 Maintenance of cell lines

HEK293T, APRE19, SH-SY5Y, hTERT-RPE1 and HELA cells were maintained in growth media containing Dulbecco's Modified Eagle Medium (DMEM) supplemented with 10 % foetal bovine serum (FBS) and 0.5 % Penicillin/Streptomycin. Cells were cultured at 37 °C in a 5 % CO_2 incubator and analysed for *mycoplasma* by polymerase chain reaction (PCR). Serum starvation was performed by culturing cells for 48 hours in starvation media comprising DMEM without supplementation of FBS and Penicillin/Streptomycin.

3.2.2.2 Passaging of cell lines

Cells were cultured up to 80 to 95 % confluence in a 10 cm dish before passaging. Passaging was performed under a laminar flow hood with sterile conditions. Following removal of the culture media, cells were washed once with 10 ml PBS (Dulbecco's Phosphate-Buffered, Saline, without $CaCl_2$ and without $MgCl_2$) and incubated with 1 ml of 0.05 % Trypsin-EDTA per

10 cm dish for 5 min at 37 °C. Next, 9 ml of FBS-containing growth media was added to inhibit trypsin activity. Cells were resuspended and transferred to a new growth media containing culture dish in the desired dilution.

3.2.2.3 Thawing of cell lines

For thawing of cells, cryotubes containing frozen cells from the liquid nitrogen storage were thawed and quickly transferred to 9 ml of growth media to dilute DMSO under sterile conditions in a laminar flow hood. Next, cells were spin down for 3 min at 500 x g, resuspended in fresh growth media and transferred to a 10 cm dish.

3.2.2.4 Freezing of cell lines

For freezing cells from a confluent 10 cm dish were harvested using 0.05 % Trypsin-EDTA as described before and centrifuged for 3 min at 500 x g. The supernatant was removed, and cells were resuspended in cryomedium comprising FBS and 10 % DMSO. Next, the cell suspension was transferred to cryotubes. Cells from one confluent 10 cm dish were distributed to four cryotubes and gradually cooled down by incubation for 15 min at 4 °C, 1 hour at -20 °C and overnight -80°C followed by long-term storage in liquid nitrogen.

3.2.3 iPSC culture and generation of iPSC-derived retinal organoids

Culture of iPSC and generation and sectioning of iPSC-derived RO was performed and provided by the group of Prof. Liebau (University of Tuebingen) as described in the doctoral thesis of Dr. Achberger [22].

3.2.4 Cloning

3.2.4.1 Gateway® cloning

3.2.4.1.1 Polymerase chain reaction using primers with attB overhangs

To generate overexpression constructs with different tags, the Gateway® cloning system was used. Therefore, first complementary DNA (cDNA) was amplified by PCR using specific primers with attB1 and attB2 recombination site overhangs. The attachment of attB1 and attB2 sites was either performed in a one-step PCR, in which the primer contains the complete attB sites or a two-step PCR, in which two subsequential PCR using attB1 and attB2 adaptor primers were performed. For canonical *CRB1* (NM_202153), *CRB2* (NM_173689) and *CRB3* (NM_139161.5) pcDNA3 plasmids from Prof. Masaki Nishimura (Molecular Neuroscience Research Centre, Shiga University of Medical Science Molecular Neuroscience Research Center, Japan) were used as cDNA template for PCR. The CRB1 extracellular isoform was partly amplified from cDNA from control iPSC-derived RO. PCR was performed using the Phusion™ High-Fidelity DNA Polymerase and the BioRad T100TM Thermal Cycler using the following protocols. All products were analysed by agarose gel electrophoresis.

Table 9| Pipetting scheme for PCR amplification of *CRB1* and CRB3 with attB1 and attB2 overhang primers

Reagent	Volume per reaction in µL
Phusion HF buffer (5x)	5
dNTPs (10 mM)	0.5
Phusion Polymerase	0.5
Primer forward (10 µM)	1.3
Primer reverse (10 µM)	1.3
Nuclease-free H_2O	15.9
Template plasmid (10 ng/µl)	0.5
Total	**25**

Table 10| PCR program for *CRB1* amplification with attB1 and attB2 overhang primers

Temperature (°C)	Time	Cycles
98	2 min	
98	30 sec	25 x
68	40 sec	
72	4:30 min (1 min per 1000bp)	
72	5 min	

Table 11| PCR program for *CRB3* amplification with attB1 and attB2 overhang primers

Temperature (°C)	Time	Cycles
98	2 min	
96	30 sec	20 x
55	40 sec	
72	1 min (1 min per 1000bp)	
72	5 min	

Table 12| Pipetting scheme for PCR amplification of *CRB2* with attB1 and attB2 overhang primers

Reagent	Volume per reaction in µL
Phusion GC rich buffer (5x)	5
dNTPs (10 mM)	0.5
Phusion Polymerase	0.25
Primer forward (10 µM)	1.25
Primer reverse (10 µM)	1.25
Nuclease-free H_2O	13.5
DMSO	2.75
Template plasmid (10 ng/µl)	0.5
Total	**25**

Table 13| PCR program for *CRB2* amplification with attB1 and attB2 overhang primers

Temperature (°C)	Time	Cycles
99	5 min	
99	1 min	20 x
68	15 sec	
72	4:30 min (1 min per 1000bp)	
72	5 min	

3.2.4.1.2 BP and LR reaction

For BP reaction, 1 µL of PCR product containing the desired cDNA with attB overhangs was incubated with 1 µL of pDONR201 vector (100 ng/µl), 1 µL of BP Clonase II and 2 µL of elution buffer from Monarch® Plasmid Miniprep kit. For LR reaction, 1 µL of pDONR contained the cDNA of interest (100 ng/ µL) was mixed with 1 µL of pDEST vector, 1 µL of LR clonase I and 2 µL of elution buffer. The reactions were incubated at 25 °C for 4 h or overnight followed by transformation in bacteria and plating on kanamycin or ampicillin plates for BP or LR reaction, respectively.

3.2.4.2 Agarose gel electrophoresis

After PCR, amplicons were analysed by agarose gel electrophoresis using a 0.8 % or 1 % agarose gel dependent on the expected amplicon size. Therefore, agarose powder was dissolved in 1x TBE under boiling conditions, cooled down and 4 % ethidium bromide were added to the liquid. Upon complete cool-down, 10-15 µL of the PCR reactions were mixed with 2-3 µL of 6x DNA loading dye and loaded. To estimate the size of the product, 8 µL of Gene Ruler 1 kb Plus were also loaded. Separation was performed for 30 to 40 min at 100 V. Images were taken using a UV-Transilluminator Box, CCD camera and the E.A.S.Y., Win32 software.

3.2.4.3 Site directed mutagenesis

Site-directed mutagenesis (SDM) using PCR was used to introduce patient mutations and to remove different EGF domains in the canonical *CRB1* in pDONR 201 vector. The following PCR protocol was used.

Table 14| PCR protocol used for Phusion polymerase

Reagent	Volume per reaction in µL
Phusion HF buffer (5x)	4
dNTPs (10 mM)	0.4
Phusion Polymerase	0.3
Primer forward (10 µM)	1
Primer reverse (10 µM)	1
Nuclease-free H_2O	12.8
Template plasmid (10 ng/µl)	0.5
Total	**20**

Table 15| PCR program for Phusion polymerase

Temperature (°C)	Time	Cycles
99	5 min	
99	1 min	29 x
68-54	15 sec	
72	8 min (1 min per 1000bp)	
72	5 min	

Following PCR, 1 µL of *DpnI* was added and incubated for 1 h at 37 °C to digest methylated templated DNA. Amplification was verified by agarose gel electrophoresis and 5 µL of *DpnI*-digested PCR reaction were used for bacteria transformation.

3.2.4.4 Transformation of chemically competent bacteria

To amplify recombinant DNA constructs, 5 µL of PCR reaction for SDM or BP/LR reaction were added to 50 µL of chemically competent bacteria followed by incubation on ice for 30 min. For all constructs, except the empty pDONR and pDEST *E. coli* - Library Efficiency® DH5α Competent Cells were used. For empty pDONR or pDEST plasmids *E. coli* - One Shot® ccdB Survival™ 2 T1® Competent Cells were used. Upon incubation of ice, DNA was transformed by heat shocking the bacteria for 45 sec at 42 °C followed by 2 min of incubation on ice. Next, 250 µL of Super optimal broth with glucose medium was added and bacteria were incubated for 60 min at 37 °C under agitation at 160 rpm. Next, bacteria were plated on antibiotic-selective LB-agar plates consisting of 1.5 % Agar-Agar in LB medium based on the resistance gene of the transformed DNA and cultured overnight at 37 °C. Ampicillin and chloramphenicol are used at a final concentration of 100 µg/mL. Kanamycin is used at a final concentration of 50 µg/mL.

3.2.4.5 Plasmid DNA purification from chemically competent bacteria

To purify Plasmid DNA from chemically competent bacteria, PureYield™ Plasmid Midiprep Kit was used according to manufacturer's instructions. In short, a single bacteria colony from LB- agar plate was cultured overnight in 50 ml of antibiotic-selective LB-media at 37°C in a shaking incubator (160 rpm). The next day, bacteria were spin down for 10 min at 4500 x g. The supernatant was removed, the pellet was resuspended in 3 ml of resuspension buffer, lysed for 3 min at RT using 3 ml of lysis buffer and neutralised with 5 ml of neutralization solution. Samples were spin down for 15 min at 12.000 x g followed by vacuum-assistant column-based purification following manufacturers protocol. Next, endotoxins were removed, and columns were washed twice with 10 ml column wash solution and dried. DNA was eluted using 500 µL of nuclease-free H_2O. Concentration and purity were determined using NanoDrop 1000 Spectrophotometer. All constructs were verified by Sanger sequencing by Microsynth Seqlab or Eurofins Genomics following companies' instructions. Results were analysed using Benchling.

3.2.5 Immunofluorescence microscopy

Slides with cryosections of iPSC-derived were kindly provided by the group of Prof. Liebau generated as described by Dr. Achberger [22]. Next, cryosections were dried for 45 min at 37 °C followed by rehydration in PBS for 30 min at RT in a staining jar according to Coplin. Sections were circled with a Pap-pen and subsequent steps were performed in a staining

chamber. Sections were blocked for 1h at RT with blocking solution containing 10 % NGS, 1 % BSA, 0.1 % Triton X-100 in PBS. Subsequently, primary antibodies diluted in blocking solution were incubated overnight at 4°C followed by three washing steps with PBS for 10 min at RT. Secondary antibodies and Phalloidin were diluted in PBS and incubated for 1 h at RT in the dark followed by three washes steps with PBS for 10 min at RT. To visualise DNA, sections were incubated with DAPI for 10 min at RT, washed twice with PBS and mounted using 50 µL of Fluoromount-G® and a coverslip. Sections were stored at 4 °C in the dark until imaging. Imaging was performed using Zeiss Axio Imager Z1 ApoTome microscope with an AxioCam MRm camera and a 63x oil immersion objective lens (NA 1.4). Z-stacks were acquired, and Zeiss ZEN 3.0 Blue Edition was used for processing and analysis of the intensity. Images that were compared were acquired with identical exposure times, γ-settings, and grey values. Statistical analysis was performed with GraphPad Prism version 5.0.1.

3.2.6 Porcine retina pull- down approach

3.2.6.1 Pig retina lysate preparation

Pig eyes were received from the local slaughterhouse and kept at 4°C until preparation. The eye was cleaned up from the connective tissue and a scalpel was used to open the eyeball in parallel to the ciliary muscle. The vitreous body, the cornea, the lens and the iris were removed and the eye cup was washed once with PBS. Using a tweezer, the retina was detached and added to tube containing lysis buffer. Per retina, 2.5 ml of lysis buffer was used per retina and four retinas were pooled. Next, samples were incubated at for 30 min at 4°C in an end-over-end shaker (35 rpm) and spin down at 10.000 x g for 10 min. The supernatant was transferred to a new tube and protein concentration was assessed using Bradford assay.

3.2.6.2 Cell seeding and transfection using polyethylenimine

At day 0, HEK293T cells were passaged 1:2 from 10 cm to 14 cm dish as described previously. At day 1, cells reached a confluence of 60-80 % and were transfected with 8000 ng of the desired FLAG-tagged construct using PEI solution. Therefore, 8000 ng of DNA were added to 1 ml of PEI solution, vortexed, incubated for 10 min at RT and added equally to the cells in a drop-wise fashion.

3.2.6.3 Cell lysis and Bradford assay

At day 3, the media was discarded, cells were washed once with PBS and lysed on ice with 1 ml of lysis buffer. Cells were detached using a cell-scraper, transferred to a 2 mL Eppendorf tube, incubated for 30 min at 35 rpm at 4 °C in an end-over-end shaker and centrifuged for 10 min for 10.000 x g. Next, supernatant was transferred to new Eppendorf tube and the protein concentration was assessed using Bradford assay. Therefore, a dilution

series of bovine serum albumin (BSA) was performed with 0 mg/mL, 0.2 mg/mL, 0.4 mg/mL, 0.6 mg/mL, 0.8 mg/mL and 1 mg/mL in HPLC H_2O as described below.

Table 16| BSA dilution series performed to assess protein concentration by Bradford assay

BSA concentration in mg/mL	Volume of BSA stock (1mg/mL) µL	Volume of HPLC H_2O in µL	Volume of lysis buffer in µL
0	0	50	5.5
0.2	10	40	5.5
0.4	20	30	5.5
0.6	30	20	5.5
0.8	40	10	5.5
1.0	50	0	5.5

To each of the 50 µL BSA dilutions, 5.5 µL of lysis buffer were added. In a 96-well plate, 5 µL of each BSA dilution were added in triplicates. For the samples, 1 µL of sample and 4 µL of HPLC H_2O were added in triplicates. Next, 250 µL of 1x Bradford in HPLC H_2O was added, incubated for 5 min and the absorbance at 595 nm was measured using Tecan Spark 10M Luminescence Reader with the SparkControl 2.2 software. Concentration was determined using the BSA standard curve.

3.2.6.4 FLAG-immunoprecipitation and porcine retinal pull-down

For FLAG-immunoprecipitation, unless not otherwise indicated, steps were performed on ice. FLAG beads were washed once with 600 µL TBS, once with 500 µL lysis buffer and twice with 500 µL wash buffer. 10 mg of protein were loaded on 25 µL of 50 % slurry FLAG beads and incubated for 1.5 hours at 4°C in an end-over-end shaker at 35 rpm. Next, samples were spin down for 1 min at 500 x g and washed twice with 500 µL wash buffer. Samples were incubated with 500 µL 0.01 % SDS in TBS for three min at RT under movement followed by three washes with 500 µL wash buffer. 4 mg of porcine retina lysate was added, and samples were incubated for 1.5 hours at 4 °C in an end-over-end shaker. Samples were centrifuged for 1 min at 500 g, supernatant was removed, and beads were transferred to a Receiver Column. Upon three washing steps with 500 µL washing buffer and samples were eluted by incubating with 100 µL FLAG-peptide for 10 min at RT in a Thermoshaker incubator at 500 rpm.

3.2.6.5 Protein precipitation and tryptic digest

Affinity purified eluates were precipitated with acetone-based protein precipitation and digested with trypsin. For this purpose, eluates were filled with ice-cold acetone to a final of 80 % acetone. After strong vortex, samples were incubated at -20 °C for 2 hours, followed by centrifugation for 10 min at 4°C and 16000 x g. The liquid phase was discarded, and the pellet was air dried for 15 min under a chemical hood. Next, the precipitated protein was re-suspended in 30 µL 50 mM ABC solution, 4 µL RapiGest and 1 µL of 100 mM DTT-solution and incubated for 10 min at 60 °C in a Thermoblock at 500 rpm. Samples were cooled down, spin down and 1 µL 0.3 M IAA solution was added and incubated for 30 min in the dark. Next,

1 µL of 0.5 µg/uL Trypsin in 50mM HAc was added followed by incubation at 37 °C overnight. Enzymatic activity was stopped by applying 1.7 µL TFA to a final concentration of 5 % and samples were transferred to a PP insert followed by incubated for 10 min at RT. Following a centrifugation for 15 min at 22°C and 16.000 x g, the clear solution was transferred to a new tube and used for desalting and clean-up.

3.2.6.6 Stop-and-go extraction tips for desalting and clean up

For desalting and clean-up of the samples for mass spectrometry, Stage Tips with a C18 matrix were activated with 20 µL 80 % ACN/5 % TFA solution, washed with 20 µL H_2O/5 % TFA solution and the complete sample was added followed by one washing step with 20 µL H_2O/5 % TFA solution. For elution, 20 µL 50 % ACN/5 % TFA solution and 20 µL 80 % ACN/5 % TFA solution were applied. Speedvac at 37 °C was used to reduce the volume to approximately 5 µL. For mass spectrometry, samples were filled up with 0.5 % TFA to a total volume of 15 µL and 7.5 µL were transferred to a glass vial for analysis.

3.2.6.7 Mass spectrometry

LC-MS/MS analysis was done using an Ultimate3000 RSLCnano systems (Thermo Scientific) attached to a Orbitrap Fusion Tribrid mass spectrometer through a nanospray ion source [1, 176]. Prepared tryptic peptide samples were administered automatically and loaded onto a nano trap column (2 mm x 10 mm, µPAC™ Trapping column, 300 nm, 100-200 Å, PharmaFluidics) with a flow rate of 10 µL/min in 0.1% TFA in HPLC-grade H_2O [1, 176]. After 3 min, peptides were eluted and separated on an analytical 50 cm µPAC™ C18 nano column (315 µm x 50 cm, 300 nm, 100-200 Å, PharmaFluidics) by a linear gradient from 2 % to 30 % of buffer B (80 % ACN and 0.08 % formic acid in HPLC-grade H_2O) in buffer A (2 % ACN and 0.1 % formic acid in HPLC-grade H_2O) at a flow rate of 300 nL/min over 147 min [1, 176]. Left-over peptides were eluted using a step gradient from 30 % to 95 % in buffer B for 5 min, followed by 5 min at constant 95 % of buffer B [1, 176]. Next, the gradient was declined quickly in 5 min to 2 % of solvent B for the final 20 min [1, 176]. For data-dependent acquisition (DDA), full-scan MS spectra were measured on the Fusion with a resolution of 70,000 in a mass-charge range from m/z 335–1500 with a cycle time of 3 sec [1, 176]. The n most abundant precursor ions were chosen with a quadrupole mass filter if they exceeded an intensity threshold range of 5e 3 – 1e20 and were at least double charged for further fragmentation using higher-energy collisional dissociation [1, 176]. Next, mass of the fragments was analysed in the ion trap and the selected ions were excluded for further fragmentation the following 60 s by dynamic exclusion [1, 176].

3.2.7 Data analysis

MS/MS data were analysed using the MaxQuant software (version 2.0.1.0) [1, 176-178]. As the digesting enzyme Trypsin/P was chosen with a maximum of 2 missed cleavages [1, 176]. Cysteine carbamidomethylation was selected for fixed modification [1, 176]. Methionine oxidation and N-term acetylation were selected for chosen for variable modifications [1, 176]. Label-free quantification (no fast LFQ) was selected for data analysis and the minimum ratio count was put at 2 [1, 176]. 20 was chosen for first search peptide tolerance [1, 176]. Main search peptide tolerance was put at 4.5 ppm and the re-quantify option was chosen [1, 176]. The Uniprot *sus scrofa* proteome database (January 2020; 49793 entries) was used and contaminants were detected using MaxQuant contaminant search [1]. Human CRB2 (hCRB2), CRB1 (hCRB1), CRB3 (hCRB3) and GFP sequence were included in the database [1]. Match between run options was chosen with an alignment time window of 20 min and a match time window of 0.7 min [1, 176]. A minimum length of 7 amino acids with a minimum peptide number of one was demanded. Razor and unique peptides were utilised for quantifications [1]. Perseus Software (version 1.6.5.0) was used for statistical analysis [1]. Six biological replicates were used, which comprised individual tissue-specific immunoprecipitation (IP) samples processed in three independent experiments [1]. Data were filtered for peptides only identified by side, potential contaminants or reverse sequence [1, 176]. Valid values were required in at least 4 out of 6 samples in each group [1, 176]. Furthermore, Imputation by 0 was done for NaN values [1]. Median values were calculated and the stability of protein enrichment within groups was determined using the students t-test (FDR 0.05) [1]. Only proteins with a significance $p < 0.05$ and a $\log_2$ ratio against GFP control >2 were defined as significantly enriched/depleted [1]. For GO enrichment analysis the graphical tool ShinyGO 0.77 was used [1, 179]. The following settings were used: FDR cut-off 0.05, pathway size 20-250, remove redundant pathways [1]. PPI networks were generated using STRING database and visualised with Cytoscape, version 3.9.1 [1, 180, 181]

3.2.8 Full proteome analysis of iPSC-derived retinal organoids

3.2.8.1 Lysis of iPSC-derived retinal organoids and digest

For full-proteome analysis of iPSC-derived RO, 15-18 iPSC-derived RO per experimental condition were obtained as a pellet in -80 from the group of Prof. Liebau. Next, iPSC-derived RO were lysed in 100 µL LB by pipetting up and down and incubated in an end-over-end shaker at 4°C for 30 min at 35 rpm. Upon centrifugation for 10 min at 10.000 x g, supernatant was transferred to a fresh 1.5 mL Eppendorf tube and protein concentration was assessed by Bradford assay. 50 µg protein were precipitated using acetone as described before, digested with trypsin and desalted and cleaned up using Stage Tips as described before. After reducing

Speedvac as described previously, samples were filled up with 0.5 % TFA to a total volume of 30 µL and 5 µL were transferred to a glass vial for analysis.

3.2.8.2 Mass spectrometry using data-independent acquisition

Mass Spectrometry analysis was executed on an Ultimate3000 RSLC system connected to an Orbitrap Tribrid Fusion mass spectrometer [182]. Tryptic peptides were injected onto a µPAC Trapping Column (2.5 µm inter-pillar distance, 18 µm pillar length/bed depth, 5 µm pillar diameter, 9% external porosity, 2 mm bed channel width and 10 mm length, 100 to 200 Å PharmaFluidic, pillars with superficially porous shell thickness of 300 nm) at a flow rate of 10 µl per min in 0.1% TFA in HPLC H_2O [182]. Next, peptides were eluted and separated on the PharmaFluidics µPAC nano-LC column (50 cm µPAC C18, 59% external porosity, 2.5 µm inter-pillar distance, 5 µm pillar diameter, 18 µm pillar length/bed depth, 315 µm bed channel width, 50 cm bed length, superficially porous pillars with a porous shell thickness of 300 nm, 100-200 Å, PharmaFluidics) by a linear gradient from 2% to 30 % of buffer B (80% ACN and 0.08% formic acid in HPLC H_2O) in buffer A (2% ACN and 0.1% formic acid in HPLC H_2O) at a flow rate of 300 nl per min [182]. The remaining peptides were eluted by a short gradient from 30% to 95% buffer B; the total gradient run was 120 min [182]. Spectra were acquired in DIA (Data Independent Acquisition) mode using 50 variable-width windows over the mass range 350-1500 m/z, MS2 scan range was set from 200 to 2000 m/z.

3.2.8.3 MS/MS date analysis using data-independent acquisition

DIA-NN 1.8.1 (PMID: 31768060) was used to analyze raw MS/MS RAW data using in library-free mode and the human database (UniProt release October 2022). First, library of precursor ions was produced using FASTA digest for library-free search together with deep learning-based Spectra prediction. For mass accuracy correction and cross-run normalization an experimental library made from the DIA-NN search was utilised. For protein quantification, only tryptic peptides (2 missed tryptic cleavages) and only high-accuracy spectra with a minimum precursor FDR of 0.01 were used. The match between runs option was switched on and no shared spectra were accepted for protein identification. Statistical analysis including label-free quantification ratios (LFQ) was performed using the Perseus software version 1.6.15.0. For the three technical replicates per group at least 2 out of 3 samples should have a valid value. Imputation was performed by replacing missing valid values from normal distribution. Median values were calculated and the stability of protein enrichment within groups was determined using the two-sided students t-test (FDR 0.05, S0=0.1). Only proteins with a significance $p < 0.05$ were defined as significantly higher or lower abundant.

3.2.9 Co-immunoprecipitation

For co-IP, in the morning HEK293T cells were transferred 1:1 from a confluent 10 cm dish to a 14 cm dish using 0.05 % Trypsin-EDTA. In the afternoon, cells were co-transfected with the desired HA and FLAG plasmid using PEI as described before. The following amount was transfected for each construct: CRB1-FLAG WT and MT (6000 ng), CRB1-HA WT and MT (3000 ng), CRB2-FLAG (4000 ng), CRB2-HA (4000 ng), CRB3-FLAG (500 ng), CRB3-HA (500 ng), GFP-FLAG (500 ng), GFP-HA (1000 ng). After 48 hours, cells were lysed, and protein amount was determined using Bradford assay as described for the porcine retinal pull-down approach. As indicated for the porcine retina pull downs, FLAG beads were washed, and equal amount of protein were loaded on 25 µL 50 % slurry FLAG beads. After 1 h to 1.5 h of incubation in an end-over-end shaker at 35 rpm at 4°C, beads were centrifuged for 1 min at 5000 x g. Proteins were either eluted using the FLAG-peptide as described or by glycine elution. For glycine elution, after centrifugation and removal of the supernatant 100 µL of 200 mM glycine buffer pH 2.5 was added and incubated for 7 min in a Thermoblock at 500 rpm. Following centrifugation, the supernatant was removed and the Glycine incubation step was repeated. Both supernatants were pooled and neutralised with 60 µL of a 1 M Tris buffer pH 8. Samples were stored at -80 until further use for western blot analysis.

3.2.10 Western blot analysis

3.2.10.1 Sodium-dodecylsulfate-polyacrylamide gel electrophoresis

To separate proteins according to molecular weight Sodium-dodecylsulfate-polyacrylamide gel electrophoresis (SDS-PAGE) was performed. For this purpose separation and stacking gels were prepared following the standard protocol from Harlow and Lane [183]. In short, separation gel was prepared and filled in the preassembled casting stand. Isopropanol was added. After the separation gel was polymerised, isopropanol was removed, the stacking gel was poured in the casting stand and the comb was inserted. After polymerization of the stacking gel were assembled in the BioRad Electrophoresis Cell following manufacturer's instructions and filled with 1x running buffer. Upon addition of 5x Laemmli-buffer, samples (lysates or eluates) were heated for 2 min at 96 °C and loaded on the SDS-PAGE. For lysates, equal amount of protein was loaded as determined by Bradford assay. For, eluates, equal volume was loaded in case of direct comparison. For electrophoresis, current of 80 V for approximately 15 min and 120 V for approximately 1 hour was applied.

3.2.10.2 Immunoblotting

After SDS-page, proteins were transferred from the SDS gel to a PVDF-membrane via tank blotting. In short, the PVDF membrane was activated in methanol and the transfer frame consisting of one sponge, two Whatman paper, the SDS-gel, the PVDF membrane, two

Whatman paper and one sponge was assembled. The transfer fame was loaded in the transfer tank filled with 1x transfer buffer. The transfer was performed with an electronic potential of 90 V for 1.5 h at 4 °C. Next, membranes were blocked with 5 % milk or 5 % BSA in 1x TBST for 1 h at RT under motion. Primary antibodies were incubated in blocking solution for 1 hour at RT or overnight at 4 °C under motion. Next, membranes were washed three times with 1x TBST for 10 min under motion followed by incubation with secondary HRP-labelled antibodies in blocking buffer for 1 h at RT. The membranes were washed three times with 1xTBST and imaged using PierceTM ECL Plus western Blotting Substrate or PierceTM ECL western Blotting Substrate. The HRP- generated chemiluminescent signal was detected by Chemi Imager Fusion FX. Images were analysed using Image Lab™, FIJI (ImageJ) 1.53q, Illustrator and GraphPad Prism version 5.0.1.

3.2.11 Whole Genome Sequencing and variant analysis

DNA was isolated from blood samples by Eva Weber and Dr. Susanne Kohl (Institute for Ophthalmic Research, University Clinics Tübingen) and send for WGS using an Illumina Sequencing and primary analysis using a standard diagnostic pipeline to the Core Facility of Medical Genetics and Applied Genomics cATG/NCCT (University of Tuebingen). Variants were filtered for an allele frequency in population cohort of below 0.1 % to identify rare variants. The variants were further analysed and filtered using Microsoft Excel. Harmful candidate variants were defined as homo- or heterozygous for patient A and WT in patient B. Protective candidate variants were defined as homo- or heterozygous for patient B and WT in patient A.

3.2.12 RNA isolation

RNA was isolated from cell lines in 6-well plates, porcine retina samples that were transferred to a 2 mL Eppendorf tube or 10-15 iPSC-derived ROs that were collected in a 2 ml Eppendorf tube. Under the chemical hood, 1 ml of Trifast was added to each of the 6-wells or sample in Eppendorf tubes and incubated for five min at RT. To ensure proper lysis of iPSC-derived RO and retinal explants, samples were dissociated by pipetting up and down slowly during the incubation and frozen overnight at -80. To separate phases, 200 µL of chloroform was added, vortexed for 15 sec and incubated for 5 min at RT. Next, samples were centrifuged for 12.000 x g for 5 min, which separated the lower red (phenol-chloroform phase), the interphase and the aqueous upper phase, which contains the RNA. The upper phase was transferred to a new 1.5 mL Eppendorf tube and 500 µL isopropanol were added to precipitate RNA. Next, samples were mixed, incubated for 10 min on ice and centrifuged for 10 min at 12.000 x g. The supernatant was removed and the precipitate was washed twice with 1 ml of 75 % ethanol. Samples were air-dried under the chemical hood and RNA was dissolved in 30 µL of nuclease-free H_2O. Concentration and purity were determined using NanoDrop 1000 Spectrophotometer. Samples stored at -80 until further processing.

3.2.13 Genomic DNA removal from RNA samples

To remove potential genomic DNA from the isolated RNA, DNAse I treatment was performed. For this purpose, 2 µg of RNA were incubated with 2 µL 10x reaction buffer with $MgCl_2$, 0.2 µL of DNAse I (10 U/µL) and nuclease-free H_2O in total volume of 20 µL for 30 min at 37°C. Next, 2 µL of 50 mM EDTA were added and incubated for 10 min at 65 °C. Next, samples were used for cDNA synthesis.

3.2.14 cDNA synthesis

To generate cDNA, DNAse treated RNA samples were incubated with 1 µL random primers (500 µg/mL) and 5 µL of nuclease-free H_2O for 5 min at 70°C. Next, samples were incubated on ice for 5 min, spin down and 10 µL M-MLV RT 5x Buffer, 8.5 µL nuclease-free H_2O, 2.5 µL dNTPs and 1 µL M-MLV polymerase was added. Samples were incubated for 10 min at 23 °C, 50 min at 50 °C and 15 min at 70 °C. Samples were stored at -20 °C until further processing.

3.2.15 Real-time quantitative polymerase chain reaction

Relative mRNA expression levels of genes of interest were determined using real-time quantitative PCR (RT-qPCR). Per reaction, 1 µL of cDNA was added to a master mix of 5.5 µL SSO Advanced SYBR Green, 0.5 µL forward primer (10 µM), 0.5 µL reverse primer (10 µM) and 3.5 µL nuclease-free H_2O. Per sample, three replicates were added to a 96 Well Lightcycler Plate. *Glycerinaldehyd-3-phosphat-Dehydrogenase (GAPDH)* or (*Hypoxanthin-Guanin Phosphoribosyltransferase (HPRT)* were used as reference gene due to a stable expression level throughout all experimental conditions. A negative control was added comprising the master mix without the addition of cDNA but 1 µL of nuclease-free H_2O. The reaction was performed using the BioRad CFX96 Real-Time System and the CFX Maestro 1.1 software with the following program:

Table 17| BioRad program for RT-qPCR analysis

Temperature (°C)	Time	Cycles
95	1 min	
95	10 sec	40 x
60	30 sec	
65	5 sec, 0.5 °C/cycle	Melting curve
95	5 sec, 0.5 °C/cycle	

Relative expression of gene of interest relative to housekeeping genes was calculated using the CFX Maestro 1.1 software using the ΔCt and the ΔΔCt method to calculate the fold-change expression. Melting curve of product was used to confirm presence of a single peak, which excludes presences of unspecific products. Statistical analysis was performed with GraphPad Prism version 5.0.1.

3.2.16 CRB1 splicing analysis

3.2.16.1 Polymerase chain reaction using DreamTaq Polymerase

To identify potential CRB1 misspliced transcript variants, PCR analysis was performed using intron spanning primers comprising exon 8-9 and exon 8-10. GAPDH was amplified as a control gene to verify equal efficiency of cDNA synthesis. For this purpose, PCR was performed using the following protocol:

Table 18| DreamTaq PCR protocol for splicing analysis

Reagent	Volume per reaction in µL
Dream Taq Green Buffer (10x)	2
dNTPs (10 mM)	1
Dream Taq DNA Polymerase 5 U/µl	0.25
Primer forward (10 µM)	1
Primer reverse (10 µM)	1
Nuclease-free H_2O	12.75
DNAse treated cDNA	1
Total	**20**

The PCR was performed using the BioRad T100TM Thermal Cycler with the following protocol:

Table 19| PCR program for Dream Taq DNA Polymerase

Temperature (°C)	Time	Cycles
95	5 min	
95	1 min	29 x
60 *(GAPDH)* 63 (*CRB1* exon 8-9) 58 (*CRB1* exon 8-10)	40 sec	
72	1 min 1.5 min for *CRB1* exon 8-10	
72	5 min	

All PCR products were analysed by agarose gel electrophoresis as described previously.

3.2.16.2 Purification of DNA from PCR products for Sanger sequencing

In case only one amplicon size was obtained after PCR, the DNA was cleaned from up from the reaction using peqGOLD PCR Clean-Up, Cycle-Pure-Kit following manufacturer protocol. In short, four times the volume of the PCR-mix of CP buffer was added, vortexed and spin down. Samples were transferred to a peqGOLD column and two washing steps with 700 µL of DNA wash buffer were performed. The column was dried by centrifugation of 2 min at 13.000 x g. DNA was eluted using 30 µL of nuclease free H_2O. Samples were sent for Sanger sequencing as described previously.

3.2.16.3 Agarose gel extraction for Sanger sequencing

In case multiple amplicons of different size were obtained after PCR, amplicons were cut out from the gel after agarose gel electrophoresis and extracted using the GeneJET Gel Extraction Kit following manufacturer's instructions. In short, binding buffer was added in a 1:1

volume: weight ratio to the excised gel slice in a 1.5 mL Eppendorf tube. Next, samples were incubated for 10 min at 60 °C until complete melting of the agarose slice and mixed. Equal amount of isopropanol was added and mixed. Samples were transferred to the GeneJET purification column, and two washes were performed with 100 µL of binding buffer and 700 µL of ethanol containing washing buffer. Columns were dried by 1 min at 12.000 x g and DNA was eluted using 30 µL of nuclease free H_2O. Products were either send for Sanger sequencing as described previously or used for PJET cloning.

3.2.16.4 PJET PCR cloning of PCR amplicons

PCR amplicons were cloned in the pJET1.2/blunt vector using the CloneJET PCR Cloning kit following manufacturer's instructions for sticky-end cloning. In short, 1-5 µL purified PCR product was incubated with 10 µL 2X reaction buffer, 1 µL DNA blunting enzyme and 1-6 µL of nuclease-free H_2O for 5 min at 70 °C to remove sticky ends. Upon 5 min on ice, 1 µL of pJET1.2/blunt cloning vector (50 ng/µL) and 1 µL of T4 DNA ligase was added and incubated for 30 min at RT. Reactions were transformed in *E. coli* - Library Efficiency® DH5α Competent Cells.

3.2.16.5 Colony PCR

To identify positive clones after pJET PCR cloning, a colony PCR was performed using the colonies on agar plates. For this purpose, a PCR master mix was prepared for DreamTaq polymerase as described previously. A single colony was touched using the pipette tip. The tip was first dipped into the PCR mix and then to a 2 mL Eppendorf tube containing antibiotic-selective LB-medium. The PCR program was performed for DreamTaq as described previously for DreamTaq polymerase and PCR products were evaluated by agarose gel electrophoreses. Positive clones were selected and transferred from the 2 mL Eppendorf to a 50 mL antibiotic-selective LB-media for overnight culture and DNA plasmid purification.

3.2.17 Porcine retina explant culture and reverse magnetofection

Porcine eyes were obtained from the local slaughterhouse and incubated at 4 °C. All steps were performed under the Thermo Scientific™ Heraguard™ ECO clean bench. Eyeballs were washed with 70 % ethanol and PBS. The connective tissue was removed and using a scalpel the eyeball was opened in parallel to the ciliary muscle. Upon removal of the vitreous body, the cornea, the lens and the iris, PBS was added. Blood vessels were used to orient, and punches were taken with a 6,0 mm puncher. Punches were carefully transferred with a Pasteur pipette with a rubber suction cup to a 6-well trans-well plate containing 1.5 mL of complete Neurobasal media in the media chamber with the photoreceptor side facing the membrane. The explants were incubated at 37 °C in a 5 % CO_2 incubator.

After 3 hours of incubation, siRNA transfection was performed using reverse magnetofection as described by Sen *et al.* [184]. In short, per transfection 2.1 µL of magnetic nanoparticles were mixed with 50 nM or 100 nM of a pool of three *CRB1* siRNAs or control in 100 µL supplement-free and serum-free Neurobasal media were allowed to complex for 30 min at RT. Next, complexes were added to the medium chamber of the transwell plate, and a magnet was placed on the lid of the plate for 30 min in a 37 °C incubator. Next, day media was refreshed and 48 hours after transfection, samples were harvested for RNA isolation.

3.2.18 Production of monoclonal antibodies for CRB1

The production of monoclonal antibodies against CRB1 was performed by the Core Facility Monoclonal Antibodies at the Helmholtz Center Munich by the group of Dr. Feederle including antigen immunization and fusion, multiplex-high throughput screening, titer assessment and sub cloning. Hybridoma supernatants pre- and post-subcloning were tested for positive recognition of porcine and human CRB1 using immunofluorescence microscopy with the help of Sylvia Bolz and western blot analysis.

3.2.18.1 Screening of hybridoma clones by western blot analysis

To screen supernatants of hybridoma clones, western blot analysis was performed using lysates and eluates of HEK293T cells overexpressing CRB1-FLAG or porcine retina lysates. Western blot analysis was performed as previously described with the following adaptations: A Mini-PROTEAN® Comb, Prep+1 well, 1.0 mm was used for preparation of a 10 % SDS-PAGE and blocking was performed using 5 % BSA in 1x TBST for 1 h at RT. The hybridoma clone supernatant was incubated 1:10 in blocking solution and 100 µL were added to each channel of the Mini-PROTEAN II Multiscreen Apparatus. Antibodies were incubated overnight at 4 °C and washed in the PROTEAN II Multiscreen Apparatus. Secondary HRP-labelled anti-subclass-specific antibodies were provided by the Core Facility Monoclonal Antibodies at the Helmholtz Center Munich and incubated 1:1000 in blocking solution for 1 h at RT followed by several washing steps. Afterwards the membrane was removed from the PROTEAN II Multiscreen Apparatus, channels were marked with a pencil and imaged as described previously.

3.2.18.2 Validation of clones by immunofluorescence microscopy

Supernatants of hybridoma clones that were able to recognise CRB1 by western blot analysis were also validated to recognise porcine or human CRB1 by immunofluorescence microscopy, which was done by Sylvia Bolz. For this cryosections of porcine retina sections or control iPSC-derived RO were used. The staining was performed similar to the immunofluorescence microscopy described previously with the following adaptations: After drying of the cryosections for 30 min at 37 °C, 3 washes with PBS were performed for 5 min

at RT. Next sections were incubated for 5 min with 1 % SDS for 5min at RT followed by 3 washes with PBS for 5 min at RT. Sections were blocked for 1 h at RT with blocking buffer consisting of 2 % BSA in 0.1 % PBST. The hybridoma supernatants were incubated 1:2 in blocking buffer overnight at 4°C. Three washing steps were performed for 5 min at RT. Anti-subclass-specific antibodies from the Core Facility Monoclonal Antibodies at the Helmholtz Center Munich were incubated 1:10 in blocking solution for 1 h at RT followed by three washing steps with PBS for 5 min at RT. Finally, a commercially available Alexa Fluor 488 labelled antibody was incubated 1:350 in blocking buffer for 1 hour at RT. After three washing steps with PBS, DAPI staining, mounting, and imaging was performed.

4. Results

Despite insights from several animal models, there is currently no treatment available to counteract or reverse vision loss in patients suffering from *CRB1*-linked IRD [20, 185]. This emphasises the importance of further investigating the disease mechanism in a human-based model and identifying modifiers of the disease severity [20, 185]. In this study, two siblings (referred to as patient A and patient B), which are diagnosed with early-onset RP were investigated. Although both patients had the same homozygous mutation *CRB1* c.2843G>A;p.C948Y (NM_201253.3), only patient A was blind, whereas patient B was less affected and still had remaining visual capacity [22]. Previously, Dr. Achberger generated iPSC-derived RO from both patients and controls, providing a promising tool to further investigate the disease mechanism and genetic modifiers in a proof-of-principle study [22].

4.1 Reduced CRB1 C948Y protein levels and OLM localisation in patient ROs

Even though both patients share the same mutation in *CRB1*, differences in their genetic backgrounds could result in different CRB1 protein levels correlating with the symptom severity. Previously, Dr. Achberger demonstrated that *CRB1* mRNA levels are similar in RO of both patients and control, whereas CRB1 localisation at the OLM is reduced in patient RO compared to controls [22]. However, differences in CRB1 levels between patient A and patient B RO were not investigated [22]. To this end, I first aimed to assess the CRB1 protein levels in the RO of patient A and patient B.

First, several commercially available anti-CRB1 antibodies were tested for western blot analysis using an overexpression construct of human canonical CRB1 fused to a Strep-tag II/FLAG tag at the N-term (CRB1-FLAG) as a positive control (**Appendix 1**). Anti-CRB1 antibody from Abnova (H00023418-A01), which recognises a peptide in the first three EGF domains of the canonical CRB1 (NM_201253.3), was verified to detect CRB1. Next, CRB1 levels in control (K5), patient A and patient B RO lysates at 90, 250 and 350 days of age were analysed by western blot (**Figure 6 A+B**). At 90 days of age, the RO contain ganglion cells, amacrine and horizontal cells and immature photoreceptor cells while Müller glia cells are not yet present [22]. At 250 and 350 days of age, RO are fully mature and contain photoreceptors with segment protrusions, Müller glia cells, bipolar cells, synapses, amacrine and horizontal cells but no ganglion cells [22]. At all time points, CRB1 protein levels were reduced in the RO of patient A and patient B compared to the control (**Figure 6 A+B**). Further quantification revealed that CRB1 protein levels were significantly reduced by at least 50 % in patient A (One-way ANOVA, n=3; $F(2,6) = 14.32$; Tuckey's Multiple Comparison Test, $p<0.05$) and patient B (One-way ANOVA, n=3; $F(2,6) = 14.32$; Tuckey's Multiple Comparison Test, $p<0.01$) compared to control. No significant difference in CRB1 levels was found between patient A and patient B

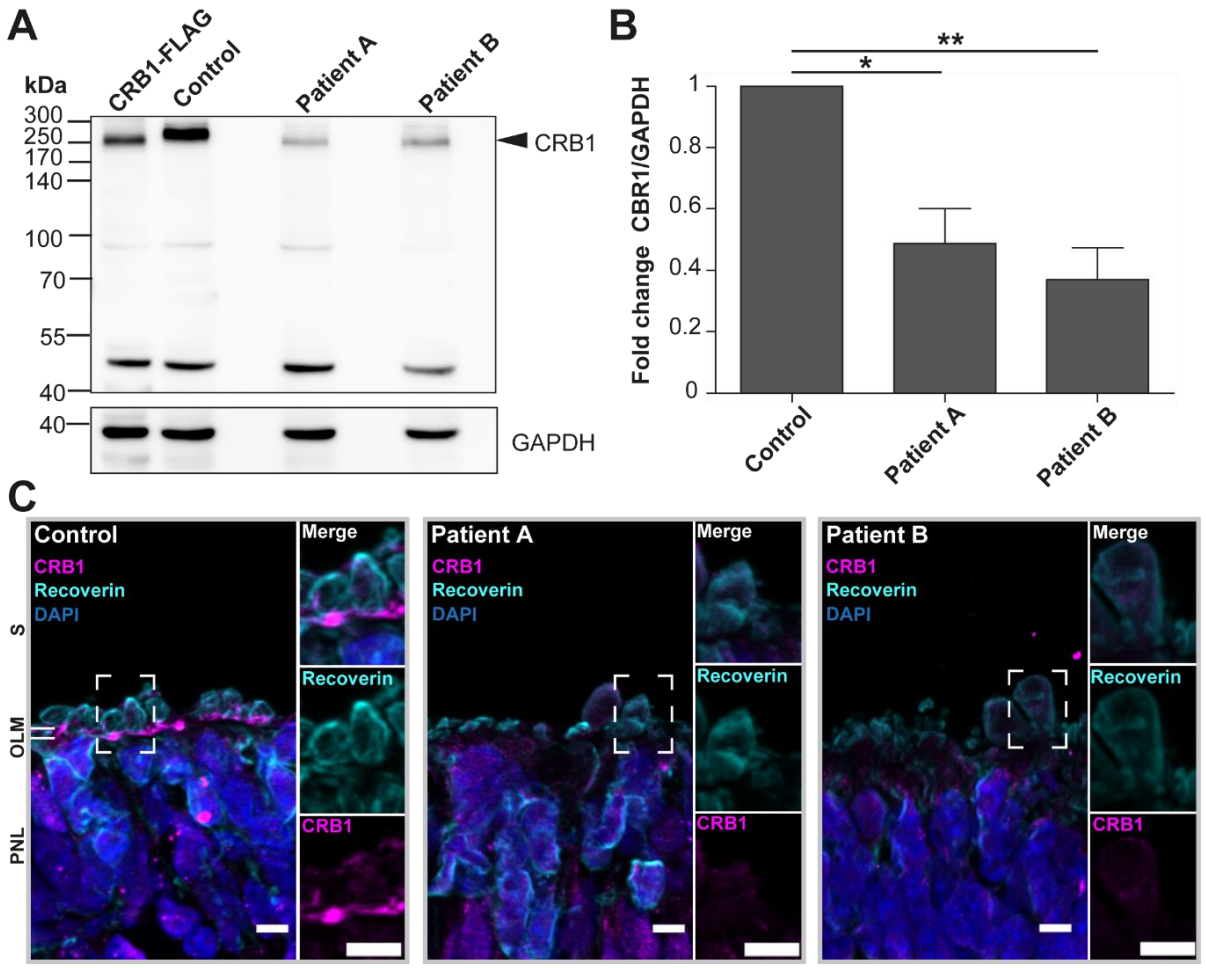

Figure 6| CRB1 patient RO showed a significant reduction in CRB1 protein levels and localisation
(A) CRB1 levels in control (K5), patient A and patient B iPSC-derived RO at 250 days of age were assessed using western blot analysis. GAPDH was used as a loading control. Lysate of HEK293T cells, that were transiently transfected with a FLAG-tagged CRB1 construct (CRB1-FLAG) was used as a positive control. **(B)** Fold change of normalised CRB1 levels relative to GAPDH in patient A and B iPSC-derived RO compared to control RO analysed by western blot. Graph depicts mean ± SEM of three independent experiments using ROs of 90, 250 and 350 days of age. A one-way ANOVA with a Tukey's Multiple Comparison Test was conducted. *p≤0.05; **p≤0.01. **(C)** Immunofluorescence microscopy analysis of CRB1 (magenta), Recoverin (pan-photoreceptor marker, cyan) and DAPI (dark blue) in control, patient A and patient B iPSC-derived RO at 260 days of age. Dashed square marks region of interest (ROI). Three left panels show ROI merge and single channels. Scale bar 5 µm. S=Segments; PNL=photoreceptor nuclear layer; OLM=outer limiting membrane

(One-way ANOVA, n=3; F (2 ,6) =14.32; Tuckey's Multiple Comparison Test, p>0.05) (**Figure 6 A+B**). During this study, a CRB1 antibody was generated together with the monoclonal antibody core facility at Helmholtz (Munich) against a peptide in the CRB1 intracellular domain, which confirmed CRB1 reduction to a similar extent in patient A and patient B RO (**Appendix 2**, see chapter 4.7.3 for detailed antibody description). In addition, CRB1 localisation was assessed by immunofluorescence microscopy using RO at 260 days of age. In control RO, CRB1 was detected above the layer of photoreceptor nuclei encompassing the base of the segment (**Figure 6 C**). In contrast, no CRB1 signal was observed at the base of the photoreceptor segments in the iPSC-derived RO of patient A and patient B.

Taken together, these data indicate that cellular processes that require the canonical full-length CRB1 protein may be affected in CRB1-patients. In addition, since CRB1 is reduced to

a similar extent in both patient RO, CRB1 levels may not explain the severity of symptoms. In the following chapters, three possible molecular mechanisms underlying the CRB1 reduction in the case of the *CRB1* c.2843G>A;p.C948Y mutation were investigated.

4.2 Molecular mechanism underlying CRB1 protein reduction by *CRB1* c.2843G>A;p.C948Y mutation

4.2.1 CRB1 C948Y did not influence BIP levels in patient RO

The CRB1 residue p.C948 has been described to form a disulfide bond with p.C681, which supports structural stability and protein folding [12]. The formation of disulfide bonds is catalysed in the ER, where misfolded proteins are degraded through the ER-associated degradation (ERAD) pathway [186]. However, when misfolded proteins accumulate in the ER, the unfolded protein response (UPR) is activated [186]. The 78-kDa binding immunoglobulin protein (BIP), is a commonly used marker of ER stress [187]. To assess if the CRB1 p.C948Y induces ER stress, BIP levels in patient and control RO were analysed by western blot (**Figure 7 A+B**). Of note, as only two independent experiments were performed, the data should be

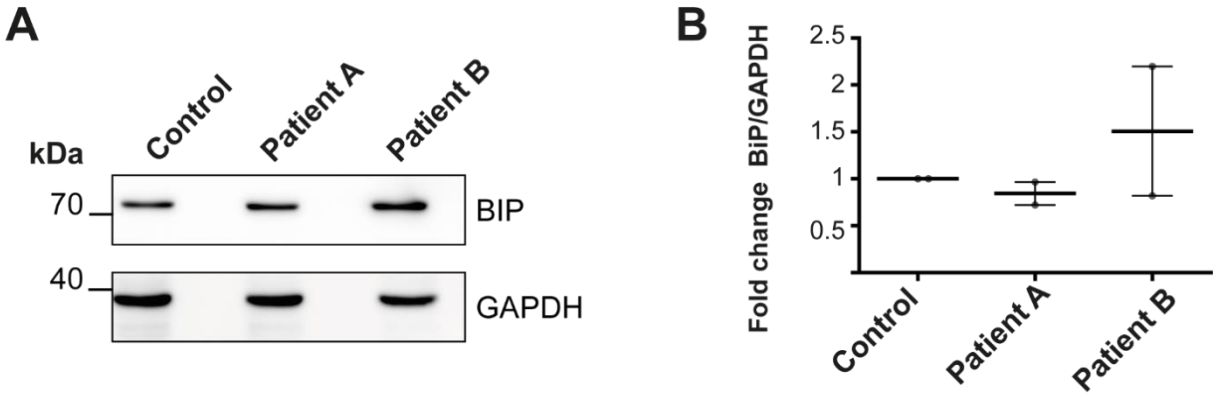

Figure 7| CRB1 p.C948Y did not influence BIP levels in patient iPSC-derived RO
BIP levels were analysed in patient A, patient B and control (K5) iPSC-derived RO of 250 and 350 days of age using western blot analysis. GAPDH was used as loading control. (A) Representative blot and (B) quantification of BIP/GAPDH levels. Data and is depicted as mean ± SEM of two independent experiments.

considered preliminary. No difference in the amount of BIP was observed between patient A and control iPSC-derived RO. For patient B, one experiment showed similar levels of BIP in patient B compared to control and the second experiment showed an approximately 2-fold increase in BIP. Since both patients showed a similar reduction in CRB1 levels but no consistent increase in BIP levels, it is concluded that CRB1 C948Y may not directly induce ER stress.

4.2.2 *CRB1* c.2843G>A led to a partially misspliced *CRB1* transcript

The *CRB1* c.2843G>A marks the first base of the splice acceptor site of exon 9 (NM_201253.3), which could lead to a misspliced *CRB1* transcript (**Figure 8 A**). This

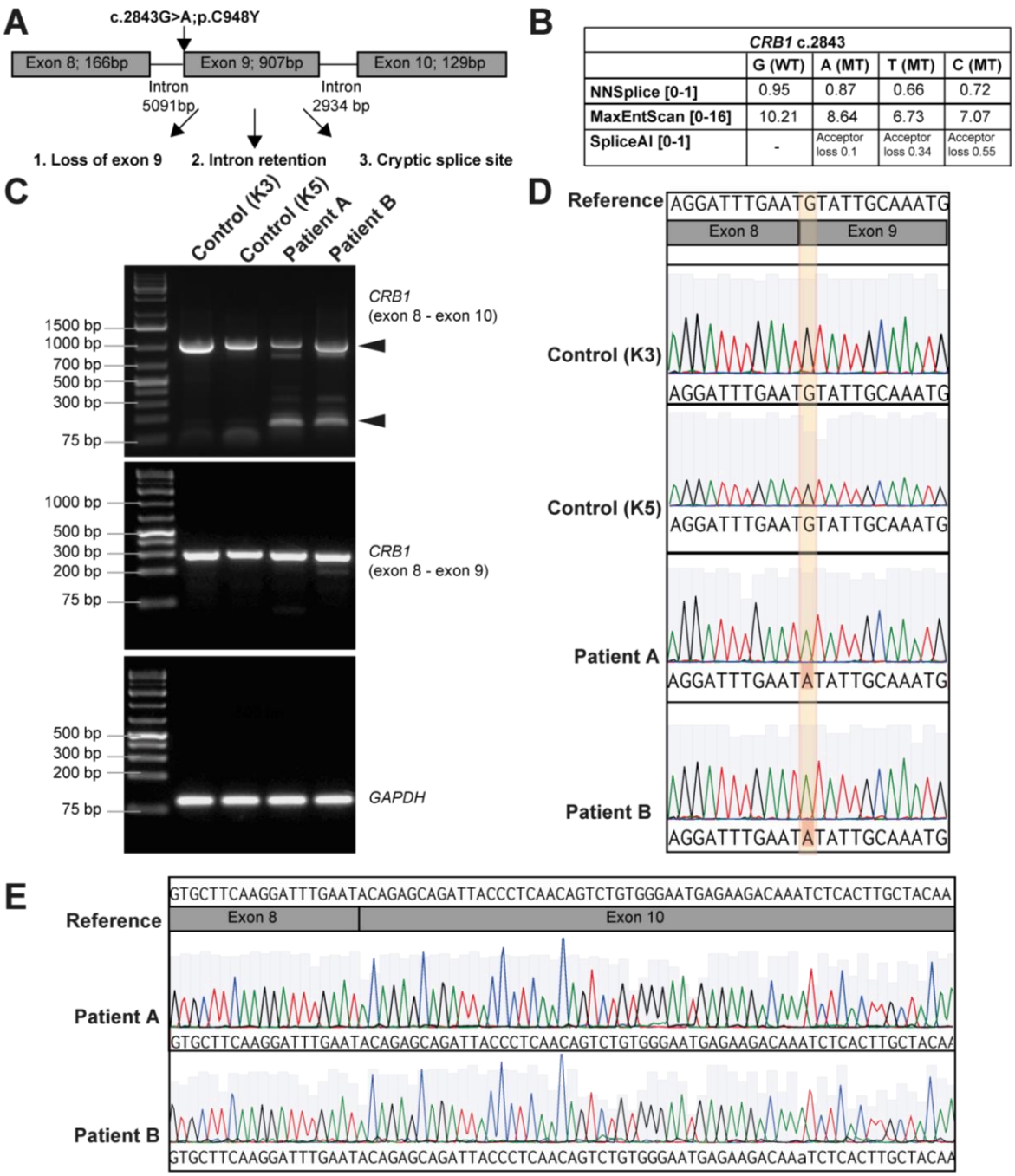

Figure 8| CRB1 c.2843G>A partially led in part to a misspliced CRB1 transcript
(A) Illustration of the exon 8- exon 10 junctions of the *CRB1* locus carrying the c.2843G>A mutation. **(B)** *In-silico* analysis of mutations at *CRB1* c.2843 using three different splice prediction tools (NNSplice, MaxEntScan and SpliceAI). **(C)** RNA was isolated from two control (K3 and K5), patient A and patient B RO. DNAse treatment and cDNA synthesis were performed. End-point PCR was executed using exon spanning primers CRB1 exon 8-10 (upper panel), CRB1 exon 8-9 (middle panel) and GAPDH (lower panel) and analysed by agarose gel electrophoresis. **(D-E)** Sanger sequencing electropherograms of the amplicons obtained with **(D)** exon-spanning primers from exon 8 to 9 or **(E)** the 100 bp amplicon obtained using exon 8 to 10 exon spanning primers. The residue of the mutation is highlighted in orange.

misspliced variant could be degraded by nonsense-mediated mRNA decay or lead to an unstable protein variant, which would explain lower CRB1 protein levels in patient RO. To assess the splicing of the *CRB1* c.2843G>A transcript, an *in silico* splice analysis was performed using three different splice prediction tools (**Figure 8 B**). Overall, c.2843G>T and

c.2843G>C were predicted to be more likely to affect *CRB1* splicing compared to c.2843G>A. All three tools showed a maximum probability of 16 % that c.2843G>A will cause an aberrant splicing pattern compared to WT. For instance, SpliceAI predicted a 10 % probability that c.2843G>A will result in a splice acceptor loss.

Next, RNA was isolated from iPSC-derived RO (330 days of age) from two controls (K3 and K5), patient A and patient B, followed by DNAse digestion and cDNA synthesis. Endpoint PCR was performed using *GAPDH* primer as an internal control, which confirmed efficient cDNA synthesis for all samples (**Figure 8 C**). Using a primer pair flanking exon 8 and 9, a specific amplicon of the expected size of approximately 299 bp was detected in both CRB1 patient samples and the control, thus excluding the retention of the intron (**Figure 8 C**). This amplicon was further validated by Sanger Sequencing, which also confirmed the c.2843G>A in both patients (**Figure 8 D**). In addition, primers flanking exon 8 to exon 10 were used to investigate potential skipping of exon 9. While the control samples showed only one amplicon of approximately 1000 bp, the CRB1 patient samples showed two prominent amplicons. One of these amplicons was seen at 1000 bp, similar to control samples, and one at approximately 100 bp, suggesting skipping of exon 9. Therefore, the 100 bp amplicon seen in the patient samples was sent for Sanger sequencing, which confirmed skipping of exon 9 in this amplicon (**Figure 8 E**).

Taken together, data suggest that c.2843G>A led to at least two *CRB1* transcript variants, one containing exon 9 and the other skipping exon 9. Skipping of exon 9 results in a frameshift and a premature stop codon after 31 aa in exon 10, which encodes the 18th EGF domain of canonical CRB1. Therefore, nonsense-mediated mRNA decay or a truncated CRB1 protein in the case of CRB1 c.2843G>A mutation may contribute in part to the CRB1 reduction. Next, the consequences of the C948Y mutation on the protein level and the CRB1-CRB1 interaction were investigated.

4.2.3 CRB1 C948Y mildly affected CRB1-CRB1 homophilic interaction

4.2.3.1 CRB1 homomer formation was mediated by the extracellular domain

Up to now, the function of the extracellular domain is poorly described [170]. Evidence in *Drosophila* germline epithelium indicate a potential role for the extracellular domain in regulating Crb membrane stability, as overexpression of the Crb extracellular domain fused to GFP localises to the apical membrane, whereas overexpression of the intracellular domain induces endocytosis of the endogenous Crumbs [23]. In addition, Zou *et al.* showed in zebrafish that Crb2a and Crb2b interact through their extracellular domains and contribute to the OLM integrity and formation of the cone mosaic [140]. Nonetheless, the interaction of human CRB1-CRB1, which may be essential for CRB1 stability and localisation, has not been investigated. Therefore, overexpression constructs of human canonical CRB1 or GFP, as a

control, fused to a FLAG-tag or HA-tag were generated. Following pairwise co-expression in HEK293T cells for 48 hours, co-IP using FLAG-beads and western blot analysis were performed. A strong interaction between CRB1-FLAG and CRB1-HA was detected (**Figure 9 A**). No interaction was observed between CRB1 and GFP excluding unspecific binding of

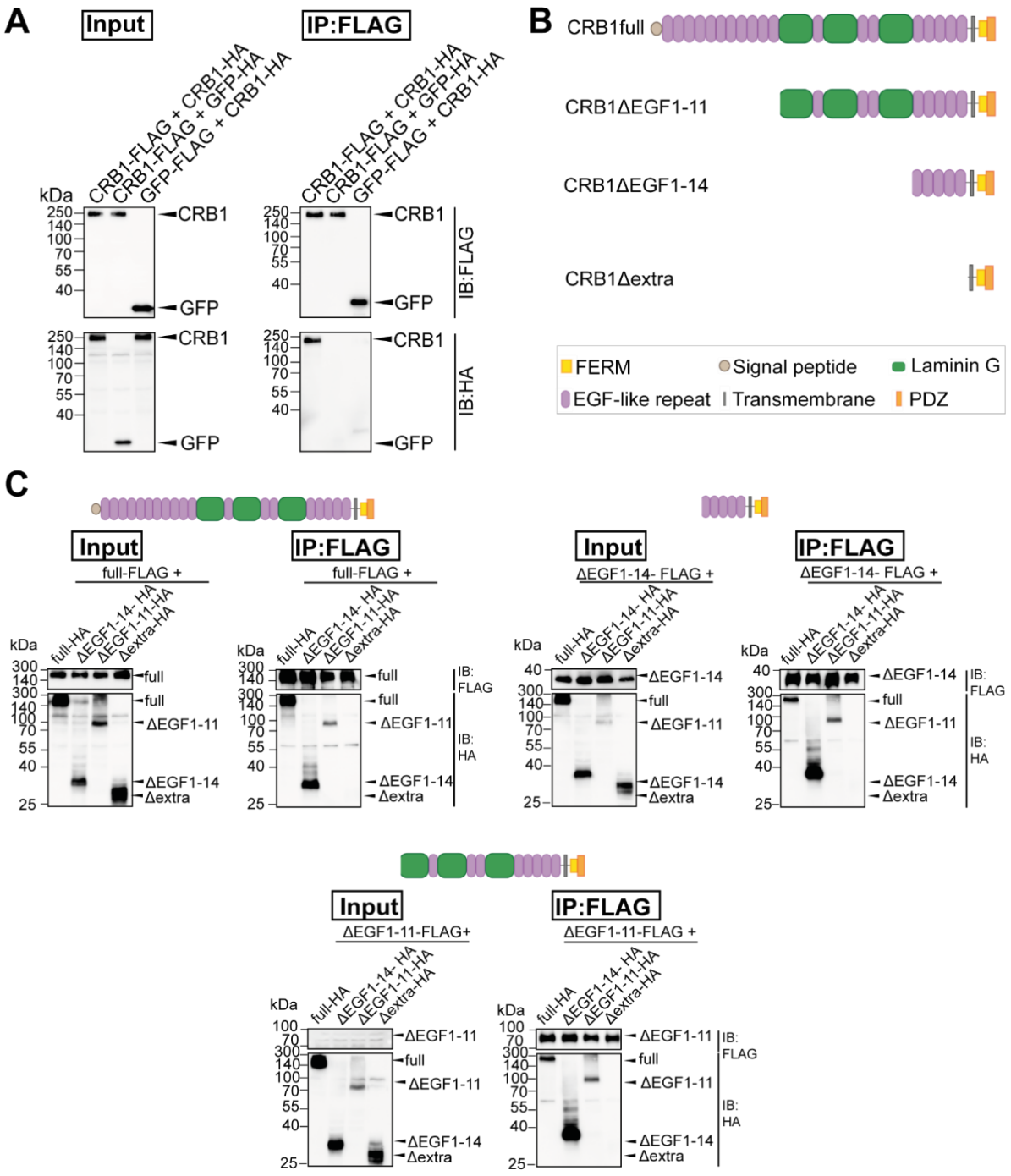

Figure 9| CRB1-CRB1 homotypic interaction was dependent on the large extracellular domain
(A) HEK293T cells were co-transfected with CRB1-FLAG or GFP-FLAG and CRB1-HA or GFP-HA. Input (left panel) and eluates upon Flag-IP (right panel) were performed and immunoblotted (IB) with FLAG and HA antibodies. Blot is representative of three independent experiments. **(B)** Schematic representation of the full-length and the truncated CRB1 construct. Colours represent the predicted protein domains. **(C)** CRB1 full-length or CRB1 truncated FLAG tagged constructs were co-transfected with full-length or truncated CRB1-HA constructs. Following FLAG-IP input (left panel) and eluates (right panel) were analysed by western blot using FLAG and HA antibodies.

CRB1 to tag or beads. The protein structure of canonical CRB1 consists of a large extracellular domain, containing a signal peptide, multiple EGF-like repeat domains and laminin G domains, a transmembrane domain and an intracellular PDZ and FERM domain [11, 12, 89]. To assess which domain is involved in the CRB1-CRB1 homotypic interaction, FLAG- or HA-tagged truncated CRB1 proteins were co-transfected in HEK293T cells followed by FLAG co-IP (**Figure 9 B**). No interaction was observed between CRB1 lacking the complete extracellular domain (CRB1Δextra) and CRB1 containing the full extracellular domain (CRB1full) indicating that the presence of the extracellular domain is essential for CRB1-CRB1 binding (**Figure 9 C**). Interestingly, the five EGFs flanking the transmembrane domain (CRB1ΔEGF1-14 and CRB1ΔEGF1-11) were sufficient to induce binding to CRB1full. Similar results were obtained when CRB1ΔEGF1-14-FLAG and CRB1ΔEGF1-11-FLAG were used as bait.

Collectively, these data indicate that the CRB1 extracellular domain is critical for the CRB1-CRB1 interaction. As a next step, the consequences of patient mutations in the extracellular domain including CRB1 C948Y were investigated.

4.2.3.2 *CRB1* missense mutations mildly influenced CRB1-CRB1 homomer formation

As the data presented above suggest that the CRB1 extracellular domain is essential for CRB1-CRB1 homophilic interactions and most of the patient mutations are located in the extracellular domain, the next aim was to assess the influence of selected mutations on the CRB1-CRB1 interaction. Several patient-described *CRB1* missense mutations were introduced into the FLAG- and HA-tagged canonical CRB1 construct by site-directed mutagenesis (SDM) (**Figure 10 A**) [8]. Mutations were selected covering regions of the extracellular domain, that are conserved in the canonical and the CRB1-B isoforms and, in particular, in the EGF-domains flanking the transmembrane domain [8, 91]. Next, FLAG- and HA- CRB1 WT or MT constructs were co-transfected in HEK293T cells. Immunoprecipitation (IP) using FLAG beads was performed followed by western blot analysis (**Figure 10 B+C**).

Overall, none of the mutations led to a significant reduction or complete loss of CRB1-CRB1 interaction. The data suggest that CRB1 p.C681Y adheres to a similar extent as CRB1 WT. A slight reduction of up to 10 % compared to WT was observed for CRB1 p.G1103R, p.Y1161C, p.C1181R and p.C1317H. CRB1 p.C480R retained approximately 88 % of the WT CRB1-CRB1 binding capacity. A loss of approximately 30 % was observed for the CRB1 p.C948Y interaction compared to CRB1 WT. A 50 % reduction in binding capacity was observed for p.C1321S, which is located in the EGF domain flanking the transmembrane domain.

Collectively, these date indicate that the majority of CRB1 missense mutations tested in this study led to a mildly impaired CRB1-CRB1 interaction *in vitro* rather than a complete loss

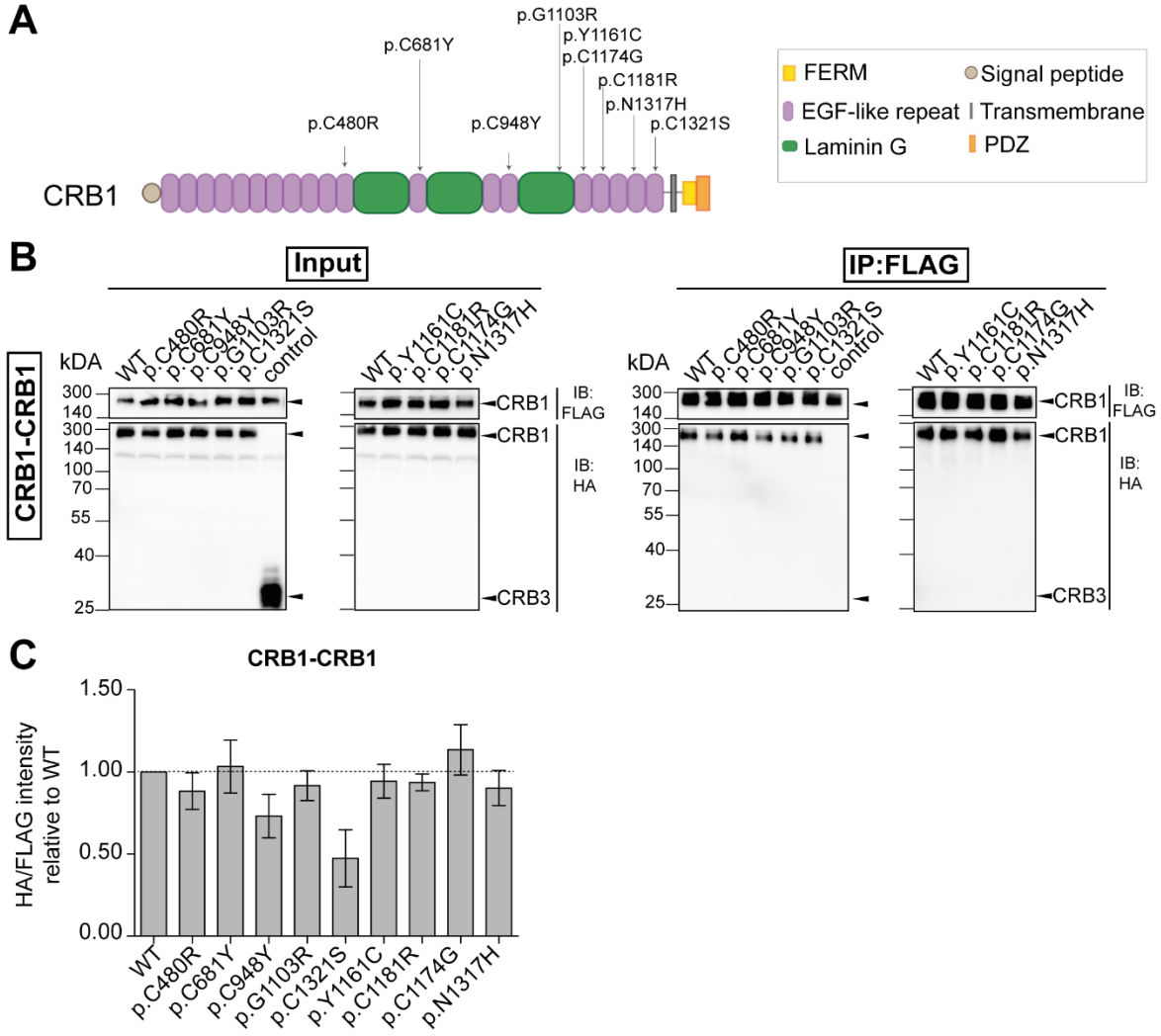

Figure 10| A panel of CRB1 missense mutations mildly influenced CRB1-CRB1 homophilic interactions
(A) Graphical illustration of canonical CRB1 and the introduced missense mutations described in patients. Colours represent described protein domains. **(B)** HA- and FLAG-tagged CRB1 WT and MT constructs were overexpressed in homozygous pairs in HEK293T cells. Western blot analysis was performed before (input) and after FLAG-IP using a FLAG- and HA-specific antibody. Representative blot of three independent experiments is shown. **(C)** Quantification of the fold change HA/FLAG of different CRB1 MT relative to WT after co-IP. Mean ± SEM of three independent experiments are depicted. For statistical analysis, a one-way ANOVA with a Tukey's Multiple Comparison Test was conducted but no significant difference was found.

of CRB1-CRB1 interaction. Next, the consequences of loss of complete EGF domains were investigated.

4.2.3.3 Loss of a single EGF domain did not disrupt CRB1-CRB1 interaction

As missense mutations did not completely disrupt CRB1-CRB1 interaction, various EGF domains were depleted in the canonical CRB1 isoform to identify, which of the 5 EGF domains flanking the transmembrane domain might be important for CRB1-CRB1 interaction. The results obtained for the p.C1321S mutation and for the truncated CRB1 construct led to the hypothesis that the last EGF domain flanking might be crucial for CRB1-CRB1 interaction. To

address this, EGF domain 15, 17, 18 and 19 were deleted by SDM in the FLAG- and HA-tagged canonical CRB1 overexpression construct (**Figure 11 A**).

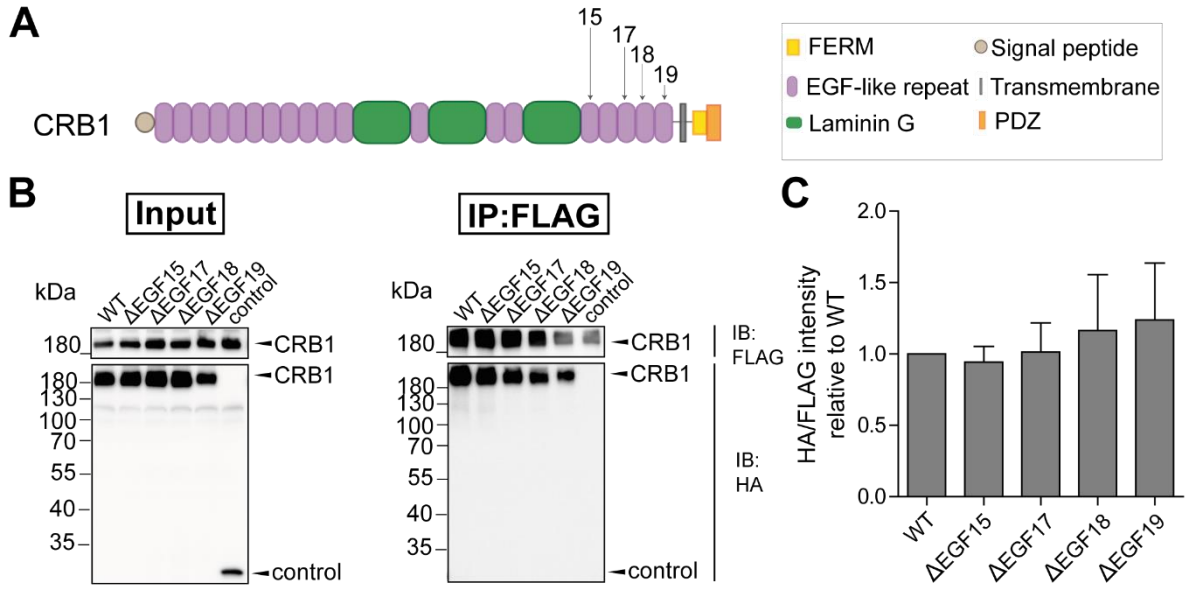

Figure 11| EGF domain 15, 17, 18 and 19 were not solely essential for CRB1-CRB1 interaction
(A) Schematic representation of canonical CRB1. Colors depict different protein domains and arrows indicate the respective EGF domain, which was deleted by SDM. **(B-C)** Co-IP was performed with the HA- and FLAG-tagged canonical CRB1 constructs lacking different EGF domain (ΔEGF), as described previously. GFP-HA was transfected as control. Input and eluates after FLAG-IP were analysed by western blot using an anti-HA and anti-FLAG antibodies. **(B)** Representative blots of one out of three independent experiments are shown. **(C)** Quantification of the ratio of the HA/FLAG intensity of three independent experiments. Graph depicts Mean ± SEM. One-way ANOVA was performed for statistical analysis. For statistical analysis, a one-way ANOVA with a Tukey's Multiple Comparison Test was conducted but no significant difference was found.

Constructs were transiently overexpressed in HEK293T cells in a pairwise homozygous manner. As previously described, FLAG-co-IP was performed and analysed by western blot analysis. Contrary to the hypothesis, deletion of any of the EGF domain 15, 17, 18 or 19, did not disrupt CRB1-CRB1 interaction (**Figure 11 B+C**). These data indicate that either multiple domains in the extracellular domain are involved in canonical CRB1 homotypic interaction or that the EGF domain 16, for which, unfortunately, no deletion construct could be obtained, is critical for the CRB1-CRB1 interaction.

Collectively, three mechanisms were analysed that might underlie the CRB1 reduction in patient RO. While no difference in the ER stress marker BIP was observed, a misspliced *CRB1* transcript lacking exon 9 was detected in patient RO carrying the *CRB1* c.2843G>A;p.C948Y mutation. Furthermore, CRB1 C948Y mildly impaired human CRB1-CRB1 interaction *in vitro*.

4.3 Retinal pull-down approach of CRB1 revealed new interactors of the crumbs complex in the retina

In the last chapter, possible molecular mechanisms underlying the CRB1 protein reduction by c.2843G>A;p.C948Y were investigated. The consequences of the CRB1 protein reduction and the loss of OLM localisation are that any cellular process that is executed or dependents

on the expression and localisation of canonical CRB1 is affected in the two patients. In the retinal context, the functions of human CRB1, particularly of the large extracellular domain, are poorly understood. PPI analysis provides a powerful method for predicting protein functions. Therefore, the next aim was to assess the retinal CRB1 PPI network.

4.3.1 CRB1 was exclusively expressed in the neuroretina

To select the optimal approach for CRB1 PPI analysis, the expression of *CRB1*, *CRB2* and *CRB3* in iPSC-derived RO and RPE, and different cell lines was explored by RT-qPCR. As Crumbs proteins are key regulators of cell polarity, HEK293T, HELA, hTERT-RPE1 and ARPE19 cells were cultured with and without serum. Serum starvation induces amongst other cilia formation and affects protein expression levels [188]. As multiple transcripts have been described for *CRB1* and *CRB2*, multiple exon spanning primer pairs were used to cover the majority of isoforms [15]. The primer pairs were previously used and validated by Pellissier *et al.* [15]. The full-length canonical isoform of *CRB1* is detected by the intron spanning primer pairs exon 4/5 and exon 11/12 [15]. The *CRB1* isoform lacking exon 4 and exon 5 is recognised by the primer pair spanning exon 2/5 and the truncated *CRB1* isoform lacking the C-term cytosolic and transmembrane domain is covered by the primer pair spanning exon 4/5 [15]. Of note, the *CRB1-C* and *CRB1-B* isoforms were not at the time of this experiment and were therefore not included in the screen [91].

The data suggest that all *CRB1* isoforms are highly expressed in iPSC-derived RO (**Figure 12 A**). In addition, relatively low levels of *CRB1* mRNA were also detected in iPSC-derived RPE cells and SH-SY5Y cells. No expression was detected in HELA, HEK293T, hTERT-RPE1 and ARPE19 cells, regardless of the cultivation with or without serum. Similar to *CRB1*, *CRB2* was highly expressed in iPSC-derived RO (**Figure 12 B**). In addition, ARPE19 cells expressed *CRB2* with or without serum cultivation. A low level expression was of *CRB2* detected in iPSC-derived RPE. In contrast to *CRB1* and *CRB2*, *CRB3* is less expressed in iPSC-derived RO but shows relatively higher expression in iPSC-derived RPE (**Figure 12 C**). Furthermore, HELA, HEK293T and ARPE19 cells express low levels of CRB3.

Taken together, these data indicate that high levels of *CRB1* were highly expressed in iPSC-derived RO. Therefore, iPSC-derived RO would provide the most optimal system to study and validate CRB1 PPI.

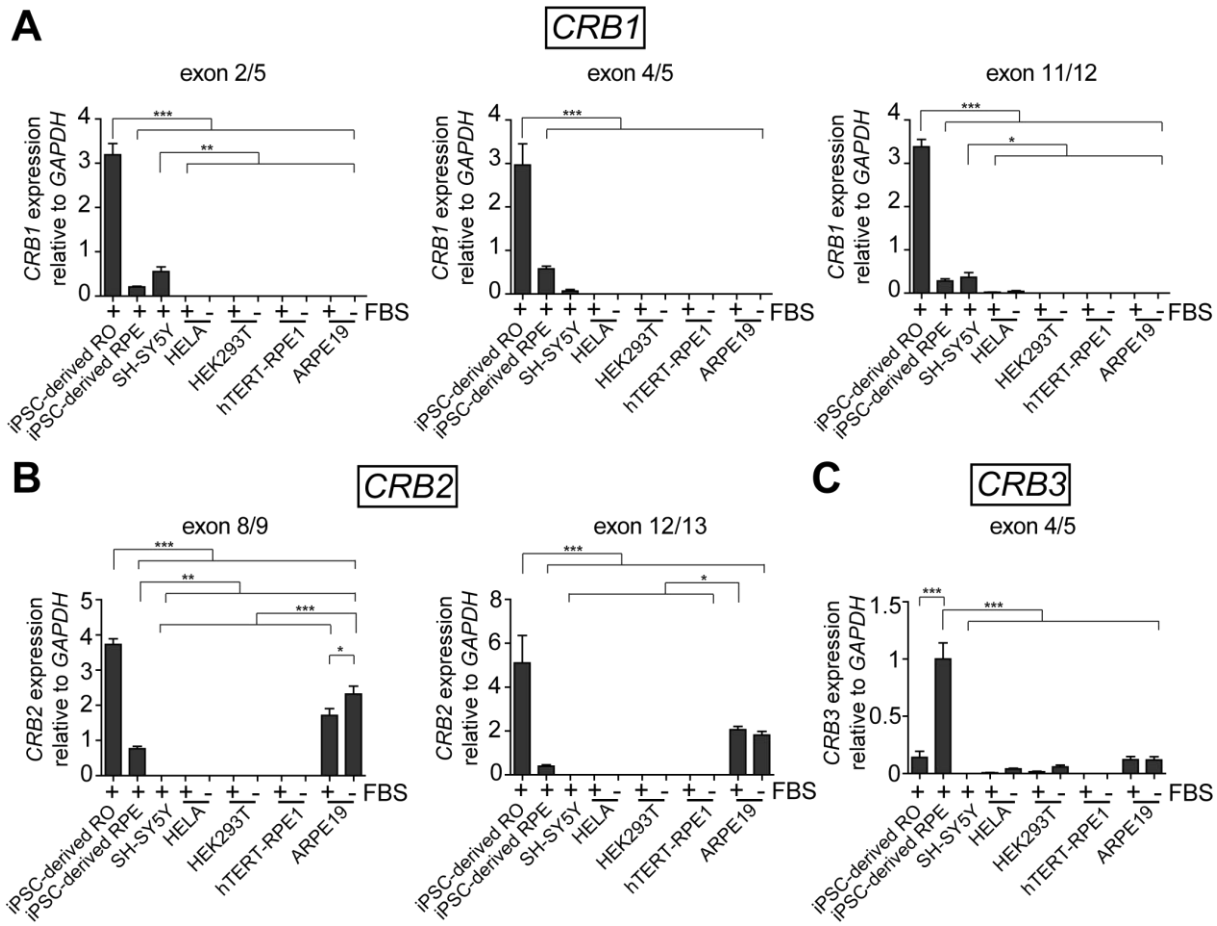

Figure 12| CRB1 and CRB2 were highly expressed in iPSC-derived retinal organoids
RNA was isolated from control iPSC-derived RO, iPSC-derived RPE and different cell lines (SH-SY5Y, HEK293T, HELA, hTERT-RPE1 and ARPE19) with and without serum (FBS) cultivation. After cDNA synthesis, the relative expression of **(A)** *CRB1* transcripts, **(B)** *CRB2* transcripts and **(C)** *CRB3* transcripts to *GAPDH* was analysed by RT-qPCR. Graph depicts mean ± SEM of three technical replicates of one biological replicate. A one-way ANOVA with a Tukey's Multiple Comparison Test was conducted. *p≤0.05; **p≤0.01, ***p≤0.001

The culture and maintenance of ROs are costly, time consuming and small scale in terms of the protein output, which is required for PPI studies. A recently published protocol by Beyer *et al.* describes a rapid and reliable pull-down approach to perform tissue- and isoform-specific protein complex analysis [176]. This would provide the opportunity to study not only the PPI of different CRB1 isoforms but also of different CRB1 MTs in a retina-specific context [176]. The porcine retina resembles the human retina regarding the neuronal structure, histological and anatomical characteristics [189]. In addition, the protein similarity is significantly higher between human and pigs then that between human and mouse [190]. This holds true for the conservation of the Crumbs protein family. Porcine and human CRB1 and CRB2 are 74.3 % and 84.5 %, identical regarding in amino acid sequence, respectively (**Appendix 3**). In addition, human and porcine CRB1 were detected at a similar height by western blot analysis using the Abnova N-term anti-CRB1 antibody, and significantly higher *CRB1* mRNA expression in the retina compared to muscle tissue was confirmed by RT-qPCR using two intron spanning primes for exon 6/7 and exon 9/10 (two-sided unpaired Student's t-test, n=3, $p < 0.001$) (**Figure 13 A+B**). Furthermore, porcine CRB1 also localises to the OLM in the porcine retina, which

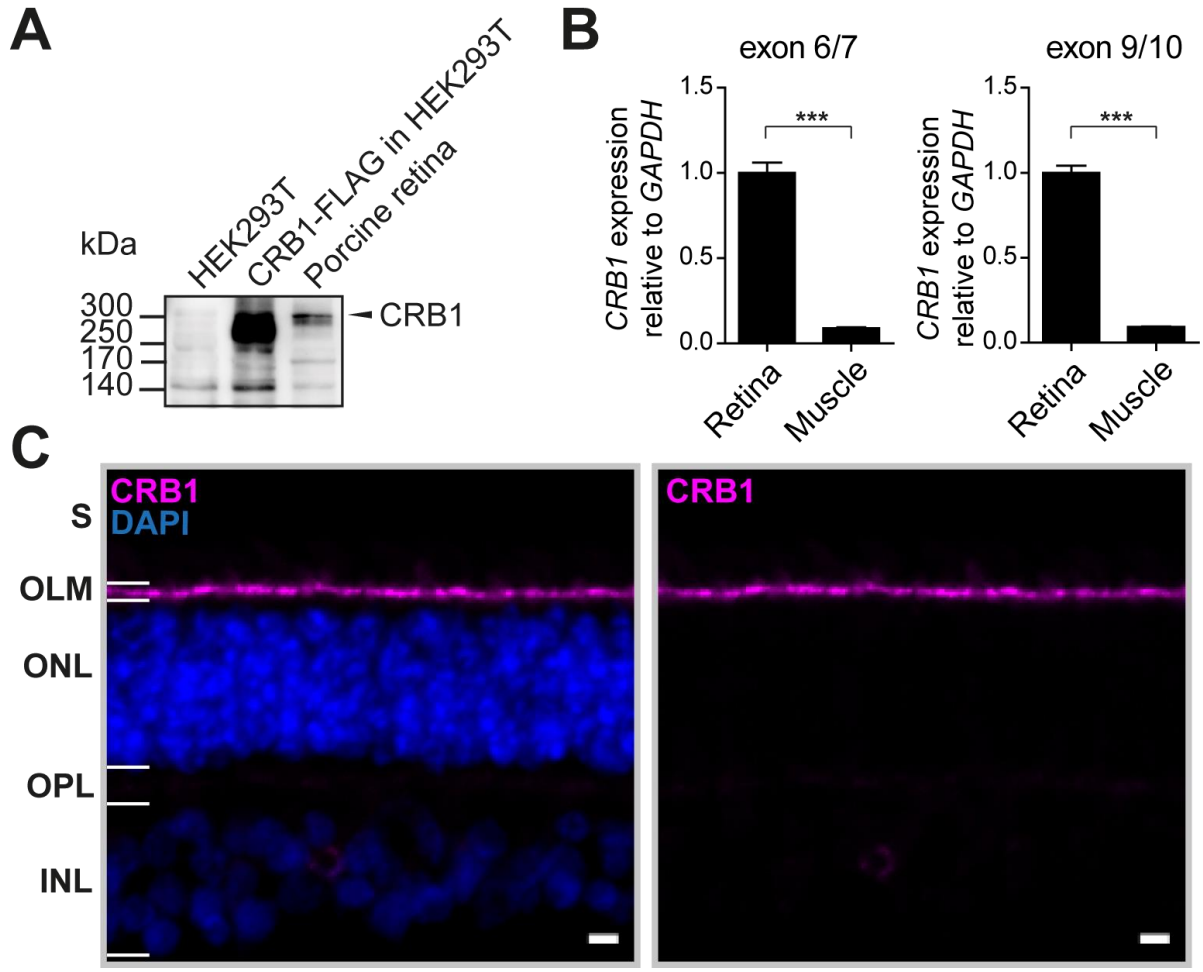

Figure 13| Porcine CRB1 localised at the OLM and was high expressed in the porcine retina
(A) Western blot analysis of lysate of non-transfected HEK293T cells, HEK293T cells transiently overexpressing a CRB1-FLAG tagged construct and porcine retina lysate. Anti-CRB1 antibody from Abnova was used for detection **(B)** RT-qPCR was performed using porcine *CRB1* specific intron spanning primers targeting exon 6-7 and exon 9-10 using cDNA from porcine retina and porcine muscle (control). Porcine specific *GAPDH* primers were used as a housekeeping control. Graph depicts mean ±SEM of three technical replicates of one biological replicate. A two-sided unpaired Student's t-test was executed. *** p≤ 0.001. **(C)** Localisation of CRB1 (magenta) in porcine retina analysed by immunohistochemistry. Intracellular CRB1 antibody (25G2) was used (described in chapter 4.7.3). S=segments, OLM=outer limiting membrane, ONL=outer nuclear layer, OPL=outer plexiform layer, scale bar 5 µM.

was confirmed by immunofluorescence microscopy using an antibody against the CRB1 intracellular domain, as described in chapter 4.7.3 (**Figure 13 C**). Given this reason, a porcine retinal pull-down approach was chosen to study CRB1 PPI in the retina.

4.3.2 Porcine retinal pull-down approach of human canonical CRB1-FLAG WT revealed novel interactors of the crumbs complex

To investigate the PPI of CRB1 in a retinal context, a porcine retinal pull-down workflow was performed (**Figure 14 A**) [176]. Therefore, human canonical CRB1 was fused to a Strep-tag II/FLAG tandem affinity purification tag at the N-term (CRB1-FLAG) [172]. Subsequently, CRB1-FLAG or GPF-FLAG (control) was transiently overexpressed in HEK293T cells. After 48 hours, FLAG-IP was performed followed by washing steps with 0.01 % SDS to purify baits from unstable HEK293T interactors. Next, purified bait proteins were incubated with or without

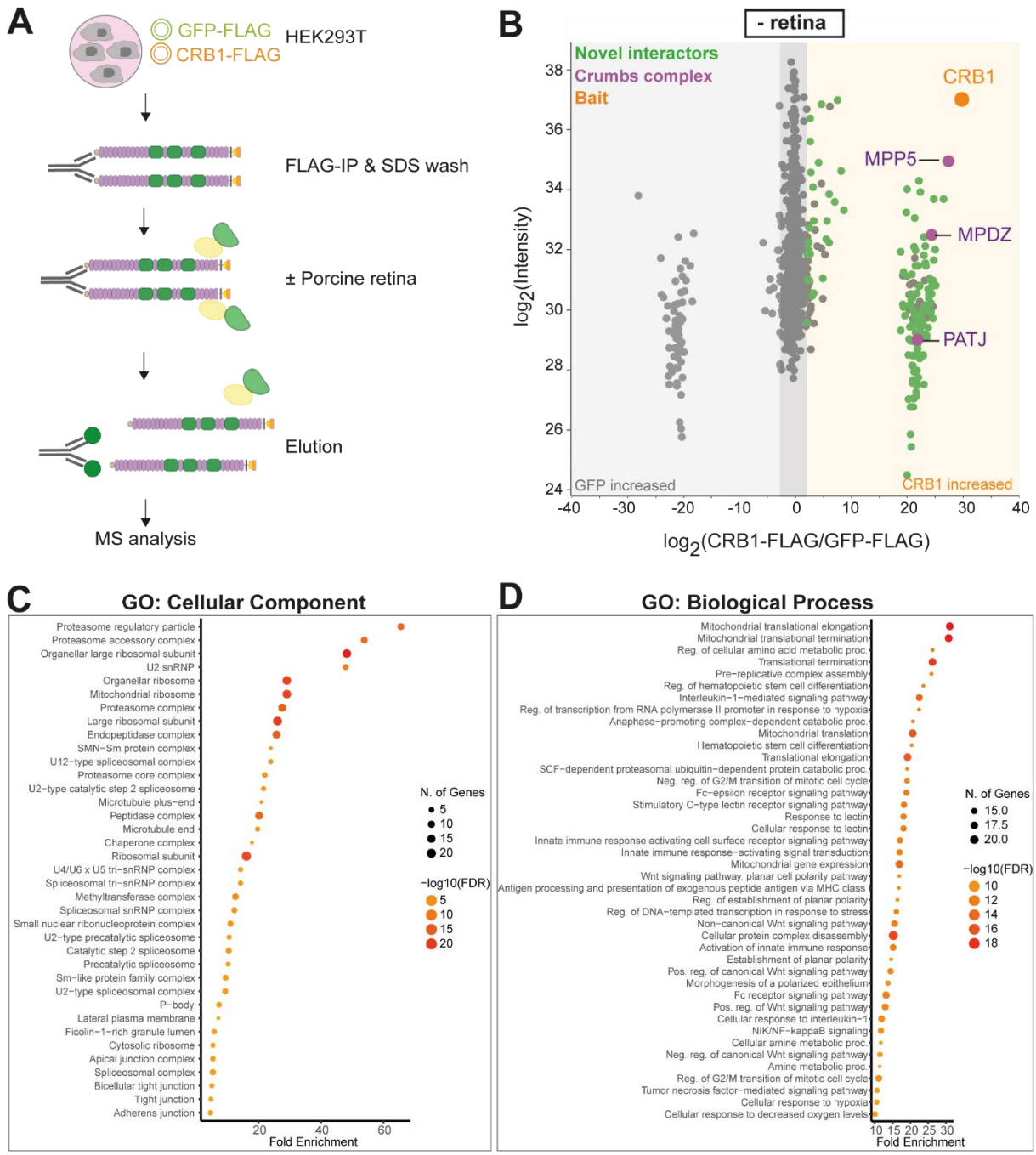

Figure 14| Significantly enriched proteins after stringent SDS washing of canonical CRB1-FLAG without porcine retinal lysate incubation

(A) N-term FLAG tagged canonical CRB1 or FLAG-tagged GFP (control) was transiently overexpressed in HEK293T cells for 48 hours. Following FLAG-IP, baits were washed with 0.01% SDS and incubated with or without porcine retinal lysates. Next, baits and interacting proteins were eluted by competitive elution with FLAG-peptide. The eluates were analysed by mass spectrometry. **(B)** Scatter plot of the $\log_2$ ratio of proteins identified in CRB1-FLAG relative to GFP-FLAG (control) without retina incubation. Every dot depicts a protein. CRB1 is shown in orange. Significant enriched proteins in CRB1-FLAG samples compared to GFP are shown in green. CRB complex members that were significantly enriched are depicted in purple (One-sample t-test, FDR 0.05, $\log_2$ ratio (CRB1-FLAG/GFP-FLAG) >2, n=6). **(C-D)** Gene ontology (GO) enrichment analysis was performed using ShinyGO in two categories, **(C)** CC and **(D)** BP using the significantly enriched proteins in CRB1-FLAG samples compared to GFP without porcine retina incubation (One-sample t-test, FDR 0.05, $\log_2$ ratio (CRB1-FLAG/GFP-FLAG) >2, n=6). Top 50 significantly enriched pathways are depicted (FDR<0.05).

porcine retinal lysate followed by elution with the competitive FLAG-peptide and analysis by mass spectrometry and DDA. All samples were analysed against the UniProt *sus scrofa* proteome database. Comparison of significant high abundance proteins in CRB1-FLAG

samples relative to GFP-FLAG, which served as a control to determine proteins unspecifically bound to beads or the FLAG-tag, allowed determination of the CRB1 PPI network. Samples that were not incubated with porcine retinal lysate allowed identification of CRB1 interactors that may have remained from HEK293T cells after SDS washing. Functional information on proteins was obtained from the UniProt database [276].

First, samples without porcine retinal lysate incubation were explored. After SDS washing, the human CRB1-FLAG bait was detected by mass spectrometry with a peptide coverage of up to 30 % (**Appendix 4**). In addition to CRB1, 138 proteins were found to be significantly more abundant in the CRB1-FLAG samples compared to control (One-sample t-test, FDR 0.05, $\log_2$ ratio >2, n=6) (**Appendix 5**). Amongst these, the core CRB complex member MPP5 and the MPP5 interactors, PATJ and MPDZ were found, indicating that the stable CRB complex was not disrupted by SDS wash (**Figure 14 B**). To further analyse the remaining interactors Gene Ontology (GO) enrichment analysis was performed, which was divided into two categories, cellular component (CC) and biological process (BP) (**Figure 14 C+D**). In the CC category, pathways associated with protein biosynthesis and degradation, for instance ribosome, proteasome, peptidase, P-body and chaperone complex were found to be significantly enriched. Other significantly enriched components included the 'lateral plasma membrane', 'tight junctions', 'adherens junctions' and the 'microtubule end' (**Figure 14 C**). In the second category of BP, in addition to pathways associated to 'mitochondria', 'translation', 'transcription', significant enriched pathways link CRB1 to 'Interleukin-1-mediated signalling' (e.g. TAB1), 'WNT signalling pathway' (e.g. SPIN1, CCDC88C), and 'Tumour necrosis factor-mediated signalling pathway' (e.g. JAK2) (**Figure 14 D + Figure 15**). In addition, proteins that

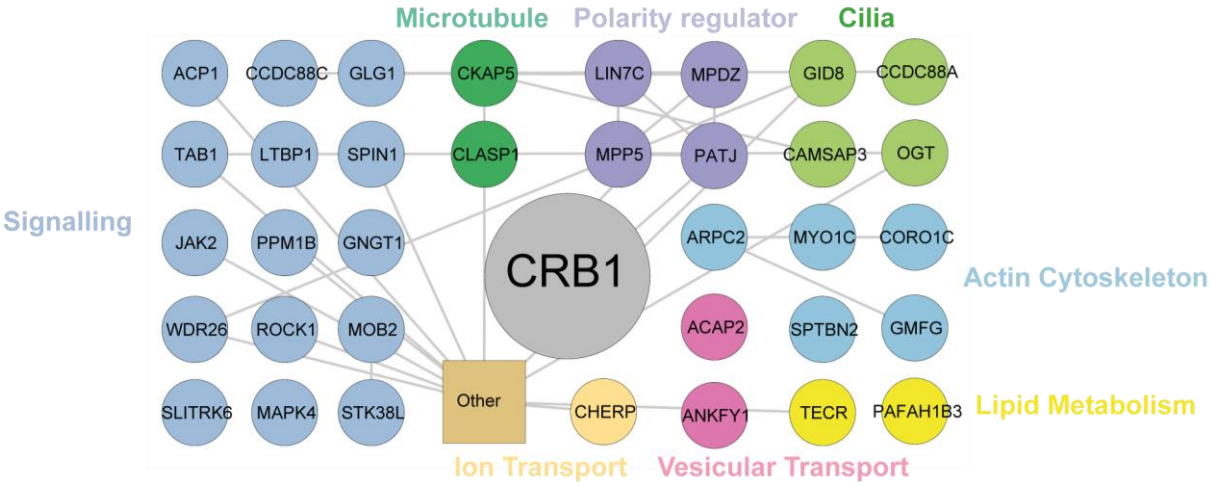

Figure 15| Significantly highly abundant proteins in CRB1-FLAG SDS washed samples included known crumbs complex members
Significantly enriched interactors in canonical CRB1-FLAG compared to GFP-FLAG without incubation of porcine retina were analysed by using String and Cytoscape (One-sample t-test, FDR 0.05, $\log_2$ ratio (CRB1-FLAG/GFP-FLAG) >2, n=6). Colours represent biological function as categorised by the UniProt database. Of note, some proteins may fit to multiple categories. Grey lines show previously reported interaction based on databases/experiments in the String database. Proteins involved in splicing, transcription, translation, metabolism, and chaperones are grouped as 'Other'. The full list of significant interactors can be found in Appendix 5.

are linked to vesicular transport (ACAP2, ANKFY1), actin cytoskeleton (APRC2, MYO1C, CORO1C, SPTBN and GMFG), cilia (GID8, CCDCC88A, CAMSAP3 and OGT) and lipid metabolism (TERC, PAFAH1B) were detected with significantly higher abundance in CRB1-FLAG compared to control (**Figure 15**).

Next, the CRB1 PPI was examined after incubation with porcine retinal lysate. As porcine and human CRB1 share 74.3 % of their amino acid sequence, specific CRB1 peptides detected by mass spectrometry were analysed (**Appendix 6**). No porcine-specific CRB1 peptides were detected indicating that canonical human CRB1 cannot pull-down porcine CRB1. After incubation with porcine retina, 341 proteins were detected with a significantly higher abundance in CRB1-FLAG samples compared to control (**Figure 16 A + Appendix 7**)**.** Of these, 83 proteins were also detected as interactors without incubation with porcine retina and are potentially derived from HEK293T cells. These included the CRB complex members MPP5, PATJ and MPDZ (**Figure 16 B**). Upon incubation with porcine retina, MPP7 and the CRB core complex member EPB41L5, which interacts with the CRB FERM domain, were significantly enriched in CRB1 samples compared to control. This suggests that the chosen proteomics approach is valid for investigating CRB1 interactors. Further analysis of the CRB1 retina interactors using GO enrichment analysis revealed additional significant enriched CC including ‘filamentous actin’, ‘axon cytoplasm’, ‘presynaptic active zone’ and ‘GABAergic synapse’ (**Figure 16 C**). Consistent with this, several significantly enriched pathways in the BP category were associated with actin, microtubule and vesicular transport (**Figure 16 D**). Illustrating this point, significantly enriched proteins in the CRB1 bait samples were actin capping proteins (TMOD2, TMOD3 and FLII), ARP2/3 complex members involved in actin nucleation (e.g. ARPC1A, ARPC5L, APRC3 and GMFG), actin motor proteins (MYO1C, MYO6 and MYO5A), actin binding proteins (e.g. DBN1, GSN), small Rho GTPases (e.g. ARHGAP32 and ARHGAP21), which are key regulators of actin cytoskeletal rearrangements, and spectrin-associated proteins (e.g. SPTBN2, SPTB), which link actin to the cell membrane (**Figure 17**). Furthermore, several proteins identified as CRB1 interactors were associated with the microtubule cytoskeleton, including components of the dynactin complex (DCTN, ACTR10), which allows transport along microtubules. Besides motor proteins, proteins linked to vesicular transport were significantly enriched in CRB1-FLAG compared to control. These included proteins involved in transport from the endoplasmic reticulum (ER) to the Golgi (e.g. BCAP9, SEC16A, TRAPPC4, TRAPPC10), endolysosomal trafficking (e.g. SPART, DNAJC13, HGS, AP3M1, AP3S2) and autophagosome formation (e.g. GABRAPL2, ATG13, RAB1B, RB1CC1). Vesicular transport is also essential to control neurotransmitter exocytosis at the synapse [49]. In line with this, proteins involved in synaptic vesicle exocytosis (e.g. SV2B, SRCN1, BSN, PCLO), synapse assembly (FARP1), and regulation of synaptic transmission (e.g. HOMER1, HOMER2, ERC2) showed significantly higher abundance in CRB1-FLAG samples compared

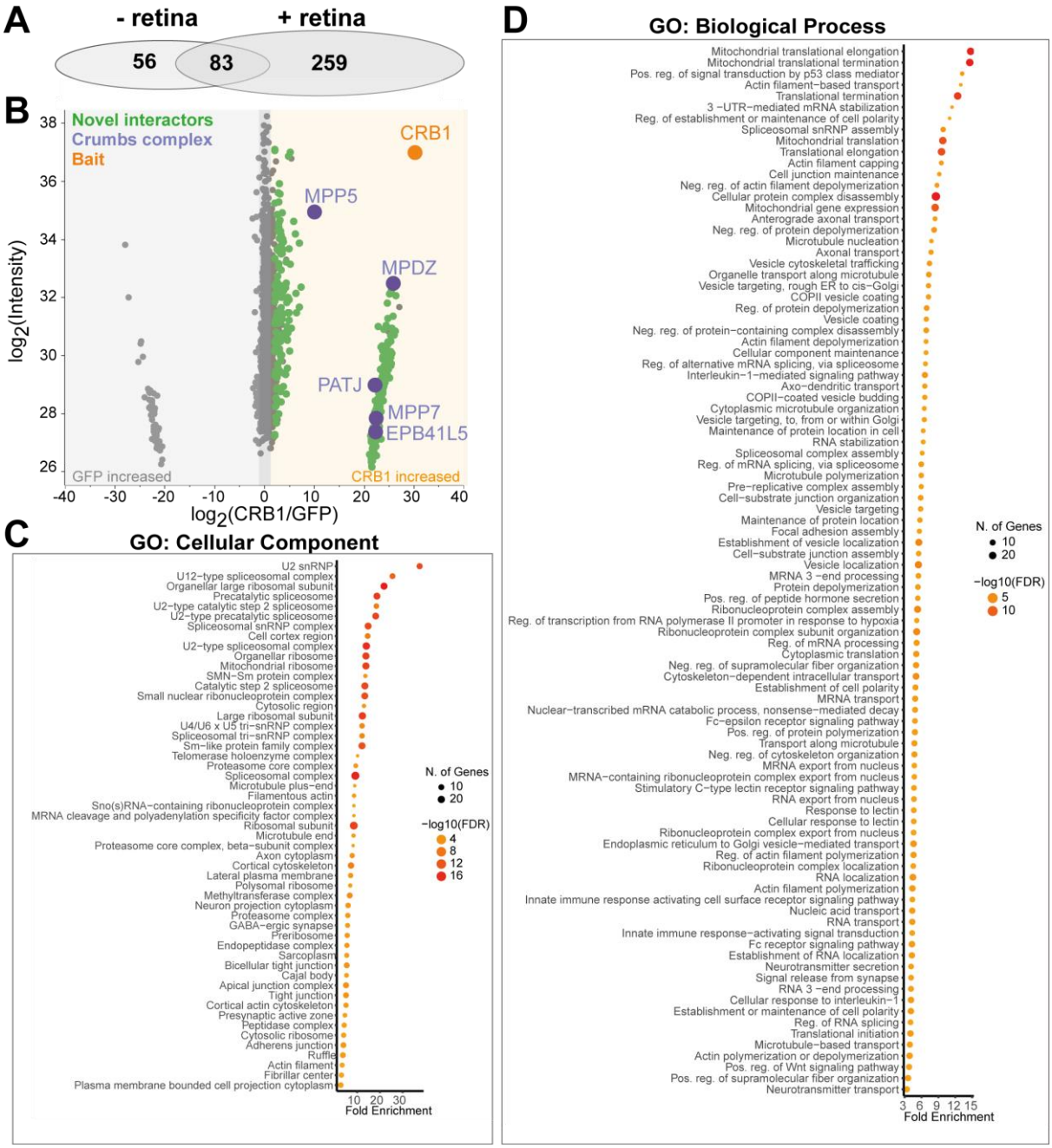

Figure 16| Incubation of canonical CRB1-FLAG with porcine retina resulted in significant enrichment of known and novel interactors

(A) Venn diagram of the significantly enriched proteins in canonical CRB1-FLAG samples compared to control without and with incubation of porcine retinal lysate (One-sample t-test, FDR 0.05, log_2 ratio (CRB1-FLAG/GFP-FLAG) >2, n=6). **(B)** Scatter plot of the log_2 ratio of proteins identified in CRB1-FLAG relative to GFP-FLAG (control) after porcine retinal lysate incubation. Each point represents a protein. CRB1 (bait) is depicted in orange. Significantly enriched proteins in CRB1-FLAG samples compared to GFP are shown in green. CRB complex members that were significantly enriched are highlighted in purple (One-sample t-test, FDR 0.05, log_2 ratio (CRB1-FLAG/GFP-FLAG) >2, n=6). **(C-D)** GO enrichment analysis using ShinyGO to identify significant enrichment **(C)** CC and **(D)** BP among the significant interactors in canonical CRB1-FLAG samples compared to control (FDR <0.05). Top 100 pathways are depicted.

to control. Furthermore, proteins involved in cilia biogenesis (e.g. CCDC88A and KIF3A), ion transport and lipid metabolism, including proteins involved in phosphoinositide (PI) regulation (e.g. MTMTR14, TTC7B, PIPK1A, PI4KA and MTMR1) were significantly enriched in

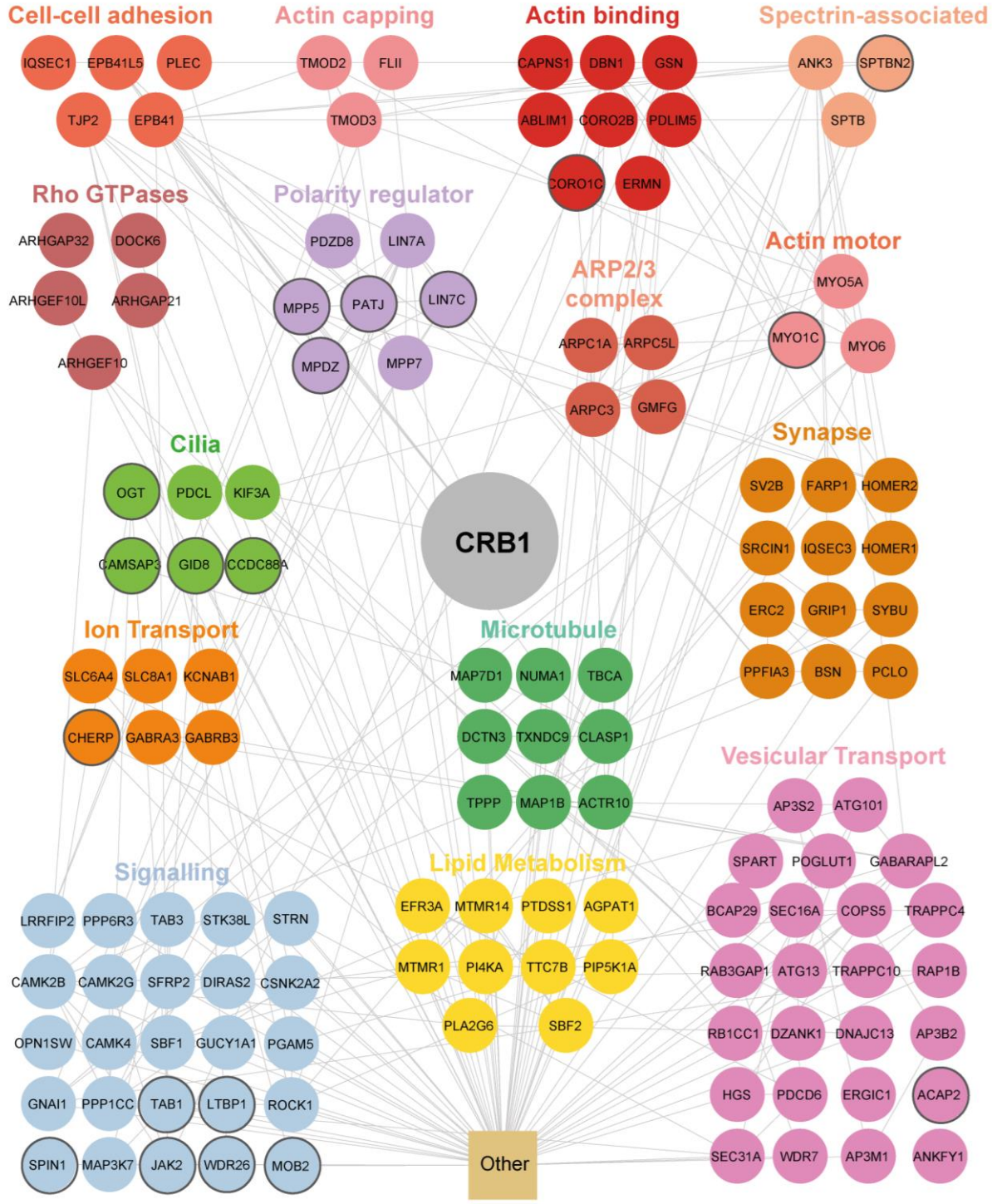

Figure 17| Retinal protein-protein interaction network of canonical CRB1 showed high abundance of proteins linked to the actin cytoskeleton
String and Cytoscape-based representation of the significant high abundant proteins detected in CRB1-FLAG samples compared to GFP control after incubation with porcine retina lysate (One-sample t-test, FDR 0.05, $\log_2$ ratio (CRB1-FLAG/GFP-FLAG) >2, n=6). Proteins are categorised and color-coded based on the biological function reported in the Uniprot database and literature. Proteins that fulfil multiple functions were categorised based on the major described function. Proteins involved in other processes such as splicing, transcription, translation, metabolism and chaperones are summarised as 'Other' and are provided in Appendix 7. Grey lines represent reported interaction in the STRING database based on databases or experiments. Proteins with a grey circled border are also identified as significant enriched in canonical CRB1-FLAG samples without incubation of porcine retina indicating a potential carry-over from the bait producing HEK293T cells.

CRB1-FLAG samples compared to control. Finally, highly abundant proteins in CRB1-FLAG link CRB1 to various signalling pathways, such as Ca^{2+}-linked (e.g. CAMK2G, CAMK2B,

CAMK4, STRN), WNT (e.g. LRRFIP2, SFRP2, CSNK2A2, SPIN1), transforming growth factor beta (TGF-ß) (e.g.TAB3, LTBP1) and MAPK signalling (e.g. WDR26, MAP3K7).

Overall, these data provide an overview of the retinal-associated interactome of canonical human CRB1. Potential novel interactors of the canonical CRB1 complex were connected to the actin cytoskeleton, vesicular transport, synapse, signalling and phospholipid metabolism.

4.3.3 Protein-protein interactions were highly overlapping between N- and C-terminal FLAG-tagged CRB1

CRB1 is a transmembrane protein with an N-term signal peptide [20]. In order not to interfere with the transport of CRB1 to the membrane, which may be essential for the acquisition of all the natural post-translational modifications of the CRB1 extracellular domain, a C-term FLAG-tagged CRB1 was initially preferred. Unfortunately, the abundance of WT and C948Y C-term FLAG-tagged CRB1 was significantly different and less stable, making comparison of the PPI networks difficult **(Appendix 8)**. In contrast, equal abundance of WT and C948Y CRB1 was observed using the N-term FLAG tag. To investigate the extent to which the PPI network of N-term compared to C-term FLAG tagged CRB1 differs, the porcine retinal pull-down approach was performed in one experiment not only with the N-term FLAG tagged CRB1, as described above, but also with the C-term FLAG tagged CRB1. Without incubation of porcine retina, 84 proteins were identified as significant interactors compared to the control using both, N-term and C-term, FLAG-tagged CRB1 (**Figure 18 A**)**.** In contrast, using only the C-term or N-term CRB1-FLAG, 25 or 55 proteins, respectively, were found to be significantly compared to the control (**Figure 18 A + Appendix 9**).

Significant interactors identified using only the N-term FLAG tagged CRB1 included the CRB complex MPP5, MPDZ and PATJ. A similar trend was observed for the samples that were incubated with porcine retina. While 261 proteins were identified as significantly enriched with both tags, additional 81 proteins or 40 proteins were only found to be significantly enriched with either the N-term FLAG or C-term tagged CRB1, respectively (**Figure 18 B + Appendix 10**). For instance, the CRB complex members LIN7C, MPDZ, MPP7 and EPB41L5 are detected as significant interactors using both the N-term and C-term tag, whereas MPP5 and PATJ are only identified as significant interactors using the N-term FLAG tagged CRB1 construct. This could be due to an interference of the C-term tag with the binding of these interactors, or due to the generally higher abundance of CRB1 and consequently of interacting proteins. This was also reflected by a higher peptide coverage detected by mass spectrometry of approximately 30 % and 17 %, respectively (**Appendix 4 + Appendix 11**).

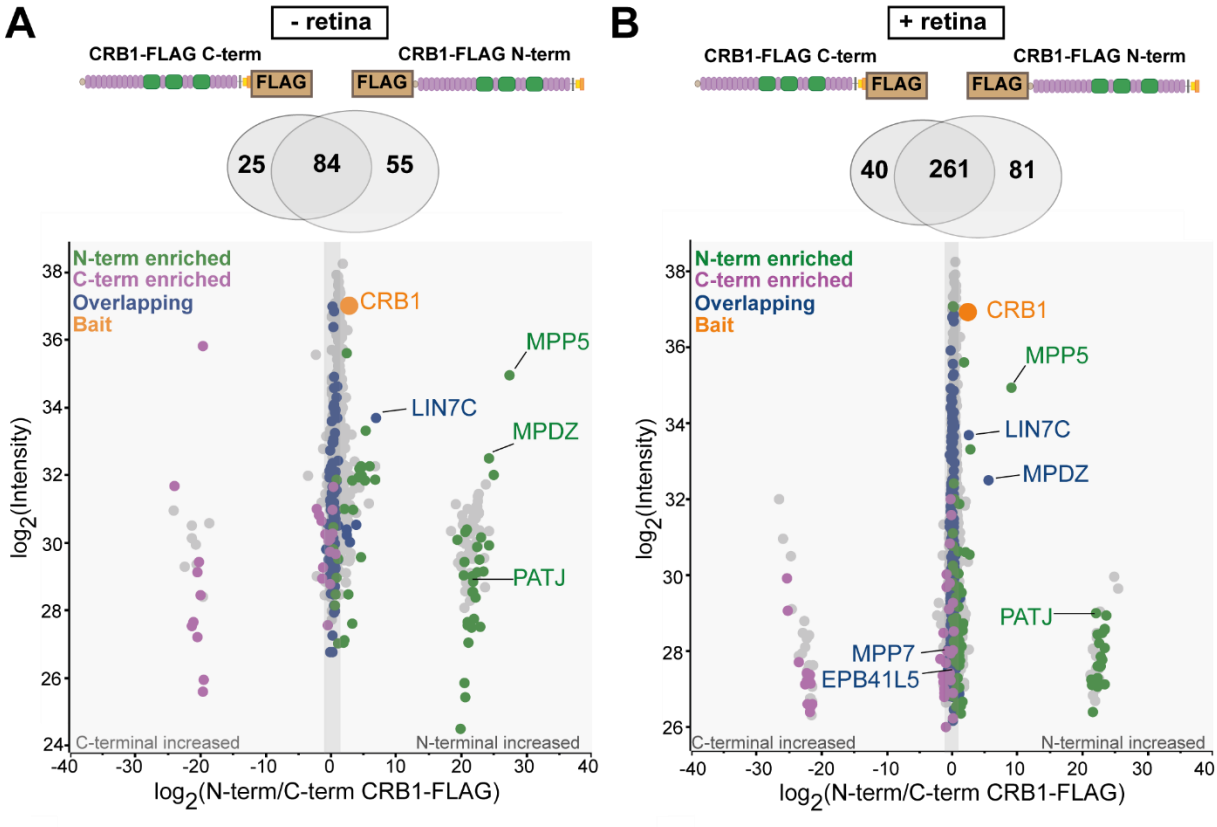

Figure 18| Crumbs complex members MPP5 and PATJ were specifically identified with the N-terminal tagged CRB1 construct
N-term and C-term FLAG-tagged canonical CRB1 were each compared with GFP-FLAG to identify significantly enriched proteins (One-sample t-test, FDR 0.05, log_2 ratio (CRB1-FLAG/GFP-FLAG) >2, n=6) for samples **(A)** without and **(B)** with incubation of porcine retina lysates. In a second step, the overlap of significantly enriched proteins for N-term and C-term FLAG tagged CRB1 was compared as represented in the Venn diagram in the upper panels. Bottom panel depicts scatter plots of the log_2 ratio of proteins identified in N-term FLAG-tagged compared to C-term FLAG-tagged canonical CRB1. Each dot represents a protein. CRB1 (bait) is depicted in orange. Significantly enriched proteins that were detected using both N-term and C-terminal FLAG tagged CRB1 compared to GFP are shown in blue. Significant interactors that are only identified when comparing N-term or C-terminal CRB1-FLAG are depicted in green or purple, respectively. CRB complex members are labelled.

Taken together, these data show that the N-term FLAG tagged CRB1 showed a higher abundance, peptide coverage and amount of significant interacting proteins. More importantly, the equal and stable abundance of CRB1 WT and C948Y using the N-term FLAG tag provides the opportunity to compare the retinal PPI.

4.3.4 Majority of retinal interactors of canonical CRB1 WT were maintained in CRB1 C948Y MT

To assess whether CRB1 WT and CRB1 C948Y show alterations in their PPI networks, which may provide insight into on the molecular mechanism underlying the patient's phenotype as well as the lower abundance of CRB1 protein in patient iPSC-derived RO, a similar porcine retinal pull-down approach was performed using N-term FLAG tagged CRB1 WT, N-term FLAG tagged CRB1 C948Y or FLAG-tagged GFP as a control. To identify potential changes in interaction partners, FLAG tagged CRB1 WT and C948Y were first compared with GFP to identify significantly enriched proteins as described above. In a second step, quantitative

changes in these interactors were identified by comparing CRB1 WT and C948Y. Data show similar abundance and peptide coverage of CRB1 WT and CRB1 C948Y by mass spectrometry (**Figure 19 A + Appendix 12**).

A

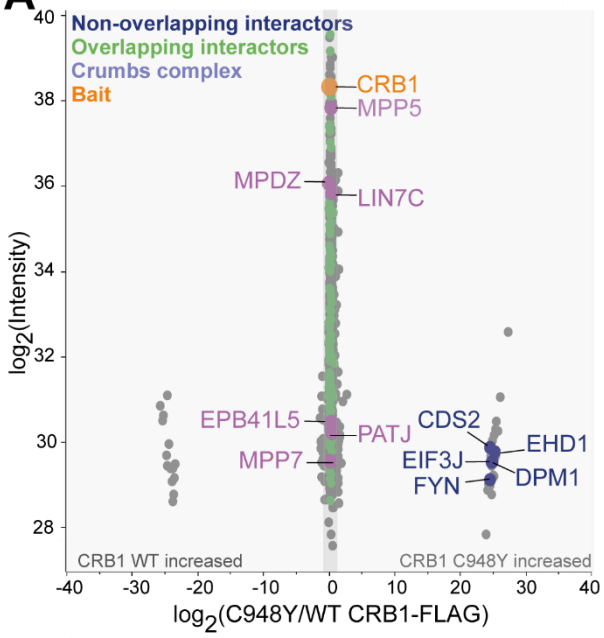

B

Gene	log_2 C948Y/WT ratio	- log_2 p-value	Function
CDS2	24.6	1.73	CDP-diacylglycerol biosynthetic process
EIF3J	24.8	2.019	Translation initiation
FYN	24.5	1.99	Kinase, immunity
EHD1	25.2	1.99	Cilium assembly, endocytosis, protein transport
DPM1	24.9	1.99	Protein mannosylation

Figure 19| Retinal interactors of canonical WT CRB1 were preserved in the C948Y mutant
(A) Scatter plot of the log_2 ratio of proteins identified in canonical CRB1 WT compared to canonical CRB1 C948Y. Every dot represents a protein. CRB1 (Bait) is marked in orange. CRB complex members are equally abundant in CRB1 WT and C948Y samples and are depicted in purple. Retinal interactors that are not significantly changed in WT and C948Y are depicted in green. Significantly enriched proteins in CRB1 C948Y compared to CRB1 WT are depicted in blue (One-sample t-test, FDR 0.05, log_2 ratio (C948Y/WT) >2, n=6) **(B)** Gene name, log_2 ratio, *p*-value and function based on the UniProt database are depicted for the significant interactors of CRB1 C948Y compared to WT.

Interestingly, this specific mutation in the extracellular domain did not disrupt the interaction with the described members of the intracellular Crumbs complex (MPP5, LIN7C, MPDZ, EPB41L5, PATJ and MPP7). In addition, no significant differences in the abundance of the novel interactors described above, were found for CRB1 C948Y compared to CRB1 WT. However, significantly higher levels of CDS2, EIF3J, FYN, EHD1 and DPM1 were detected in CRB1 C948Y compared to CRB1 WT (**Figure 19 A+B**).

Collectively, the above data indicate that CRB1 C948Y and CRB1 WT share the majority of retinal interactors while CRB1 C948Y showed a significantly higher abundance of five proteins, none of which have a described extracellular function or domain.

4.3.5 Porcine retinal pull-down using the CRB1 extracellular isoform revealed new potential extracellular interactors

The interactors of the large extracellular domain of canonical CRB1 are to date, poorly defined [170]. As the majority of patient mutations are located in the extracellular domain, further insights into potential interactors could provide valuable cues to the potential disease

mechanism [8]. To further investigate potential interactors of the extracellular domain, the porcine retinal pull-down approach was performed using the extracellular CRB1 isoform lacking the C-conserved FERM and PDZ domain, as described by Knust *et al.*, and instead containing an alternative exon 11 [89]. GFP-FLAG was used as a control and samples were incubated with or without porcine retina lysates to assess interactors that were potentially derived from HEK293T cells but remaining after SDS washing. All samples were analysed using the Uniprot *sus scrofa* proteome database. Comparison of significant high abundance proteins in the C-term FLAG tagged CRB1 extracellular samples relative to GFP-FLAG allowed the determination of CRB1 extracellular isoform interactors. Protein functional information was obtained from UniProt database [276].

After SDS washing but without incubation of porcine retinal lysate the CRB1 extracellular isoform was detected by mass spectrometry with a peptide coverage of 16 % and, as expected, no peptides for the canonical intracellular domain were detected (**Appendix 13**). Besides CRB1 extracellular, 213 proteins remained significantly enriched in CRB1 extracellular-FLAG samples compared to control (**Appendix 14**). Of these, 68 significant proteins were also detected in the pull-down approach using the canonical CRB1 isoform (**Figure 20 A**). It should be noted that the canonical and extracellular CRB1 isoform were not directly compared in one experiment and, hence, comparison should be interpreted with caution. As expected, none of the known Crumbs complex members, that bind to the intracellular FERM and PDZ domain, were significantly enriched in the CRB1-extracellular-FLAG compared to the control. For further analysis of the 214 proteins that potentially remained attached after SDS washing, GO enrichment analysis was performed (**Figure 20 B+C**). In the CC category, significant enrichment of components amongst others linked to splicing, ribosome, desmosomes, cortical cytoskeleton, actin filament and lamellipodium was shown (**Figure 20 B**). Among the significantly enriched BP, twelve out of 50 pathways were linked to the regulation of the actin cytoskeleton (**Figure 20 C**). This includes members of the ARP2/3 complex involved in actin nucleation (e.g. ARPC1A, ARPC1B), spectrin-associated proteins (e.g. SPTBN2, SPTAN1), actin motor proteins (e.g. MYL6, MYH7B), actin capping (e.g. TMOD2, TMOD3) and actin binding proteins (e.g. GSN, CORO1C) (**Figure 20 D**). Furthermore, proteins with a significantly higher abundance in CRB1 extracellular FLAG samples compared to control were linked to microtubule (e.g. CLASP1), vesicular transport (e.g. ANKFY1, ACAP2), cell-cell adhesion (e.g. CADM1), cilia (e.g. CCDC88A, CAMSAP3), lipid transport (e.g. FABP7) as well as multiple signalling pathways including MAPK signalling (e.g. WDR26, MAP3K7, TAB1), WNT signalling (e.g. WDR26, PPM1B, CCDC88C), insulin-like growth factor receptor signalling pathway (e.g. IGFBP2), TGF beta signalling (e.g. PPM1A, LTBP1), NIK/NF-kappaB signalling (e.g. TAB2, TAB1, PPM1B, TAB3) and mTOR signalling (e.g. RRAGC). Among these, seven significantly enriched candidates in the CRB1-extracellular-FLAG compared to control were described in

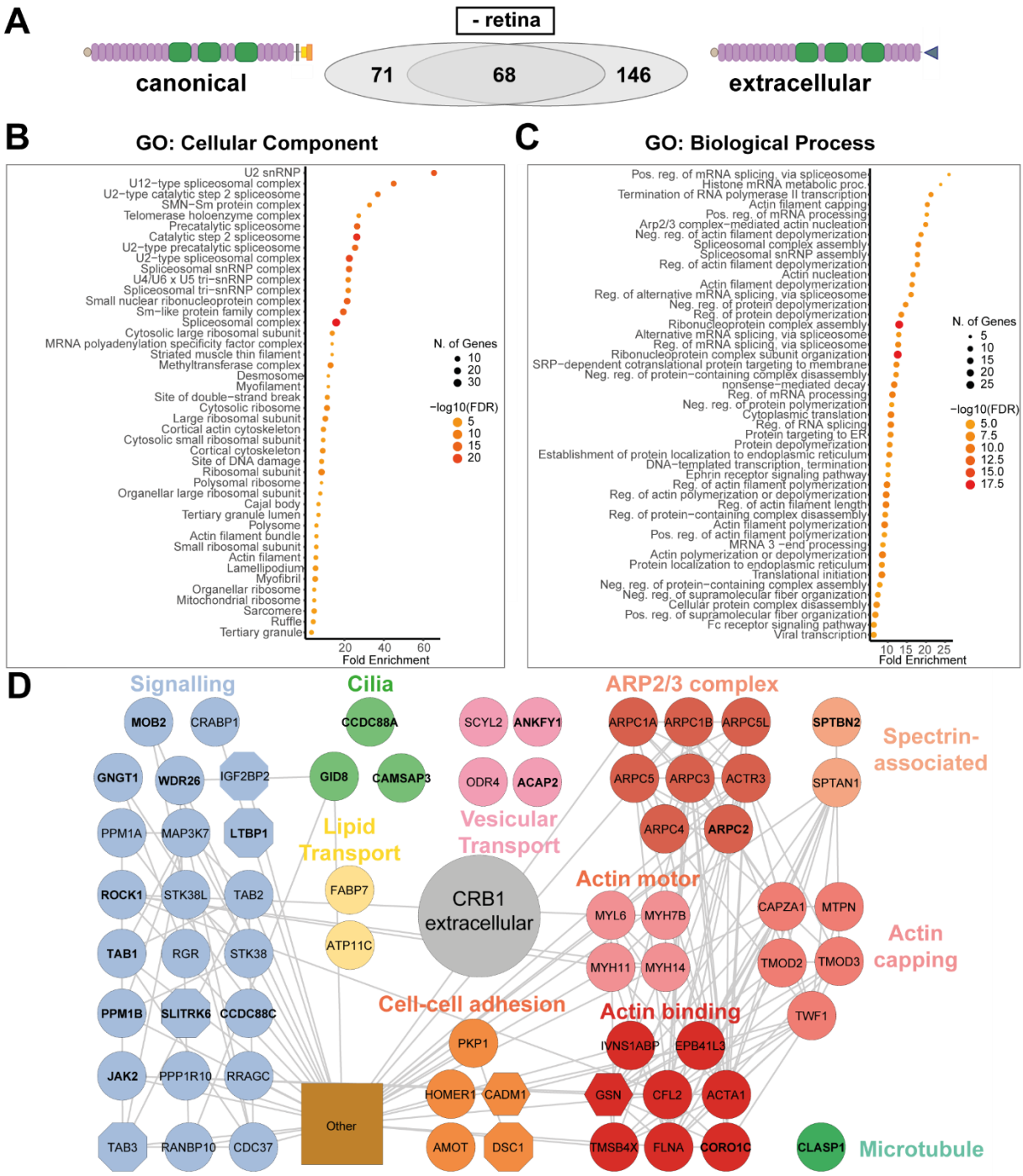

Figure 20| Without incubation with porcine retinal lysate, interactors of the CRB1 extracellular isoform were linked to processes involving or associated with the actin cytoskeleton
(A) Venn diagram showing the overlap of significant interactors identified for the extracellular isoform and the canonical form of CRB1 before incubation with porcine retinal lysate. **(B-C)** GO enrichment analysis was performed using ShinyGO for the significantly enriched proteins in the CRB1 extracellular samples compared to GFP without incubation with porcine retinal lysate (FDR<0.05). Two categories were analysed, **(B)** CC and **(C)** biological pathways. Top 50 pathways are depicted. **(D)** Representation of the significant interactors of the CRB1 extracellular domain without incubation of porcine retina using String and Cytoscape. Proteins were clustered and coloured based on their function as described in the UniProt database. Note that some proteins may fit into more than one category. Grey lines represent interactions reported in the STRING database based on databases and experiments. Proteins depicted in octal shape are described to have an extracellular domain or localisation. Proteins in bold were also identified using the canonical isoform (One-sample t-test, FDR 0.05, log_2 ratio (CRB1/GFP) >2, n=6)

the UniProt database as having an extracellular domain or extracellular localisation, involved in signalling (LTBP1, SLITRK6, TAB3, IGF2BP2), cell adhesion (CADM1, DSC1) and actin cytoskeleton (GSN).

Next, the significantly enriched proteins in the CRB1-extracellular FLAG samples upon incubation with porcine retina were examined. after incubation of CRB1 extracellular-FLAG with porcine retina, 417 proteins were significantly enriched in CRB1-extracellular FLAG samples compared to control (**Figure 21 A + Appendix 15**). Of these, 117 proteins were also identified as significantly enriched without the addition of porcine retina. Furthermore, 190 proteins that were identified as significantly enriched in CRB1 extracellular FLAG compared to control overlapped with the significant interactors identified using canonical CRB1-FLAG (**Figure 21 B**). Except for MPDZ, all other members of the intracellular crumbs complex were either not detected or not significantly enriched in the CRB1-extracellular FLAG samples compared to control (**Figure 21 C**). GO enrichment analysis showed that significantly enriched components in the CRB1 extracellular FLAG samples compared to control included spliceosome, ribosome, microtubule, actin filament bundle, filopodium, growth cone, cell projections and exocytic vesicles (**Figure 21 E**). Correspondingly, pathways enriched in the BP category include processes related to the actin and microtubule cytoskeleton regulation, cell-cell and cell-matrix junctions, vesicular localisation, axonal and ER-Golgi transport (**Figure 21 D**). Similar to the significant interactors identified for the canonical CRB1, significant proteins enriched CRB1 extracellular FLAG included proteins involved in cell adhesion (e.g. TJP2, PLEC), actin capping (e.g. TMOD2, TMOD3), actin binding (e.g. GSN, CORO1C, DBN1), spectrin cytoskeleton (e.g. SPTBN2, ANK3), actin motor proteins (e.g. MYO1C), ARP2/3 complex (e.g. ARPC5L, ARPC1A), Rho GTPases (ARHGEF10L, ARHGAP32), polarity regulation (e.g. MPDZ, LLGL2) (**Figure 22**). In addition, proteins associated with cilia, including cilia-basal body membrane docking (e.g. RAB3IP), cilia assembly (e.g. CCDC88A, CAMSAP3), lipid metabolism with a strong majority of PI lipid regulators (e.g. PLCL2, FAM126B, VAC14, SBF2, NUDT3, PIP5K1C), ion transporters for chloride, potassium, Ca^{2+} and sodium ions (e.g. GABRB3, GABRA1), proteins involved amongst others in microtubule assembly (e.g. EML5, SLAIN2, CLASP1) and transport along microtubules (e.g. KIF5B, ACTR10, DCTN1 DYNLL1). Furthermore, proteins significantly enriched in CRB1 extracellular FLAG compared to control contain proteins linked to vesicular processes including transport from the ER to the Golgi (e.g. TRAPPC6B, TRAPPC3), endocytosis and endolysosomal transport (e.g. TOM1L2, TBC1D17, ACAP2, SYNRG), autophagosome formation (e.g. RB1CC1, ATG101, ATG13), exocytosis (e.g. RIMS2, ARFGEF1, EXOC1). Closely related to the vesicle-based process, proteins significantly enriched in the CRB1 extracellular have a described function in synaptic processes such as synaptic transmission (e.g. HOMER1, HOMER2) and neurotransmitter exocytosis (e.g. RIMS1, PCLO, SYT5, RPH3A, ERC2).

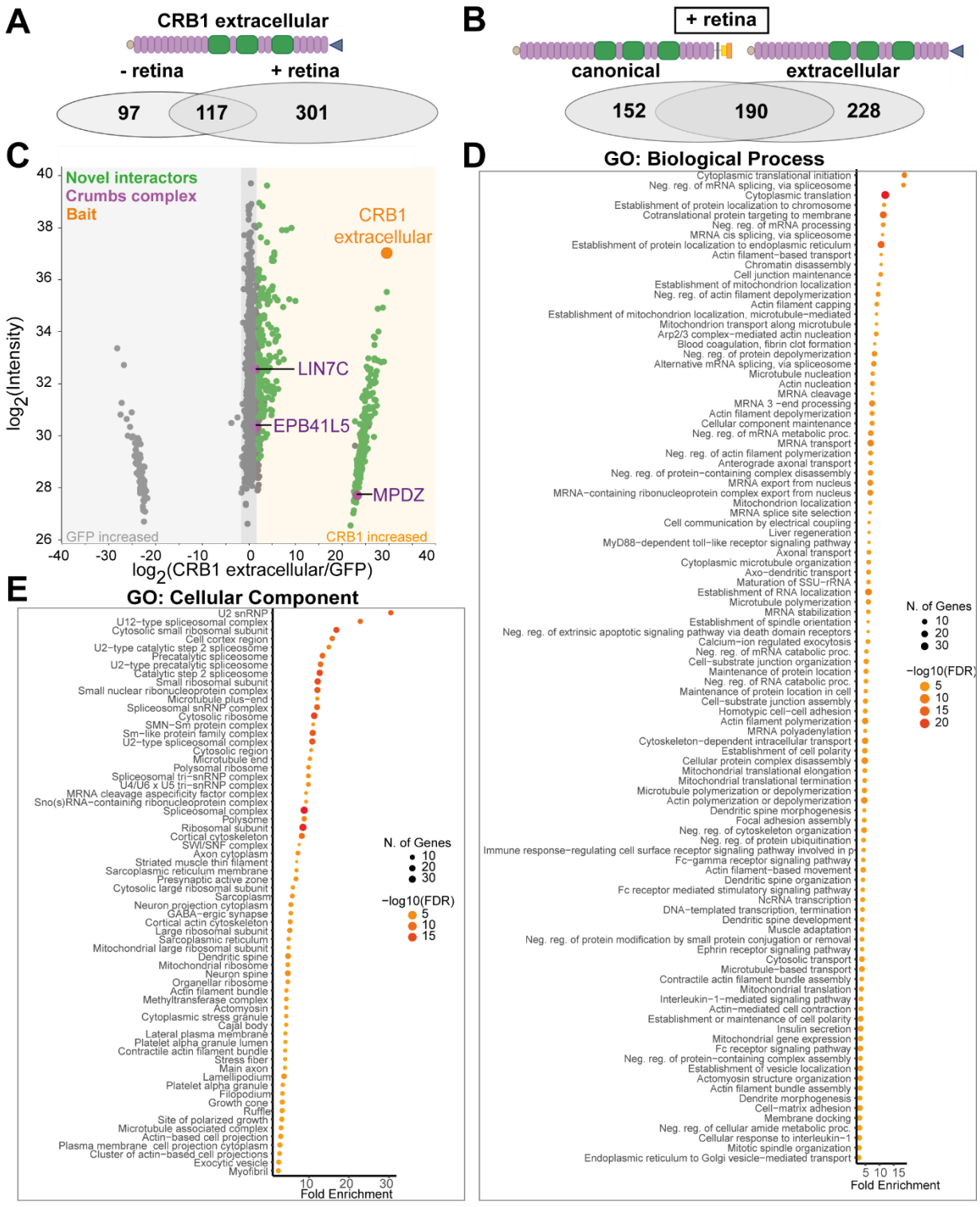

Figure 21| Retinal interactors of the CRB1 extracellular isoform and the canonical isoform were involved in similar biological processes

(A) Venn diagram of the overlap of significant interactors identified in CRB1 extracellular isoform samples with and without incubation with porcine retinal lysate **(B)** Venn diagram comparing the overlap between significant retinal interactors of canonical and extracellular domain CRB1 upon incubation with retinal lysate. **(C)** Scatter plot of the $\log_2$ ratio of proteins identified in the CRB1 extracellular isoform compared to GFP upon incubation with porcine retinal lysates. CRB1 (bait) is shown in orange. Significantly more abundant proteins in the CRB1 extracellular sample are highlighted in green. Except for MPDZ, crumbs complex members of the intracellular domain (purple) are either not detected or not significantly enriched. (One-sample t-test, FDR 0.05, $\log_2$ ratio (CRB1/GFP) >2, n=6). **(D-E)** GO enrichment analysis was performed to identify significantly enriched **(E)** CC and **(D)** BP among the significant retinal interactors identified in the CRB1 extracellular isoform samples compared to control (FDR<0.05). Top 100 pathways are depicted.

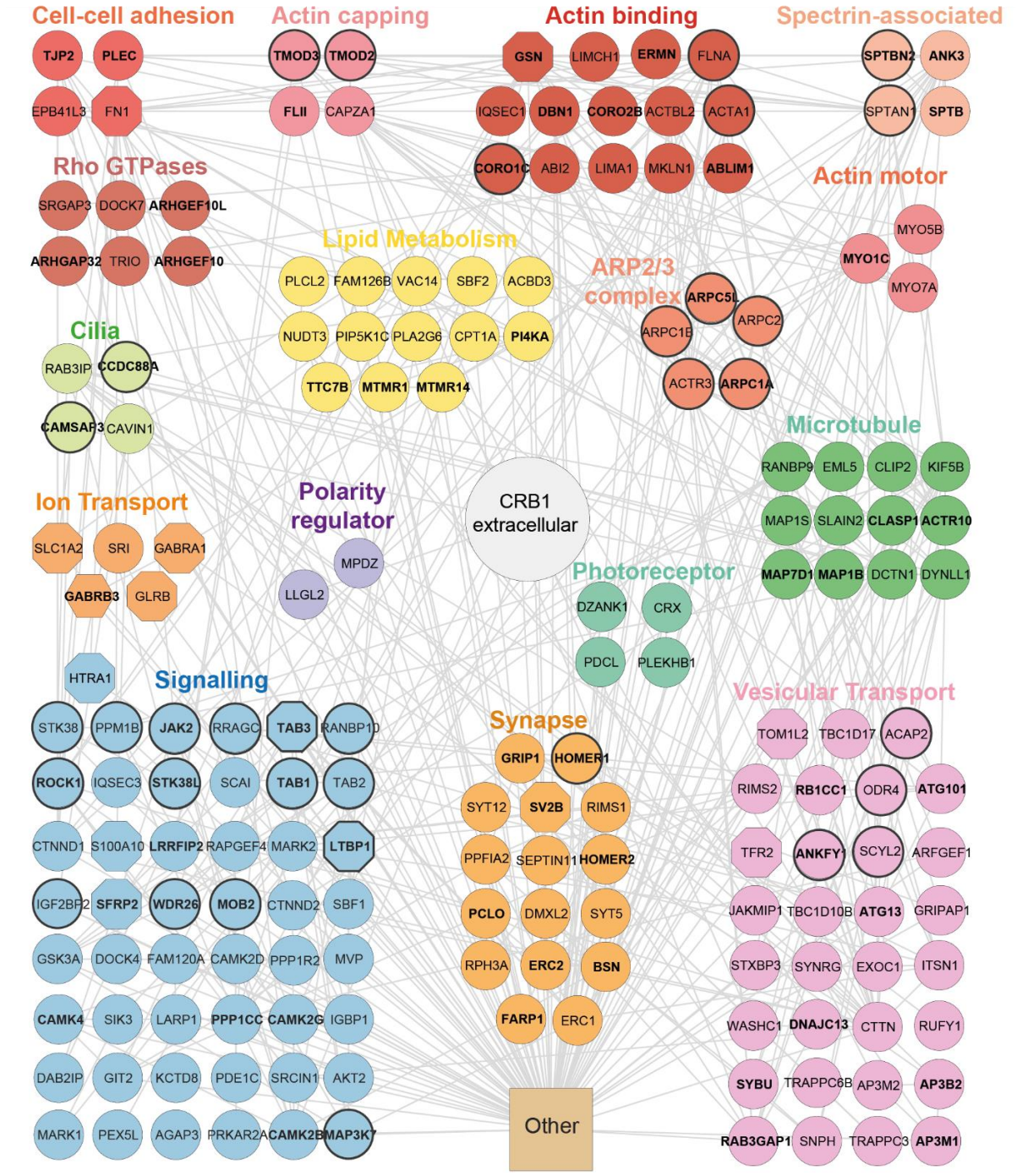

Figure 22| Protein-protein interaction network of the CRB1 extracellular isoform revealed new candidate interactors of the extracellular domain
Significantly enriched interactors in CRB1 extracellular isoform samples compared to control upon incubation with porcine retina were analysed using STRING and Cytoscape. (One-sample t-test, FDR 0.05, $\log_2$ ratio (CRB1/GFP) >2, n=6). Protein colours indicate major function based on the Uniprot database. Some proteins may fit into two categories. Grey lines represent interactions reported in the String database based on experiments or databases. Proteins with other functions, for instance ribosomal, splicing or mitochondria are grouped as other and can be found in Appendix 15. Ocular shaped proteins are known to have an extracellular domain or localisation. Proteins in bold were also identified as significant interactors using the canonical CRB1 isoform. Black border line depicts proteins that were also identified as significant interactors for the CRB1 extracellular domain without incubation of porcine retina and are most likely derived from HEK293T cells.

Moreover, proteins involved in NF-kappa-B activation (e.g. PPM1B, TAB3, TAB1), mTORC1 signalling (e.g. RRAGC, SIK3, LARP1, MAP3K7), Rho protein signalling transduction (e.g. SCAI), WNT signalling (e.g. CTNND1, LRRFIP2, MARK2, SFRP2, WDR26,

CTNND2, GSK3A), TGF-beta signalling (e.g. LTBP1), insulin-like growth factor receptor signalling pathway (e.g. IGFBP2), MAPK signalling (e.g. WDR26) and Ca^{2+}-linked signalling (e.g. CAMK4, CAMK2G, CAMK2B) were found. Furthermore, 13 of the highly abundant significant proteins were described to have an extracellular domain or localisation according to the UniProt database, which are described to have a function in the extracellular matrix (e.g. FN1), ion transport (e.g. SLC1A2, GABRA1, GABRB3, GLRB), signalling (e.g. HTRA1, TAB3, LTBP1, S100A10, SRFP2, IGF2BF2), synapse (e.g. SV2B) and actin regulation (e.g. GSN).

Together, these data provide novel candidate interactors of the CRB1 extracellular domain. Similar to the canonical form of CRB1, several significantly enriched proteins in CRB1 extracellular isoform samples are involved in actin cytoskeleton-based processes, vesicular transport, PPI metabolism and signalling.

4.3.6 Porcine retinal pull-down showed no significant differences in the retinal interactors of WT and C948Y CRB1 extracellular domain

To further investigate the molecular mechanisms underlying the C948Y mutation, the C948Y mutation was additionally introduced into the C-term FLAG tagged CRB1 extracellular domain construct. Next, a porcine retinal pull-down approach was performed using the C-term FLAG tagged WT and C948Y constructs of the CRB1 extracellular domain or GFP-FLAG as a control. Similar to the canonical form, the FLAG tagged CRB1 extracellular domain WT and C948Y were first compared with GFP-FLAG to determine significantly enriched proteins. In a second step, quantitative changes in significant proteins were identified by comparing CRB1 extracellular domain WT and C948Y.

Results obtained indicated that approximately similar peptide coverage of CRB1 extracellular and CRB1 C948Y were obtained by mass spectrometry. Consistent with the data obtained for the canonical CRB1 isoform, none of the described interactors were significantly altered in CRB1 extracellular domain C948Y compared to WT (**Figure 23**). Overall, these data showed that the retinal interactions of the CRB1 extracellular domain were not significantly disturbed by the introduction of the C948Y mutation.

In conclusion, CRB1 retinal PPI analysis revealed a strong association of CRB1 with the regulation of the actin cytoskeleton and actin-based processes such as vesicular transport and cell-adhesion. However, the co-localisation in retinal tissue and the functional relevance of these potential interactors in relation to CRB1 need to be further verified. To this end, the localisation and functional relevance of actin regulators identified as potential CRB1 interactors will be investigated in control and patient RO in the next chapter.

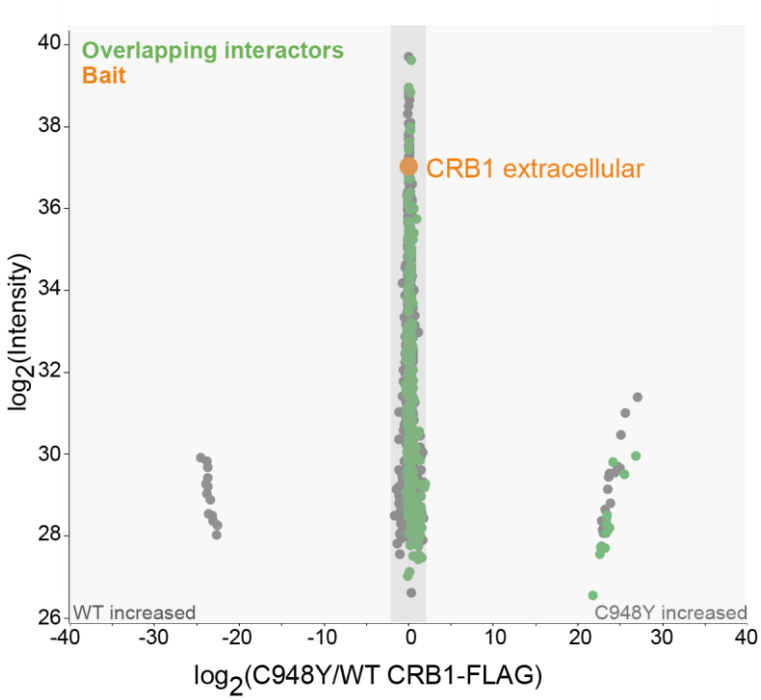

Figure 23| No significant loss or gain of protein-protein interactions was identified in CRB1 extracellular WT and C948Y mutant
Scatter plot of the log_2 ratio of proteins identified in CRB1 extracellular isoform WT compared to C948Yafter incubation with porcine retinal lysate. CRB1 extracellular domain is depicted in orange. Previously identified CRB1 extracellular domain interactors shown in green were not significantly changed between WT and C948Y mutant. n=6

4.4 Investigation of CRB1 and the regulation of the actin cytoskeleton

4.4.1 CRB1 localised closely to F-actin and various actin regulators in control RO

The actin cytoskeleton is involved in several cellular processes such as vesicular transport, exocytosis, cilia and signalling [191]. In particular photoreceptors, as the most metabolically active and specialised cells, rely on a tight regulation of the actin cytoskeleton to maintain the constant renewal of the OS, which is linked to the ARP2/3 complex and rhodopsin trafficking from the IS to the OS [191, 192]. Given the high abundance of proteins involved in the regulation of the actin cytoskeleton as well as proteins involved in actin-driven cellular processes in the CRB1 PPI analysis, the next aim was to further investigate the localisation of F-actin and CRB1 in the control RO using immunofluorescence microscopy. Results obtained showed that CRB1 and F-actin localised to the OLM in control RO (**Figure 24 A**). In particular, CRB1 was detected at the top of the F-actin ring at the base of the segment-like protrusions overlying the photoreceptor nuclei, which further emphasises the critical role of both at the

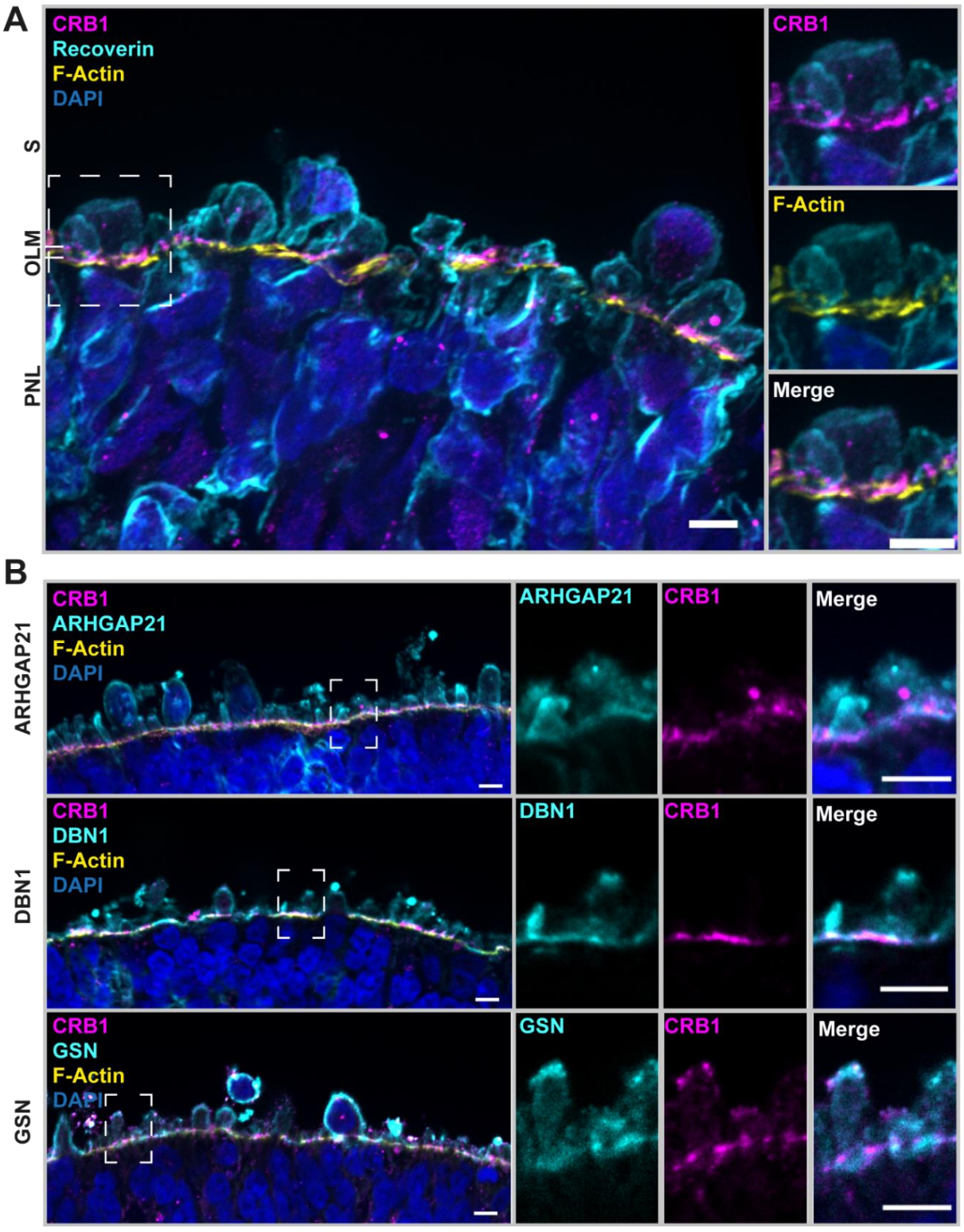

Figure 24| CRB1 localised together with F-actin, GSN, DBN1 and ARHGAP21 at the base of the segment-like protrusion in control iPSC-derived RO
Immunofluorescence microscopy images of control iPSC-derived RO at 260 days of age. **(A)** Localisation of CRB1 (magenta), the pan-photoreceptor marker Recoverin (cyan), F-actin (Phalloidin, yellow). DAPI (dark blue) was used to visualise the nuclei. Right panel depicts merged overview. Dashed square marks the ROI shown in the left panels. **(B)** Localisation of CRB1 (magenta) and ARHGAP21 (top pane, cyan), DBN1 (middle panel, cyan) and GSN (bottom panel, cyan). F-actin is stained with Phalloidin (yellow) and nuclei are shown with DAPI (dark blue). Dashed square marks ROI depicted in the left three panels. Scale bar 5 µm. Data show representative image from three images taken of three organoids of one differentiation.

OLM. ARHGAP21, DBN1 (Drebrin) and GSN (Gelsolin) were identified as potential interactors of CRB1 in the porcine retinal pull down approach. ARHGAP21 belongs to the family of small

Rho GTPases and acts as Rho GTPase inhibitor by inducing the catalysis from GTP to GDP [193]. By regulating the activity of FAK, PK1, Cdc42, RhoA, RhoC and ARP2/3, ARHGAP21 has been shown to regulate various cytoskeletal processes including cell migration, adhesion, secretion and stress fibre formation [193]. DBN1 is an F-actin binding protein that increases filament stiffness, thereby regulating synaptic plasticity and communication [194]. In addition, GSN is an actin-binding protein involved polymerization at the pointed end and capping at the barbed ends [191, 195]. Dysfunction of GSN is associated with photoreceptor degradation [191, 195]. Therefore, the localisation of ARGHAP21, DBN1 and GSN was examined in relation to CRB1 in control RO was investigated (**Figure 24 B**). Data obtained indicate that all three actin regulatory proteins localised to the area of the OLM similarly to F-actin and CRB1. ARHGAP21, DBN1 and GSN were present within the segment-like protrusions, but also partially overlapped with CRB1 at the base of the segment.

Overall, these data further validate the retinal CRB1 PPI network and confirm the localisation of CRB1 together with ARHGAP21, DBN1 and GSN in the subapical region of the OLM in control iPSC-derived RO.

4.4.2 F-actin intensity was significantly reduced in patient A and patient B RO

Disturbance in the regulation of the actin cytoskeleton are observed in IRD [191]. As the above data allow to hypothesise that CRB1 may be involved in the regulation of the cytoskeleton and actin-based processes, the next aim was to investigate the actin cytoskeleton in the patient RO, which showed reduced levels of CRB1. To this end, the abundance and localisation of F-actin was analysed using by immunofluorescence microscopy using phalloidin in control (K3 and K5), patient A and patient B RO of 260 days of age.

Data indicated that in addition to CRB1, F-actin was reduced at the OLM in both patients compared to control (**Figure 25 A**). Further quantification of three to four RO of one differentiation suggested a significant reduction of F-actin intensity of approximately 30 % and 60 % in patient A and patient B, respectively, compared to the independent controls (K3 and K5) (One-way ANOVA, n=3-6, $F(3,11)=14.99$, Tukey's Multiple Comparison test, $p<0.05$) (**Figure 25 B**). In addition, F-actin intensity was significantly lower at the OLM of patient B compared to RO of patient A (One-way ANOVA, n=3-6, $F(3,11)=14.99$, Tukey's Multiple Comparison test, $p>0.05$) (**Figure 25 B**). No difference was observed between patient A, patient B and control (K5) when ß-actin levels were analysed by western blot of total-RO lysates (**Appendix 16**).

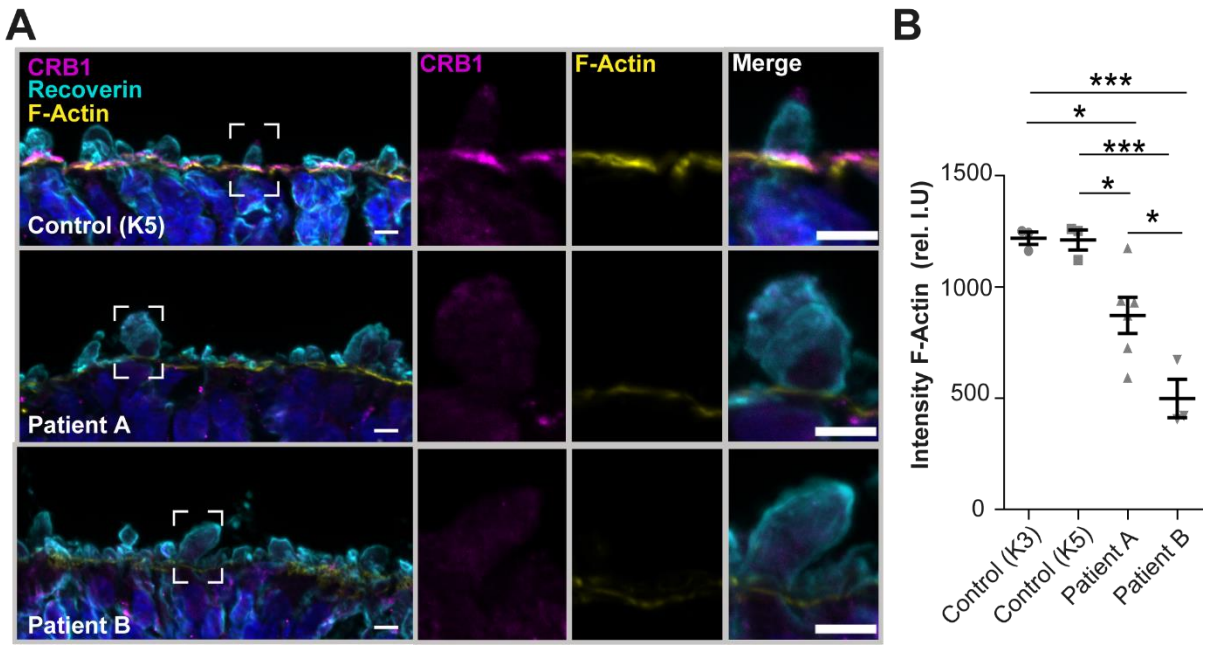

Figure 25| RO of patient A and patient B showed a significant reduction in F-actin intensity at the OLM
(A) Immunofluorescence microscopy of control (K5, top panel), patient A (middle panel) and patient B (bottom panel) iPSC-derived RO of 260 days of age. Left panel depicts an overview with the ROI marked with a white dashed square. Left three panels depict the ROI. Staining was performed for F-actin (phalloidin, yellow), CRB1 (magenta), Recoverin (pan-photoreceptor marker, cyan), DAPI (nuclei, dark blue) **(B)** Quantification of F-actin intensity of three to six images taken from three to four organoids per condition (K3, K5, patient A and patient B) of one differentiation. Graph depicts mean ± SEM. One way-way ANOVA with a Tukey's multiple comparison test was performed for statistical analysis. n.s. $p>0.05$; *$p<0.05$; ***$p<0.001$

Taken together, these preliminary data indicated that both patient ROs showed a reduction in F-actin at the OLM, which needs to be further validated using RO from additional RO differentiations to exclude differentiation specific effects.

4.4.3 Full-proteome analysis revealed downregulation of actin-based processes in CRB1 patients

To further evaluate the consequences of the CRB1 C948Y mutation on RO homeostasis, full-proteome analysis was performed. For this purpose, 15 to 16 ROs from control, patient A and patient B at 330 days of age were lysed and, after tryptic digestion, the samples were analysed by mass spectrometry using DIA (**Figure 26 A**). Principle component analysis (PCA) confirmed the clustering of the three technical replicates of control, patient A and patient B, excluding any experimental outliers within the groups (**Figure 26 B**). The replicates of control, patient A and patient B were grouped, filtered for valid values in at least two out of the three technical replicates and missing values were replaced from a normal distribution.

First, the abundance of CRB1 and the described CRB complex members was analysed (two-sample t-test, FDR 0.05, S0=0.1, n=3) (**Figure 26 C+D**). In line with previous findings, both patients RO showed a significant reduction in CRB1 abundance compared to the control. Further analysis of the peptides detected for CRB1 revealed a strong reduction of all peptides detected along the extracellular domain of canonical CRB1, which incorporates the residue of

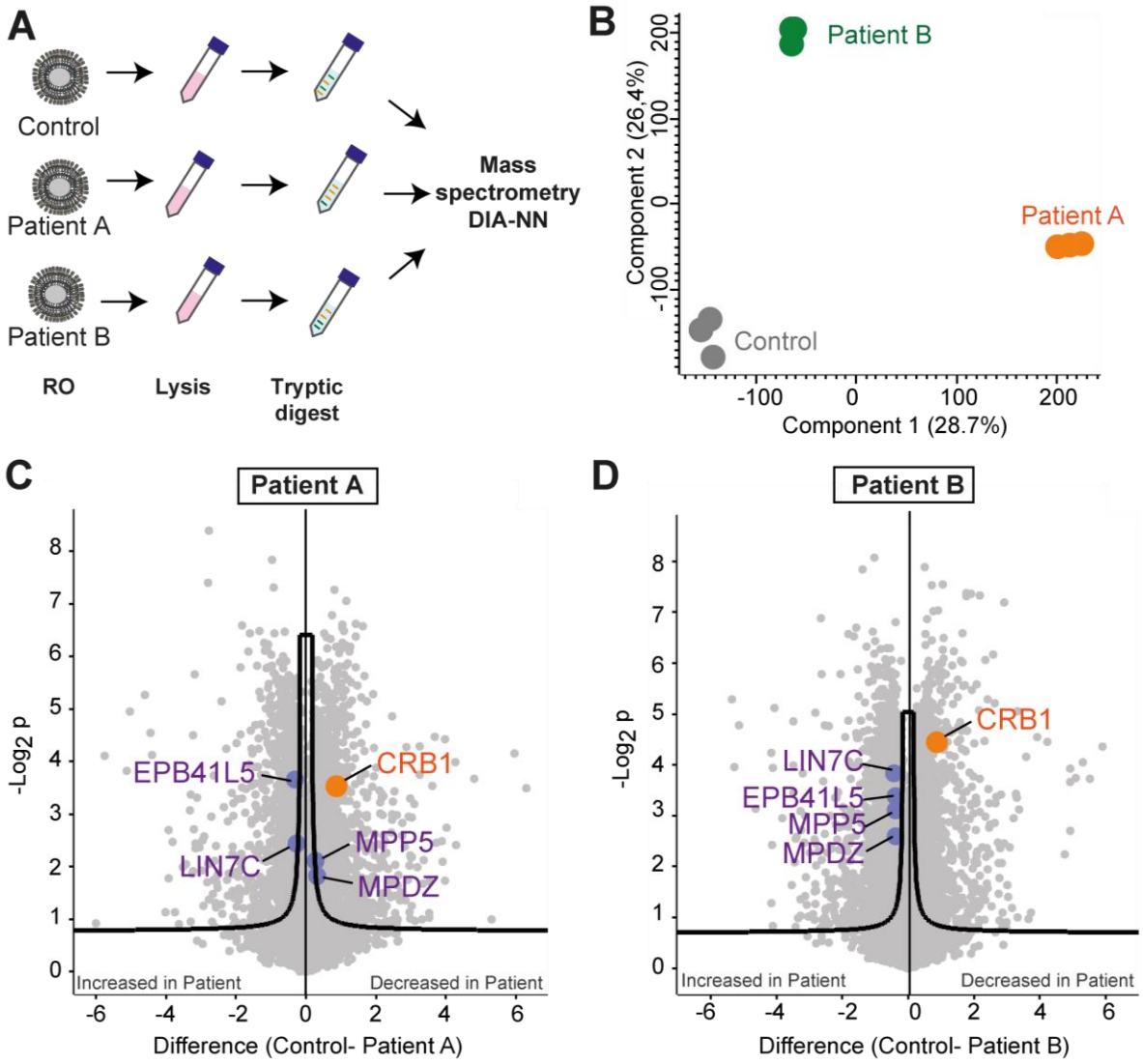

Figure 26| Full proteome analysis showed reduced CRB1 and partially increased Crumbs complex members abundance in patient RO compared to control
(A) Graphical illustration of the experimental approach. 15-16 control, patient A and patient B iPSC-derived RO at 350 days of age were lysed and, after tryptic digest, peptides were analysed by mass spectrometry using database independent analysis **(B)** PCA of the variance in the three replicates analysed for patient A (orange), patient B (green) and control (grey). 28.7 % and 26.4 % of the variation was explained by components 1 and 2, respectively. **(C-D)** Volcano plot of the difference in mean intensity in control minus patient samples versus the $-\log_2$ p-value. Every dot represents a protein. CRB1 (orange) and CRB complex members (purple) are highlighted. Three technical replicates of lysates from 15-16 RO of one differentiation are shown. (Two-sided t-test, FDR 0.05, S0=0.1, n=3)

the C948Y variant (**Appendix 17**). No difference was observed in the abundance of the intracellular CRB1 peptide, which was detected in only two of the three replicates for both patients. In parallel with the reduction in CRB1, the intracellular CRB complex members EPB41L5 and LIN7C were slightly but significantly increased in both patient RO compared to the control. Interestingly, the other CRB complex members MPP5 and MDPZ were significantly upregulated in the less affected patient B compared to control, whereas both proteins were significantly downregulated in the more affected patient A compared to the control. Together, these data further confirmed the reduction of CRB1 in peptides covering the entire extracellular

domain and the slight increase of the previously described CRB complex members in patient iPSC-derived RO.

Next, the abundance of proteins, other than CRB1 and the known CRB complex members, were investigated to identify changes associated with the CRB1 C948Y mutation. For this purpose, proteins that were significantly altered in both patients compared to control were determined. Secondly, proteins that did not follow the same trend in both patients were excluded. For instance, proteins that were of significant upregulated in patient A compared to control, but downregulated in patient B compared to the control, were excluded.

Out of a total of 8827 proteins detected, 625 and 581 proteins were significantly up- and downregulated, respectively, in both patients compared to the control (**Appendix 18 + Appendix 19**). GO enrichment analysis using two categories, CC and BC, revealed that CC, which were significantly higher abundant in CRB1 patient RO were linked to the photoreceptor IS and OS, cilia, basolateral membrane, synaptic vesicles and tight junctions, amongst others **(Figure 27 A + Figure 28**). Similarly, the significantly higher BP in patient RO included pathway related to visible light detection, photoreceptor cell maintenance and cellular response to heat suggesting that, in contrast to the loss of vision in patients, RO show significantly high abundance of proteins related to light detection. Moreover, GO enrichment analysis of the proteins with a significantly lower abundance in CRB1 patient RO compared to control showed that CRB1 patient RO show a reduction in CC and BC, including actin filaments, growth cones, early endosomal membrane, response to reactive oxygen species and cell-matrix adhesion (**Figure 27 B + Figure 28**). Among the proteins that were significantly different in both patients compared to the control, 71 proteins were identified as interactors of the CRB1 canonical or CRB1 extracellular isoform (**Figure 28**). These included members of the ARP2/3 complex (ARPC2, ARPC3), actin binding proteins (DBN1, GSN1, FLNA), actin motor proteins (MYO5B, MYO1C), lipid metabolism regulators (CPT1A, TTC7B, PIP5K1A), spectrin-associated proteins (ANK3), cilia proteins (e.g. PDCL), photoreceptor-linked proteins (CRX, OPN1SW) and signalling (e.g. CAMK2B, ARHGEF10).

Taken together, data obtained confirmed a decreased abundance of proteins associated with the actin cytoskeleton and actin-based processes such as growth cone, cell-matrix adhesion and actin-based projections in both patient RO compared to control RO. As these processes are affected in both patients RO, one could hypothesise that these alterations may be related to the homozygous CRB1 C948Y mutation and potential disease mechanisms. To prove this, isogenic controls would be required.

Collectively, data in this chapter revealed that both patient RO show alterations in the actin cytoskeleton and actin-based processes. Next, the differences between the two patients and candidate modifiers were investigated.

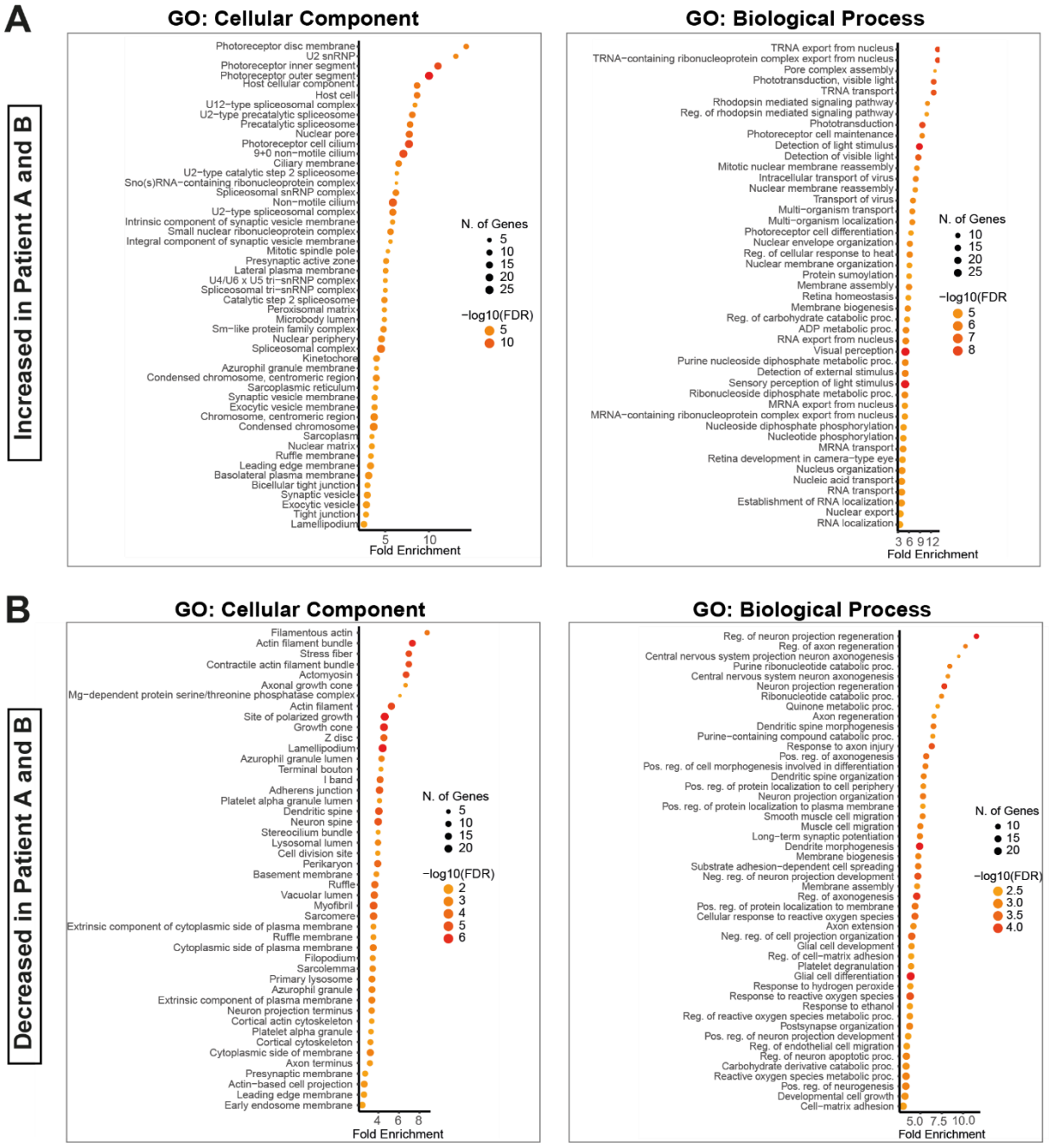

Figure 27| CRB1 patient RO showed high abundance of phototransduction proteins and decreased abundance of actin-associated proteins
Go enrichment analysis of the top 50 significantly enriched CC (left panels) and biological process (right panels) among the proteins that were significantly **(A)** increased or **(B)** decreased in CRB1 patient A and B RO compared to control. Analysis was performed using ShinyGO (FDR 0.05).

4.5 Identification of candidate modifiers of disease severity between CRB1 patient brothers

The two patients described in this study provide a key example of relatives carrying the same CRB1 mutation, but with a striking difference in disease severity. Given this reason, the aim of this chapter was to further identify potential harmful and protective candidates, that may underlie the difference in disease severity. To this end, the initial differences in the full-proteome of RO from the more affected patient A and the less affected patient B were analysed using

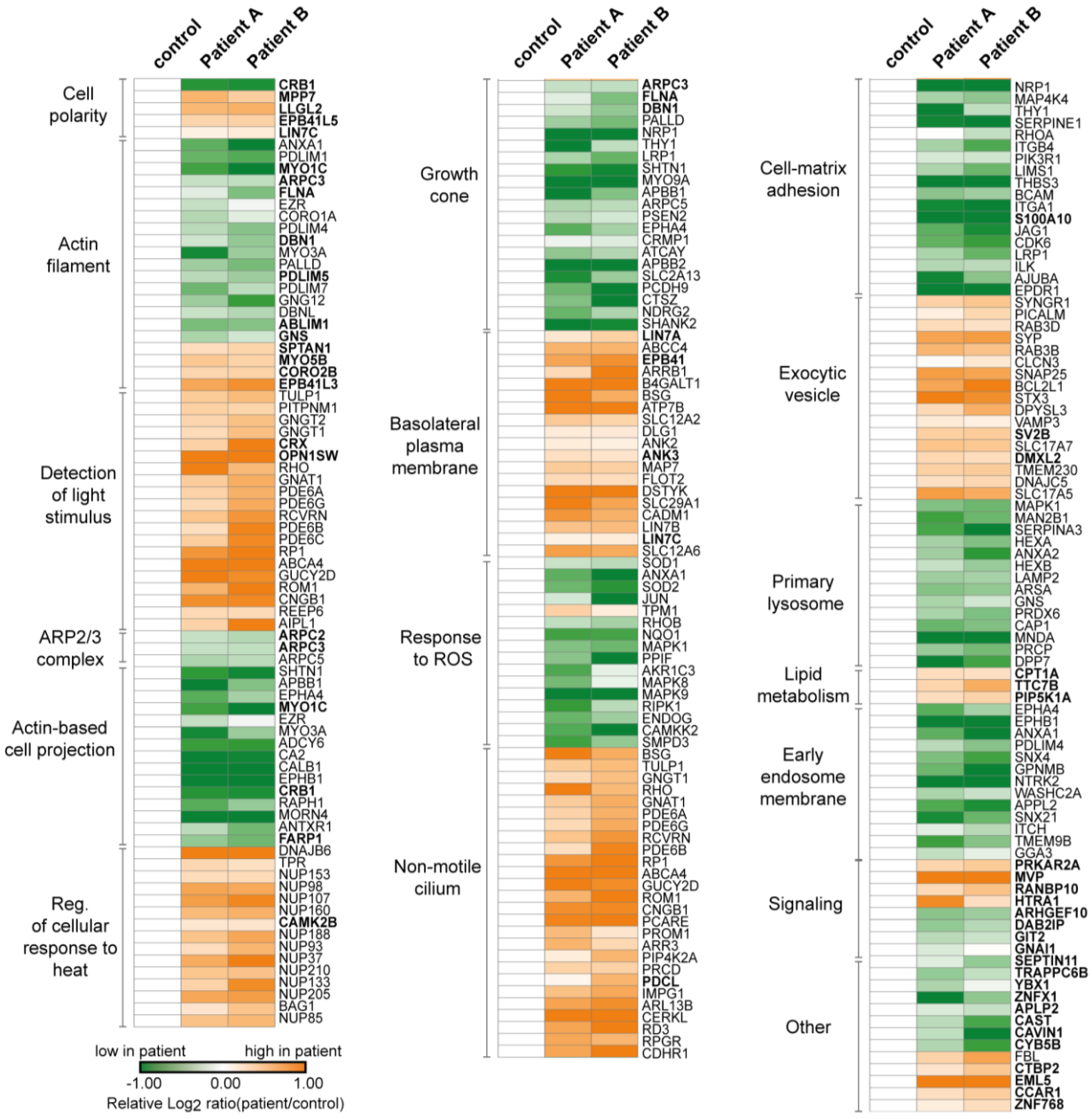

Figure 28| Proteins linked to actin filament, cell-matrix adhesion, growth cone, lysosomes and endosomes were significantly reduced in patient iPSC-derived RO
Heat map of the relative log_2 ratios of proteins that were significantly changed in patients compared to control. Proteins were clustered based on CC or BP identified by ShinyGO. Proteins depicted in bold were identified as interactors of canonical or extracellular CRB1.

mass spectrometry and DIA. This allowed the identification of potential downstream processes affected by the potentially harmful or protective modifying candidate(s). Second, to identify the primary candidate modifier, WGS was performed on blood samples from patient A and B and harmful and protective genetic variants were identified.

4.5.1 Full-proteome analysis of patient RO revealed differentially abundant biological processes

To identify differences that might contribute to the variable clinical phenotype of the two patients, a full-proteome analysis was performed on RO from patient A, patient B and control

(K5) at 330 days of age, as described previously. Using mass spectrometry and DIA, proteins with a significantly different abundance in either RO of patient A or B compared to the control were identified (Two-sided t-test, FDR 0.05, S0=0.1, n=3). Secondly, of those proteins, that did not differ significantly in abundance between samples from patient A and patient B were excluded (Two-sided t-test, FDR 0.05, S0=0.1, n=3). In this way, 3119 proteins were identified as significantly different in abundance between the two patients (data not shown). Of these, 1274 proteins were significantly increased in patient A compared to patient B (decreased in patient B), while 1845 proteins were significantly decreased in patient A compared to patient B (increased in patient B) (data not shown). Next, GO enrichment analysis was performed to identify significantly enriched BP and CC among the proteins that were significantly more abundant in the RO of the more affected patient A compared to patient B (**Figure 29 A**). Significantly enriched pathways in RO of patient A compared to RO of patient B included components and processes linked to the actin cytoskeleton (e.g. myofilament, stress fibres, actomyosin), lysosomal lumen and unfolded protein response (**Figure 29 A + Figure 30 A**). Further analysis using KEGG pathway enrichment showed a significant increase in HIF1 signalling components in the RO of patient A compared to patient B (**Appendix 20**). Next, GO enrichment analysis was performed in the CC and BC categories using proteins that were of significantly less abundant in patient A compared to patient B. Significantly reduced pathways in the RO of the more affected patient A include proteins associated with the photoreceptor (e.g. disc membrane, IS and OS), cilia (e.g. intraciliary transport particles, non-motile cilium, ciliary membrane), detection of light stimulus (e.g. phototransduction, sensory perception of light stimulus, signal release from the synapse) and signal transduction by p53 class mediators (**Figure 29 B + Figure 30 A**). KEGG pathway analysis further revealed a significant enrichment of proteins involved in NOTCH signalling, WNT signalling and RAS signalling among the low abundant proteins in patient A compared to patient B RO (**Appendix 20**).

Furthermore, 149 and 56 proteins identified as retinal interactor of CRB1 (canonical or extracellular) were of significant higher abundance in patient A and patient B RO, respectively (**Figure 30 B + Figure 31**). These included proteins involved in the actin cytoskeleton (e.g. FLNA), lysosome (e.g. TXNDC5), response to unfolded protein (e.g. CLGN, DNAJC3), detection of light stimulus (e.g. PLEKHB1), regulation of signal transduction by p53 class mediator (CSNK2A2, ZNF385A), WNT signalling (e.g.. SFRP2), RAS signalling (e.g. PLA2G6,

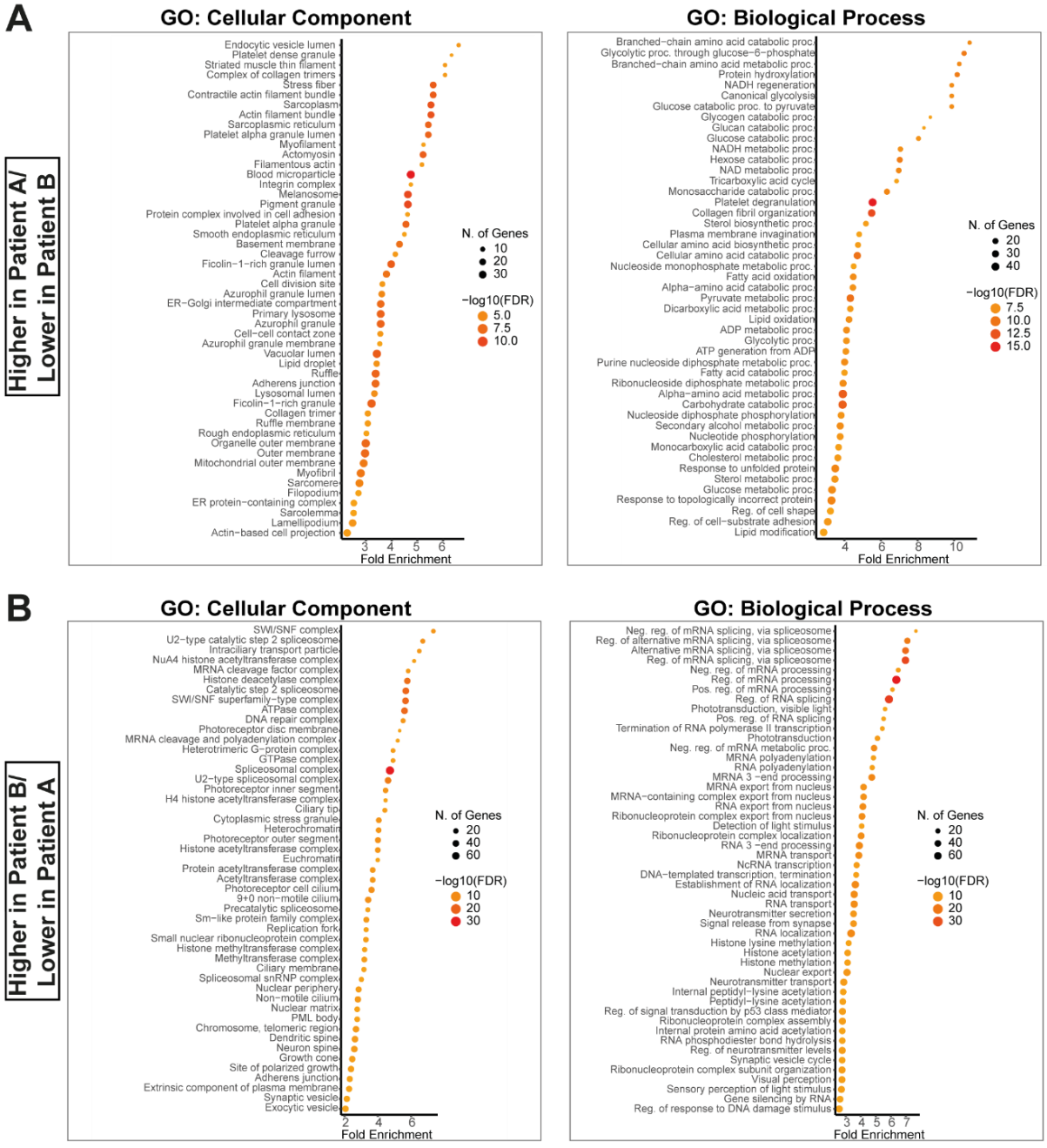

Figure 29| Patients RO show differences in pathways related to UPR, phototransduction and cilia
GO enrichment analysis in the CC (left panels) and BP (right panels) was performed using ShinyGO to identify significantly enriched pathways among proteins that are **(A)** significantly increased in patient A compared to patient B RO samples or **(B)** significantly decreased in patient A compared to patient B. Top 50 significantly enriched pathways/components are depicted (FDR 0.05).

AKT2), signal release from the synapse (e.g. PPIA2, RIMS2) and Notch signalling (e.g. CTBP2) (**Figure 31**).

Collectively, these data revealed that patient RO differ in the abundance of proteins related to the light-stimulus detection and synaptic signal release, which correlates with the previous Ca^{2+} imaging data and the clinical phenotype of the patients [22]. To further define discrete candidate genetic modifiers, WGS was performed as described in the next chapter.

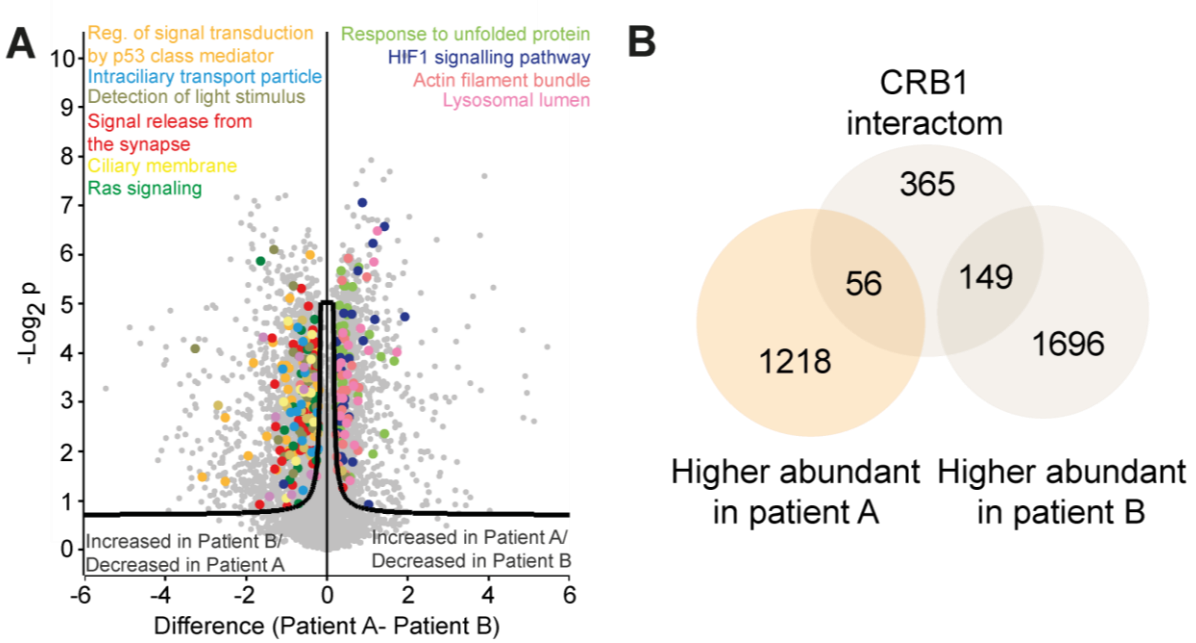

Figure 30| Lower abundant proteins in patient A RO are linked to cilia, synapse, light detection and signalling
(A) Volcano plot of the log difference (patient A- patient B) relative to the - $\log_2$ p value of proteins identified by full-proteome analysis using mass spectrometry and data-independent analysis of RO lysates from patient A compared to patient B. Each grey dot depicts a protein. Proteins that are significantly different are depicted in colours based on the function/component identified using ShinyGO GO enrichment analysis. **(B)** Venn diagram representing the overlap of CRB1 retinal interactors (canonical and extracellular) and the proteins that are significantly different between RO from patient A and patient B.

Collectively, these data revealed that patient RO differ in the abundance of proteins related to the light-stimulus detection and synaptic signal release, which correlates with the previous Ca^{2+} imaging data and the clinical phenotype of the patients [22]. To further define discrete candidate genetic modifiers, WGS was performed as described in the next chapter.

4.5.2 Potential candidate modifiers identified by short-read WGS

To identify potential disease modifiers, WGS using blood-extracted DNA and variant identification was performed by the Institute of Medical Genetics and Applied Genomics cATG/NCCT (Tuebingen) following their standard diagnostic pipeline. As expected, the homozygous G>A variant in the *CRB1* gene (c.2843G>A;p.C948Y) was confirmed as causal variant in both patients (**Appendix 22**). To identify candidate modifiers, variants were filtered for an allele frequency of below 0.1 % in the population cohort. Next, protein codon variants (missense, splice, stop and frameshift mutations), which could directly affect protein function and potential regulatory variants (3'UTR, 5'UTR, upstream, downstream), which could affect protein expression or stability, were selected. Additionally, potential regulatory variants (3'UTR, 5'UTR, upstream, downstream) were excluded if no significant change was observed in the full-proteomic analysis in between the patient and to the control (chapter 4.4.3). Subsequently, candidates that were not detected in full-proteome analysis of control RO lysate or were not

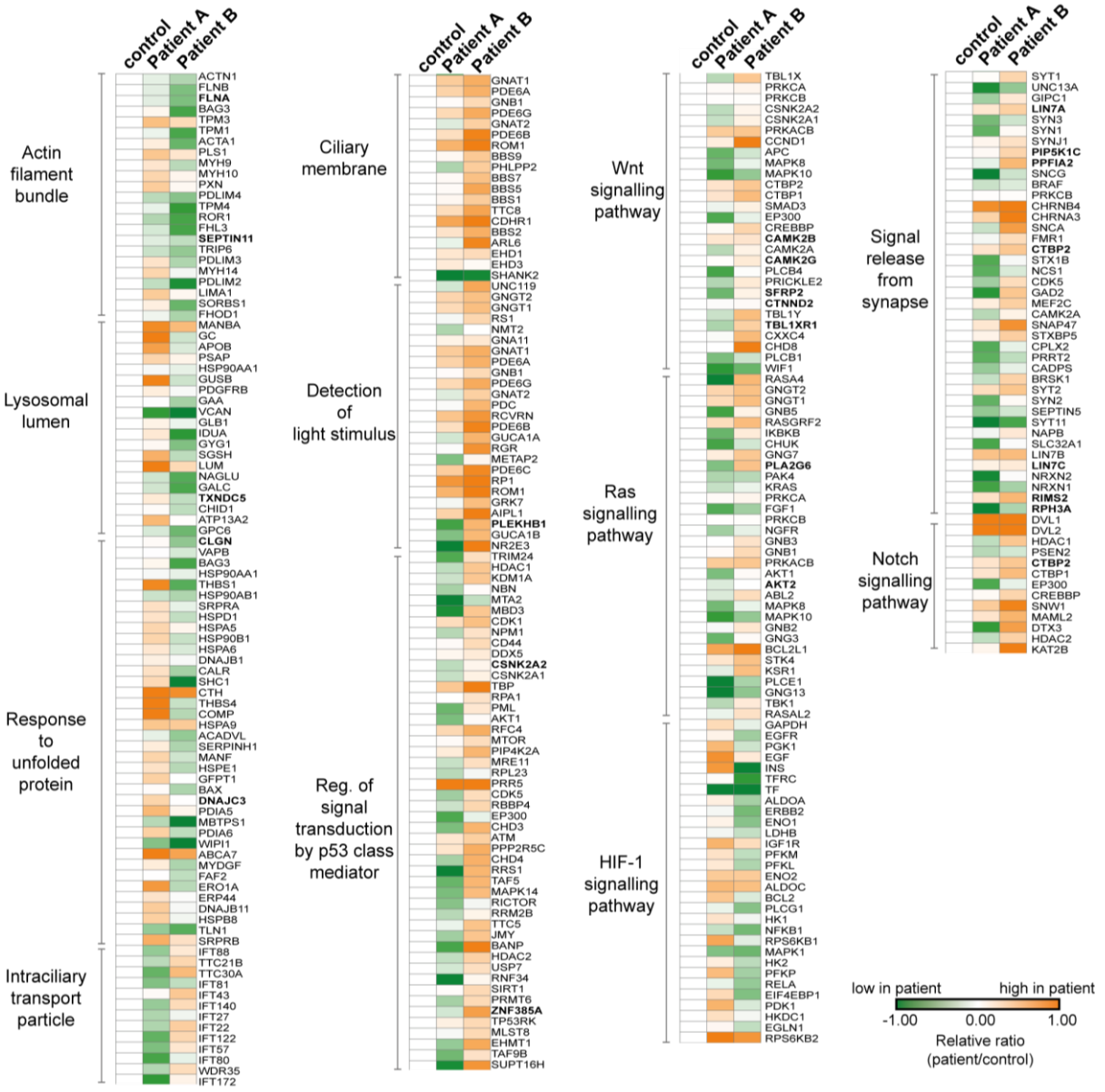

Figure 31| Patient A and patient B RO showed difference in the abundance of proteins linked to cilia, phototransduction, UPR and signalling
Heat map of the relative ratio of protein detected in patient A/control and patient B/control. Colour represents relative abundance compared to control. Proteins are grouped based on the categories detected in the GO enrichment analysis. Retinal interactors of either canonical or extracellular CRB1 are depicted in bold. (Two-sided t-test, FDR 0.05, S0=0.1, n=3). Raw data are presented in Appendix 21.

confirmed on protein level in the Human protein atlas database were excluded [196]. Finally, harmful variants were considered to occur homozygous or heterozygous in patient A and WT in patient B. Protective variants were selected to be homozygous or heterozygous in patient B and WT in patient A. Functional information on the proteins encoded by the candidate genes was obtained using the UniProt database [276].

4.5.2.1 Potentially harmful candidates of disease severity identified in the more affected patient A

Among the 62 potential harmful variants selected, three were previously identified as CRB1 interactors and three were associated with diseases with a retinal phenotype (**Appendix 23 + Table 20**). These included a heterozygous missense variant in *MAP7D1* identified in

Table 20| Potentially harmful candidate modifiers identified in patient A WGS was performed using blood samples from patient A and patient B. Upon diagnostic pipeline filtering, variants were filtered to be homo- or heterozygous in patient A and WT in patient B. Variants were filtered for missense, splice, frameshift, stop mutation. Variants in regulatory regions (upstream, downstream of a gene, 5'UTR, 3'UTR) were selected if their abundance in the full-proteome analysis was significantly different between patient A and B as well as to the control. Candidates depicted in this table are heterozygous in patient A and WT in patient B. Proteins in bold were previously identified as CRB1 interactors.

Gene	Variant type	Annotation/location	Function	OMIM
MAP7D1	Missense	c.1565A>C:p.Gln522Pro (ENST00000316156.8)	Microtubule, Cell cycle	
CDH23	Missense	c.9979G>A:p.Ala3327Thr (ENST00000224721.12)	Visual perception	Usher syndrome type 1D
CC2D2A	Missense	c.298A>C:p.Met100Leu (ENST00000389652.11)	Cilia assembly, Smoothened signalling	Joubert syndrome, Meckel-Gruber syndrome
CCDC88A	Upstream	chr2:55285997 G>A	Cilia biogenesis	PEHO syndrome-like
FAM120A	3'UTR Deletion	chr9:93565146 del:ATACA	Oxidative stress response	
RLBP1	Upstream insertion	chr15:89225800 ins:AAATA	Visual perception	

patient A, which is involved in cell cycle regulation and is part of the microtubule cytoskeleton. MAP7D1 protein levels were equal between RO lysates from patient A, patient B and control, suggesting that this modifier could potentially affect its functional activity rather than protein levels. Second, patient A carried a heterozygous SNV upstream of *CCDC88A*, a regulator of the actin cytoskeleton, cilium assembly and protein transport, which has been identified as a retinal CRB1 interactor. In addition, slightly but significantly lower levels of CCDC88A were observed in the RO lysates of patient A compared to patient B (**Figure 32**). Furthermore, a

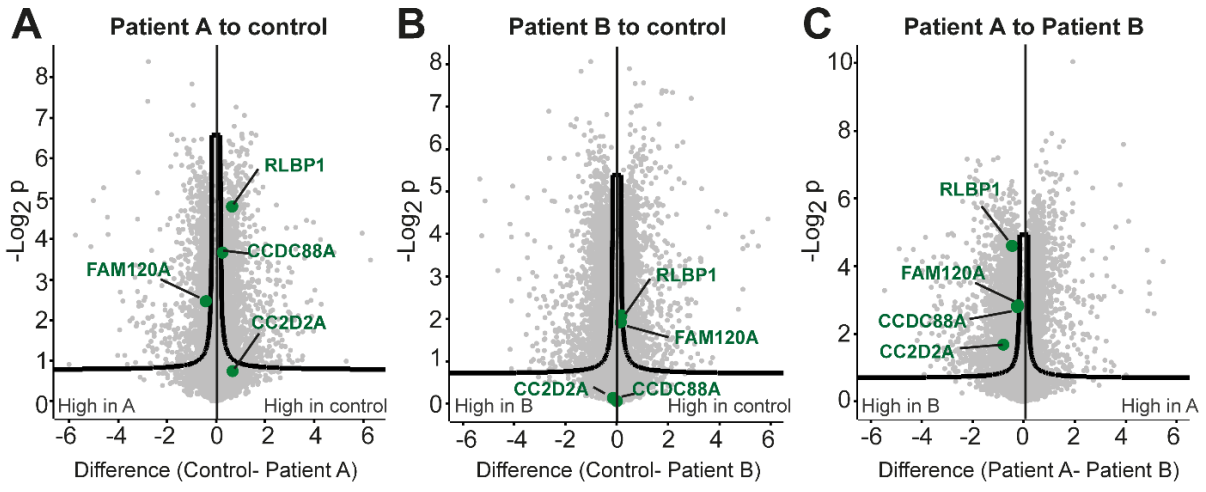

Figure 32| Potential candidate modifiers were mildly reduced in patient A RO lysate compared to patient B Full-proteome analysis was performed on RO lysates from patient A, patient B and control as described previously. Volcano plot of the difference in abundance depicted between **(A)** Control and patient A, **(B)** control and patient B and **(C)** patient A and patient B relative to the $-\log_2$ p value. Every grey dot represents a protein. Significantly changed candidates are marked in green. Experiment was performed with three technical replicates (chapter 4.4.3).

heterozygous deletion in the 5'UTR region of *FAM120A*, a regulator of the oxidative stress response, was detected, which was accompanied by a mild reduction in FAM120A protein levels in the RO lysates of patient A compared to patient B. In addition to the candidate modifiers within the CRB1 interactome, several variants in genes related to visual perception or retinal diseases were identified. First, patient A carried a heterozygous missense mutation in *CDH23*, which is involved in visual perception and is associated with Usher syndrome type 1D. Similar protein levels of CDH23 were detected in iPSC-RO from patient A, patient B and control, indicating that the variant may not affect CDH23 protein levels. Furthermore, a heterozygous missense variant in the Joubert syndrome protein *CC2D2A*, a regulator of cilia assembly, was identified in patient A. Interestingly, significantly lower levels of CC2D2A were observed in RO lysates from patient A compared to patient B. Finally, a significantly lower abundance of RLBP1, a regulator of visual perception was identified in RO lysates from patient A compared to patient B and control alongside with a heterozygous insertion upstream of *RLBP1* in patient A. Collectively, a panel of potential harmful candidate modifiers that could exacerbate the phenotype of patient A was identified based on WGS, PPI analysis and RO full-proteome analysis. Next, candidate modifiers that could prevent the development of severe symptoms in patient B were examined.

4.5.2.2 Potentially protective candidates of disease severity identified in the less affected patient B

To identify potential protective modifiers of disease severity, a similar approach was performed and with a filter for hetero- or homozygous variants detected in patient B. A total of 67 candidates were identified, of which eight were either associated with a retinal disease, vision, or identified as CRB1 interactors (**Appendix 24+ Table 21**). ARHGEF10 was identified

Table 21| Potential protective candidates in patient B include CRB2 Candidates were filtered to be homo- or heterozygous in patient B and WT in patient A, identified as CRB1 interactors, linked to vision or diseases associated with symptoms leading to vision loss. All variants are heterozygous in patient B and WT in patient A compared to the reference genome. Interactors are depicted in bold. shown

Gene	Variant type	Annotation/location	Function	OMIM
ARHGEF10	**missense**	**c.3544G>A:p.Ala1182Thr ENST00000349830.8**	**Actin cytoskeleton organization**	**Slowed nerve conduction velocity**
SPTB	**missense**	**c.1606G>A:p.Asp536Asn ENST00000389720.4**	**Spectrin cytoskeleton**	**Anemia, Elliptocytosis**
ARMC9	downstream	chr2: 231377515 G>A	Ciliogenesis, Sonic Hedgehog signalling	Joubert syndrome 30
CRB2	upstream	chr9: 123351196 G>T	Cell polarity	Focal segmental glomerulosclerosis 9, RP
PLEKHB1	**5'UTR**	**chr11: 73646286 G>T**	**Phototransduction**	
RBP3	upstream	chr10: 47346224	Visual pigment	RP
RDH12	upstream	chr14: 67699083T>G chr14:67699209C>T chr:14:67701643C>T	Photoreceptor cell maintenance	LCA
SRRT	**Upstream**	**chr7: 100874220A>T**	**Transcription regulation**	

as CRB1 interactor and is an important regulator of the actin cytoskeleton. Interestingly, a heterozygous missense variant in *ARHGEF10* was identified in patient B. As no significant differences in the abundance of ARHGEF10 were detected in full-proteome analysis of RO lysates from patient A, patient B and control, this variant, if any, may impair ARHGEF10 activity rather than stability (**Figure 33**).

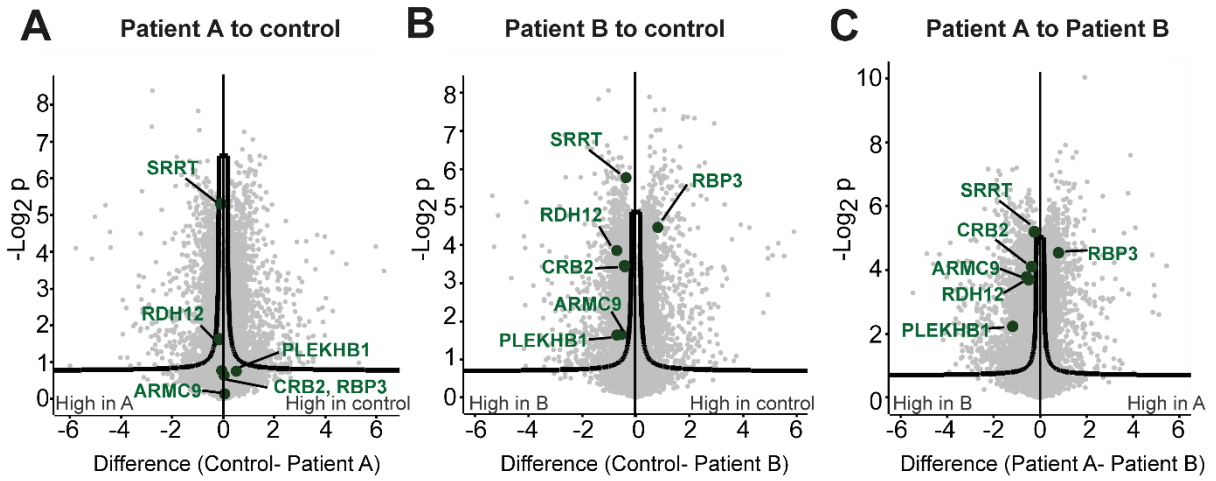

Figure 33| Protective candidates in patient B included the crumbs complex member CRB2
Volcano plot of the difference between **(A)** control and patient A **(B)** control and patient B and **(C)** patient A and patient B relative to the $-\log_2$ p value. Graph depicts the abundance of proteins in patient A, patient B and control RO lysates analysed by mass spectrometry and DIA-NN as described previously. Each dot depicts a protein. Significantly changed candidates between patient A and patient B are highlighted in green.

Furthermore, patient B carries a heterozygous missense variant in the CRB1 interactor *SPTB*, which is a member of the spectrin cytoskeleton. Again, this variant did not alter SPTB protein levels in RO lysates from the patient and control RO as analysed by mass spectrometry (Chapter 4.4.3). Furthermore, a small but significant increase in ARMC9 abundance was detected in RO lysates from patient A compared to patient B and control (**Figure 33**). ARMC9 is important for the localisation of the basal body to the cilium and has been described in patients with Joubert syndrome, which includes IRD. WGS revealed that patient B carries a rare heterozygous SNV downstream of *ARMC9*, which could potentially alter ARMC9 expression. In patient B, a 5'UTR variant and an upstream heterozygous variant were detected in, *PLEKHB1* and *SRRT,* respectively, both of which were identified as CRB1 interactors. In addition, PLEKHB1, which localises to the photoreceptor OS and has been suggested to modulate phototransduction, was significantly upregulated in RO lysates from patient B compared to patient A or control. Furthermore, patient B carried two upstream heterozygous variants in *RBP3* and *RDH12*, which are both linked to IRD. While RO lysates from patient B showed significantly higher levels of RDH12 compared to control or patient A, RBP3 levels were significantly decreased in patient B compared to patient A or control RO lysates. Finally, a heterozygous rare variant upstream of *CRB2* was identified in patient B, alongside with slightly but significantly increased levels of this protein in patient B compared to control and patient A RO lysate. Further analysis of the identified peptides revealed that not all, but the

majority of the peptides detected for CRB2 showed increased abundance in patient B compared to patient A RO lysate (**Appendix 25**). Taken together, these data provide valuable candidates for further analysis as protective candidates in the context of CRB1-linked IRD.

4.5.3 Both patients had an heterozygous variant of unknown significance in *GUCA1B* c.560G>A;p.S187N

The genetic analysis identified a variant of unknown significance was identified in *GUCA1B* c.560G>A;p.S187N. In addition, GUCA1B was one of the proteins whose abundance was significantly different between patient A and patient RO lysate (chapter 4.5.1). *GUCA1B* encodes for the neuronal Ca^{2+} sensor GCAP2, which is expressed in rod and cone photoreceptors [197]. GCAP2 binds to guanylate cyclases and stimulates their activity to produce cGMP at low Ca^{2+} concentrations [197]. In this way, GCAP2 is crucial to restore cGMP levels upon activation of phototransduction. GCAP2 contains four EF-hand domains with a helix-loop-helix structure, of which EF-hand 1 interacts with guanylate cyclases and EF-hand domains 2-4 are involved in Ca^{2+} binding [197]. GCAP2 p.S187N is located at the C-term end and not in any of the EF-hand domains (**Figure 34 A**). As other autosomal dominant mutations

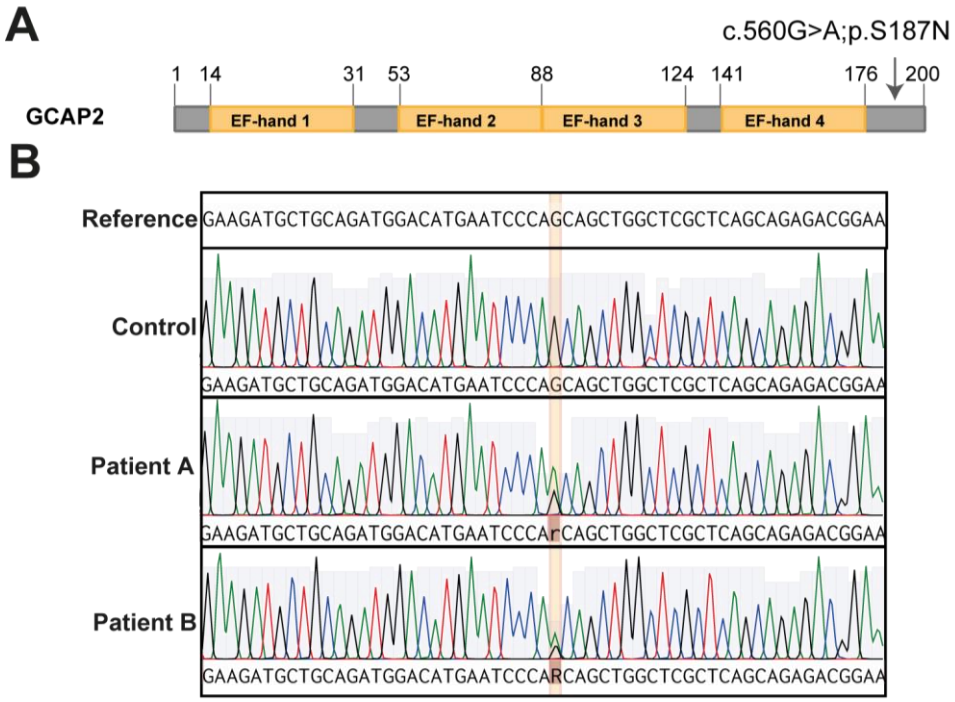

Figure 34| Both patients carried a heterozygous variant of unknown significance in *GUCA1B* c.560G>A;p.S187N encoding GCAP2
(A) Illustration of the protein structure of GCAP2 (encoded by *GUCA1B*) carrying four EF hand domains. The position of the mutation is indicated with an arrow. **(B)** The region of the variant was amplified from patient DNA samples by PCR and the amplicons analysed by Sanger sequencing. As a control, DNA from ARPE19 cell lines was used. Variant of unknown significance *GUCA1B* c.560G>A is highlighted in orange.

in GCAP2 have been described in patients with RP and dysfunction of GCAP2 could explain the phenotype observed during Ca^{2+} imaging of RO, further confirmation that the mutation is present in both patients was of high interest. Therefore, the region of the variant of unknown

significance was amplified by endpoint PCR and analysed by Sanger sequencing (**Figure 34 B**). Results obtained confirmed that both patients were carriers of the heterozygous *GUCA1B* c.560G>A variant indicating that this mutation alone could not explain the severe phenotype seen in patient A.

Collectively, these data show that both patients carry a heterozygous variant of unknown significance in *GUCA1B*, which is located outside of the Ca^{2+} binding domains. In addition, the variant was confirmed in both patients, leading to the conclusion that it cannot be a primary explanation for the clinical variance seen in between the two brothers and the RO.

In conclusion, in this chapter, the differences in the RO of the severely affected patient A and the less affected patient B were investigated and a panel of potential protective and harmful candidate modifiers was selected. Among the protective candidates the CRB family member CRB2 was identified, which has already been shown to rescue the phenotype in a CRB1-linked mouse model and in CRB1 patients-derived RO [94, 167]. As the molecular mechanism underlying the protective effects of CRB2 is still poorly described, the relationship between CRB1 and CRB2 in the retina was further investigated in the next chapter.

4.6 Investigation of the molecular mechanism underlying CRB2 as a potential modifier in CRB1-linked retinal degenerations

Several lines of evidence point to CRB2 as a potential modifier in CRB1-linked IRD [24, 94, 167]. However, the underlying molecular mechanisms remain under investigated. Given that CRB2 was additionally identified as one of the protective candidate modifiers, that was increased in the RO of the less affected patient B, the next aim was to further investigate the relationship between CRB1 and CRB2 regarding their interaction and the retinal interactome. Of note, this chapter 4.6 is taken and adapted from a manuscript, which is under revision at Life Science Alliance [1].

4.6.1 Human CRB1 and CRB2, but not CRB3, adhered homo- and heterotypically

The localisation of CRB1 and CRB2 at the OLM has been previously described by Pellissier *et al.* and Quinn *et al.* [14, 15]. Given this, the next aim was to investigate whether human CRB1, which interacts homotypically as shown in chapter 4.2.3, also binds to the other members of CRB protein family, CRB2 and CRB3, as previously shown for zebrafish CRB2a and CRB2b [140]. CRB1 and CRB2 both have a large extracellular domain of multiple EGF repeats and Laminin G domains, which is absent in CRB3 (**Figure 35 A**) [16]. Therefore, canonical human CRB1, CRB2, CRB3A were tagged with a FLAG or HA-tag followed by pairwise overexpression of these constructs in HEK293T cells [1]. GFP-HA was transfected as a negative control to exclude unspecific binding to the beads or tag [1]. After 48 hours of

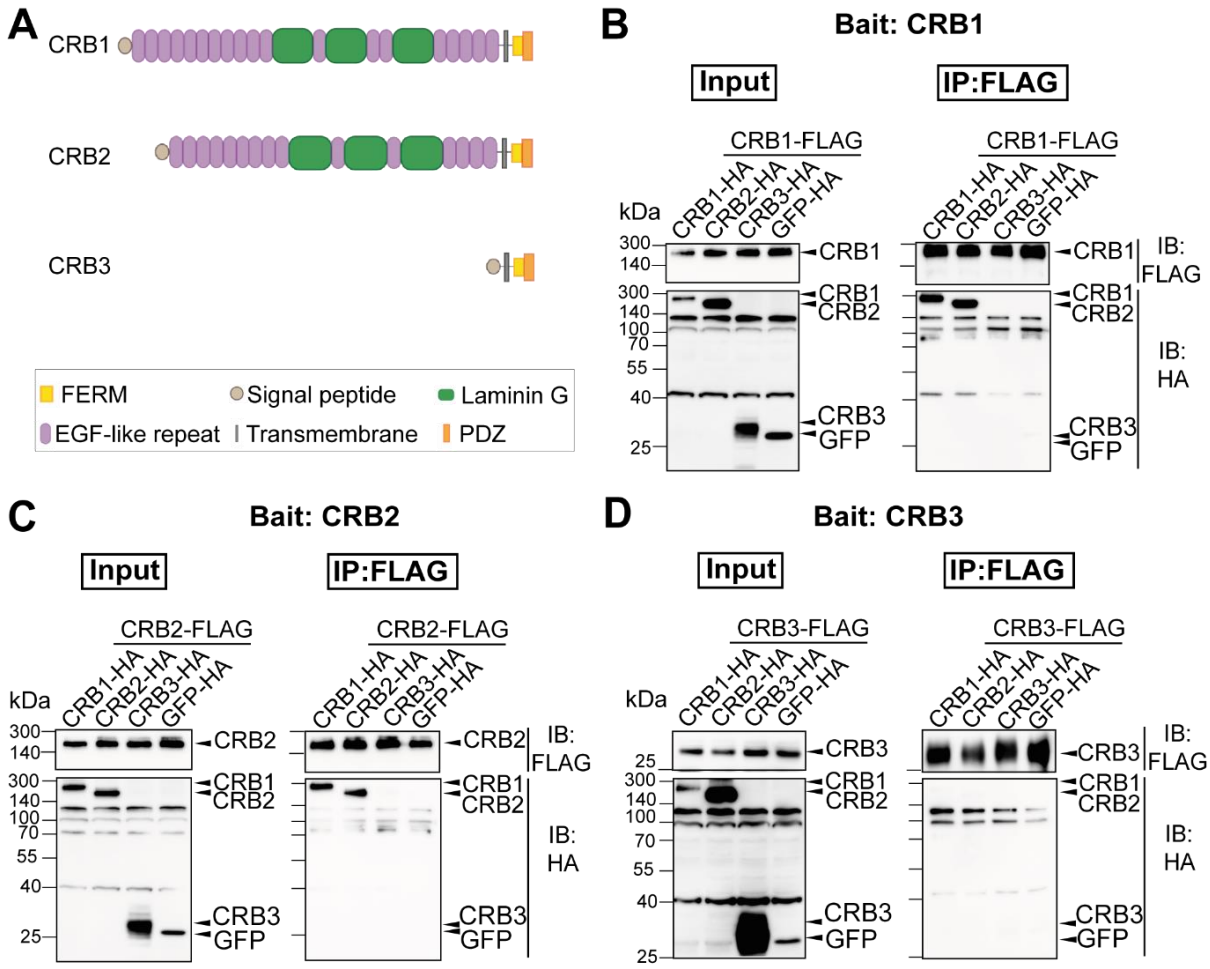

Figure 35| Human canonical CRB1 and CRB2 interacted homo- and heterotypically
(A) Schematic illustration of the protein structure of human canonical CRB1, CRB2 and CRB3. Colours represent the predicted protein domain. **(B)** CRB1-FLAG, **(C)** CRB2-FLAG, **(D)** CRB3-FLAG were co-transfected with CRB1-HA, CRB2- HA, CRB3-HA or GFP-HA as negative control in HEK293T cells. Inputs (left panel) and eluates after FLAG-IP (right panel) were analysed by western blot using an anti-HA and anti-FLAG antibodies. Representative blots of three independent experiments are depicted. This figure and figure legend are part of the manuscript [1]

transient overexpression, cells were lysed, and lysates (input) and eluates after FLAG-IP were analysed by western blot [1]. Western blot analysis of the input confirmed expression of all constructs. Using human canonical CRB1-FLAG as a bait, binding of CRB1 to CRB1 and CRB2 but not to CRB3 or GFP was demonstrated (**Figure 35 B**) [1]. Similarly, CRB2-FLAG, as a bait, interacted with CRB1 and CRB2 but not with CRB3 or GFP (**Figure 35 C**) [1]. Finally, using CRB3-FLAG as bait, no interaction was observed with any of the CRB family protein members and GFP (**Figure 35 D**) [1]. Taken together, these data show that human CRB1 and CRB2, but not CRB3, form homo- and heteromeric interactions hinting towards a role for the extracellular domain in this interaction [1].

4.6.2 CRB2 pulled-down endogenous CRB1 from retinal tissue

An interaction between CRB1 and CRB2 hints towards a possible interdependence of CRB1 and CRB2 at the OLM in the retina [1]. In addition, several studies allow to hypothesise a possible functional redundancy of CRB1 and CRB2 [94, 167, 168]. To further investigate this

interdependence and the role of CRB1-CRB2 interaction in the retina, the porcine retinal pull-down approach described for CRB1 in chapter 4.3, was performed using FLAG-tagged human CRB2 as a bait [1]. Briefly, human CRB2-FLAG or GFP-FLAG (control) was transiently overexpressed in HEK293T cells followed by FLAG-IP [1]. Baits bound to FLAG-beads were washed with 0.01 % SDS and incubated with or without porcine retinal lysate. After elution, the protein complexes were analysed by mass spectrometry and DDA [1].

After SDS washing and without incubation with porcine retinal lysate, 144 proteins remained significantly enriched in the CRB2 bait samples compared to the GFP control (One-sample t-test, FDR 0.05, log_2 ratio (CRB2/GFP)>2) (**Appendix 26**) [1]. Next, the PPI network of human CRB2 was explored after the addition of porcine retinal lysate [1]. 300 proteins were significantly enriched in the CRB2 bait samples compared to the control upon incubation with porcine retinal lysate (**Figure 36 A + Appendix 27**) [1]. Of these, 212 proteins were specifically

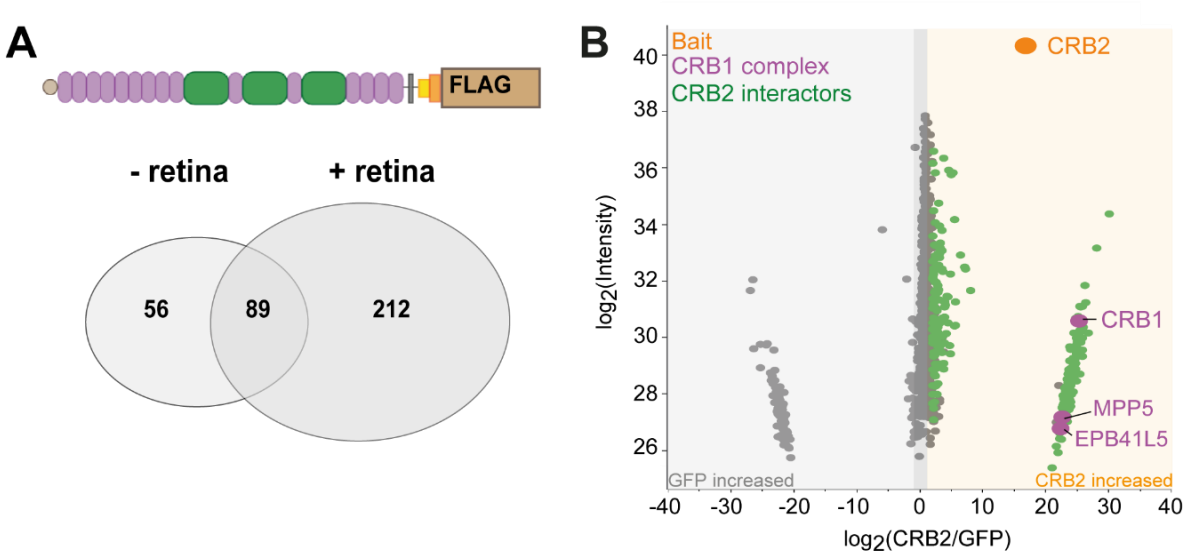

Figure 36| CRB2 pulled-down endogenous CRB1 from retinal tissue
Porcine retina pull-down approach was performed for human CRB2-FLAG relative to GFP-FLAG (control) with and without incubation of retinal lysate. **(A)** Venn diagram of the significantly enriched proteins in CRB2-FLAG compared to GFP with and without incubation of porcine retina. **(B)** Scatter plots of the log_2 ratio of proteins identified in CRB2-FLAG relative to GFP-FLAG (control) after porcine retinal lysate incubation. Each dot depicts a protein. Bait proteins are depicted in orange. Significantly enriched proteins in bait-FLAG samples compared to GFP are shown in green. Crumbs complex members that were significantly enriched in the CRB2-FLAG samples are depicted in purple (One-sample t-test, FDR 0.05, log_2 ratio (bait-FLAG/GFP-FLAG) >2, n=6). **[1]**

detected as significant CRB2 interactors upon incubation with porcine retina, including CRB1 and the two CRB complex members MPP5 and EPB41L5 (**Figure 36 B**) [1]. As previous data revealed that CRB1 is not expressed in HEK293T cells, the detected CRB1 was most likely derived from the porcine retina [1]. To further confirm this, specific CRB1 peptides detected by mass spectrometry were analysed [1]. Despite the high similarity between porcine and human CRB1, the detected peptides confirmed the pull-down of porcine CRB1 by human CRB2

(**Appendix 28**) [1]. Taken together, these data suggest a strong interaction between CRB1 and CRB2 in a retinal context [1].

4.6.3 Retinal protein-protein interaction network of CRB1 and CRB2 were highly overlapping

The fact that human CRB1 and CRB2 interact in the retina together with previously published studies, allows to hypothesise a corroborative role in the retina [1]. Given this reason, the retinal PPI network of CRB2 was further explored [1].

A total of 174 proteins were identified in the retinal interactome of CRB2-FLAG and canonical CRB1-FLAG (**Figure 37 A**) [1]. GO enrichment analysis was performed using the

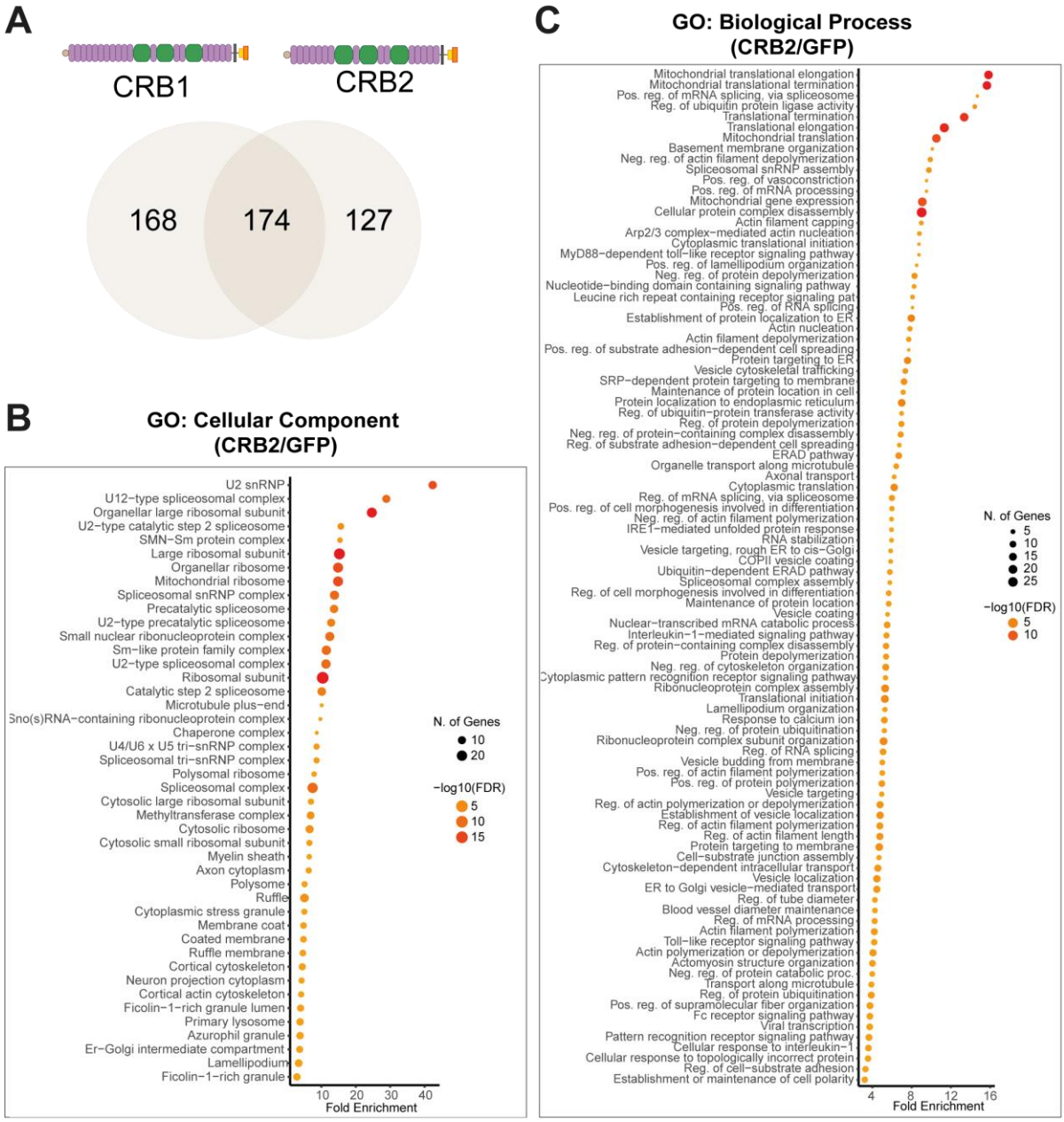

Figure 37| Retinal protein-protein interaction linked CRB2 to actin cytoskeleton and vesicular transport
(A) Venn diagram of the overlap of the characterised retinal interactors of canonical CRB1-FLAG and CRB2-FLAG **(B-C)** GO enrichment analysis of the significantly enriched **(B)** CC and **(C)** BP using the CRB2-FLAG retinal interactor. Top 100 significantly enriched pathways are shown (FDR<0.05). [1]

significantly enriched proteins in CRB2-FLAG samples compared to GFP upon incubation with porcine retinal lysate [1]. In line with the canonical CRB1 retinal interactor, significantly enriched components in the CRB2-FLAG interactome include ‘axon cytoplasm’, ‘cortical actin cytoskeleton’ and ‘microtubule plus-end’ (**Figure 37 B**) [1]. In contrast to the canonical CRB1-FLAG, ‘presynaptic active zone’ and ‘GABAergic synapse’ were not significantly enriched components in the CRB2-FLAG retinal PPI network [1]. In addition, several BP associated with the actin cytoskeleton, vesicular transport and microtubule cytoskeleton were significantly enriched in the CRB2-FLAG similar to the CRB1-FLAG retinal interactome (**Figure 37 C**) [1]. This includes proteins involved in cell-cell adhesion (e.g. EPB41, TJP2, EPB41L3), actin capping (e.g. TMOD2, FLII), actin binding (e.g. GSN and ABLIM1), ARP2/3 complex (e.g. ARPC2, ARPC1A), actin motor proteins (e.g. MYO5A, MYO1C), Rho GTPases (e.g. ARHGEF10, ARHGAP21) as significant retinal interactors of CRB2 similar to CRB1 (**Figure 38**) [1]. Similar to the CRB1 retinal interactome, the CRB2 interactome comprised proteins involved in microtubules (e.g. CALSP1, DCTN2), signalling (e.g. LTBP1, STK38, TAB1), lipid metabolism (e.g. EFR3A, PTDSS1) and vesicular transport (e.g. ARL8A, PDCD6) [1]. Compared to CRB1-FLAG, BP including ‘neurotransmitter secretion’ and ‘signal release from the synapse’ were not significantly enriched in the CRB2-FLAG retinal PPI network [1]. Illustrating this point, only four of the identified proteins linked to synapse were part of the CRB2 retinal interactome (e.g. SV2B, FARP1, DMXL2 and HOMER1) [1]. In contrast, ‘response to Ca^{2+} ions’ (e.g. CAV1 and GUCA1A1) were identified among the significantly enriched pathways in the CRB2-FLAG retinal PPI network [1]. In addition, other photoreceptor-related proteins were identfied as part of the CRB2 interactome (e.g. RDH11, CLCC1, CRYBB3 and SLC24A1) [1].

Taken together, these data indicate that the CRB2 retinal interactome not only includes CRB1 and the core CRB complex members but also shows a high overlap with retinal interactors involved in the cytoskeleton, vesicular transport, signalling, cilia and lipid metabolism [1].

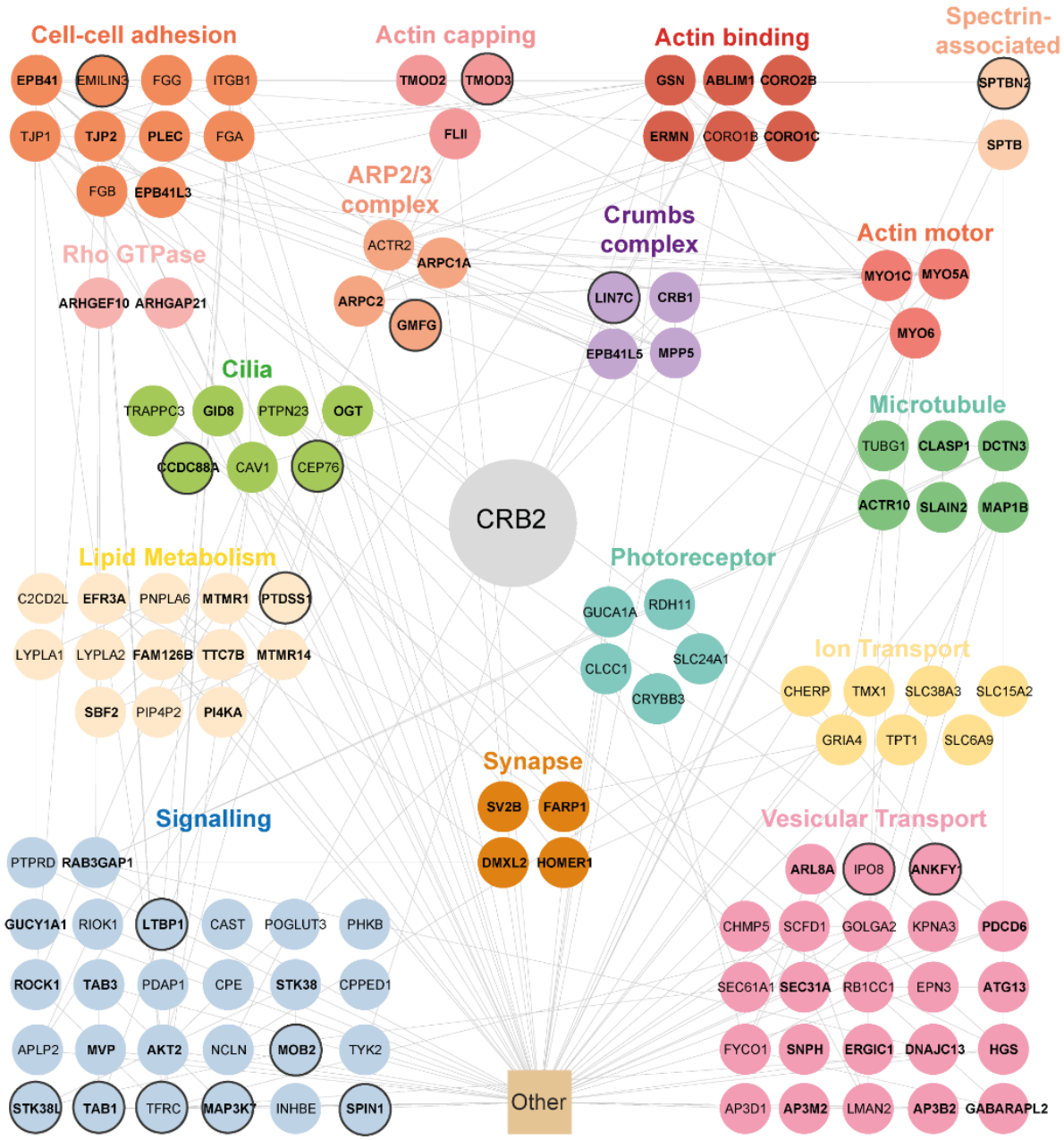

Figure 38| CRB2 protein-protein retinal interaction network included proteins involved in signalling, lipid metabolism, cytoskeleton, cilia and ion transport
Significantly more abundant proteins in CRB2-FLAG compared to control after incubation with porcine retinal lysates were analysed using String and Cytoscape. Colours represent BP based on Uniprot database and literature. Grey lines indicate reported interactions based on database/experiment. Proteins involved in mitochondria, transcription, DNA binding, splicing and chaperones are grouped as other. Proteins with a grey circled border are also identified as significantly enriched without incubation of porcine retina, indicating a possible carry-over from the bait-producing HEK293T cells. Proteins depicted in bold are identified as part of the CRB1 retinal PPI network**.** [1]

4.6.4 Missense mutations in the CRB1 extracellular domain only mildly influenced CRB1-CRB2 interaction *in vitro*

Since patient-described missense mutations in the CRB1 extracellular domain slightly influence CRB1-CRB1 interaction, the next aim was to investigate the effect of these missense mutations on the binding of canonical CRB1 and CRB2 [1]. To address this aim, co-IP was performed upon pairwise overexpression of canonical FLAG-tagged human canonical CRB1 WT or CRB1 MT (p.C480R, p.C681Y., p.C948Y, p.G1103R, p.Y1161C, p.C1174G and p.N1317H) together with HA-tagged CRB2 (**Figure 39 A**) [1].

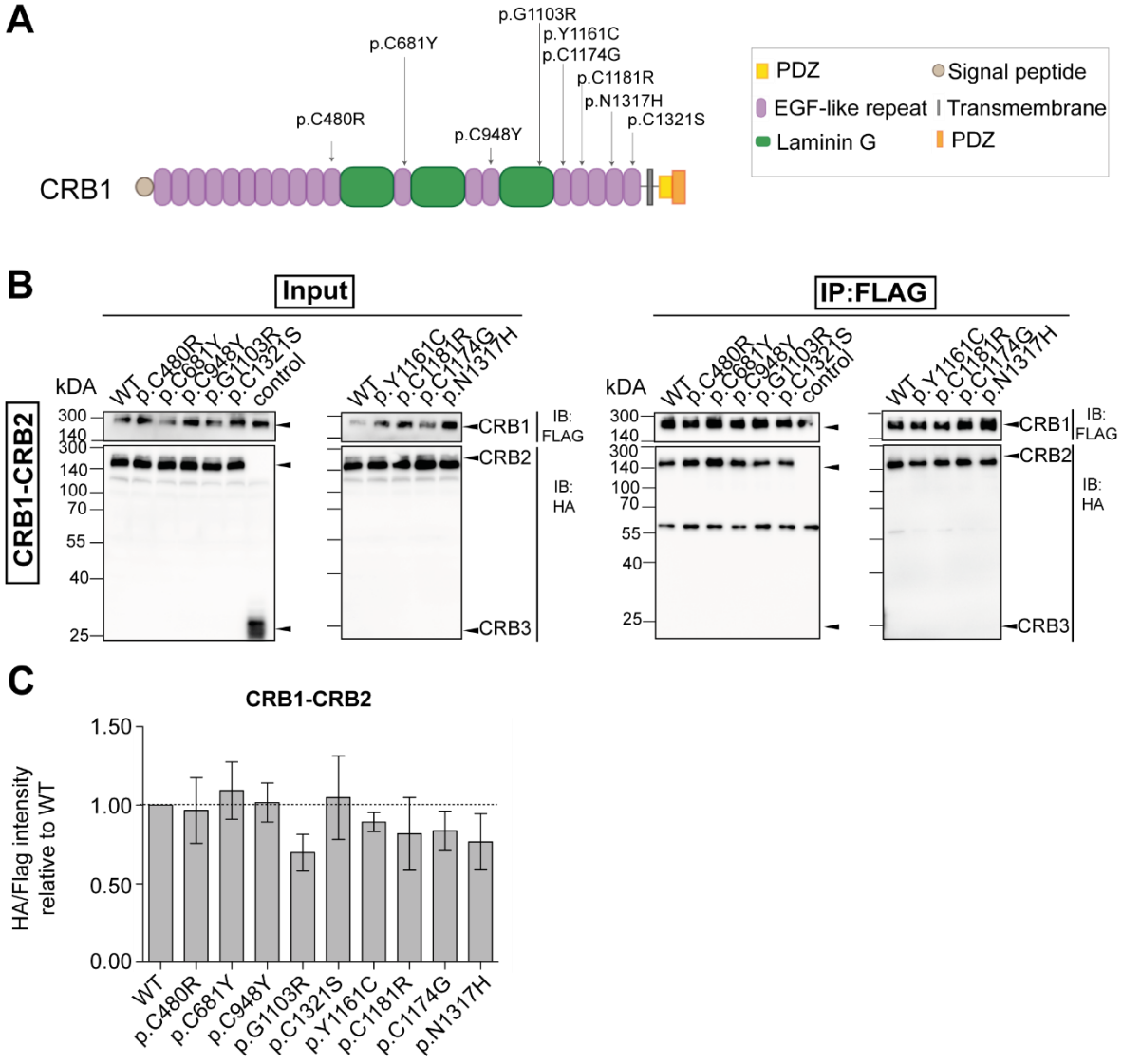

Figure 39| CRB1 missense mutations tested did not or mildly alter CRB1-CRB2 interaction
(A) Graphical illustration of the patient's missense mutations introduced in the canonical CRB1 construct. **(B)** CRB1-FLAG constructs WT or MT were co-transfected with CRB2-HA in HEK293T cells. CRB3-HA was co-transfected as control. Upon FLAG-IP, input (Left panel) and eluates (right panel) were analysed by western blot with HA- and FLAG antibodies. **(C)** Quantification of the signal intensity HA/FLAG in eluates after FLAG-IP relative to WT of three biological replicates. Data depicts mean ± SEM. This figure and figure legend are part of the manuscript. [1]

After 48 hours, the input and eluates upon FLAG-IP were analysed by western blotting. In general, none of the mutations resulted in a complete loss of CRB1-CRB2 interaction (**Figure 39 B+C**) [1]. Illustrating this point, CRB1 p.C681Y, p.C984Y and p.C1321S show similar binding to CRB2 compared to CRB1 WT [1]. Similarly, CRB1 p.C480R retains approximately 96 % of the ability to bind CRB2 compared to CRB1 WT [1]. Nonetheless, certain mutations showed a mild, although not significant, effect on the CRB1-CRB2 interaction [1]. A slight decrease of 11 %, 19 %, 17 % and 24 % was observed for CRB1 p.Y1161C, p.C1181R, p.C1174G and p.C1317H, respectively [1]. Furthermore, CRB1 p.G1103R, which is located in the last Laminin G domain, reduced CRB1-CRB2 adhesion by approximately 30 % compared to CRB1 WT [1]. Overall, these data indicate a mild but not significant impact of certain, but not all, CRB1 missense mutations in the extracellular domain on the CRB1-CRB2 interaction [1].

In conclusion, results obtained indicated a strong interaction of CRB1 and CRB2 in the retina, which was only slightly affected by the missense mutations described in *CRB1* patients. In addition, a high overlap was observed in the PPI of CRB2 and CRB1, further strengthening CRB2 as a potential modifier in *CRB1*-linked retinal diseases. In order to further assess the panel of candidate modifiers including CRB2, a large-scale analysis would be beneficial to complement studies on iPSC-derived RO. Therefore, in the next chapter, the first steps towards establishing a porcine retinal explant system to study CRB1 modifiers will be presented.

4.7 Establishment of a porcine retinal explant system to screen for candidate modifiers in CRB1-linked retinal degenerations

ROs provide a powerful tool for studying disease mechanisms and drug efficacy and toxicity [271]. However, the culture of RO is time-consuming, costly and tend to be small-scale [272]. This chapter aimed to evaluate an alternative approach to narrow down the list of candidate modifiers, to be tested in RO. Recently, gene silencing by reverse magnetofection has proven to be highly effective in retinal explants of rats [184]. Given the high similarity of human and porcine CRB1, the aim was to establish a porcine retinal explant system, that would allow silencing of *CRB1* and candidate modifiers by reverse magnetofection or chemical inhibition. This will allow to screening and narrowing down the list of candidate modifiers prior to evaluation in ROs.

4.7.1 Expression of CRB1 was variable in different regions of the pig retina and different eyes

Studies in mice suggest that Crb1, which is only expressed in Müller glia cells in the murine retina, is highly expressed in the superior retina compared to the inferior retina [15]. In contrast Crb2, which is expressed in photoreceptor and Müller glia cells, is highly expressed in the inferior region [15]. Given this reason, the aim was to investigate the levels of CRB1 in different region of the porcine retina. To address this aim, punches were taken from different regions of the porcine retina and CRB1 expression was analysed by RT-qPCR and western Blot (**Figure 40 A**). Preliminary data showed variable expression of CRB1 in different regions of the retina.

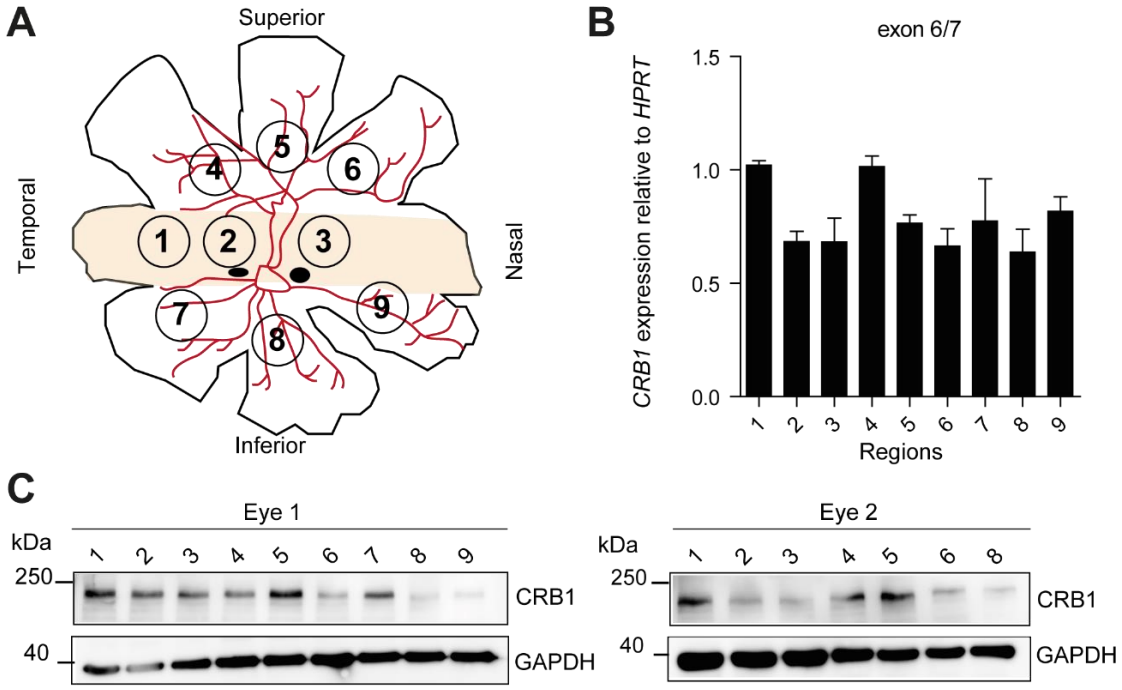

Figure 40| Expression of CRB1 varied in different regions of the porcine retina
(A) Schematic representation of the porcine retina, adapted from Armento *et al*. [269]. Red lines indicate blood vessels. Orange area represents the visual streak (cone-rich region). Circles represent the punched area. **(B)** Relative expression of *CRB1* in different regions of the porcine retina relative to the *HPRT* housekeeping gene. Data depict mean ± SEM of two biological replicates performed with three technical replicates. **(C)** CRB1 protein levels were analysed in different porcine retina explant regions of two donor eyes (left and right panel) by western blot analysis. GAPDH was used as a loading control. Anti-CRB1 antibody from Abnova was used.

In the superior region, there was a tendency for higher expression in the more temporal and central side (region 4 and 5) (**Figure 40 B+C**). In the inferior region, CRB1 levels were similar to the central region with one eye showing higher expression in the temporal side (region 7). In the cone-rich area, the temporal section (region 1) had high levels of CRB1 at both mRNA and protein levels compared to the central region (2+3). In the central region (2+3), CRB1 levels seemed to be lower, however, reproducibly equal using both western blot and RT-qPCR. Therefore, region 2 and 3 were selected to perform siRNA mediated silencing using a *CRB1* siRNAs or control. Taken together, these preliminary data suggest a variable expression of

CRB1 in the porcine retina with a trend towards higher expression in the temporal and superior regions.

4.7.2 Preliminary knockdown experiments of *CRB1* in porcine retina explants by reverse magnetofection

In a next step, the aim was to test silencing of *CRB1* in porcine retinal explants. To this end, three porcine retinal explants were taken in the central part of the retina (region 1 and 2) of two retinas and cultured on transwells (**Figure 41 A**). After 6 hours, siRNAs were complexed

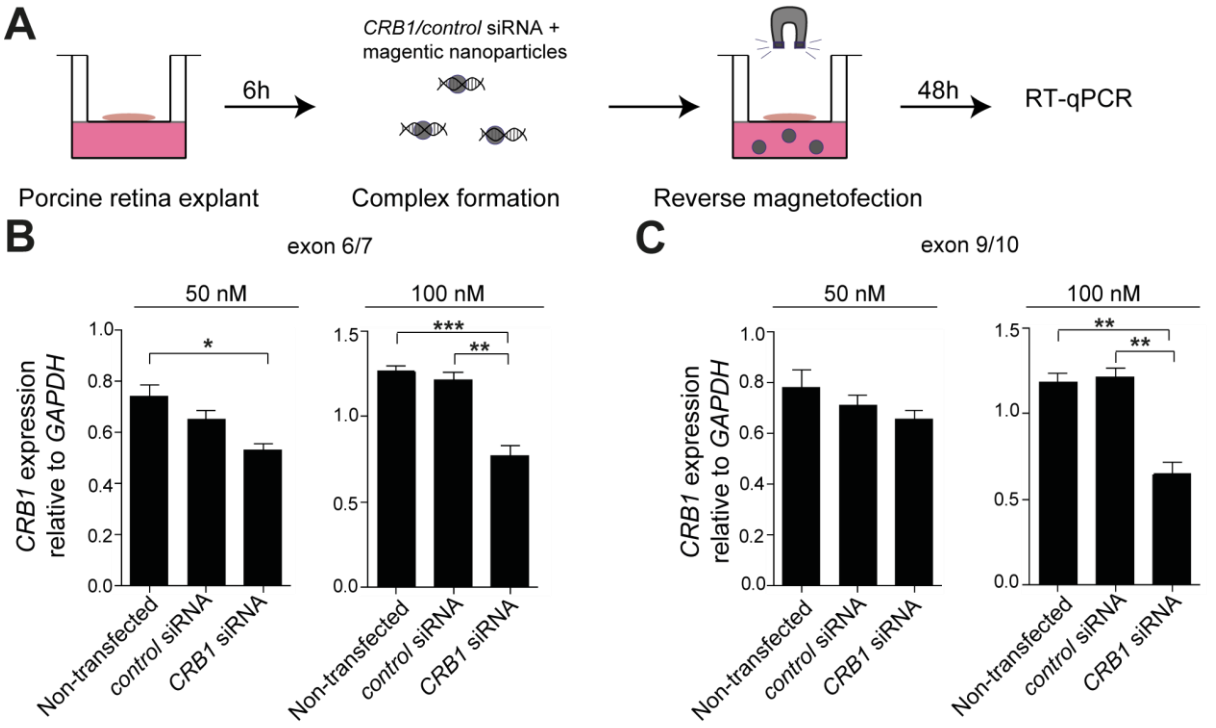

Figure 41| Preliminary data on CRB1 silencing in porcine retina explants
(A) Schematic representation of the experimental workflow. Retinal explants were extracted and cultured on trans-well plates. After 6 hours, control or a pool of three *CRB1* siRNAs were complexed with magnetic nanoparticles and transfected into porcine retinal explants by reverse magnetofection. After 48 hours, RNA was isolated and converted to cDNA and analysed by RT-qPCR. **(B)** mRNA expression of *CRB1* relative to *GAPDH* 48h after transfection with 50 nM or 100 nM of siRNA. CRB1 exon spanning primers from exon 6 to 7 (left panel) and from exon 9 to 10 (right panel) were used. Graph depicts mean ± SEM of three technical replicates of one biological replicate. For statistical comparison a one-way ANOVA with a Tukey's Multiple Comparison Test was performed. *p≤0.05; **p≤0.01, ***p≤0.001

with magnetic nanoparticles followed by reverse magnetofection. In short, RNA-magnetic nanoparticle complexes were added to the medium chamber and a magnet was placed on top of the plate. For *CRB1*, three siRNAs were used as a pool. A negative scramble siRNA (control siRNA) and magnetic nanoparticles alone (non-transfected) were used as controls. Three retinal explants from the first retina were used for non-transfected, control siRNA and 50 nM *CRB1* siRNA. The three explants from the second retina were used for non-transfected, control siRNA and 100 nM *CRB1* siRNA. After 48 hours, RNA was isolated followed by cDNA synthesis and RT-qPCR. Results obtained indicate that 50 nM of *CRB1* siRNA reduces *CRB1* levels by

approximately 19 % and 9 % using exon 6/7 primers and exon 9/10 intron spanning primers, respectively, compared to control siRNA (**Figure 41 B**). The differences in *CRB1* mRNA levels were statistically significant using exon 6/7 primers (One-way ANOVA, n=3, $F(2,6)= 9.08$, $p < 0.05$) between non-transfected and 50 nM of *CRB1* siRNA transfected samples (Tukey's Multiple Comparison Test, $p < 0.05$). *CRB1* silencing using 100 nM significantly reduced CRB1 levels by approximately 37 % and 47 % using exon 6/7 primers (One-way ANOVA, n=3, $F(2,6)= 31.05$, $p < 0.001$, Tukey's Multiple Comparison Test, $p < 0.01$) and exon 9/10 (One-way ANOVA, n=3, $F(2,6)= 28.21$, $p < 0.001$, Tukey's Multiple Comparison Test, $p < 0.01$) primers, respectively, compared to control siRNA. No significant difference was found between control siRNA and *CRB1* siRNA transfected condition, indicating that the control siRNA does not affect CRB1 expression, as expected. Of note, a difference in the initial expression of *CRB1* was observed in the eyes used for 50 nM and 100 nM. Therefore, the experiment should be repeated to assess the optimal concentration for efficient silencing. Nonetheless, these preliminary data indicate that silencing of *CRB1* may principally work in porcine retinal explants, but further determination of the experimental condition is required.

4.7.3 Generation of monoclonal antibodies against human and porcine CRB1 and CRB2

To improve the assessment of the *CRB1* knockdown in the porcine retina and its subsequent consequences, the lack of a working CRB1 antibody in the porcine retinal section provided a major challenge. In addition, the CRB1 Abnova only recognises the human canonical isoform of CRB1, while CRB1-B and CRB1-C are not detected. Therefore, the next step was to generate and validate CRB1 monoclonal antibodies that recognise both human and porcine CRB1. Additionally, the aim was to generate a CRB1 antibody recognising the three major isoforms in the human retina CRB1 A-C [91]. Three peptides were selected for CRB1 and two peptides were selected for CRB2 (**Table 22 + Appendix 29**).

Table 22| Overview of the antigen peptides used for monoclonal antibody production Table depicts the given name of the peptide with the according information regarding the protein, species and peptide sequence.

Name	Protein	Peptide information	Peptide sequence
CRB1A	CRB1	Pig sequence N-term	LDKDCDDEKDPCF
CRB1B	CRB1	Human sequence exon 6 (all CRB1 isoforms)	YQCDCHRPYEGPNC
CRB1C	CRB1	Human sequence C-term intracellular	NKRATQGTYSPSRQEK
CRB2A	CRB2	Human and pig N-term	LDLDECQSQPCAH
CRB2B	CRB2	Human and pig C-term	KRRQSEGTYSPSQQE

The generation of monoclonal antibodies was carried out together with the Core Facility Monoclonal Antibodies at the Helmholtz Center Munich, which performed antigen immunisation and fusion, multiplex-high throughput screening, titre assessment and subcloning.

For a first screening of the hybridoma supernatants, human canonical CRB1 or CRB2 tagged with a FLAG tag was transiently overexpressed in HEK293T cells, which were lysed after 48 hours. Subsequently, lysates were analysed by western blot analysis using a multiscreen device. Positive clones were validated on porcine retinal lysate by western blot analysis and immunofluorescence microscopy using porcine retinal slices, human donor retina and human iPSC-derived ROs. Out of a total of 111 hybridoma supernatants, five were shown to recognise human CRB2 but not porcine CRB2 by western blot analysis (**Appendix 30**). In addition, none of the five clones was able to detect CRB2 at the OLM in porcine retina, human iPSC-derived RO and human retina. For CRB1, two clones (CRB1C 25G2 and CRB1B 27A5) were able to detect human and porcine CRB1 using western blot analysis (**Figure 42 + Appendix 30**). CRB1C 25G2, is directed against a peptide in the conserved intracellular domain of CRB1, whereas CRB1B 27A5 recognises a peptide in exon 6, which is conserved in the three major isoforms described by Ray *et al* [91]. Furthermore, CRB1C 25G2 was shown to detect CRB1 at the OLM in human iPSC-derived RO and porcine retinal sections using immunofluorescence microscopy while CRB1B 27A5 was shown to detect in human iPSC-derived RO (**Figure 42 C+D**). In porcine retina section, CRB1B 27A5 does not detect CRB1 at the OLM but rather stained the IS. Next, the CRB1C 25G2 and CRB1B 27A5 clones were re-cloned by the Core Facility Monoclonal Antibodies at the Helmholtz Center Munich. After re-cloning, the CRB1 specificity was verified and compared with the original clones by western blot analysis (**Appendix 31**).

In conclusion, a monoclonal antibody CRB1 C25G2 against the intracellular domain was generated, allowing the analysis of human and porcine CRB1 by western blot analysis and immunofluorescence microscopy. The monoclonal antibody CRB1B 27A5 recognises CRB1 A-C and detects CRB1 by western blot analysis and immunofluorescence microscopy. Thereby, both antibodies provide valuable tools for further analysis of CRB1 function in human and porcine retinal models.

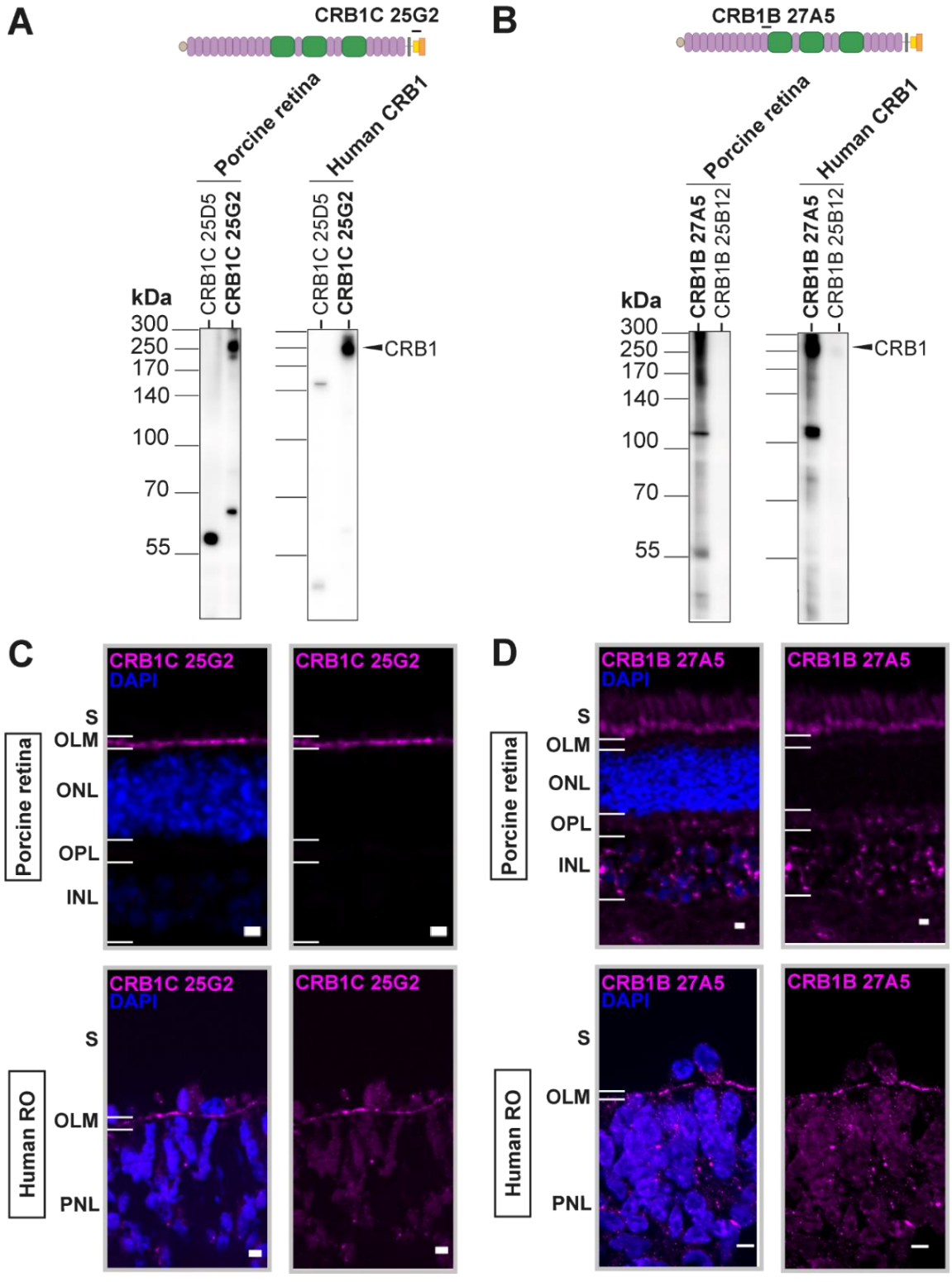

Figure 42| CRB1C 25G2 and CRB1B 27A5 detect CRB1 using western blot and immunofluorescence microscopy
First screening of hybridoma supernatants revealed two positive clones CRB1C 25G2, which recognises a peptide in the intracellular domain **(A, upper panel)** and CRB1B 27A5, which binds to a peptide in the extracellular domain **(B, upper panel)** that is conserved in the three major isoforms described in the human retina by Ray *et al*.[91] Hybridoma supernatants were tested by western blot analysis **(A-B)** using porcine retina lysate (left panel) or HEK293T lysate upon overexpression of canonical human CRB1 or CRB2 (right panel). As a control two negative clone (CRB1C 25G2 and CRB1B 25B12) are depicted. Arrow indicates expected CRB1 kDa size **(C-D)** Immunofluorescence microscopy of control human iPSC-derived RO (lower panel) and porcine retina (upper panel) stained with **(C)** CRB1C 25G2 (magenta) or **(D)** CRB1B 27A5 (magenta) and DAPI (dark blue). Scale bar 5 µm. S=Segments; PNL=Photoreceptor nuclei layer; OLM=Outer limiting membrane; ONL=Outer nuclear layer; OPL=Outer plexiform layer

5. Discussion

Bi-allelic mutations in the transmembrane protein CRB1 are one of the major causes of IRD [7-9]. No treatment is currently available to halt or reverse vision loss in these patients [20, 185]. Various animal models have contributed significantly to elucidating the function of the intracellular CRB complex [19]. Nonetheless, given the species-specific differences in the number and localisation of CRB proteins, the molecular functions and disease mechanisms of human CRB1 are still poorly described [20]. Furthermore, genetic modifiers of the *CRB1*-associated disease severity represent a current gap of knowledge. Using a multi-modal approach, this study provides novel insights into the disease mechanism and candidate modifiers in two siblings carrying the same homozygous *CRB1* c.2843G>A;C948Y mutation with a substantial difference in the disease manifestation (**Figure 43**).

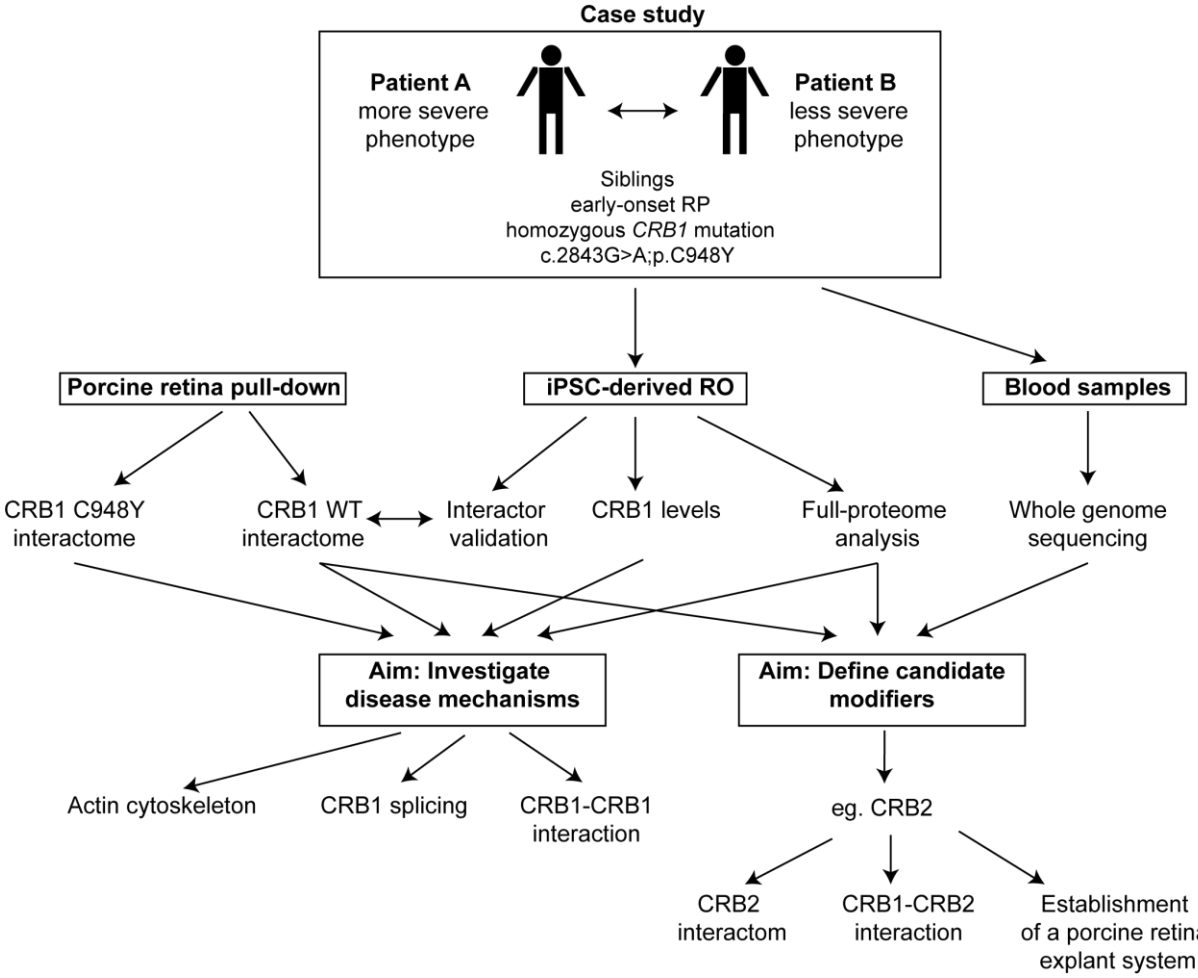

Figure 43| Multimodal approach to investigate disease mechanism and candidate modifiers in two siblings with early-onset RP
Two siblings, both carrying the same homozygous *CRB1* mutation with significant differences in the disease severity, served as a proof-of-concept. To gain new insights into disease mechanisms and to define candidate modifiers, a multi-modal approach was performed, including a porcine retinal pull-down approach to define retinal interactors of CRB1, full-proteome analysis using mass spectrometry and DIA of patient and control iPSC-derived RO and WGS of patient blood samples.

5.1 Human CRB1 and CRB2 formed homo- and heteromeric complexes at the OLM

Previous studies have shown that human CRB1 and CRB2 both localise to the OLM in human iPSC-derived RO and human foetal retina [14, 94, 168]. Using co-IP in HEK293T cells and a porcine retinal pull-down approach, the data obtained in this study revealed that CRB1 and CRB2 not only both localise to the OLM, but also form homo- and heterotypic complexes. CRB3, which lacks the large extracellular domain, was unable to interact with the other two members of the CRB family. These findings are in line with the observations by Zou *et al.,* that zebrafish Crb2a and Crb2b interact through their extracellular domains [140].

Interestingly, only human CRB2 and not human CRB1 was able to pull-down porcine CRB1 from retinal tissue. This may be due to the affinity and nature of the CRB-CRB interaction. Human CRB1 and CRB2 may be present as homomeric complexes bound to FLAG-beads when offered as bait to porcine retinal lysates. It is not known whether CRB1 and CRB2 only form dimeric or also multimeric complexes and whether homotypic or heterotypic interactions are equally dominant. As only CRB2 was able to pull-down porcine CRB1, the affinity of heterotypic interactions of CRB proteins may be higher compared to homotypic interactions. This hypothesis is supported by the observations of Hoa *et al.*, who showed that the affinity of heterophilic interactions of zebrafish Crb2a and Crb2b is higher compared to homophilic interactions [139].

In addition, neither human CRB1 nor CRB2 were able to pull-down porcine CRB2, which may be a technical limitation of the protein detection method. Up to date, the abundance of CRB2 in the adult porcine retina has not been published and may be significantly lower compared to CRB1. The TopTen LC-MS/MS data-dependent acquisition used in this study is biased towards the identification of high abundance proteins. Alternatively, enriched proteins after porcine retinal pull-down could be analysed by western blot if species-specific CRB antibodies are available. Furthermore, pull-down samples could be analysed by DIA or a targeted MS-based approach to improve the detection of low abundant CRB2.

Data presented here provide strong evidence that the interaction of human CRB1-CRB1 and human CRB1-CRB2 is mediated by the extracellular domain, as truncations of the CRB1 extracellular domain (CRB1Δextra) led to a loss of CRB1-CRB1 interaction and CRB3 did not interact with CRB1 and CRB2. However, none of the introduced *CRB1* patient missense mutations, deleted EGF domains (EGF15, EGF17, EGF18 and EGF19) or truncated CRB1 constructs completely abolished the CRB1-CRB1 interaction *in vitro*. The effect of EGF16 remains of great interest, but deletion of EGF16 by SDM was unsuccessful. Nonetheless, these data allow to hypothesise that several residues in the extracellular domain may be involved in the CRB-CRB interaction. Furthermore, *CRB1* missense mutations differentially

affected CRB1-CRB1 and CRB1-CRB2 interaction indicating that distinct residues could be involved in homo- and heterotypic interaction. Unfortunately, a 3D structure of the dimeric CRB1-CRB1 and CRB2-CRB1 interaction could not be obtained using AlphaFold-based modelling, which would be a promising strategy to identify candidate residues and help to understand whether CRB interact in *cis*- or *trans* or both. Further insight into the molecular nature of the CRB-CRB interaction would help to better understand the function of this interaction.

In conclusion, the data obtained in this study demonstrate a novel and strong homotypic and heterotypic interaction of human canonical CRB1 and CRB2, which is only slightly affected by patient mutations in the extracellular domain.

5.2 Function of the CRB-CRB interaction and the role of the extracellular domain

The strong homotypic and heterotypic interaction of CRB1 and CRB2 suggests an important function of this complex in the retina. One could hypothesise that these interactions are important to 1) localise and stabilise CRB at the OLM, 2) modulate cellular signalling as a transmembrane receptor in *cis* or *trans*, or 3) to mediate cell-cell adhesion as a novel type of adhesion molecule between photoreceptor and Müller glia cells.

First, a role for the extracellular domain in the localisation and stability of CRB at the OLM has been suggested by several lines of evidence [23, 170]. In *Drosophila* germline epithelium Fletcher *et al.* showed that overexpression of the Crb extracellular domain fused to GFP localised similarly to endogenous Crb, whereas overexpression of the intracellular domain induced endocytosis of the endogenous Crb [23]. Furthermore, AAV-based gene therapy of human CRB2 in a $Crb1^{-/-}Crb2^{F/+}$ mouse model demonstrated that only when targeting both photoreceptors and Müller Glia, CRB2 localised to the OLM [95]. In contrast, targeting only photoreceptors led to CRB2 expression mainly in the IS, indicating that CRB2-CRB2 interactions in *trans* are important for OLM localisation [95]. The role of the extracellular domain in CRB1 stability, turnover or localisation at the OLM is further affirmed by the fact that iPSC-derived RO from patients carrying missense mutations in the extracellular domain (c.3122T>C;p.M1041T; c.2983G>T;p.E995∗; c.1892A>G,p.Y631C, c.2843G>A;p.C948Y) show a reduction of CRB1 at the OLM [94, 141]. In line with these data, results presented here confirmed reduced CRB1 signal at the OLM in the RO of two patients carrying the homozygous c.2843G>A;p.C948Y mutation. To investigate whether patient described missense mutations in the extracellular domain influence the CRB-CRB interaction, co-IP was performed. Results showed that only a few missense mutations slightly altered the CRB1-CRB1 or CRB1-CRB2 interaction *in vitro* suggesting that loss of CRB-CRB interaction may not be a universal disease mechanism for all *CRB1* mutations in the extracellular domain. However, as a mild decrease

in vitro may have profound consequences at the OLM depending on the turnover of CRB1, further evaluation of these mutations under physiological conditions or photoreceptor cell stress would be interesting. In addition, more sensitive *in vitro* methods such as mass photometry would be beneficial.

Second, the extracellular domain has been linked to cellular signalling pathways. For several transmembrane receptors, dimerisation can either be stimulated after- or is necessary before ligand binding to induce downstream signalling activity [198]. Recently, NOTCH1, which localises Müller glia cell villi at the OLM, was found to be significantly reduced at the OLM in RO from *CRB1* patients compared to controls [141]. In line with this, data shown in this study revealed, between the two patient RO lysates, significant differences in the abundance of Notch signalling components. Furthermore, binding of the CRB extracellular domain to the extracellular domain of Notch has been shown in iPSC-derived RO, zebrafish and *Drosophila* [141, 147, 148, 199]. In this study, neither CRB1 nor CRB2 was able to pull-down the NOTCH receptor from the porcine retinal lysate. However, NOTCH was identified as a CRB2 interactor from HEK293T cell lysate. NOTCH receptors are highly expressed during development and are upregulated in Müller Glia cells following injury [200-202]. It is therefore possible that NOTCH receptors are present at low levels in the healthy adult porcine retina and are thus not identifiable in the pull-down approach.

Besides NOTCH signalling, CRB proteins have been implicated in the Hippo signalling pathway, which regulates growth factor signalling, proliferation, wound healing and cell contact inhibition [203-205]. Thompson *et al.* have hypothesised that a potential interaction of the extracellular domain of CRB in *trans* may serve as a sensor of cell-cell contact through regulation of the Hippo signalling pathway by the CRB intracellular domain [170]. In the murine retina, loss of Crb1 or Crb2, respectively, leads to a reduction in YAP, a key regulator of the Hippo signalling [25]. In *Drosophila*, loss of Crb activates the Hippo-Yorkie signalling pathway [206, 207]. Increased levels of CRB3 were shown to stabilise Kibra, which promotes YAP phosphorylation [208, 209]. Accordingly, siRNA-assistant depletion of *CRB3* causes nuclear localisation of YAP [210]. In this study, several proteins involved in the Hippo pathway were identified as part of the CRB1 retinal PPI network including MOB2, STK38 and STK38L. Besides the classical core components of the Hippo pathway consisting of the serine/threonine protein kinases MST1 and MST2, the serine/threonine protein kinases LATS1 and LATS2 and the transcriptional co-activators YAP and TAZ, STK38 and STK38L (also known as NDR1/2) can be phosphorylated by MST1/2 and function as YAP kinases [211-214]. MOB2 is a member of the Mob protein family, which is known to regulate the Hippo signalling pathway [215]. Depletion of MOB2 increases NDR kinase activity [216]. It would be of interest to further investigate if CRB regulates the Hippo pathway by initial interaction of the CRB extracellular

domain in *trans* leading to downstream modulation of STK38/STK38L and MOB2 by the CRB intracellular domain.

Furthermore, the CRB1 retinal PPI analysis revealed additional extracellular ligands for the CRB extracellular domain, that may induce or require CRB multimer formation. These included the secreted glycoprotein SFRP2, an extracellular regulator of the WNT signalling pathway [217]. SFRP2 can act as an antagonist of the canonical WNT pathway by sequestering of soluble WNT ligands, thereby preventing its binding to the Frizzled receptor [217]. In addition, SFRP2 has been reported to have agonistic effects on the canonical WNT pathway, possibly through direct binding to the Frizzled receptor or through the WNT ligand Wnt3a [217]. Furthermore, SFRP2 activates non-canonical WNT pathways [217]. WNT signalling components, including SFRP, have not only been implicated in retinal development but also in human retinal diseases [218-221]. In this study, alterations in WNT signalling pathway components were observed between RO of the two patients using full-proteome analysis, emphasising the need to further investigate the role of CRB1 in WNT signalling. In line with these observations, Dr. Achberger previously showed changes in mRNA expression of *WNT* genes in patient RO compared to control [22]. These data allow to hypothesise that binding of SFRP2 to the CRB1 extracellular domain reduces soluble SFRP2 may lead to decreased activation of the non-canonical WNT pathway. Besides SFRP2, LTBP1, which is involved in TGFβ signalling, was identified as a candidate interactor of the CRB1 extracellular domain. LTBP1 interacts with the TGFβ propeptide (or latency-associated peptide), assisting in its folding, secretion and providing traction to activate TGFβ in the extracellular matrix [222]. In the retina, TGFβ signalling has been shown to be neuroprotective [223, 224]. Whether the interaction of the CRB1 extracellular domain with LTBP1 could provide an additional pulling force to detach active TGFβ from the latent complex remains to be investigated.

Finally, the interaction of the CRB extracellular domain revealed in this study postulates CRB1 as a novel class of cell-cell adhesion molecules in *trans* or cell-matrix adhesion molecules in *cis,* as hypothesised for zebrafish CRB by Zou *et al.* [140]. In HEK293T cells, expression of zebrafish Crb2a and Crb2b induced cell aggregation through the extracellular domain [140]. In mice and *Drosophila*, CRB has been shown to be important for the development and integrity of the OLM [99, 116, 117, 159, 225]. Furthermore, at a certain age, patient iPSC-derived RO exhibit ectopic photoreceptor spreading in regions of OLM interruption [14, 94]. In line with these findings, data obtained in this study showed that both CRB1 C948Y patient iPSC-derived RO had reduced CRB1 levels as well as significantly lower abundance of proteins associated with cell-matrix adhesion compared to control RO. In addition, PPI analysis of CRB1 revealed fibronectin (FN) and gelsolin (GSN) as potential extracellular matrix interactors, which may contribute to the adhesion of CRB to the extracellular matrix.

Collectively, these data indicate that the CRB-CRB interaction may regulate CRB localisation, signalling such as Notch, Hippo, WNT or TGF-ß or cell adhesion.

5.3 CRB1 protein levels were reduced in homozygous CRB1 C948Y mutation

In general, *CRB1* null mutations leading to a premature stop codon, are more frequently found in patients with a severe and early-onset IRD phenotype compared to variants leading to an altered protein (missense or in-frame deletions) [8]. Yet, the most common CRB1 C948Y mutation is an exception to this correlation as it is also frequently reported in patients with a LCA and EORD phenotype [8]. Data presented here showed that CRB1 localisation at the OLM was decreased alongside with a significant reduction in total CRB1 protein in patient RO with a homozygous C948Y mutation. This suggests that CRB1 C948Y does not manifest as a conventional missense mutation, which may explain why it is frequently found in patients with a severe and early-onset phenotype.

As iPSC-derived RO from other patients carrying the CRB1 C948Y mutation also display reduction of CRB1 at the OLM, this observation is not specific to the two brothers investigated in this study, but rather seems to be a general consequence of the C948Y mutation [22, 94, 141]. Previously, Pellikka *et al.* introduced the C948Y mutation into the corresponding residue in *Drosophila*, C1540Y, and expressed either the full-length or the C1540Y MT in a $crb^{-/-}$ background [156]. In contrast to the human iPSC-derived RO, higher levels of Crb along with mislocalisation to the rhabdomeres were shown at 50 % of pupal development in the Crb-C1540Y compared to the Crb WT [156]. The difference in CRB1 abundance in case of the C948Y/C1540Y mutation between human RO and *Drosophila* may reflect species-specific differences in the function of this residue. In addition, Pellikka *et al.* used overexpression, which was not driven by the endogenous Crb promotor and natural epigenetic regulation [156]. Furthermore, the overexpression construct used by Pellikka *et al.*, did not contain introns flanking the C948/C1540 residue and, hence, alterations in the splicing pattern of *CRB1/crb* due to the C948Y/C1540Y can not be assessed. Similarly, in this study, overexpression of the C948Y and WT FLAG-tagged CRB1 cDNA lacking the introns in HEK293T cells resulted in equal abundance of CRB1, which does not reflect the endogenous CRB1 reduction observed in CRB1 C948Y patient derived RO.

Results obtained here indicate that CRB1 c.2843G>A;p.C948Y, which is widely classified as a missense mutation, results in a WT and a misspliced *CRB1* transcript. The misspliced transcript exon 9 causes a frameshift mutation with a premature stop codon in exon 10. As an endpoint PCR was used, which favours small amplicons and is not quantitative and no inhibitor of nonsense-mediated mRNA decay was applied prior to isolation of RNA, no conclusions can be drawn about the ratio of misspliced *CRB1* compared to WT transcript [273]. Using a luciferase-based *in vitro* splicing assay, Bellingrath *et al.* showed that c.2843G>A led to exon

skipping in 60 % of transcripts, while only 36 % were correctly spliced (ARVO Annual Meeting Abstract 2022 [226]). As not all transcripts seem to skip exon 9, it would be interesting to investigate whether missplicing affects specific CRB1 isoforms.

Consequently, the misspliced *CRB1* transcript could either be degraded by nonsense-mediated mRNA decay or translated into a truncated CRB1 protein lacking the last EGF and the intracellular domain. No changes in *CRB1* mRNA levels were observed by Boon *et al.* and Dr. Achberger between patient and control RO suggesting that the misspliced transcript may be of low abundance or not degraded by nonsense-mediated mRNA decay [22, 94]. In this study, CRB1-specific peptides before and after the CRB1 c.2843G>A;p.C948Y mutation residue were of similar abundance in patient iPSC-derived RO indicating that a stable truncated CRB1 protein is not present. Future studies should investigate if the misspliced *CRB1* transcript variant leads to an unstable truncated CRB1 protein that could competitively bind to the extracellular domain of WT CRB1. In this way, the misspliced *CRB1* transcript could exert a dominant negative effect on the remaining WT protein leading to degradation of both proteins.

While partial missplicing of *CRB1* induced by c.2843G>A remains a possibility, the CRB1 C948Y missense mutation also revealed a 20 % reduction in CRB1-CRB1 interaction *in vitro*. This may have significant implications *in vivo* at the OLM or under light stress if the CRB-CRB interaction is required for stable complex formation in polarised cells. Furthermore, the consequences of the C948Y mutation on post-translational modifications such as protein glycosylation were not investigated in this study. Protein O-glucosyltransferase 1 (Poglut1), which adds O-glucose to serine residues in the C^1XSXPC^2 for EGF-like domains, has been shown to O-glycosylate Crb2 [227]. This O-glycosylation was essential for the membrane localisation of Crb2 in mice [227]. Although C948 is not part of the POGLUT1 motif, alteration in other post-translational modifications such as phosphorylation could alter the stability, function and localisation of CRB1.

Taken together, this study revealed that the c.2843G>A;p.C948Y mutation resulted in a fraction of misspliced *CRB1* transcript at mRNA level and protein levels, mildly affected CRB1-CRB1 interaction and significantly reduced endogenous CRB1 protein levels in patient RO.

5.4 The CRB1 retinal protein-protein interaction network provides novel insights on the retinal Crumbs complex

In this study, the CRB1 retinal interactome was investigated using a porcine retinal pull-down approach. Although the retinal interactions were not significantly lost in in the CRB1 C948Y, as initially speculated, the results obtained provide novel insights into the retinal CRB1 complex and allow to define new hypotheses on the function of WT CRB1 in the retina. In addition, several patient missense mutations, including C948Y, are accompanied by a

reduction of canonical CRB1 at the OLM, indicating that any function requiring the full-length WT protein may be altered in CRB1 patients [94].

Various lines of evidence indicate that CRB1 is involved in the regulation of the endo-lysosomal system and that vesicular trafficking is important for the recycling of CRB1/Crb at the OLM [141, 149]. Delivery of Crb proteins to the apical membrane requires vesicular transport involving Rab11-endosomes along polarised microtubules through dynein and F-actin through interaction with MyoV [149, 228-230]. Furthermore, the interaction of MyoV and Crb is also important for the regulation of rhodopsin transport in *Drosophila* [230]. In accordance with these observations, the retinal PPI network of CRB1 contained the actin motor protein MYO5A and proteins of the dynein-dynactin microtubule motor complex including DCTN3 and ACTR10 emphasising the role of CRB1 in retinal vesicular transport.

Defective intracellular transport and vesicular misrouting is one of the hallmarks of retinal degenerations [49]. In crb MT *Drosophila* retina, Arl8-positive lysosomal vesicles are significantly increased in size, intensity and proximity to Atg8-positive compartments (autophagosomes and autolysosomes) prior to light-induced degeneration [149]. Similarly, patient RO display less late endosomes (RAB7+, VSP35+) and recycling endosomes (Rab11A+) but more early endosomes (EEA1+) and endo-lysosomal compartments for degradation (ARL8+, LAMP1+) as demonstrated by Buck *et al.* [94, 141]. In this study, alterations in the abundance of endolysosomal proteins were observed in patients compared to control RO by full-proteome analysis of RO lysates. In contrast to Buck *et al.*, a significantly higher abundance of exocytic vesicles was observed in patient RO, accompanied by a lower abundance of lysosomes and early endosomes in the patient iPSC-derived RO compared to control [141]. The differences to the results obtained by Buck *et al.* could be originating from the different experimental setup. Buck *et al.* investigated the localisation of single marker proteins in the ONL by immunofluorescence, while in this study proteomic analysis of whole organoid lysates was performed [141]. In addition, Buck *et al.* used isogenic controls, which are required to confirm that observations are caused by the CRB1 mutation [141]. Therefore, the generation of isogenic controls for the two patients used in this study is important for further investigations. Finally, effects of CRB1 on the endo-lysosomal system may be mutation dependent. Several proteins with a role in vesicular trafficking, such as DZANK1, have been identified as part of the CRB1 retinal interactome. DZANK1 regulates vesicular transport towards the base of the photoreceptor connecting cilium, which is required for photoreceptor development [231]. In the future, it would be interesting to investigate DZANK1 in patient RO with different *CRB1* mutations.

The changes in vesicular trafficking and the endo-lysosomal system could also be a secondary consequence of CRB1 loss. For instance, loss of apical-basal polarity due to alterations in WNT by CRB1 could impair polarity-dependent processes such as directed

transport [274]. Moreover, multiple proteins involved in PI metabolism have been identified as part of the CRB1 retinal PPI. PI are differentially distributed within the endo-lysosomal network to regulate cargo sorting and their dysregulation has been linked to blindness [232, 233]. In *Drosophila* salivary gland epithelium, loss of Crb is accompanied by the accumulation of $PI(4,5)P_2$, reduced apical trafficking and secretion [234]. Loss of Pten, which catalyses $PI(3,4,5)P_3$ to $PI(4,5)P_2$, counteracts the accumulation of $PI(4,5)P_2$ in the Crb knockdown salivary gland [234]. Therefore, Lattner *et al*. hypothesised that Crb indirectly regulates Pten through its interactors MyoV and β-Spectrin, although the exact mechanism remains unknown [234]. Here, PIP-5 kinase (PIP5K1A), which converts PI(4)P to $PI(4,5)P_2$, was identified as part of the retinal CRB1 complex. Since increased activity of PIP5K1A would lead to the accumulation of $PI(4,5)P_2$, it would be of high interest if CRB1 negatively regulates PIP5K1A and if inhibition of PIP5K1A would prevent the accumulation of $PI(4,5)P_2$ upon loss of CRB1.

Photoreceptors rely on a tightly regulated actin cytoskeleton to drive OS formation, rhodopsin transport from the IS to the OS, and synaptic vesicle release [235]. Furthermore, dysfunction of actin regulators such as GSN induces photoreceptor cell death [191, 195]. Analysis of the CRB1 retinal interactome revealed a high abundance of multiple regulators of the actin cytoskeleton, indicating a role for CRB1 in the regulation of the retinal actin cytoskeleton. Furthermore, both CRB1 patient RO showed reduced intensity of F-actin at the OLM and significantly lower abundance of proteins linked to actin filaments, ARP2/3 complex and actin-based cell projection compared to control. In *Drosophila*, Crb has been implicated in the regulation of the actin cytoskeleton, supporting the results of this study [236]. Illustrating this point, spectrin and moesin interact with Crb to stabilise the apical membrane cytoskeleton during epithelial morphogenesis [236]. In line with these findings, in this study SPTB and SPTBN2, members of the spectrin family, were identified in the CRB1 PPI analysis. Furthermore, Crb has been shown to regulate actomyosin dynamics and adherens junctions during dorsal closure in *Drosophila*, which was mediated by Rho1-GTPase, ARP2/3 and moesin [237]. In line with those findings, various proteins involved in Rho protein signalling (ARHGAP21, ARHGEF10 and ARHGAP32) as well as components of the ARP2/3 complex (ARPC3, ARPC5L, ARPC1A) were identified as part of the CRB1 PPI network.

The other two family members of the human CRB family, CRB2 and CRB3, have been shown to regulate the F-actin [238, 239]. Podocytes from a podocyte-specific CRB2 KO mouse model and human podocytes depleted for CRB2 display less F-actin and reduced cell adhesion emphasising the role of human CRB proteins in regulating the actin cytoskeleton [238]. Furthermore, CRB3 was shown to interact with the ARP2/3 complex indicating that the regulation of F-actin is mediated by the conserved intracellular domain [239, 240]. However, many actin regulating proteins were also identified in the PPI analysis of the extracellular isoform of CRB1, which lacks the canonical FERM and PDZ domain. A possible explanation

could be that the alternative C-term part of the CRB1 extracellular isoform interacts with regulators of the actin cytoskeleton. The localisation of CRB1 extracellular is debatable, as, on one hand, it has been reported that it lacks the transmembrane and intracellular domain and may be secreted whereas another study predicted that it encodes a transmembrane and a 22 amino acid intracellular domain [11, 15, 89]. Furthermore, overexpression of the CRB1 extracellular isoform may allow binding of the full-length porcine CRB1, which allows binding of actin regulators. Finally, the binding of actin regulators to the CRB1 extracellular isoform could be indirect through other proteins. For instance, extracellular isoform GSN could bind the extracellular domain of CRB1 as well as actin regulatory proteins.

Interestingly, RO from patient B, who is less affected, also had a lower abundance of proteins involved in actin bundling compared to RO from patient A and control in the full proteome analysis. Concurrently, proteins involved in intraciliary transport and ciliary membrane are less abundant in RO from patient A compared to patient B. Interestingly, reduced actin bundling has been shown to enhance ciliogenesis [241]. Therefore, it would be interesting to further investigate the effects of CRB1 on ciliogenesis as multiple proteins with a known function in cilia biology were identified as part of the retinal CRB1 complex.

Overall, results of this study provide new insights into the CRB1 retinal interactome linking CRB1 to regulators of the actin cytoskeleton, lipid metabolism and vesicular transport.

5.5 Novel candidate modifiers of disease severity in *CRB1*-linked retinal degenerations

Emerging evidence from other IRD, such as the Bardet-Biedl syndrome and PRPH2-associated macular dystrophy, have revealed the involvement of multiple alleles in the development of clinical phenotypes [242-245]. Taking advantage of the use of two siblings carrying the same *CRB1* mutation with substantial differences in disease manifestation, novel candidate modifiers for CRB1-associated IRD have been defined using a multi-step approach including WGS of patient blood samples, full-proteome analysis of patient RO and the CRB1 retinal interactome analysis.

On one hand, this approach has several limitations that need to be considered. First, this study focused on rare genetic variants such as single nucleotide variants and small indels. This excludes larger insertions or deletions, structural variants, inversions, copy number variations, tandem repeats, transposable repeats or quantitative trait loci, which may contribute to the variation of disease severity [246]. Furthermore, other filters have been applied to reduce the number of candidates, for instance the exclusion of common variants, which is debatable.

Second, environmental factors and the immune system were not considered in this study. Recent studies have described alterations in the composition of lymphocytes, dendritic cells

and complement factors in blood samples from CRB1 patients compared to controls [247, 248]. As the patient RO used in this study, lack immune cells, but still show a variable phenotype in the light sensitivity that correlates with the clinical phenotype, the findings serve as a proof-of concept to define candidate genetic variants [22, 249-251].

Third, this study is limited by the small number of patients. As siblings, the two patients share 50 % of their genetic information, which is promising for the identification genetic variants. However, as they are not monozygotic twins, many candidate modifiers have been identified. In addition, it remains to be investigated whether those candidates are specific to the two patients or general modifiers in CRB1-linked patients. Moreover, it is not possible to distinguish the impact of the CRB1 mutation from the impact of the modifier in the full-proteome analysis of the RO. One possibility would be to establish isogenic control lines. Additionally, future experiments should involve the pharmacological or genetic modulation of candidate modifiers in the patient RO to evaluate consequences on the light sensitivity. Furthermore, porcine retinal explants in combination with siRNA-assisted silencing of *CRB1* and candidate modifiers could be used to narrow down promising candidates.

Fourth, the full-proteome analysis was performed using three technical replicates on a pool of RO. Additional replicates would be beneficial to further confirm stable differences between patients and the control and to improve the signal-to-noise ratio. As there is variation even between RO from the same differentiation, ideally one would aim to analyse compare the proteome of individual RO [270, 272]. However, this is technically challenging due to the low amount of protein in a single RO.

Finally, it is debatable whether the modifier has to belong to the CRB1 PPI network. Given the large protein scaffold organised by CRB1, any dysfunction in this scaffold could be expected to contribute to the patient's phenotype. In line with this hypothesis, Jak3 was previously identified as an enhancer of the neovascularisation phenotype in *Crb1* rd8 mice [160]. Here, another member of janus kinase family, JAK2, was identified as part of the CRB1 retinal interactome. Furthermore, *Arhgef12* was found to modulate the phenotype of *Crb1* rd8 mice and ARHGEF10 was identified as a component of the retinal CRB1 complex [164]. Nonetheless, not all previously described modifiers are part of the retinal CRB1 interactome. For instance, *AIPL1*, a photoreceptor-specific co-chaperone for cGMP-specific PDE-6, has been identified, as a modulator in a patient independent of any interaction with CRB1 described in this or other studies [157, 158].

On the other hand, and besides these limitations, this study provides interesting candidate modifiers, which could protect patient B (protective candidate) or intensify the phenotype of patient A (harmful candidate). A panel of the identified candidates are related to cilia biology such as the potential harmful candidates (*CC2D2A*, *CDH23* and *CCDC88A*) and the potential

protective candidate (*ARMC9*). Interestingly, heterozygous variants in ciliopathy-associated genes such as *BBS7*, *NPHS1* and *BBS17* are described as potential modifiers in *CRB2*-related syndrome indicating that cilia-associated processes may influence CRB-related (patho-) mechanisms [152]. For instance, patient A carries a heterozygous missense mutation M100L in *CC2D2A*, a key regulator of ciliogenesis and sonic hedgehog signalling, along with significantly lower CC2D2A protein levels in RO lysates compared to patient B [253, 254]. According to the ClinVar database, this variant has been identified as variant of unknown significance in patients with autosomal recessive Joubert syndrome 9, RP 93, and Meckel-Gruber syndrome [252]. CC2D2A localises to the ciliary transition zone and basal body and interacts with CEP290 through the N-term domain (1-998 amino acid) [253, 254]. It would be interesting to further investigate the localisation of CC2D2A in patient and control RO and whether the M100L mutation affects the interaction with CEP290.

Another interesting potential harmful candidate is *CDH23*, in which the more affected patient A carries a heterozygous missense mutation c.9979G>A:p.A3327T. The transmembrane protein CDH23 is a member of the cadherin family of Ca^{2+}-dependent cell adhesion molecules and involved in cell-cell adhesion and cell-matrix adhesion [255-257]. The A3327T mutation is located in the intracellular domain and has been described in a patient with Usher syndrome type 1 in the ClinVar database [252]. However, as Usher patients typically present hearing problems, which to the best of my knowledge, is not the case in the two CRB1 patients, the heterozygous A3327T mutation may only be pathogenic in combination with the *CRB1* mutation. Finally, *ARHGEF10* was identified as a CRB1 interactor and as a potential protective candidate in patient B, who carries a heterozygous missense mutation c.3544G>A:p.A1182T. Previously, disruption of *Arhgef12* was shown to accelerate the phenotype in the *CRB1*^{rd8} mouse model [164]. As ARHGEF10 has been shown to be involved in vesicular transport and nerve fibre development, it remains of high interest whether the A1182T mutation enhances ARHGEF10 activity and thereby partially rescues the impaired endo-lysosomal trafficking due to CRB1 disruption [258, 259].

In conclusion, this proof-of-concept study describes novel protective and harmful candidate modifiers in two siblings with the same CRB1 C948Y mutation but with a substantial difference in the disease severity.

5.6 The role of CRB2 in modulating CRB1-linked retinal degenerations

The most interesting protective candidate identified in this study is the CRB family member CRB2. Using full-proteome analysis by mass spectrometry, the RO of the less affected patient B showed a small but significant increase in CRB2 levels compared to RO of patient A and control. Concomitantly, a heterozygous single base variant was identified upstream of the *CRB2* in patient B at chr9:123351196 G>T.

Various lines of evidence support CRB2 as a protective modulator of CRB1-IRD. First, loss of *Crb2* in *Crb1*-deficient murine Müller glia cells or immature photoreceptors enhances the phenotype [24, 25, 166]. Similarly, heterozygous KO of *Crb2* in homozygous *Crb1* MT mice resulted in an earlier and more severe retinal degeneration phenotype compared to a heterozygous KO of *Crb2* in heterozygous *Crb1* MT mice [15]. Furthermore, Boon *et al.* demonstrated that supplementation of CRB1 or CRB2 by adeno-associated viral vectors improves the histological and transcriptional changes in the endo-lysosomal system in CRB1 patient iPSC-derived RO and CRB1 KO iPSC-derived RO [94, 168]. Similarly, in a mid-onset *Crb1* RP mouse model expression of *Crb2* in both, photoreceptor and Müller glia cells, improved retinal function [95, 167]. Together, these data emphasise CRB2 as a potential protective modifier.

Nonetheless, the protein levels of CRB2 are only slightly increased in the RO of patient B compared to control and patient A in the full proteome analysis. Therefore, it remains important to verify the localisation and abundance of CRB2 using western blot and immunofluorescence. As the rescue ability of CRB2 in the *Crb1* KO mouse model only occurred when photoreceptor and Müller glia cells were targeted, one would expect CRB2 levels to be increased in both photoreceptors and Müller Glia of patient B RO [95]. Two reasons could explain the only mild increase in CRB2. First, CRB2 may not be the only modifier that explains the difference in phenotype severity between the two brothers. It could be that multiple protective and harmful factors contribute to the phenotypic difference between the two patients. To test this hypothesis, the level of CRB2 in the RO of patient B would have to be reduced to a similar level as in the RO of patient A, for example by siRNA-mediated knock-down. Alternatively, the abundance of CRB2 in the RO of patient A would have to be increased to the level observed in the RO of patient B, for example by adeno-associated viral vectors. Next, Ca^{2+} imaging and full-proteome analysis should be performed to evaluate the extent to which CRB2 could minimise the difference between RO of patient A and patient B. In addition, various studies have shown that the levels of CRB proteins are balanced and that highly elevated and highly decreased levels of CRB lead to loss of apical-basal polarity and defects in the embryonic epithelial formation [88, 137, 138, 146]. Therefore, a slight increase in CRB2 may be sufficient to protect but, yet, not enough to induce adverse effects.

A possible explanation for the increased CRB2 levels could be the heterozygous upstream variant chr9:123351196 G>T, which could influence CRB2 expression levels. According to the Human Genome Browser, there are no H3K27Ac marks in this region and no known enhancer regions [275]. To investigate whether this residue affects *CRB2* expression, the variant could be introduced using a CRISPR-based strategy into ARPE19 or iPSC for RO generation to assess if it modulates CRB2 levels. In addition, qPCR should be performed to investigate if the variant affects *CRB2* mRNA expression. Besides this variant, other mechanisms could lead to

a higher abundance of CRB2, supporting the idea of multiple modifiers. These could be proteins that regulate the stability, localisation or turnover of CRB2. Therefore, further research is required to identify the molecular mechanisms underlying the elevated levels in patient B RO.

The comparable rescue ability of CRB1 and CRB2 in CRB1 patient iPSC-derived RO, allow to hypothesise that CRB1 and CRB2 are functionally redundant to some extent [112]. Therefore, higher levels of CRB2 could compensate for the loss of CRB1. This is supported by the homotypic and heterotypic CRB-CRB interaction and by the high overlap of protein-protein interactors for CRB1 and CRB2 described in this study from HEK293T cells and retinal lysate. Therefore, it would be interesting to further evaluate the levels of CRB2 in patients with CRB1-linked retinal degenerations of different disease severity. Van den Hurk *et al*. previously sequenced the *CRB2* gene in patients with RP or LCA and identified a panel of heterozygous missense variants [260]. A similar approach could be performed in patients with CRB1 mutations and different disease severity.

Up to now, 37 patients with bi-allelic *CRB2* mutations have been described [93, 261-266]. These patients present various phenotypes ranging from severe prenatal abnormalities to isolated postnatal kidney dysfunction due to the broader expression of CRB2 in multiple epithelial-derived tissues [92]. Similar to patient mutations in *CRB1*, the majority of patient mutations identified in *CRB2* are located in the extracellular domain, further emphasising the importance of the CRB extracellular domain in the disease pathogenesis [152]. Nonetheless, only a few patients with *CRB2* mutations develop retinal symptoms [92, 93]. On one hand, it could be that the level of CRB1 is sufficient to rescue the function of CRB2 in the retina in the majority of patients. It would be interesting to sequence the *CRB1* gene and determine if the protein levels are altered in the *CRB2*-patients with IRD. On the other hand, there are just a few patients with *CRB2*-related syndrome with a poor initial life expectancy [152]. Only two patients have been reported to survive up to the ages of six and seven years, while other reports mention six patients, who did not survive longer than seven months [152]. In *CRB1*-linked IRD, the beginning of symptom varies from 0 to 47 years of age with a median age of 4 years [9]. Therefore, given the low life expectancy, *CRB2* patients may often be too young to develop retinal symptoms.

Finally, it remains to be investigated how CRB2 could contribute to the therapy of *CRB1*-linked IRD. Studies from Pellissier *et al.* have shown advantages of CRB2 gene therapy compared to CRB1 in a CRB1 KO mouse model [95, 167]. First, CRB2 is smaller compared to CRB1 and can therefore be more easily packed [95, 167]. Second, only targeting Müller Glia cells and photoreceptors with CRB2 improved retinal function, while expression of CRB1 did not improve retinal function [95, 167]. In contrast, expression of CRB1 induced an immune

response leading to tissue degeneration [95, 167]. These data indicate that the broader expression of CRB2 may be of advantage in CRB1-linked IRD as it is less immunogenic.

Taken together, this study provides novel insights into the disease mechanism underlying CRB1-linked IRD caused by the c.2843G>A;p.C948Y mutation. Furthermore and for the first time, molecular differences and potential modifiers have been described using a multi-modal approach in two siblings with the same CRB1 c.2843G>A;p.C948Y mutation but with substantial differences in the disease severity.

6. References

1. Stehle, I.F., et al., *Human CRB1 and CRB2 form homo- and heteromeric protein complexes in the retina,* Life Sci Alliance, 2024.
2. Hutmacher, F., *Why Is There So Much More Research on Vision Than on Any Other Sensory Modality?* Front Psychol, 2019. **10**: p. 2246.
3. A, W., W. RB, and M. MA, *Making Eye Health a Population Health Imperative: Vision for Tomorrow*. 2016: National Academies of Sciences, Engineering, and Medicine; Health and Medicine Division; Board on Population Health and Public Health Practice; Committee on Public Health Approaches to Reduce Vision Impairment and Promote Eye Health.
4. Erskine, L. and E. Herrera, *Connecting the Retina to the Brain.* ASN Neuro, 2014. **6**(6): p. 1759091414562107.
5. Hussey, K.A., S.E. Hadyniak, and R.J. Johnston, Jr., *Patterning and Development of Photoreceptors in the Human Retina.* Front Cell Dev Biol, 2022. **10**: p. 878350.
6. Cremers, F.P.M., et al., *Special Issue Introduction: Inherited Retinal Disease: Novel Candidate Genes, Genotype-Phenotype Correlations, and Inheritance Models.* Genes (Basel), 2018. **9**(4).
7. Daich Varela, M., et al., *CRB1-Associated Retinal Dystrophies: Genetics, Clinical Characteristics, and Natural History.* American Journal of Ophthalmology, 2023. **246**: p. 107-121.
8. Bujakowska, K., et al., *CRB1 mutations in inherited retinal dystrophies.* Human mutation, 2012. **33**(2): p. 306-315.
9. Talib, M., et al., *Genotypic and Phenotypic Characteristics of CRB1-Associated Retinal Dystrophies: A Long-Term Follow-up Study.* Ophthalmology, 2017. **124**(6): p. 884-895.
10. Alves, C.H., et al., *Loss of CRB2 in the mouse retina mimics human retinitis pigmentosa due to mutations in the CRB1 gene.* Hum Mol Genet, 2013. **22**(1): p. 35-50.
11. den Hollander, A.I., et al., *Mutations in a human homologue of Drosophila crumbs cause retinitis pigmentosa (RP12).* Nat Genet, 1999. **23**(2): p. 217-21.
12. den Hollander, A.I., et al., *CRB1 mutation spectrum in inherited retinal dystrophies.* Hum Mutat, 2004. **24**(5): p. 355-69.
13. Hu, Y., et al., *Dissecting the transcriptome landscape of the human fetal neural retina and retinal pigment epithelium by single-cell RNA-seq analysis.* PLoS Biol, 2019. **17**(7): p. e3000365.
14. Quinn, P.M., et al., *Human iPSC-Derived Retinas Recapitulate the Fetal CRB1 CRB2 Complex Formation and Demonstrate that Photoreceptors and Müller Glia Are Targets of AAV5.* Stem Cell Reports, 2019. **12**(5): p. 906-919.
15. Pellissier, L.P., et al., *CRB2 acts as a modifying factor of CRB1-related retinal dystrophies in mice.* Hum Mol Genet, 2014. **23**(14): p. 3759-71.
16. Quinn, P.M., L.P. Pellissier, and J. Wijnholds, *The CRB1 Complex: Following the Trail of Crumbs to a Feasible Gene Therapy Strategy.* Front Neurosci, 2017. **11**: p. 175.
17. Margolis, B., *The Crumbs3 Polarity Protein.* Cold Spring Harb Perspect Biol, 2018. **10**(3).
18. Fan, S., et al., *Polarity Proteins Control Ciliogenesis via Kinesin Motor Interactions.* Current Biology, 2004. **14**(16): p. 1451-1461.
19. Gosens, I., et al., *Composition and function of the Crumbs protein complex in the mammalian retina.* Experimental Eye Research, 2008. **86**(5): p. 713-726.
20. Boon, N., J. Wijnholds, and L.P. Pellissier, *Research Models and Gene Augmentation Therapy for CRB1 Retinal Dystrophies.* Front Neurosci, 2020. **14**: p. 860.
21. Talib, M. and C.J.F. Boon, *Retinal Dystrophies and the Road to Treatment: Clinical Requirements and Considerations.* Asia Pac J Ophthalmol (Phila), 2020. **9**(3): p. 159-179.
22. Achberger, K., *Human retinal organoids - Exploration of a human induced pluripotent stem cell-derived in vitro model*, in *Medical Faculty*. 2021, University of Tuebingen: Medical Faculty. p. 187.
23. Fletcher, G.C., et al., *Positive feedback and mutual antagonism combine to polarize Crumbs in the Drosophila follicle cell epithelium.* Curr Biol, 2012. **22**(12): p. 1116-22.

24. Quinn, P.M., et al., *Loss of CRB2 in Müller glial cells modifies a CRB1-associated retinitis pigmentosa phenotype into a Leber congenital amaurosis phenotype.* Hum Mol Genet, 2019. **28**(1): p. 105-123.

25. Pellissier, L.P., et al., *Targeted ablation of CRB1 and CRB2 in retinal progenitor cells mimics Leber congenital amaurosis.* PLoS Genet, 2013. **9**(12): p. e1003976.

26. Majid, A., et al., *Differential coding of perception in the world's languages.* Proc Natl Acad Sci U S A, 2018. **115**(45): p. 11369-11376.

27. Klauke, S., C. Sondocie, and I. Fine, *The impact of low vision on social function: The potential importance of lost visual social cues.* Journal of Optometry, 2023. **16**(1): p. 3-11.

28. London, A., I. Benhar, and M. Schwartz, *The retina as a window to the brain—from eye research to CNS disorders.* Nature Reviews Neurology, 2013. **9**(1): p. 44-53.

29. Tworig, J.M. and M.B. Feller, *Müller Glia in Retinal Development: From Specification to Circuit Integration.* Frontiers in Neural Circuits, 2022. **15**.

30. Li, F., D. Jiang, and M.A. Samuel, *Microglia in the developing retina.* Neural Development, 2019. **14**(1): p. 12.

31. Hasel, P., et al., *Neurons and neuronal activity control gene expression in astrocytes to regulate their development and metabolism.* Nature Communications, 2017. **8**(1): p. 15132.

32. Zhang, K.Y. and T.V. Johnson, *The internal limiting membrane: Roles in retinal development and implications for emerging ocular therapies.* Exp Eye Res, 2021. **206**: p. 108545.

33. Ptito, M., M. Bleau, and J. Bouskila, *The Retina: A Window into the Brain*, in *Cells*. 2021: Switzerland.

34. Yang, S., J. Zhou, and D. Li, *Functions and Diseases of the Retinal Pigment Epithelium.* Front Pharmacol, 2021. **12**: p. 727870.

35. Nag, T.C. and S. Wadhwa, *Ultrastructure of the human retina in aging and various pathological states.* Micron, 2012. **43**(7): p. 759-81.

36. Strauss, O., *The Retinal Pigment Epithelium in Visual Function.* Physiological Reviews, 2005. **85**(3): p. 845-881.

37. Steinberg, R.H., *Interactions between the retinal pigment epithelium and the neural retina.* Documenta Ophthalmologica, 1985. **60**(4): p. 327-346.

38. Diamond, J.S., *Inhibitory Interneurons in the Retina: Types, Circuitry, and Function.* Annual Review of Vision Science, 2017. **3**(1): p. 1-24.

39. Franke, K. and T. Baden, *General features of inhibition in the inner retina.* The Journal of Physiology, 2017. **595**(16): p. 5507-5515.

40. Baylor, D.A., T.D. Lamb, and K.W. Yau, *Responses of retinal rods to single photons.* J Physiol, 1979. **288**: p. 613-34.

41. Nathans, J., D. Thomas, and D.S. Hogness, *Molecular genetics of human color vision: the genes encoding blue, green, and red pigments.* Science, 1986. **232**(4747): p. 193-202.

42. Bowmaker, J.K., H.J. Dartnall, and J.D. Mollon, *Microspectrophotometric demonstration of four classes of photoreceptor in an old world primate, Macaca fascicularis.* The Journal of Physiology, 1980. **298**(1): p. 131-143.

43. Molday, R.S. and O.L. Moritz, *Photoreceptors at a glance.* J Cell Sci, 2015. **128**(22): p. 4039-45.

44. Lamb, T.D., *Photoreceptor physiology and evolution: cellular and molecular basis of rod and cone phototransduction.* J Physiol, 2022. **600**(21): p. 4585-4601.

45. Sjöstrand, F.S., *The ultrastructure of the outer segments of rods and cones of the eye as revealed by the electron microscope.* Journal of Cellular and Comparative Physiology, 1953. **42**(1): p. 15-44.

46. Molday, R.S. and L.L. Molday, *Differences in the protein composition of bovine retinal rod outer segment disk and plasma membranes isolated by a ricin-gold-dextran density perturbation method.* J Cell Biol, 1987. **105**(6 Pt 1): p. 2589-601.

47. Cohen, A.I., *Further studies on the question of the patency of saccules in outer segments of vertebrate photoreceptors.* Vision Research, 1970. **10**(6): p. 445-IN14.

48. Steinberg, R.H., S.K. Fisher, and D.H. Anderson, *Disc morphogenesis in vertebrate photoreceptors.* J Comp Neurol, 1980. **190**(3): p. 501-8.

49. Nagel-Wolfrum, K. and U. Wolfrum, *Vesicle transport and photoreceptor death: fishing for molecular links.* Dev Cell, 2013. **25**(5): p. 435-6.

50. Khanna, H. *Photoreceptor Sensory Cilium: Traversing the Ciliary Gate*. Cells, 2015. **4**, 674-686 DOI: 10.3390/cells4040674.

51. Gilliam, J.C., et al., *Three-dimensional architecture of the rod sensory cilium and its disruption in retinal neurodegeneration.* Cell, 2012. **151**(5): p. 1029-41.

52. Pearring, J.N., et al., *Protein sorting, targeting and trafficking in photoreceptor cells.* Prog Retin Eye Res, 2013. **36**: p. 24-51.

53. Chen, J.V., et al., *Rootletin organizes the ciliary rootlet to achieve neuron sensory function in Drosophila.* Journal of Cell Biology, 2015. **211**(2): p. 435-453.

54. Buchwalter, R.A., et al., *Centrosome in Cell Division, Development and Disease*, in *Encyclopedia of Life Sciences*. 2016. p. 1-12.

55. Arshavsky, V.Y., T.D. Lamb, and E.N. Pugh, Jr., *G proteins and phototransduction.* Annu Rev Physiol, 2002. **64**: p. 153-87.

56. Jastrzebska, B., Y. Tsybovsky, and K. Palczewski, *Complexes between photoactivated rhodopsin and transducin: progress and questions.* Biochem J, 2010. **428**(1): p. 1-10.

57. Gao, Y., et al., *Structures of the Rhodopsin-Transducin Complex: Insights into G-Protein Activation.* Mol Cell, 2019. **75**(4): p. 781-790.e3.

58. Zhou, X.E., K. Melcher, and H.E. Xu, *Structure and activation of rhodopsin.* Acta Pharmacologica Sinica, 2012. **33**(3): p. 291-299.

59. Vöcking, O., L. Leclère, and H. Hausen, *The rhodopsin-retinochrome system for retinal re-isomerization predates the origin of cephalopod eyes.* BMC Ecology and Evolution, 2021. **21**(1): p. 215.

60. Burns, M.E., *Deactivation mechanisms of rod phototransduction: the Cogan lecture*, in *Invest Ophthalmol Vis Sci*. 2010: United States. p. 1282-8.

61. Hsieh, C.L., et al., *Arrestin Facilitates Rhodopsin Dephosphorylation in Vivo.* J Neurosci, 2022. **42**(17): p. 3537-3545.

62. Wilden, U., S.W. Hall, and H. Kühn, *Phosphodiesterase activation by photoexcited rhodopsin is quenched when rhodopsin is phosphorylated and binds the intrinsic 48-kDa protein of rod outer segments.* Proc Natl Acad Sci U S A, 1986. **83**(5): p. 1174-8.

63. Chen, C.K., et al., *Modulation of mouse rod response decay by rhodopsin kinase and recoverin.* J Neurosci, 2012. **32**(45): p. 15998-6006.

64. Choi, E.H., et al., *Retinoids in the visual cycle: role of the retinal G protein-coupled receptor.* Journal of Lipid Research, 2021. **62**: p. 100040.

65. Reichenbach, A. and A. Bringmann, *New functions of Müller cells.* Glia, 2013. **61**(5): p. 651-78.

66. Kobat, S.G. and B. Turgut, *Importance of Müller Cells.* Beyoglu Eye J, 2020. **5**(2): p. 59-63.

67. Wang, Y.P., et al., *Development of normal retinal organization depends on Sonic hedgehog signaling from ganglion cells.* Nat Neurosci, 2002. **5**(9): p. 831-2.

68. Bachleda, A.R., L.H. Pevny, and E.R. Weiss, *Sox2-Deficient Müller Glia Disrupt the Structural and Functional Maturation of the Mammalian Retina.* Invest Ophthalmol Vis Sci, 2016. **57**(3): p. 1488-99.

69. Wohl, S.G., et al., *Müller glial microRNAs are required for the maintenance of glial homeostasis and retinal architecture.* Nat Commun, 2017. **8**(1): p. 1603.

70. Saint-Geniez, M., et al., *Endogenous VEGF is required for visual function: evidence for a survival role on müller cells and photoreceptors.* PLoS One, 2008. **3**(11): p. e3554.

71. Bai, Y., et al., *Müller cell-derived VEGF is a significant contributor to retinal neovascularization.* J Pathol, 2009. **219**(4): p. 446-54.

72. Yoshida, S., et al., *Interleukin-6 (IL-6) production by cytokine-stimulated human Müller cells.* Curr Eye Res, 2001. **22**(5): p. 341-7.

73. Otori, Y., et al., *Marked increase in glutamate-aspartate transporter (GLAST/GluT-1) mRNA following transient retinal ischemia.* Brain Res Mol Brain Res, 1994. **27**(2): p. 310-4.

74. Rauen, T., J.D. Rothstein, and H. Wässle, *Differential expression of three glutamate transporter subtypes in the rat retina.* Cell Tissue Res, 1996. **286**(3): p. 325-36.

75. Bringmann, A., et al., *Role of retinal glial cells in neurotransmitter uptake and metabolism.* Neurochem Int, 2009. **54**(3-4): p. 143-60.

76. Izumi, Y., et al., *Müller cell swelling, glutamate uptake, and excitotoxic neurodegeneration in the isolated rat retina.* Glia, 1999. **25**(4): p. 379-89.

77. Izumi, Y., et al., *Glutamate transporters and retinal excitotoxicity.* Glia, 2002. **39**(1): p. 58-68.

78. Pow, D.V. and D.K. Crook, *Direct immunocytochemical evidence for the transfer of glutamine from glial cells to neurons: use of specific antibodies directed against the d-stereoisomers of glutamate and glutamine.* Neuroscience, 1996. **70**(1): p. 295-302.

79. Goldman, D., *Müller glial cell reprogramming and retina regeneration.* Nature Reviews Neuroscience, 2014. **15**(7): p. 431-442.

80. Franze, K., et al., *Muller cells are living optical fibers in the vertebrate retina.* Proc Natl Acad Sci U S A, 2007. **104**(20): p. 8287-92.

81. Too, L.K. and M.P. Simunovic, *Retinal Stem/Progenitor Cells Derived From Adult Müller Glia for the Treatment of Retinal Degeneration.* Frontiers in Cell and Developmental Biology, 2021. **9**.

82. Salman, A., M.E. McClements, and R.E. MacLaren, *Insights on the Regeneration Potential of Müller Glia in the Mammalian Retina.* Cells, 2021. **10**(8).

83. Graca, A.B., C. Hippert, and R.A. Pearson, *Müller Glia Reactivity and Development of Gliosis in Response to Pathological Conditions.* Adv Exp Med Biol, 2018. **1074**: p. 303-308.

84. Henderson, R.H., *Inherited retinal dystrophies.* Paediatrics and Child Health, 2020. **30**(1): p. 19-27.

85. Berger, W., B. Kloeckener-Gruissem, and J. Neidhardt, *The molecular basis of human retinal and vitreoretinal diseases.* Prog Retin Eye Res, 2010. **29**(5): p. 335-75.

86. Chen, T.-C., et al., *Genetic characteristics and epidemiology of inherited retinal degeneration in Taiwan.* npj Genomic Medicine, 2021. **6**(1): p. 16.

87. Jürgens, G., et al., *Mutations affecting the pattern of the larval cuticle inDrosophila melanogaster.* Wilhelm Roux's archives of developmental biology, 1984. **193**(5): p. 283-295.

88. Tepass, U., C. Theres, and E. Knust, *crumbs encodes an EGF-like protein expressed on apical membranes of Drosophila epithelial cells and required for organization of epithelia.* Cell, 1990. **61**(5): p. 787-99.

89. den Hollander, A.I., et al., *CRB1 has a cytoplasmic domain that is functionally conserved between human and Drosophila.* Human Molecular Genetics, 2001. **10**(24): p. 2767-2773.

90. Klebes, A. and E. Knust, *A conserved motif in Crumbs is required for E-cadherin localisation and zonula adherens formation in Drosophila.* Curr Biol, 2000. **10**(2): p. 76-85.

91. Ray, T.A., et al., *Comprehensive identification of mRNA isoforms reveals the diversity of neural cell-surface molecules with roles in retinal development and disease.* Nat Commun, 2020. **11**(1): p. 3328.

92. Jaron, R., et al., *Expanding the phenotype of CRB2 mutations – A new ciliopathy syndrome?* Clinical Genetics, 2016. **90**(6): p. 540-544.

93. Tessier, A., et al., *Bi-allelic variations in CRB2, encoding the crumbs cell polarity complex component 2, lead to non-communicating hydrocephalus due to atresia of the aqueduct of sylvius and central canal of the medulla.* Acta Neuropathologica Communications, 2023. **11**(1): p. 29.

94. Boon, N., et al., *AAV-mediated gene augmentation therapy of CRB1 patient-derived retinal organoids restores the histological and transcriptional retinal phenotype.* Stem Cell Reports, 2023. **18**(5): p. 1123-1137.

95. Pellissier, L.P., et al., *Gene therapy into photoreceptors and Müller glial cells restores retinal structure and function in CRB1 retinitis pigmentosa mouse models.* Hum Mol Genet, 2015. **24**(11): p. 3104-18.

96. Paniagua, A.E., et al., *CRB2 completes a fully expressed Crumbs complex in the Retinal Pigment Epithelium.* Scientific Reports, 2015. **5**(1): p. 14504.

97. van Rossum, A.G., et al., *Pals1/Mpp5 is required for correct localization of Crb1 at the subapical region in polarized Muller glia cells.* Hum Mol Genet, 2006. **15**(18): p. 2659-72.

98. den Hollander, A.I., et al., *Isolation of Crb1, a mouse homologue of Drosophila crumbs, and analysis of its expression pattern in eye and brain.* Mech Dev, 2002. **110**(1-2): p. 203-7.

99. van de Pavert, S.A., et al., *Crumbs homologue 1 is required for maintenance of photoreceptor cell polarization and adhesion during light exposure.* Journal of Cell Science, 2004. **117**(18): p. 4169-4177.

100. Guo, C., et al., *Zebrafish Crb1, Localizing Uniquely to the Cell Membranes around Cone Photoreceptor Axonemes, Alleviates Light Damage to Photoreceptors and Modulates Cones' Light Responsiveness.* J Neurosci, 2020. **40**(37): p. 7065-7079.

101. Omori, Y. and J. Malicki, *oko meduzy and related crumbs genes are determinants of apical cell features in the vertebrate embryo.* Curr Biol, 2006. **16**(10): p. 945-57.

102. Fan, S., et al., *A novel Crumbs3 isoform regulates cell division and ciliogenesis via importin beta interactions.* J Cell Biol, 2007. **178**(3): p. 387-98.

103. Li, P., et al., *Crumbs protein homolog 3 (CRB3) expression is associated with oestrogen and progesterone receptor positivity in breast cancer.* Clin Exp Pharmacol Physiol, 2019. **46**(9): p. 837-844.

104. Iioka, H., et al., *Crumbs3 is a critical factor that regulates invasion and metastasis of colon adenocarcinoma via the specific interaction with FGFR1.* Int J Cancer, 2019. **145**(10): p. 2740-2753.

105. Park, B., et al., *PALS1 is essential for retinal pigment epithelium structure and neural retina stratification.* J Neurosci, 2011. **31**(47): p. 17230-41.

106. Bachmann, A., et al., *Drosophila Stardust is a partner of Crumbs in the control of epithelial cell polarity.* Nature, 2001. **414**(6864): p. 638-643.

107. Hong, Y., et al., *Drosophila Stardust interacts with Crumbs to control polarity of epithelia but not neuroblasts.* Nature, 2001. **414**(6864): p. 634-8.

108. Hong, Y., et al., *Distinct roles of Bazooka and Stardust in the specification of Drosophila photoreceptor membrane architecture.* Proc Natl Acad Sci U S A, 2003. **100**(22): p. 12712-7.

109. Nam, S.C. and K.W. Choi, *Interaction of Par-6 and Crumbs complexes is essential for photoreceptor morphogenesis in Drosophila.* Development, 2003. **130**(18): p. 4363-72.

110. Berger, S., et al., *Unraveling the genetic complexity of Drosophila stardust during photoreceptor morphogenesis and prevention of light-induced degeneration.* Genetics, 2007. **176**(4): p. 2189-200.

111. Wei, X. and J. Malicki, *nagie oko, encoding a MAGUK-family protein, is essential for cellular patterning of the retina.* Nat Genet, 2002. **31**(2): p. 150-7.

112. Wei, X., et al., *Nok plays an essential role in maintaining the integrity of the outer nuclear layer in the zebrafish retina.* Exp Eye Res, 2006. **83**(1): p. 31-44.

113. Gosens, I., et al., *FERM protein EPB41L5 is a novel member of the mammalian CRB-MPP5 polarity complex.* Exp Cell Res, 2007. **313**(19): p. 3959-70.

114. Hsu, Y.C., et al., *Mosaic Eyes is a novel component of the Crumbs complex and negatively regulates photoreceptor apical size.* Development, 2006. **133**(24): p. 4849-59.

115. Laprise, P., et al., *The FERM protein Yurt is a negative regulatory component of the Crumbs complex that controls epithelial polarity and apical membrane size.* Dev Cell, 2006. **11**(3): p. 363-74.

116. Pellikka, M., et al., *Crumbs, the Drosophila homologue of human CRB1/RP12, is essential for photoreceptor morphogenesis.* Nature, 2002. **416**(6877): p. 143-9.

117. Izaddoost, S., et al., *Drosophila Crumbs is a positional cue in photoreceptor adherens junctions and rhabdomeres.* Nature, 2002. **416**(6877): p. 178-83.

118. Lee, J.D., et al., *The FERM protein Epb4.1l5 is required for organization of the neural plate and for the epithelial-mesenchymal transition at the primitive streak of the mouse embryo.* Development, 2007. **134**(11): p. 2007-16.

119. Kantardzhieva, A., et al., *MPP5 recruits MPP4 to the CRB1 complex in photoreceptors.* Invest Ophthalmol Vis Sci, 2005. **46**(6): p. 2192-201.

120. Kantardzhieva, A., et al., *MPP3 is recruited to the MPP5 protein scaffold at the retinal outer limiting membrane.* Febs j, 2006. **273**(6): p. 1152-65.

121. Gosens, I., et al., *MPP1 links the Usher protein network and the Crumbs protein complex in the retina.* Hum Mol Genet, 2007. **16**(16): p. 1993-2003.

122. Dudok, J.J., et al., *MPP3 regulates levels of PALS1 and adhesion between photoreceptors and Müller cells.* Glia, 2013. **61**(10): p. 1629-44.

123. Aartsen, W.M., et al., *Mpp4 recruits Psd95 and Veli3 towards the photoreceptor synapse.* Hum Mol Genet, 2006. **15**(8): p. 1291-302.

124. Yang, J., et al., *Mpp4 is required for proper localization of plasma membrane calcium ATPases and maintenance of calcium homeostasis at the rod photoreceptor synaptic terminals.* Hum Mol Genet, 2007. **16**(9): p. 1017-29.

125. Lemmers, C., et al., *hINADl/PATJ, a homolog of discs lost, interacts with crumbs and localizes to tight junctions in human epithelial cells.* J Biol Chem, 2002. **277**(28): p. 25408-15.

126. Roh, M.H., et al., *The Maguk protein, Pals1, functions as an adapter, linking mammalian homologues of Crumbs and Discs Lost.* J Cell Biol, 2002. **157**(1): p. 161-72.

127. Roh, M.H., et al., *The carboxyl terminus of zona occludens-3 binds and recruits a mammalian homologue of discs lost to tight junctions.* J Biol Chem, 2002. **277**(30): p. 27501-9.

128. Hamazaki, Y., et al., *Multi-PDZ domain protein 1 (MUPP1) is concentrated at tight junctions through its possible interaction with claudin-1 and junctional adhesion molecule.* J Biol Chem, 2002. **277**(1): p. 455-61.

129. Nam, S.C. and K.W. Choi, *Domain-specific early and late function of Dpatj in Drosophila photoreceptor cells.* Dev Dyn, 2006. **235**(6): p. 1501-7.

130. Richard, M., F. Grawe, and E. Knust, *DPATJ plays a role in retinal morphogenesis and protects against light-dependent degeneration of photoreceptor cells in the Drosophila eye.* Dev Dyn, 2006. **235**(4): p. 895-907.

131. Hurd, T.W., et al., *Direct interaction of two polarity complexes implicated in epithelial tight junction assembly.* Nat Cell Biol, 2003. **5**(2): p. 137-42.

132. Lemmers, C., et al., *CRB3 binds directly to Par6 and regulates the morphogenesis of the tight junctions in mammalian epithelial cells.* Mol Biol Cell, 2004. **15**(3): p. 1324-33.

133. Joberty, G., et al., *The cell-polarity protein Par6 links Par3 and atypical protein kinase C to Cdc42.* Nat Cell Biol, 2000. **2**(8): p. 531-9.

134. Lin, D., et al., *A mammalian PAR-3-PAR-6 complex implicated in Cdc42/Rac1 and aPKC signalling and cell polarity.* Nat Cell Biol, 2000. **2**(8): p. 540-7.

135. Whitney, D.S., et al., *Binding of Crumbs to the Par-6 CRIB-PDZ Module Is Regulated by Cdc42.* Biochemistry, 2016. **55**(10): p. 1455-61.

136. Pichaud, F., *PAR-Complex and Crumbs Function During Photoreceptor Morphogenesis and Retinal Degeneration.* Front Cell Neurosci, 2018. **12**: p. 90.

137. Wodarz, A., et al., *Expression of crumbs confers apical character on plasma membrane domains of ectodermal epithelia of Drosophila.* Cell, 1995. **82**(1): p. 67-76.

138. Wodarz, A., F. Grawe, and E. Knust, *CRUMBS is involved in the control of apical protein targeting during Drosophila epithelial development.* Mechanisms of Development, 1993. **44**(2): p. 175-187.

139. Hao, Q., et al., *Crumbs proteins stabilize the cone mosaics of photoreceptors and improve vision in zebrafish.* Journal of Genetics and Genomics, 2021. **48**(1): p. 52-62.

140. Zou, J., X. Wang, and X. Wei, *Crb apical polarity proteins maintain zebrafish retinal cone mosaics via intercellular binding of their extracellular domains.* Dev Cell, 2012. **22**(6): p. 1261-74.

141. Buck, T.M., et al., *CRB1 is required for recycling by RAB11A+ vesicles in human retinal organoids.* Stem Cell Reports, 2023. **18**(9): p. 1793-1810.

142. Lin, Y., et al., *The extracellular and intracellular regions of Crb2a play distinct roles in guiding the formation of the apical zonula adherens.* Biomedicine & Pharmacotherapy, 2020. **125**: p. 109942.

143. Röper, K., *Anisotropy of Crumbs and aPKC drives myosin cable assembly during tube formation.* Dev Cell, 2012. **23**(5): p. 939-53.

144. Letizia, A., et al., *A functional role of the extracellular domain of Crumbs in cell architecture and apicobasal polarity.* Journal of Cell Science, 2013. **126**(10): p. 2157-2163.

145. Richard, M., et al., *A role for the extracellular domain of Crumbs in morphogenesis of Drosophila photoreceptor cells.* Eur J Cell Biol, 2009. **88**(12): p. 765-77.

146. Das, S. and E. Knust, *A dual role of the extracellular domain of Drosophila Crumbs for morphogenesis of the embryonic neuroectoderm.* Biology Open, 2018. **7**(1): p. bio031435.

147. Ohata, S., et al., *Dual Roles of Notch in Regulation of Apically Restricted Mitosis and Apicobasal Polarity of Neuroepithelial Cells.* Neuron, 2011. **69**(2): p. 215-230.

148. Herranz, H., et al., *Self-refinement of Notch activity through the transmembrane protein Crumbs: modulation of γ-Secretase activity.* EMBO reports, 2006. **7**(3): p. 297-302.

149. Kraut, R.S. and E. Knust, *Changes in endolysosomal organization define a pre-degenerative state in the crumbs mutant Drosophila retina.* PLoS One, 2019. **14**(12): p. e0220220.

150. Ehrenberg, M., et al., *CRB1: one gene, many phenotypes.* Semin Ophthalmol, 2013. **28**(5-6): p. 397-405.

151. Khan, K.N., et al., *A clinical and molecular characterisation of CRB1-associated maculopathy.* Eur J Hum Genet, 2018. **26**(5): p. 687-694.

152. Slavotinek, A.M., *The Family of Crumbs Genes and Human Disease.* Mol Syndromol, 2016. **7**(5): p. 274-281.

153. Talib, M., et al., *CRB1-associated retinal dystrophies in a Belgian cohort: genetic characteristics and long-term clinical follow-up.* Br J Ophthalmol, 2022. **106**(5): p. 696-704.

154. Tsang, S.H., et al., *Whole exome sequencing identifies CRB1 defect in an unusual maculopathy phenotype.* Ophthalmology, 2014. **121**(9): p. 1773-82.

155. Mairot, K., et al., *CRB1-Related Retinal Dystrophies in a Cohort of 50 Patients: A Reappraisal in the Light of Specific Müller Cell and Photoreceptor CRB1 Isoforms.* Int J Mol Sci, 2021. **22**(23).

156. Pellikka, M. and U. Tepass, *Unique cell biological profiles of retinal disease-causing missense mutations in the polarity protein Crumbs.* J Cell Sci, 2017. **130**(13): p. 2147-2158.

157. Yzer, S., et al., *CRB1 heterozygotes with regional retinal dysfunction: implications for genetic testing of leber congenital amaurosis.* Invest Ophthalmol Vis Sci, 2006. **47**(9): p. 3736-44.

158. Sacristan-Reviriego, A., et al., *Clinical and functional analyses of AIPL1 variants reveal mechanisms of pathogenicity linked to different forms of retinal degeneration.* Scientific Reports, 2020. **10**(1): p. 17520.

159. Mehalow, A.K., et al., *CRB1 is essential for external limiting membrane integrity and photoreceptor morphogenesis in the mammalian retina.* Hum Mol Genet, 2003. **12**(17): p. 2179-89.

160. Chang, B., et al., *Spontaneous Posterior Segment Vascular Disease Phenotype of a Mouse Model, rnv3, Is Dependent on the Crb1rd8 Allele.* Invest Ophthalmol Vis Sci, 2018. **59**(12): p. 5127-5139.

161. Luhmann, U.F., et al., *Differential modulation of retinal degeneration by Ccl2 and Cx3cr1 chemokine signalling.* PLoS One, 2012. **7**(4): p. e35551.

162. Kwon, Y.S., et al., *Cytoglobin deficiency potentiates Crb1-mediated retinal degeneration in rd8 mice.* Dev Biol, 2020. **458**(2): p. 141-152.

163. Markand, S., et al., *Mthfr as a modifier of the retinal phenotype of Crb1(rd8/rd8) mice.* Exp Eye Res, 2016. **145**: p. 164-172.

164. Weatherly, S.M., et al., *Identification of Arhgef12 and Prkci as genetic modifiers of retinal dysplasia in the Crb1rd8 mouse model.* PLOS Genetics, 2022. **18**(6): p. e1009798.

165. Richert, E., et al., *CRB1(rd8) mutation influences the age-related macular degeneration phenotype of NRF2 knockout mice and favors choroidal neovascularization.* Adv Med Sci, 2020. **65**(1): p. 71-77.

166. Quinn, P.M., et al., *CRB2 in immature photoreceptors determines the superior-inferior symmetry of the developing retina to maintain retinal structure and function.* Human Molecular Genetics, 2018. **27**(18): p. 3137-3153.

167. Buck, T.M., et al., *AAV-CRB2 protects against vision loss in an inducible CRB1 retinitis pigmentosa mouse model.* Mol Ther Methods Clin Dev, 2021. **20**: p. 423-441.

168. Boon, N., et al., *Characterization and AAV-mediated CRB gene augmentation in human-derived CRB1(KO) and CRB1(KO)CRB2(+/-) retinal organoids.* Mol Ther Methods Clin Dev, 2023. **31**: p. 101128.

169. den Hollander, A.I., et al., *Leber congenital amaurosis: genes, proteins and disease mechanisms.* Prog Retin Eye Res, 2008. **27**(4): p. 391-419.

170. Thompson, B.J., F. Pichaud, and K. Röper, *Sticking together the Crumbs — an unexpected function for an old friend.* Nature Reviews Molecular Cell Biology, 2013. **14**(5): p. 307-314.

171. Nygard, A.B., et al., *Selection of reference genes for gene expression studies in pig tissues using SYBR green qPCR.* BMC Mol Biol, 2007. **8**: p. 67.

172. Gloeckner, C.J., et al., *A novel tandem affinity purification strategy for the efficient isolation and characterisation of native protein complexes.* Proteomics, 2007. **7**(23): p. 4228-34.

173. Demichev, V., et al., *DIA-NN: neural networks and interference correction enable deep proteome coverage in high throughput.* Nat Methods, 2020. **17**(1): p. 41-44.

174. Robinson, J.T., et al., *Integrative genomics viewer.* Nature Biotechnology, 2011. **29**(1): p. 24-26.

175. Waterhouse, A.M., et al., *Jalview Version 2—a multiple sequence alignment editor and analysis workbench.* Bioinformatics, 2009. **25**(9): p. 1189-1191.

176. Beyer, T., et al., *Tissue- and isoform-specific protein complex analysis with natively processed bait proteins.* Journal of Proteomics, 2021. **231**: p. 103947.

177. Cox, J. and M. Mann, *MaxQuant enables high peptide identification rates, individualized p.p.b.-range mass accuracies and proteome-wide protein quantification.* Nature Biotechnology, 2008. **26**(12): p. 1367-1372.

178. Cox, J., et al., *A practical guide to the MaxQuant computational platform for SILAC-based quantitative proteomics.* Nature Protocols, 2009. **4**(5): p. 698-705.

179. Ge, S.X., D. Jung, and R. Yao, *ShinyGO: a graphical gene-set enrichment tool for animals and plants.* Bioinformatics, 2020. **36**(8): p. 2628-2629.

180. Szklarczyk, D., et al., *The STRING database in 2023: protein-protein association networks and functional enrichment analyses for any sequenced genome of interest.* Nucleic Acids Res, 2023. **51**(D1): p. D638-d646.

181. Shannon, P., et al., *Cytoscape: a software environment for integrated models of biomolecular interaction networks.* Genome Res, 2003. **13**(11): p. 2498-504.

182. Scholz, N., et al., *Molecular sensing of mechano- and ligand-dependent adhesion GPCR dissociation.* Nature, 2023. **615**(7954): p. 945-953.

183. Harlow, E. and D. Lane, *Antibodies. A laboratory manual.* 1988.

184. Sen, M., et al. *Efficient Ocular Delivery of VCP siRNA via Reverse Magnetofection in RHO P23H Rodent Retina Explants*. Pharmaceutics, 2021. **13**, DOI: 10.3390/pharmaceutics13020225.

185. Lopes da Costa, B., et al. *Clinical and Therapeutic Evaluation of the Ten Most Prevalent CRB1 Mutations*. Biomedicines, 2023. **11**, DOI: 10.3390/biomedicines11020385.

186. Adams, C.J., et al., *Structure and Molecular Mechanism of ER Stress Signaling by the Unfolded Protein Response Signal Activator IRE1.* Frontiers in Molecular Biosciences, 2019. **6**.

187. Mozos, A., et al., *The expression of the endoplasmic reticulum stress sensor BiP/GRP78 predicts response to chemotherapy and determines the efficacy of proteasome inhibitors in diffuse large b-cell lymphoma.* Am J Pathol, 2011. **179**(5): p. 2601-10.

188. Santos, N. and J.F. Reiter, *Building it up and taking it down: the regulation of vertebrate ciliogenesis.* Dev Dyn, 2008. **237**(8): p. 1972-81.

189. Murali, A., et al., *Retinal explant culture: A platform to investigate human neuro-retina.* Clinical & Experimental Ophthalmology, 2019. **47**(2): p. 274-285.

190. Dawson, H.D., et al., *An in-depth comparison of the porcine, murine and human inflammasomes; lessons from the porcine genome and transcriptome.* Veterinary Microbiology, 2017. **202**: p. 2-15.

191. Megaw, R. and T.W. Hurd, *Photoreceptor actin dysregulation in syndromic and non-syndromic retinitis pigmentosa.* Biochemical Society Transactions, 2018. **46**(6): p. 1463-1473.

192. Spencer, W.J., et al., *Photoreceptor disc membranes are formed through an Arp2/3-dependent lamellipodium-like mechanism.* Proceedings of the National Academy of Sciences, 2019. **116**(52): p. 27043.

193. Rosa, L.R.O., et al., *ARHGAP21 as a master regulator of multiple cellular processes.* Journal of Cellular Physiology, 2018. **233**(11): p. 8477-8481.

194. Butkevich, E., et al., *Drebrin-like protein DBN-1 is a sarcomere component that stabilizes actin filaments during muscle contraction.* Nature Communications, 2015. **6**(1): p. 7523.

195. Megaw, R., et al., *Gelsolin dysfunction causes photoreceptor loss in induced pluripotent cell and animal retinitis pigmentosa models.* Nature Communications, 2017. **8**(1): p. 271.

196. Uhlén, M., et al., *Proteomics. Tissue-based map of the human proteome.* Science, 2015. **347**(6220): p. 1260419.

197. Hunt, D.M., P. Buch, and M. Michaelides, *Guanylate cyclases and associated activator proteins in retinal disease.* Molecular and Cellular Biochemistry, 2010. **334**(1): p. 157-168.

198. Schlessinger, J., *Cell Signaling by Receptor Tyrosine Kinases.* Cell, 2000. **103**(2): p. 211-225.

199. Nemetschke, L. and E. Knust, *Drosophila Crumbs prevents ectopic Notch activation in developing wings by inhibiting ligand-independent endocytosis.* Development, 2016. **143**(23): p. 4543-4553.

200. Ghai, K., C. Zelinka, and A.J. Fischer, *Notch signaling influences neuroprotective and proliferative properties of mature Müller glia.* J Neurosci, 2010. **30**(8): p. 3101-12.

201. Louvi, A. and S. Artavanis-Tsakonas, *Notch signalling in vertebrate neural development.* Nat Rev Neurosci, 2006. **7**(2): p. 93-102.

202. Hayes, S., et al., *Notch signaling regulates regeneration in the avian retina.* Dev Biol, 2007. **312**(1): p. 300-11.

203. Gumbiner, B.M. and N.G. Kim, *The Hippo-YAP signaling pathway and contact inhibition of growth.* J Cell Sci, 2014. **127**(Pt 4): p. 709-17.

204. Yu, F.X., B. Zhao, and K.L. Guan, *Hippo Pathway in Organ Size Control, Tissue Homeostasis, and Cancer.* Cell, 2015. **163**(4): p. 811-28.

205. Grusche, F.A., et al., *The Salvador/Warts/Hippo pathway controls regenerative tissue growth in Drosophila melanogaster.* Developmental Biology, 2011. **350**(2): p. 255-266.

206. Ling, C., et al., *The apical transmembrane protein Crumbs functions as a tumor suppressor that regulates Hippo signaling by binding to Expanded.* Proc Natl Acad Sci U S A, 2010. **107**(23): p. 10532-7.

207. Chen, C.L., et al., *The apical-basal cell polarity determinant Crumbs regulates Hippo signaling in Drosophila.* Proc Natl Acad Sci U S A, 2010. **107**(36): p. 15810-5.

208. Mao, X., et al., *CRB3 regulates contact inhibition by activating the Hippo pathway in mammary epithelial cells.* Cell Death Dis, 2017. **8**(1): p. e2546.

209. Szymaniak, Aleksander D., et al., *Crumbs3-Mediated Polarity Directs Airway Epithelial Cell Fate through the Hippo Pathway Effector Yap.* Developmental Cell, 2015. **34**(3): p. 283-296.

210. Varelas, X., et al., *The Crumbs Complex Couples Cell Density Sensing to Hippo-Dependent Control of the TGF-β-SMAD Pathway.* Developmental Cell, 2010. **19**(6): p. 831-844.

211. Hergovich, A., *The Roles of NDR Protein Kinases in Hippo Signalling.* Genes (Basel), 2016. **7**(5).

212. Zhang, L., et al., *NDR functions as a physiological YAP1 kinase in the intestinal epithelium.* Curr Biol, 2015. **25**(3): p. 296-305.

213. Hergovich, A., et al., *NDR kinases regulate essential cell processes from yeast to humans.* Nat Rev Mol Cell Biol, 2006. **7**(4): p. 253-64.

214. Hergovich, A., *Regulation and functions of mammalian LATS/NDR kinases: looking beyond canonical Hippo signalling.* Cell & bioscience, 2013. **3**(1): p. 1-12.

215. Duhart, J.C. and L.A. Raftery, *Mob Family Proteins: Regulatory Partners in Hippo and Hippo-Like Intracellular Signaling Pathways.* Front Cell Dev Biol, 2020. **8**: p. 161.

216. Kohler, R.S., et al., *Differential NDR/LATS Interactions with the Human MOB Family Reveal a Negative Role for Human MOB2 in the Regulation of Human NDR Kinases.* Molecular and Cellular Biology, 2010. **30**(18): p. 4507-4520.

217. van Loon, K., E.J.M. Huijbers, and A.W. Griffioen, *Secreted frizzled-related protein 2: a key player in noncanonical Wnt signaling and tumor angiogenesis.* Cancer and Metastasis Reviews, 2021. **40**(1): p. 191-203.

218. Lad, E.M., S.H. Cheshier, and M.Y.S. Kalani, *Wnt-signaling in retinal development and disease.* Stem cells and development, 2009. **18**(1): p. 7-16.

219. Jones, S.E., et al., *Modulated expression of secreted frizzledrelated proteins in human retinal degeneration.* Neuroreport, 2000. **11**(18): p. 3963-3967.

220. Alves, C.H., L.P. Pellissier, and J. Wijnholds, *The CRB1 and adherens junction complex proteins in retinal development and maintenance.* Progress in Retinal and Eye Research, 2014. **40**: p. 35-52.

221. Robitaille, J., et al., *Mutant frizzled-4 disrupts retinal angiogenesis in familial exudative vitreoretinopathy.* Nature genetics, 2002. **32**(2): p. 326-330.

222. Robertson, I.B., et al., *Latent TGF-β-binding proteins.* Matrix Biol, 2015. **47**: p. 44-53.

223. Bielmeier, C.B., et al., *Deficiency in Retinal TGFβ Signaling Aggravates Neurodegeneration by Modulating Pro-Apoptotic and MAP Kinase Pathways.* Int J Mol Sci, 2022. **23**(5).

224. Wang, S.K., Y. Xue, and C.L. Cepko, *Microglia modulation by TGF-β1 protects cones in mouse models of retinal degeneration.* J Clin Invest, 2020. **130**(8): p. 4360-4369.

225. Pearson, R.A., et al., *Targeted disruption of outer limiting membrane junctional proteins (Crb1 and ZO-1) increases integration of transplanted photoreceptor precursors into the adult wild-type and degenerating retina.* Cell Transplant, 2010. **19**(4): p. 487-503.

226. Bellingrath, J.-S., et al., *Development of a functional assay for the assessment of two common CRB1 mutations.* Investigative Ophthalmology & Visual Science, 2022. **63**(7): p. 1766 – F0315-1766 – F0315.

227. Ramkumar, N., et al., *Protein O-Glucosyltransferase 1 (POGLUT1) Promotes Mouse Gastrulation through Modification of the Apical Polarity Protein CRUMBS2.* PLOS Genetics, 2015. **11**(10): p. e1005551.

228. Aguilar-Aragon, M., G. Fletcher, and B.J. Thompson, *The cytoskeletal motor proteins Dynein and MyoV direct apical transport of Crumbs.* Dev Biol, 2020. **459**(2): p. 126-137.

229. Li, B.X., A.K. Satoh, and D.F. Ready, *Myosin V, Rab11, and dRip11 direct apical secretion and cellular morphogenesis in developing Drosophila photoreceptors.* J Cell Biol, 2007. **177**(4): p. 659-69.

230. Pocha, S.M., A. Shevchenko, and E. Knust, *Crumbs regulates rhodopsin transport by interacting with and stabilizing myosin V.* J Cell Biol, 2011. **195**(5): p. 827-38.

231. Dona, M., et al., *NINL and DZANK1 Co-function in Vesicle Transport and Are Essential for Photoreceptor Development in Zebrafish.* PLoS Genet, 2015. **11**(10): p. e1005574.

232. Cullen, P.J. and J.G. Carlton, *Phosphoinositides in the mammalian endo-lysosomal network.* Subcell Biochem, 2012. **59**: p. 65-110.

233. Wensel, T.G., *Phosphoinositides in Retinal Function and Disease.* Cells, 2020. **9**(4).

234. Lattner, J., et al., *Crumbs organizes the transport machinery by regulating apical levels of PI(4,5)P2 in Drosophila.* eLife, 2019. **8**: p. e50900.

235. Corral-Serrano, J.C., et al., *PCARE and WASF3 regulate ciliary F-actin assembly that is required for the initiation of photoreceptor outer segment disk formation.* Proceedings of the National Academy of Sciences, 2020. **117**(18): p. 9922-9931.

236. Médina, E., et al., *Crumbs interacts with moesin and beta(Heavy)-spectrin in the apical membrane skeleton of Drosophila.* J Cell Biol, 2002. **158**(5): p. 941-51.

237. Flores-Benitez, D. and E. Knust, *Crumbs is an essential regulator of cytoskeletal dynamics and cell-cell adhesion during dorsal closure in Drosophila.* eLife, 2015. **4**: p. e07398.

238. Tanoue, A., et al., *Podocyte-specific Crb2 knockout mice develop focal segmental glomerulosclerosis.* Scientific Reports, 2021. **11**(1): p. 20556.

239. Gao, Y., et al., *Polarity protein Crumbs homolog-3 (CRB3) regulates ectoplasmic specialization dynamics through its action on F-actin organization in Sertoli cells.* Scientific Reports, 2016. **6**(1): p. 28589.

240. Dominique, M.-H., et al., *CRB3 and ARP2/3 regulate cell biomechanical properties to set epithelial monolayers for collective movement.* bioRxiv, 2023: p. 2023.04.18.537332.

241. Smith, C.E.L., A.V.R. Lake, and C.A. Johnson, *Primary Cilia, Ciliogenesis and the Actin Cytoskeleton: A Little Less Resorption, A Little More Actin Please.* Frontiers in Cell and Developmental Biology, 2020. **8**.

242. Katsanis, N., et al., *Triallelic inheritance in Bardet-Biedl syndrome, a Mendelian recessive disorder.* Science, 2001. **293**(5538): p. 2256-9.

243. Katsanis, N., J.R. Lupski, and P.L. Beales, *Exploring the molecular basis of Bardet-Biedl syndrome.* Hum Mol Genet, 2001. **10**(20): p. 2293-9.

244. Zernant, J., et al., *Rare and common variants in ROM1 and PRPH2 genes trans-modify Stargardt/ABCA4 disease.* PLoS Genet, 2022. **18**(3): p. e1010129.

245. Poloschek, C.M., et al., *ABCA4 and ROM1: implications for modification of the PRPH2-associated macular dystrophy phenotype.* Invest Ophthalmol Vis Sci, 2010. **51**(8): p. 4253-65.

246. Cheng, J., et al., *Integrating Genome-Wide CNVs Into QTLs and High Confidence GWAScore Regions Identified Positional Candidates for Sheep Economic Traits.* Front Genet, 2020. **11**: p. 569.

247. Moekotte, L., et al., *CRB1-Associated Retinal Dystrophy Patients Have Expanded Lewis Glycoantigen-Positive T Cells.* Invest Ophthalmol Vis Sci, 2023. **64**(13): p. 6.

248. Moekotte, L., et al., *Elevated Plasma Complement Factors in CRB1-associated Inherited Retinal Dystrophies.* medRxiv, 2023: p. 2023.11.10.23298334.

249. Nashun, B., P.W. Hill, and P. Hajkova, *Reprogramming of cell fate: epigenetic memory and the erasure of memories past.* Embo j, 2015. **34**(10): p. 1296-308.

250. Bilwes, A.M., et al., *Structural basis for inhibition of receptor protein-tyrosine phosphatase-alpha by dimerization.* Nature, 1996. **382**(6591): p. 555-9.

251. Bilic, J. and J.C. Izpisua Belmonte, *Concise review: Induced pluripotent stem cells versus embryonic stem cells: close enough or yet too far apart?* Stem Cells, 2012. **30**(1): p. 33-41.

252. Landrum, M.J., et al., *ClinVar: improving access to variant interpretations and supporting evidence.* Nucleic Acids Res, 2018. **46**(D1): p. D1062-d1067.

253. Gorden, N.T., et al., *CC2D2A is mutated in Joubert syndrome and interacts with the ciliopathy-associated basal body protein CEP290.* Am J Hum Genet, 2008. **83**(5): p. 559-71.

254. Tallila, J., et al., *Identification of CC2D2A as a Meckel syndrome gene adds an important piece to the ciliopathy puzzle.* Am J Hum Genet, 2008. **82**(6): p. 1361-7.

255. Astuto, L.M., et al., *CDH23 Mutation and Phenotype Heterogeneity: A Profile of 107 Diverse Families with Usher Syndrome and Nonsyndromic Deafness.* The American Journal of Human Genetics, 2002. **71**(2): p. 262-275.

256. Bolz, H., et al., *Mutation of CDH23, encoding a new member of the cadherin gene family, causes Usher syndrome type 1D.* Nat Genet, 2001. **27**(1): p. 108-12.

257. Singaraju, G.S., et al., *Structural basis of the strong cell-cell junction formed by cadherin-23.* The FEBS Journal, 2020. **287**(11): p. 2328-2347.

258. Shibata, S., et al., *ARHGEF10 directs the localization of Rab8 to Rab6-positive executive vesicles.* J Cell Sci, 2016. **129**(19): p. 3620-3634.

259. Verhoeven, K., et al., *Slowed Conduction and Thin Myelination of Peripheral Nerves Associated with Mutant Rho Guanine-Nucleotide Exchange Factor 10.* The American Journal of Human Genetics, 2003. **73**(4): p. 926-932.

260. van den Hurk, J.A., et al., *Characterization of the Crumbs homolog 2 (CRB2) gene and analysis of its role in retinitis pigmentosa and Leber congenital amaurosis.* Mol Vis, 2005. **11**: p. 263-73.

261. Adutwum, M., et al., *Six new cases of CRB2-related syndrome and a review of clinical findings in 28 reported patients.* Clinical Genetics, 2023. **103**(1): p. 97-102.

262. Chen, X., et al., *CRB2 mutation causes autosomal recessive retinitis pigmentosa.* Experimental Eye Research, 2019. **180**: p. 164-173.

263. Ebarasi, L., et al., *Defects of CRB2 Cause Steroid-Resistant Nephrotic Syndrome.* The American Journal of Human Genetics, 2015. **96**(1): p. 153-161.

264. Lamont, R.E., et al., *Expansion of phenotype and genotypic data in CRB2-related syndrome.* European Journal of Human Genetics, 2016. **24**(10): p. 1436-1444.

265. Udagawa, T., et al., *Altered expression of Crb2 in podocytes expands a variation of CRB2 mutations in steroid-resistant nephrotic syndrome.* Pediatric Nephrology, 2017. **32**(5): p. 801-809.

266. Zhang, L., et al., *Genetic and preimplantation diagnosis of cystic kidney disease with ventriculomegaly.* Journal of Human Genetics, 2020. **65**(5): p. 455-459.

267. Grigoryan, E.N. *Self-Organization of the Retina during Eye Development, Retinal Regeneration In Vivo, and in Retinal 3D Organoids In Vitro*. Biomedicines, 2022. **10**, DOI: 10.3390/biomedicines10061458.

268. Klapper, S.D., et al., *Biophysical Properties of Optogenetic Tools and Their Application for Vision Restoration Approaches.* Front Syst Neurosci, 2016. **10**: p. 74.

269. Armento, A., et al. *Complement Factor H Loss in RPE Cells Causes Retinal Degeneration in a Human RPE-Porcine Retinal Explant Co-Culture Model*. Biomolecules, 2021. **11**, DOI: 10.3390/biom11111621.

270. Wahle, P., et al., *Multimodal spatiotemporal phenotyping of human retinal organoid development.* Nature Biotechnology, 2023. **41**(12): p. 1765-1775.

271. Achberger, K., et al., *Merging organoid and organ-on-a-chip technology to generate complex multi-layer tissue models in a human retina-on-a-chip platform.* eLife, 2019. **8**: p. e46188.

272. Zhang, Z., et al., *Retinal Organoid Technology: Where Are We Now?* Int J Mol Sci, 2021. **22**(19).

273. Smith, C.J. and A.M. Osborn, *Advantages and limitations of quantitative PCR (Q-PCR)-based approaches in microbial ecology.* FEMS Microbiology Ecology, 2009. **67**(1): p. 6-20.

274. Karner, C., K.A. Wharton, and T.J. Carroll, *Apical-basal polarity, Wnt signaling and vertebrate organogenesis.* Semin Cell Dev Biol, 2006. **17**(2): p. 214-22.

275. Kent, W.J., et al., *The human genome browser at UCSC.* Genome Res, 2002. **12**(6): p. 996-1006.

276. The UniProt, C., *UniProt: the Universal Protein Knowledgebase in 2023.* Nucleic Acids Research, 2023. **51**(D1): p. D523-D531.

7. Acknowledgements

I would like to thank my supervisor **Prof. Marius Ueffing** for giving me the opportunity to work in his laboratory on the CRB1 project. Thank you, Marius, for your constant support, great scientific ideas, trust and enthusiasm throughout my PhD allowing me to learn and grow as a scientist.

I am very grateful to my advisory board members, **Prof. Melanie Phillip** and **Dr. Johannes Gloeckner**, who always provided new ideas and interesting discussions about my project during the advisory board meetings. Furthermore, I would also like to thank **Prof. Dr. Stefan Liebau**, **Dr. Kevin Achberger** and **Virginia Cora** for the iPSC-derived RO and the discussions on the CRB1 project. In addition, I am grateful to **Dr. Peter MJ Quinn** for his input on the manuscript.

I would like to express my gratitude to **Dr. Karsten Boldt** and **Dr. Tina Beyer** for 'adopting' me into the cilia group and always having an open door for questions. I think that we can now consider Crumbs to be a cilia protein. This project, the thesis and the manuscript would never have been what it is now without your mentoring, ideas, support and encouragement. I would also like to thank you, Tina, for proofreading my thesis.

I would also like to thank **Sylvia Bolz**, **Christine Henes** and **Selina Kugler** for their help with microscopy-related questions and the microscopic validation of the CRB monoclonal antibodies. In addition, I would also like to thank **Prof. Dr. Regina Feederle** and **Dr. Katharina Bäuer** for the discussions and production of the CRB monoclonal antibodies at the Helmholtz Zentrum Munich.

Furthermore, I would like to thank **Prof. Dr. Katarina Stingl** and **Dr. Susanne Kohl** for their help with clinical questions and ethical agreements. For the help and input on the analysis of the CRB1 splicing, I would like to thank **Dr. Nicole Weißschuh** and **Dr. Peggy Reuter**.

For the analysis and help with the WGS, I am very thankful to **Dr. Nicolas Casadei**, **Dr. Elena Buena Atienza**, **Dr. Theresia Zuleger**, **Jakob Admard** and **Caspar Gross**.

I am very grateful to all the wonderful members of the **Ueffing Lab,** who make it such a pleasure to work every day. **Dr. Mohamed Ali Jarboui**, thank you, for the help with the DIA analysis and all the fancy analysis tools. I would like to thank **Franziska Klose** for taking care of the mass spectrometer and every single sample that I had to measure. Thank you, **Katrin Dahlke**, for all your support in the lab with ordering, experimental methods and great lab tips. I would especially like to thank **Franziska Wörz, Felix Hoffmann, Ana Cristina Almansa García**, **Tobias Leonhard**, **Nicola Horn,** and **Shibu Antony** for all the support and fun we had in and out of the lab! Thank you for being not only wonderful colleagues, but friends!

8. Appendix

Appendix 1| Anti-CRB1 antibody from Abnova specifically recognises human canonical CRB1

To validate anti-CRB1 commercially available antibodies, HEK293T cells were transiently transfected with GFP (control) or FLAG-tagged CRB1 (NSF-CRB1) for 48 hours followed by western blot analysis. Anti-CRB1 antibodies were used from Thermo (PA5-34491), Sigma (HPA061250), Abnova (H00023418-A01) and Merck (MABN1572). Anti-Flag antibody was used as a control to verify expression of NSF-CRB1.

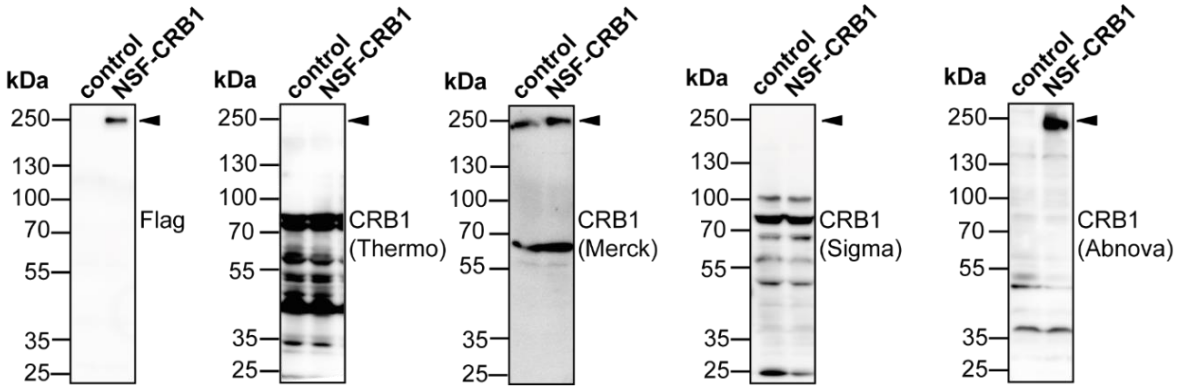

Appendix 2| Lower level of CRB1 protein in CRB1-patient RO using a C-term CRB1 antibody CRB1C 25G2 Western blot analysis of lysates of control, patient A and patient B iPSC-derived ROs of 90 days of age. CRB1 was analysed using CRB1C 25G2 a home-made antibody that recognises a peptide in the CRB1 intracellular domain. Further details on this antibody are described in chapter 4.73. GAPDH was used as a loading control.

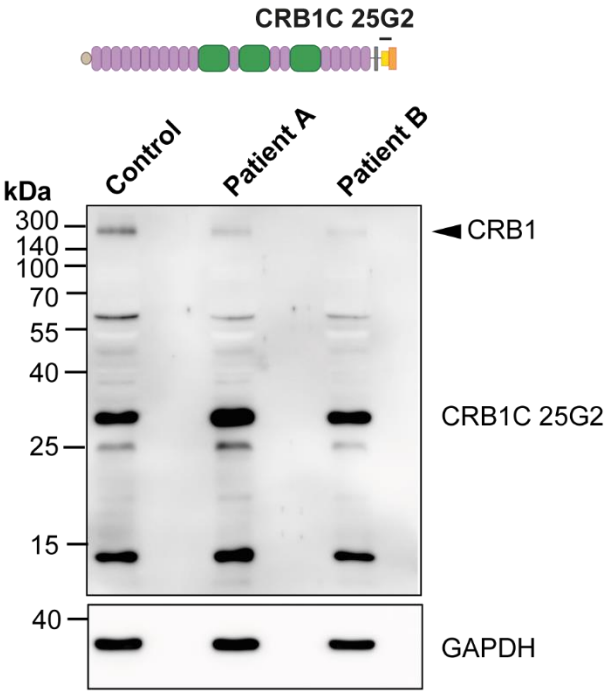

Appendix 3| Porcine and human CRB1 and CRB2 are highly conserved (A) Alignment of *CRB2* protein sequence from homo sapiens (H.sapiens, bottom sequence, NP_775960.4) and sus scrofa (S.scrofa, upper sequence, XP_003122203.3) together with the consensus sequence (B) Alignment of CRB1 protein sequence of H.sapiens (bottom strand, NP_957705.1) and S.scrofa (top strand, XP_020920141.1) with consensus.

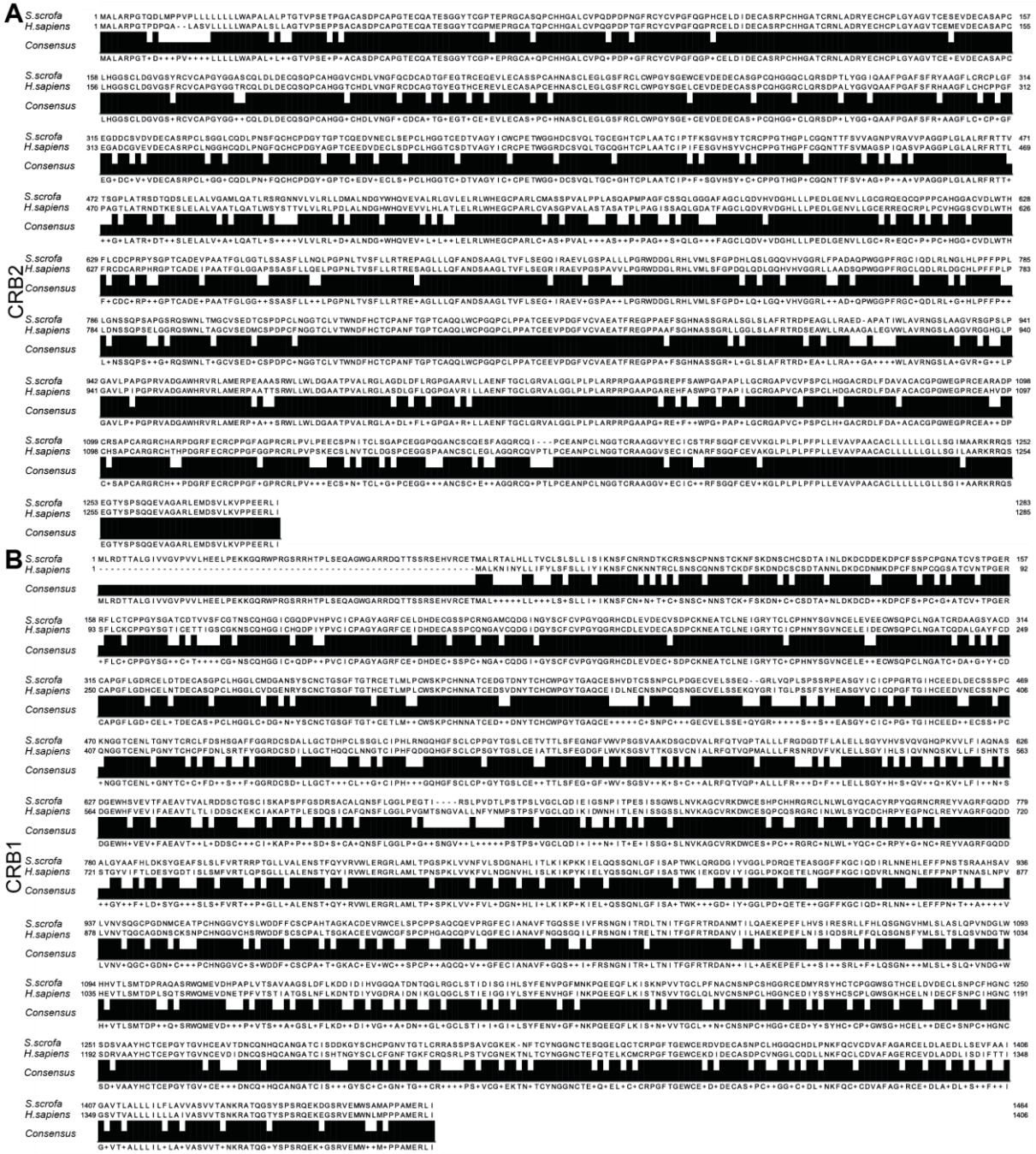

Appendix 4| Peptide coverage of CRB1 with the N-term FLAG tag Scaffold was used to identify unique exclusive peptides for CRB1 (*homo sapiens*). Amino acids similar to the MS/MS spectra are depicted in yellow. Green residues have a post-translational modification. Coverage 30 %

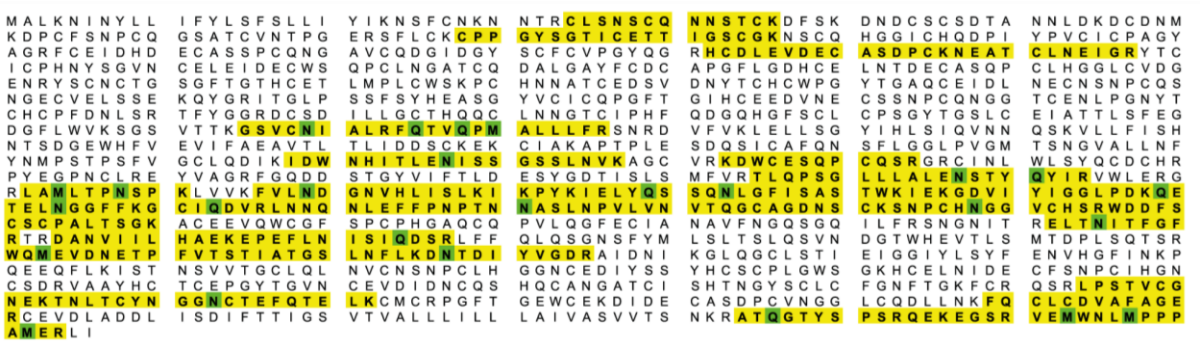

Appendix 5| Significant enriched proteins in CRB1-FLAG after SDS washing and without incubation of porcine retina lysate CRB1-FLAG and GFP-FLAG were transiently overexpressed in HEK293T cells, followed by FLAG-IP and SDS washing. Upon elution, samples were analysed by mass spectrometry using DDA. Table shows the significant higher abundant proteins in CRB1-FLAG samples compared to GFP-FLAG together with the log_2 ratio and the $-log_2$ p-value (One-sample t-test, FDR 0.05, log_2 ratio (CRB1-FLAG/GFP-FLAG) >2, n=6)

Gene	Log_2 ratio (CRB1/GFP)	$-log_2$ p-value	Gene	Log_2 ratio (CRB1/GFP)	$-log_2$ p-value	Gene	Log_2 ratio (CRB1/GFP)	$-log_2$ p-value
CRB1	29.67	5.07	**MRPL48**	22.20	3.56	**SUMF2**	20.54	2.30
MPP5	27.39	3.94	**RPS15**	22.18	14.44	**UBE2L3**	20.52	2.29
LIN7C	26.42	12.73	**PRPF31**	22.03	3.14	**SLAIN2**	20.49	2.29
MRPL43	25.07	16.57	**FKBP10**	21.98	15.76	**CLASP1**	20.46	2.21
PTMA	24.91	2.29	**PPHLN1**	21.96	3.55	**MYO1C**	20.36	2.30
GNGT1	24.75	2.10	**CCDC88A**	21.90	14.07	**RANBP9**	20.18	2.29
MOB2	24.65	2.80	**LTBP1**	21.87	16.13	**RCL1**	20.18	2.29
MRPL49	24.53	4.02	**LOC100626015**	21.86	19.70	**JAK2**	19.98	2.34
MRPL13	24.52	15.76	**FHL1**	21.82	2.42	**KEAP1**	19.91	2.30
MRPL39	24.35	16.18	**PATJ**	21.76	3.51	**TNRC6B**	19.88	3.56
SELENOF	24.30	15.36	**RANBP10**	21.76	2.30	**ANKFY1**	19.79	3.53
MRPL15	24.30	14.99	**PAFAH1B3**	21.71	2.27	**ROCK1**	19.60	3.55
MPDZ	24.27	10.92	**ARPC2**	21.69	2.29	**CKAP5**	19.34	2.07
MRPL37	24.23	2.29	**DNAJC3**	21.66	3.56	**CHERP**	19.31	2.27
PSMB6	24.15	2.18	**SDF2**	21.65	3.70	**ACAP2**	19.20	2.29
MRPL46	23.95	3.56	**SDF2L1**	21.63	2.29	**U2SURP**	18.85	2.25
TET2	23.94	19.12	**NGLY1**	21.61	3.57	**CDC5L**	18.83	2.29
PSMA3	23.88	3.80	**CAMSAP3**	21.57	3.56	**UGGT2**	8.71	2.76
RPL36A	23.83	2.29	**LOC100526148**	21.52	3.57	**THRAP3**	8.13	2.85
MRPL20	23.75	3.57	**SPTBN2**	21.50	2.11	**EIF4B**	7.49	2.25
MRPL27	23.69	3.56	**MAP3K7**	21.44	3.51	**SNRPD2**	7.03	2.30
PTS	23.43	3.57	**WDR5**	21.39	3.57	**BCLAF1**	6.07	2.13
PSMB1	23.42	15.78	**ARL6IP5**	21.37	2.09	**OBI1**	6.00	2.34
PSMA2	23.39	18.50	**SF3B2**	21.35	2.54	**SNRPD1**	5.60	2.19
MRPL32	23.32	15.10	**SLITRK6**	21.25	16.36	**OGT**	5.53	1.95
SPINDOC	23.30	15.49	**GID8**	21.23	2.29	**SNRPN**	4.93	2.13
IVNS1ABP	23.22	13.56	**MGA**	21.22	3.57	**WDR77**	4.60	5.91
MRPL38	23.21	3.57	**HNRNPUL1**	21.20	2.29	**ERH**	4.19	6.20
H1-4	23.18	15.12	**USP15**	21.17	3.57	**PSPC1**	3.32	7.13
HDX	23.10	3.57	**WDR26**	21.17	3.56	**MRPL9**	3.21	1.94
TECR	23.06	2.11	**ZNF768**	21.10	3.55	**STK38L**	3.17	3.96
MAGT1	22.96	16.45	**MAPK4**	21.05	3.57	**MRPL1**	3.07	1.91
OTUD4	22.90	11.84	**TXNDC5**	20.98	3.57	**SPIN1**	2.73	4.97
RPS20	22.90	15.04	**HNRNPH2**	20.97	2.10	**EIF3A**	2.68	1.88
E2F8	22.88	18.06	**GMFG**	20.94	2.29	**CANX**	2.60	4.33
PROSER1	22.79	3.57	**SLC30A9**	20.93	3.57	**PPM1B**	2.59	4.52
SRPRB	22.76	3.57	**CSRP2**	20.89	2.06	**MRPL12**	2.50	4.03
MRPL16	22.72	3.55	**PHKB**	20.88	3.57	**PSMA1**	2.49	4.92
IPO8	22.68	3.57	**TAF4B**	20.86	3.57	**PSMC3**	2.44	5.16
MRPL28	22.68	3.56	**GLG1**	20.79	3.57	**PSMD1**	2.43	4.66
MRPL55	22.44	2.29	**CORO1C**	20.76	2.45	**PSMD2**	2.38	5.51
PSMD8	22.40	2.29	**CPSF7**	20.70	3.57	**PSMC4**	2.36	4.38
TAB1	22.34	3.02	**CBX4**	20.64	2.30	**PSMC2**	2.33	5.59
SPIN3	22.30	20.16	**DDX6**	20.63	2.29	**PSMC6**	2.27	5.56
SNRPE	22.21	2.29	**CCDC88C**	20.61	2.30	**PSMA4**	2.18	6.44
PSMC1	2.17	4.98						
PSMC5	2.11	4.39						
DNAJB11	2.08	5.58						
PSMB3	2.04	4.58						

Appendix 6| CRB1 peptides detected by mass spectrometry Alignment of porcine and human CRB1. Specific peptides detected by mass spectrometry are depicted in green. Except for one peptide, which is also highlighted in the porcine CRB1 sequence, all peptides were specific for human CRB1 as they differ by at least one amino acid from porcine CRB1. This image was generated using Jalview software.

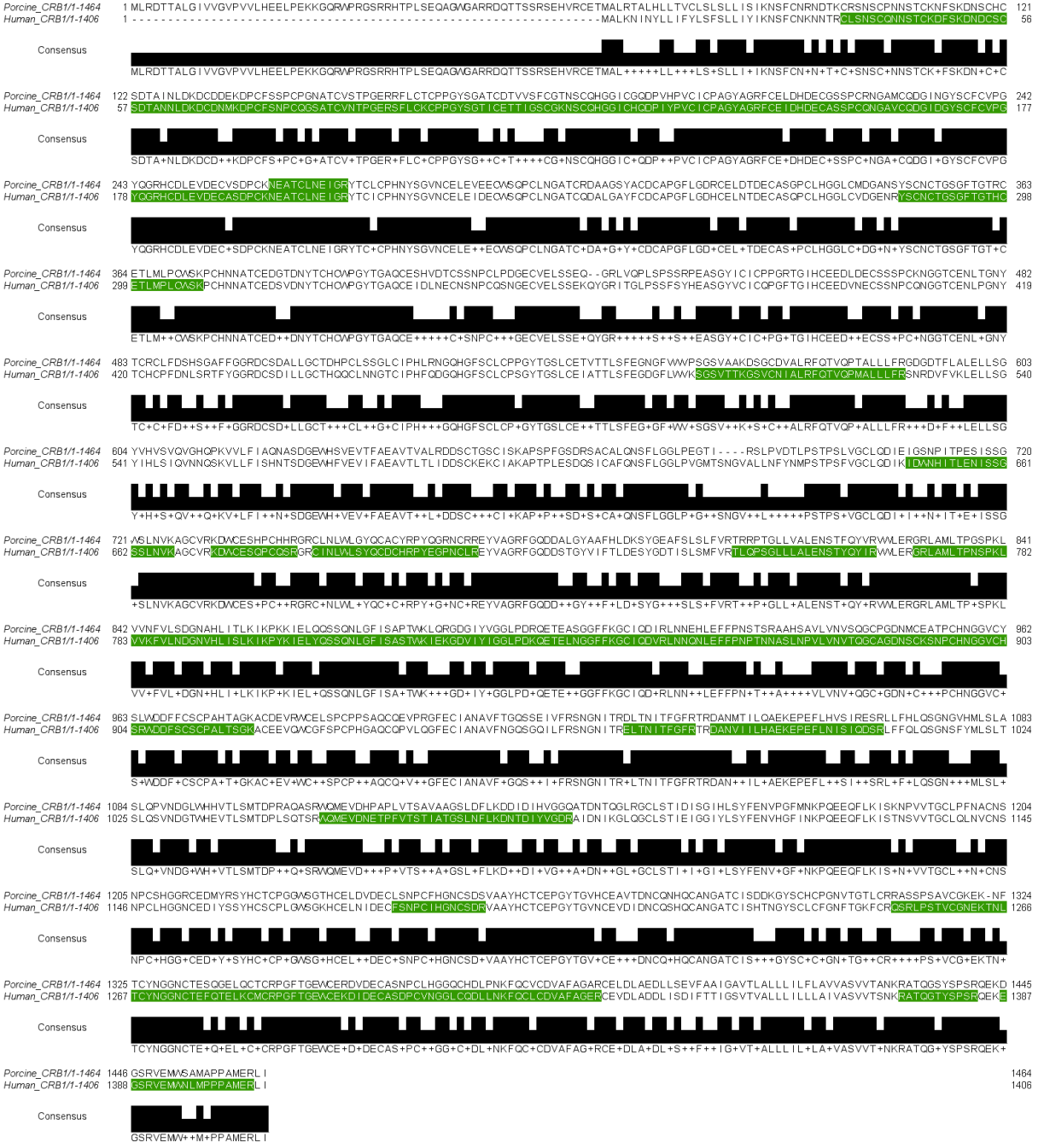

Appendix 7 Overview of the significant enriched proteins in CRB1-FLAG samples compared to GFP-FLAG upon incubation with porcine retina lysate together with the log_2 ratio and the $-log_2$ p-value (One-sample t-test, FDR 0.05, log_2 ratio (CRB1-FLAG/GFP-FLAG) >2, n=6)

Gene	Log_2 ratio (CRB1/ GFP)	$-log_2$ p-value	Gene	Log_2 ratio (CRB1/ GFP)	$-log_2$ p-value	Gene	Log_2 ratio (CRB1/GFP)	$-log_2$ p-value
CRB1	30.14	17.76	**AP3M1**	22.74	3.57	**MRPL39**	3.92	2.01
RIOK1	26.32	4.25	**PRKCB**	22.72	3.57	**TAB1**	3.81	6.45
DAZAP1	26.27	3.94	**GPATCH11**	22.72	2.30	**ABLIM1**	3.79	4.97
ATP5F1E	26.04	16.79	**MYO1C**	22.72	16.29	**GID8**	3.78	1.96
RPL8	25.76	2.48	**RSBN1**	22.71	15.57	**ZSCAN26**	3.75	1.64
MPDZ	25.75	3.42	**AGPAT1**	22.69	3.58	**CTBP2**	3.72	4.42
MRPL15	25.58	19.74	**KPNA4**	22.68	2.29	**ROCK1**	3.66	1.61
SF3B4	25.58	19.58	**SLC30A9**	22.68	2.56	**FGB**	3.65	5.32
NUMA1	25.49	2.30	**SBF2**	22.67	16.45	**SF3B1**	3.60	6.97
OBI1	25.40	23.32	**RANBP9**	22.67	2.52	**ERH**	3.56	8.26
MRPL3	25.35	17.60	**AGAP3**	22.65	2.30	**VWA8**	3.56	5.11
MRPL46	25.35	20.78	**GNAI1**	22.63	2.32	**DBN1**	3.54	5.07
MRPL27	25.34	4.03	**COPS6**	22.62	2.29	**TMOD2**	3.48	8.00
MRPL37	25.34	4.01	**MBD2**	22.60	15.71	**SPINDOC**	3.43	5.99
IVNS1ABP	25.14	18.22	**RAP1B**	22.60	2.02	**PSMB1**	3.39	1.80
RPS29	25.12	2.30	**RANBP10**	22.57	18.60	**MOB2**	3.36	6.57
MRPL45	25.08	3.85	**DIRAS2**	22.56	2.08	**CLGN**	3.31	5.79
MRPL32	24.89	20.97	**PPP1CC**	22.55	2.29	**FGA**	3.31	5.80
DCTN3	24.86	16.43	**MTHFD1L**	22.53	2.45	**MTMR14**	3.31	7.62
MRPL2	24.82	3.57	**ANK3**	22.53	3.68	**SNRPD1**	3.31	6.12
CHERP	24.79	17.32	**TXNDC12**	22.52	2.34	**FGG**	3.30	5.55
MRPL1	24.79	3.90	**GOLGA2**	22.51	2.47	**HNRNPC**	3.30	1.67
MRPL17	24.77	2.77	**OPN1SW**	22.49	2.30	**STK38L**	3.29	7.08
OTUD4	24.61	16.45	**DZANK1**	22.48	16.34	**ERMN**	3.27	5.82
NDUFB11	24.60	15.59	**RSL1D1**	22.48	2.40	**CAMK2G**	3.23	1.74
FLII	24.55	2.54	**ARHGEF10L**	22.48	2.30	**SART1**	3.22	1.89
MRPL20	24.51	3.47	**PYM1**	22.46	2.29	**MTRES1**	3.22	1.87
MRPL16	24.46	2.70	**SMARCD1**	22.46	3.57	**ROGDI**	3.21	1.87
RBM6	24.38	13.81	**TRAPPC9**	22.41	2.05	**SNRPB2**	3.20	1.83
TET2	24.36	4.28	**SEC31A**	22.41	2.22	**IQSEC3**	3.19	1.86
FBXO44	24.34	3.73	**PDCL**	22.37	14.80	**PRPF31**	3.16	6.68
PSMA2	24.23	3.65	**TXNDC9**	22.36	15.91	**AP3B2**	3.15	7.71
PTS	24.19	17.37	**GUCY1A1**	22.35	14.15	**PLEC**	3.12	6.71
TAB3	24.18	4.34	**APLP2**	22.34	2.09	**EIF3E**	3.08	1.81
SRRM2	24.10	3.58	**UBXN1**	22.33	2.29	**CCAR1**	3.07	5.50
MRPL38	24.09	4.06	**TIMM10**	22.33	2.29	**ARPC1A**	3.05	4.88
ZRANB2	24.06	3.91	**TXNDC5**	22.32	20.07	**SNRPG**	3.03	1.90
ATG13	24.05	2.88	**CAMK4**	22.32	15.73	**PCLO**	2.98	6.65
MORC3	24.00	4.53	**KCNAB1**	22.31	14.75	**RPL36A**	2.97	1.83
EIF3H	24.00	2.44	**MPP7**	22.31	3.67	**JAK2**	2.93	6.84
PLD3	23.99	2.45	**TAF4B**	22.31	3.57	**SPIN1**	2.91	7.39
HOMER1	23.98	17.45	**PPP6R3**	22.29	15.29	**TNRC6B**	2.90	5.38
HDX	23.96	3.57	**MAP7D1**	22.29	15.40	**SF3B2**	2.87	5.65
SYBU	23.94	4.20	**OTX2**	22.28	2.29	**SPART**	2.86	7.40
ARHGEF10	23.92	15.27	**EPB41L5**	22.27	2.47	**GSN**	2.85	5.77
IPO8	23.89	17.06	**SRCIN1**	22.27	15.67	**AP3S2**	2.84	1.80
RBM5	23.83	16.08	**PFDN1**	22.26	2.29	**MYO5A**	2.83	5.06
MRPL48	23.82	3.97	**ZNF768**	22.26	2.30	**SNRPD2**	2.82	6.85
FARP1	23.81	15.67	**TOP1**	22.25	2.29	**MRPL24**	2.81	1.53
YBX3	23.81	3.57	**THOC6**	22.24	3.57	**SF3B6**	2.78	8.47
PBRM1	23.80	14.60	**PPFIA3**	22.23	2.30	**CANX**	2.78	5.54
PDCD6	23.76	15.99	**BCAP29**	22.22	3.63	**PSMA5**	2.77	1.82
MRPL40	23.75	3.57	**DKC1**	22.20	3.69	**PSMB2**	2.70	1.82
MTMR1	23.73	2.60	**ACIN1**	22.19	15.77	**MYO6**	2.70	4.50

ACOT9	23.72	2.70	**CPSF4**	22.19	2.30	**MRPL12**	2.65	8.76
ACAP2	23.72	15.97	**RCL1**	22.18	3.57	**IQSEC1**	2.63	1.72
PSMB7	23.69	3.57	**MGA**	22.16	16.55	**PSMB4**	2.62	1.81
SLC8A1	23.68	17.30	**DOCK6**	22.15	18.03	**RPS7**	2.59	1.79
CYB5B	23.68	2.40	**PYCR1**	22.15	16.49	**TJP2**	2.57	1.81
GLYR1	23.67	2.87	**ZFR**	22.10	3.57	**SV2B**	2.57	6.58
MRPL14	23.65	2.19	**PATJ**	22.09	12.09	**EPB41**	2.56	5.04
POGLUT3	23.65	2.84	**PRPF4**	22.05	3.49	**WDR17**	2.55	1.78
LIN7A	23.63	15.64	**CSNK2A2**	22.04	2.30	**SPTB**	2.52	3.36
ACTR10	23.63	2.43	**MTA3**	22.00	15.71	**CPSF6**	2.50	6.25
L3MBTL1	23.60	3.65	**BRCC3**	21.99	3.57	**SF3B3**	2.50	6.55
ATG101	23.55	15.59	**PDLIM5**	21.99	2.32	**PI4KA**	2.47	4.42
ARHGAP21	23.54	15.50	**BMS1**	21.91	15.93	**WDR7**	2.44	4.11
HOMER2	23.53	16.94	**GRIP1**	21.89	16.98	**SPTBN2**	2.44	6.00
CAPNS1	23.52	3.75	**THOC2**	21.80	3.57	**PGAM5**	2.42	5.62
COPS5	23.51	2.43	**PLA2G6**	21.77	2.08	**CLASP1**	2.41	3.63
KIAA0513	23.51	2.38	**TFR2**	21.76	2.30	**EEF1E1**	2.40	1.77
SBF1	23.44	4.50	**GATAD2B**	21.69	2.29	**GABRB3**	2.36	1.78
DNAJC3	23.43	16.77	**SEC16A**	21.67	2.02	**MPI**	2.36	1.64
CHTOP	23.43	2.30	**KIF3A**	21.67	2.30	**PRPSAP1**	2.36	3.62
TBCA	23.36	15.37	**MRPS21**	21.61	2.29	**STK38**	2.34	6.87
CISD3	23.35	20.45	**IK**	21.58	2.10	**RAB3GAP1**	2.33	1.73
POGLUT1	23.35	3.57	**PRDM11**	21.54	2.30	**SRRT**	2.32	3.33
TTC7B	23.34	15.57	**ZNFX1**	21.48	2.29	**SFRP2**	2.27	3.34
TARDBP	23.32	3.58	**PTDSS1**	21.44	2.48	**NOP56**	2.26	6.05
MOGS	23.32	2.35	**SUN2**	21.44	2.29	**EFR3A**	2.26	4.36
MVP	23.24	2.78	**CAMSAP3**	21.42	3.57	**FHL1**	2.25	1.72
PPID	23.20	2.05	**DNAJC12**	21.38	2.30	**TRAPPC4**	2.24	1.71
SMNDC1	23.17	2.52	**LOC100526148**	21.32	2.30	**AIMP2**	2.24	1.70
LSM8	23.16	2.46	**PRPF40A**	21.07	2.29	**PRPF8**	2.24	4.70
GABARAPL2	23.13	15.61	**MPP5**	9.92	9.30	**CORO1C**	2.23	4.75
LRRFIP2	23.12	18.04	**BSN**	7.32	2.51	**PIP5K1A**	2.22	4.82
ERGIC1	23.10	2.35	**BCLAF1**	7.01	8.93	**TPPP**	2.17	1.74
GMFG	23.06	3.56	**RBM17**	6.94	2.25	**SNRPD3**	2.15	3.23
PFKFB3	23.06	4.09	**MAP3K7**	6.40	1.98	**EIF3A**	2.15	3.58
TOMM22	23.06	2.27	**DNAJC13**	6.26	2.15	**NADK2**	2.15	1.75
WTAP	23.05	18.63	**CLNS1A**	6.18	2.23	**RPS20**	2.12	4.08
SLC6A4	23.04	2.16	**THRAP3**	5.83	10.85	**CAMK2B**	2.11	3.08
EIF2AK3	23.03	3.57	**PHF5A**	5.42	2.15	**SPTAN1**	2.11	5.23
RBM8A	23.02	13.59	**RBM10**	5.33	7.00	**MAP1B**	2.10	5.16
FKBP10	23.00	16.25	**EIF4B**	5.14	6.78	**OPLAH**	2.09	5.74
POLDIP3	22.99	2.44	**RB1CC1**	5.12	4.61	**ARPC3**	2.08	4.11
ARPC5L	22.93	3.56	**SLAIN2**	5.08	2.01	**TOR1AIP2**	2.07	5.05
ERC2	22.92	16.35	**U2SURP**	4.97	7.86	**EIF3S8**	2.07	3.03
AMH	22.92	3.72	**CORO2B**	4.91	6.28	**VARS1**	2.06	4.36
LTBP1	22.91	18.41	**LIN7C**	4.90	5.23	**EEF1D**	2.06	4.08
PSMD10	22.88	3.66	**CCDC88A**	4.89	1.89	**THEM6**	2.05	6.36
WDR37	22.86	16.85	**WDR77**	4.86	7.85	**CDC5L**	2.05	4.56
SRRM1	22.85	2.39	**UTP6**	4.69	1.83	**PDZD8**	2.04	1.73
ARHGAP32	22.84	15.50	**RPS15 RIG**	4.66	1.98	**STRN**	2.03	1.67
TBL1XR1	22.84	3.51	**FBL**	4.66	1.62	**PSMC1**	2.01	4.43
E2F8	22.84	18.40	**SELENOF**	4.63	1.74	**DHX16**	2.01	5.94
SUMO1	22.84	3.57	**WDR26**	4.61	2.07			
GABRA3	22.83	3.74	**MRPL47**	4.54	2.08			
PRPF6	22.83	3.57	**LSM14A**	4.51	7.08			
SNRNP40	22.82	2.41	**TMOD3**	4.43	6.59			
KIAA1217	22.81	15.66	**UBC**	4.41	1.98			
TERF2	22.81	3.56	**NT5C2**	4.36	5.71			
ZNF385A	22.81	2.26	**ANKFY1**	4.36	6.90			
DHX38	22.80	2.30	**UGGT2**	4.36	5.84			
NGLY1	22.80	17.74	**SLC4A1AP**	4.25	2.02			

CIAO1	22.79	2.29	**OGT**	4.23	6.69
HGS	22.79	14.44	**MRPL22**	4.09	2.02
TRAPPC10	22.77	2.10	**SPIN3**	3.93	2.00

Appendix 8| CRB1 WT and C948Y are not equally abundant using the C-term FLAG tag Scatter plot of the log_2 ratio of C-term FLAG tagged CRB1 WT and C948Y mutant. Each dot depicts a protein. Bait is depicted in orange. N=6

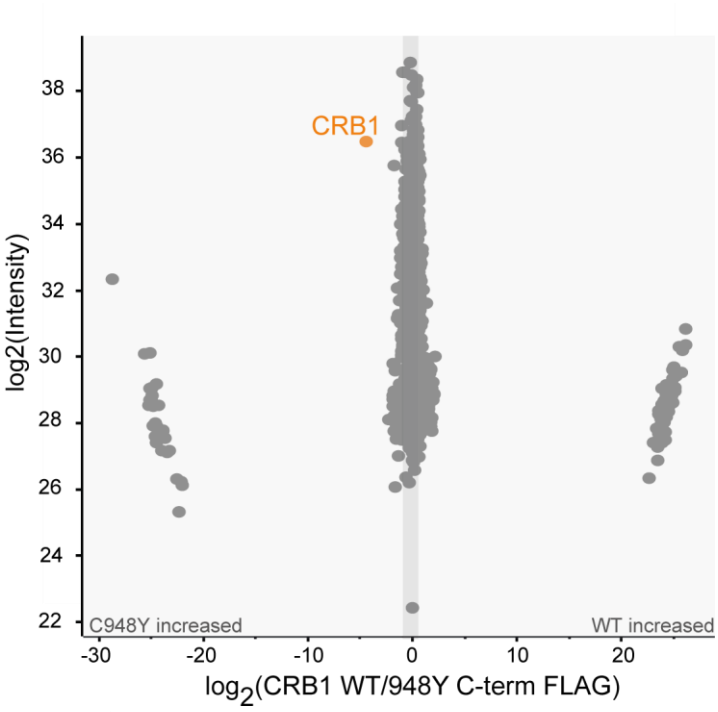

Appendix 9| Overview of the proteins that were identified as significant enriched using only the N-term or C-term CRB1-FLAG construct compared to GFP without incubation of porcine retina lysate. Gene names are depicted together with the Log_2 ratio and the $-log_2$ p-value N=6; n.a.= not available. One-sample t-test, FDR 0.05, log_2 ratio (CRB1-FLAG/GFP-FLAG) >2, n=6)

N-term FLAG specific	Log_2 ratio (N-term CRB1 /GFP)	$-log_2$ p-value (N term CRB1 vs GFP)	Log_2 ratio (C-term CRB1 /GFP)	$-log_2$ p-value (C-term CRB1 vs GFP)	C term FLAG specific	Log_2 ratio (C-term CRB1 /GFP)	$-log_2$ p-value (C term CRB1 vs GFP)	Log_2 ratio (C-term CRB1 /GFP)	$-log_2$ p-value (C term CRB1 vs GFP)
CAMSAP3	21.57	3.56	n.a	n.a	**ACIN1**	n.a	n.a	19.99	2.30
CANX	2.60	4.33	0.18	0.65	**AMOTL1**	n.a	n.a	19.46	2.30
CBX4	20.64	2.30	n.a	n.a	**ARMC8**	n.a	n.a	19.45	2.29
CKAP5	19.34	2.07	n.a	n.a	**ARRB1**	n.a	n.a	24.06	2.29
CLASP1	20.46	2.21	n.a	n.a	**BMS1**	n.a	n.a	20.48	2.30
CSRP2	20.89	2.06	n.a	n.a	**CHCHD3**	22.38	1.34	21.61	2.00
DDX6	20.63	2.29	n.a	n.a	**CYB5B**	n.a	n.a	20.23	2.29
DNAJB11	2.08	5.58	-1.13	0.00	**DSC1**	n.a	n.a	20.16	2.29
DNAJC3	21.66	3.56	n.a	n.a	**LOC100516036**	n.a	n.a	19.61	2.37
EIF3A	2.68	1.88	1.82	1.73	**LSM11**	n.a	n.a	19.59	2.29
FHL1	21.82	2.42	n.a	n.a	**LSM14A**	n.a	n.a	19.70	3.57
FKBP10	21.98	15.76	n.a	n.a	**MRPL11**	22.22	1.47	22.00	2.24
GLG1	20.79	3.57	n.a	n.a	**MRPL24**	23.62	1.53	23.70	2.66
GMFG	20.94	2.29	n.a	n.a	**MRPL4**	n.a	n.a	23.17	2.29
KEAP1	19.91	2.30	n.a	n.a	**MRPL42**	n.a	n.a	21.13	2.30
LOC100626015	21.86	19.70	n.a	n.a	**MYH4**	n.a	n.a	20.19	2.03
MAGT1	22.96	16.45	n.a	n.a	**ODR4**	n.a	n.a	21.28	22.84
MPDZ	24.27	10.92	n.a	n.a	**PFKFB3**	n.a	n.a	20.47	17.16
MPP5	27.39	3.94	n.a	n.a	**PRPF8**	n.a	n.a	17.12	2.16
MRPL1	3.07	1.91	2.76	1.84	**RBM17**	n.a	n.a	17.86	3.54
MRPL37	24.23	2.29	n.a	n.a	**RBMX**	22.12	1.47	22.29	2.55
MRPL55	22.44	2.29	n.a	n.a	**SF3B4**	n.a	n.a	21.51	2.29
MYO1C	20.36	2.30	n.a	n.a	**SNRNP200**	n.a	n.a	17.04	2.28
NGLY1	21.61	3.57	n.a	n.a	**SUMO4**	23.07	1.25	22.87	2.06
PAFAH1B3	21.71	2.27	21.39	1.33	**TAB3**	n.a	n.a	21.15	2.29
PATJ	21.76	3.51	n.a	n.a					
PHKB	20.88	3.57	n.a	n.a					
PPHLN1	21.96	3.55	n.a	n.a					
PSMA1	2.49	4.92	-0.95	0.07					
PSMA2	23.39	18.50	n.a	n.a					
PSMA4	2.18	6.44	0.06	0.70					
PSMB3	2.04	4.58	-2.57	0.01					
PSMC1	2.17	4.98	-4.56	0.01					
PSMC2	2.33	5.59	-3.57	0.01					
PSMC3	2.44	5.16	-2.32	0.04					
PSMC4	2.36	4.38	-1.89	0.04					
PSMC5	2.11	4.39	-2.22	0.00					
PSMC6	2.27	5.56	-2.95	0.01					
PSMD1	2.43	4.66	-2.15	0.02					
PSMD2	2.38	5.51	-2.34	0.03					
PSMD8	22.40	2.29	n.a	n.a					
PTMA	24.91	2.29	-1.01	0.26					
RCL1	20.18	2.29	n.a	n.a					
SDF2	21.65	3.70	n.a	n.a					
SDF2L1	21.63	2.29	n.a	n.a					
SLC30A9	20.93	3.57	n.a	n.a					
SLITRK6	21.25	16.36	n.a	n.a					
SNRPE	22.21	2.29	n.a	n.a					
SRPRB	22.76	3.57	n.a	n.a					
SUMF2	20.54	2.30	n.a	n.a					
TECR	23.06	2.11	n.a	n.a					
TXNDC5	20.98	3.57	n.a	n.a					
UBE2L3	20.52	2.29	n.a	n.a					
UGGT2	8.71	2.76	3.35	1.72					
ZNF768	21.10	3.55	n.a	n.a					

Appendix 10 CRB1 interactors that were specifically detected with the N-term or C-term tagged construct compared to GFP upon incubation with porcine retina lysate. Table depicts the gene name along with the Log_2 ratio and the $-log_2$ p-value. N=6, n.a. not available, one-sample t-test, FDR 0.05, log_2 ratio (CRB1-FLAG/GFP-FLAG) >2, n=6)

N-term FLAG specific	Log_2 ratio (N-term CRB1 /GFP)	$-log_2$ p-value (N term CRB1 vs GFP)	Log_2 ratio (C-term CRB1 /GFP)	$-log_2$ p-value (C term CRB1 vs GFP)	C-term FLAG specific	Log_2 ratio (N-term CRB1 /GFP)	$-log_2$ p-value (N term CRB1 vs GFP)	Log_2 ratio (C-term CRB1 /GFP)	$-log_2$ p-value (C term CRB1 vs GFP)
AGAP3	22.65	2.30	n.a	n.a	**ARID1A**	n.a	n.a	21.95	3.57
AGPAT1	22.69	3.58	n.a	n.a	**ATP1A3**	n.a	n.a	25.30	2.29
AP3S2	2.84	1.80	2.49	0.58	**CLIP2**	n.a	n.a	21.48	3.57
ARHGEF10L	22.48	2.30	n.a	n.a	**CNOT1**	24.77	0.86	25.10	2.35
ARPC5L	22.93	3.56	n.a	n.a	**DDX19B**	2.26	0.93	2.07	1.68
CAMK2B	2.11	3.08	1.81	3.68	**DENR**	21.50	1.34	21.72	2.05
CAMSAP3	21.42	3.57	n.a	n.a	**DKK3**	n.a	n.a	22.29	2.29
CANX	2.78	5.54	1.01	2.45	**EIF5**	n.a	n.a	22.11	3.57
CIAO1	22.79	2.29	n.a	n.a	**FAU**	1.62	0.93	2.52	1.75
CISD3	23.35	20.45	n.a	n.a	**FYCO1**	24.51	1.39	24.40	2.39
CLASP1	2.41	3.63	1.78	2.77	**GIT1**	n.a	n.a	22.14	2.29
CLGN	3.31	5.79	1.25	2.56	**GRIA4**	n.a	n.a	23.49	2.29
CPSF4	22.19	2.30	n.a	n.a	**HP1BP3**	1.87	4.88	2.09	4.96
DNAJC3	23.43	16.77	n.a	n.a	**IGF2BP2**	n.a	n.a	21.99	2.29
EEF1D	2.06	4.08	1.88	4.39	**LARP1**	n.a	n.a	22.58	2.07
EEF1E1	2.40	1.77	2.32	0.97	**MAEA**	n.a	n.a	21.95	2.29
FBL	4.66	1.62	4.36	1.55	**MAPK8IP3**	n.a	n.a	21.67	2.29
FHL1	2.25	1.72	n.a	n.a	**MARK2**	n.a	n.a	21.97	3.57
FKBP10	23.00	16.25	n.a	n.a	**MRPL43**	24.93	1.43	25.31	2.22
GATAD2B	21.69	2.29	n.a	n.a	**MRPL44**	n.a	n.a	24.39	2.22
GMFG	23.06	3.56	n.a	n.a	**MRPS17**	n.a	n.a	22.27	2.46
GNAI1	22.63	2.32	22.19	0.86	**MYO5B**	n.a	n.a	21.65	2.30
GOLGA2	22.51	2.47	21.78	0.88	**NFS1**	22.43	1.30	22.75	3.45
IK	21.58	2.10	n.a	n.a	**NOL4**	n.a	n.a	22.17	2.30
KPNA4	22.68	2.29	n.a	n.a	**OLA1**	n.a	n.a	22.14	2.29
LOC100526148	21.32	2.30	n.a	n.a	**PPHLN1**	n.a	n.a	23.19	2.29
LOC110260088	2.07	3.03	n.a	n.a	**RAPGEF4**	n.a	n.a	22.54	3.57
MAP1B	2.10	5.16	1.89	5.65	**RPS19**	1.99	4.55	2.08	4.97
MOGS	23.32	2.35	22.39	0.83	**RRBP1**	n.a	n.a	21.78	2.29
MPI	2.36	1.64	1.79	0.90	**SCRN3**	n.a	n.a	25.24	2.30
MPP5	9.92	9.30	0.89	0.42	**SMARCA4**	n.a	n.a	20.96	3.57
MRPL14	23.65	2.19	23.26	1.42	**SRGAP3**	n.a	n.a	23.11	2.29
MRPL24	2.81	1.53	2.66	1.53	**SYT12**	22.58	1.42	22.77	3.92
MRPL40	23.75	3.57	n.a	n.a	**TFAM**	23.40	0.87	23.85	2.36
MRPL45	25.08	3.85	24.82	1.40	**THOC1**	n.a	n.a	22.20	3.57
MRPS21	21.61	2.29	n.a	n.a	**TPD52L1**	n.a	n.a	22.98	18.59
NADK2	2.15	1.75	1.90	1.71	**U2AF1**	2.59	0.96	2.41	1.73
NGLY1	22.80	17.74	n.a	n.a	**USP39**	21.91	1.37	21.81	2.10
OPN1SW	22.49	2.30	n.a	n.a	**VCPIP1**	n.a	n.a	21.78	2.29
OTX2	22.28	2.29	n.a	n.a	**WDR33**	21.48	1.41	21.39	2.18
PATJ	22.09	12.09	n.a	n.a					
PDLIM5	21.99	2.32	21.39	1.34					
PDZD8	2.04	1.73	1.56	1.68					
PFDN1	22.26	2.29	n.a	n.a					
POGLUT1	23.35	3.57	n.a	n.a					
PPP1CC	22.55	2.29	n.a	n.a					
PRPF4	22.05	3.49	21.75	1.32					
PRPF40A	21.07	2.29	n.a	n.a					
PSMA2	24.23	3.65	23.28	1.32					
PSMA5	2.77	1.82	1.83	0.94					
PSMB1	3.39	1.80	2.44	1.63					
PSMB2	2.70	1.82	1.29	0.54					
PSMB4	2.62	1.81	1.64	0.93					
PSMB7	23.69	3.57	n.a	n.a					
PSMC1	2.01	4.43	0.90	2.93					
PSMD10	22.88	3.66	22.41	1.36					
PTDSS1	21.44	2.48	20.12	0.86					
RAP1B	22.60	2.02	n.a	n.a					

ROCK1	3.66	1.61	3.55	1.59
RPS29	25.12	2.30	n.a	n.a
SEC16A	21.67	2.02	21.56	1.33
SELENOF	4.63	1.74	n.a	n.a
SLC30A9	22.68	2.56	n.a	n.a
SLC6A4	23.04	2.16	22.96	1.41
SNRNP40	22.82	2.41	22.63	1.39
SNRPG	3.03	1.90	2.92	1.02
SPTAN1	2.11	5.23	1.99	5.82
STRN	2.03	1.67	1.16	0.53
SUMO1	22.84	3.57	n.a	n.a
TBCA	23.36	15.37	n.a	n.a
TBL1XR1	22.84	3.51	21.73	1.32
TIMM10	22.33	2.29	n.a	n.a
TOMM22	23.06	2.27	n.a	n.a
TRAPPC4	2.24	1.71	1.85	0.93
TXNDC12	22.52	2.34	21.92	1.35
UBC	4.41	1.98	2.78	0.96
UBXN1	22.33	2.29	n.a	n.a
UGGT2	4.36	5.84	1.53	2.65
ZNF768	22.26	2.30	n.a	n.a
ZNFX1	21.48	2.29	n.a	n.a
ZSCAN26	3.75	1.64	3.69	1.63

Appendix 11| Coverage of C-term FLAG-tagged CRB1 is lower compared to N-term FLAG-tagged
Unique exclusive peptides for human CRB1 (C-term FLAG) were identified using Scaffold. Amino acids equal to the MS/MS spectra are depicted in yellow. Green residues have a post-translational modification. Coverage 17 %

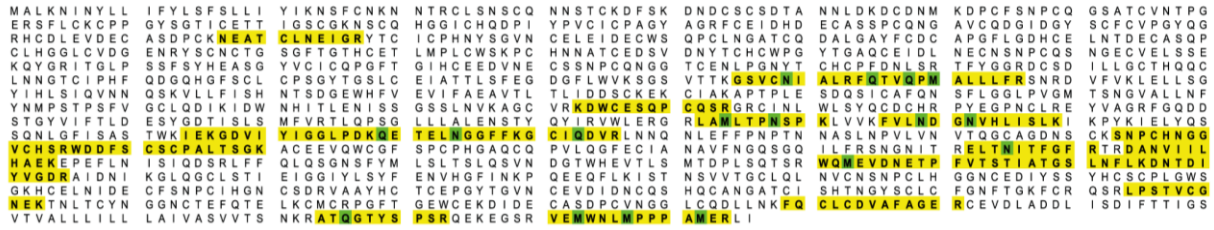

Appendix 12| Specific peptide coverage of CRB1-FLAG WT and C948Y Unique exclusive peptides for human CRB1 WT were identified using Scaffold for **(A)** CRB1 WT samples and **(B)** CRB1 C948Y samples. Amino acids equal to the MS/MS spectra are depicted in yellow. Green residues have a post-translational modification. Red circle marks the mutated residue. Coverage 19 %

A **CRB1 WT**

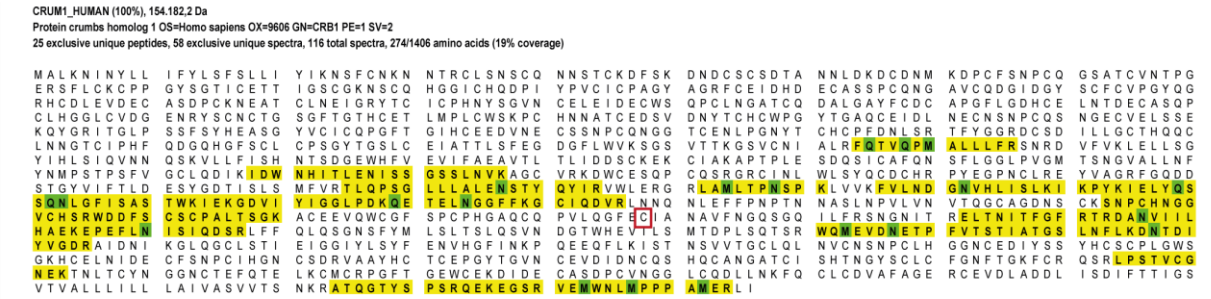

B **CRB1 C948Y**

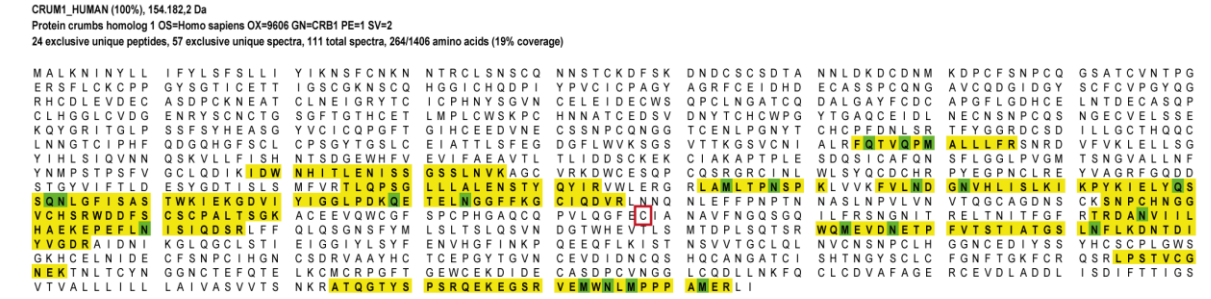

Appendix 13 Specific peptide coverage of CRB1-extracellular FLAG Unique exclusive peptides for CRB1 extracellular FLAG samples were identified using Scaffold against the canonical CRB1 protein. Amino acids equal to the MS/MS spectra are depicted in yellow. Green residues have a post-translational modification. Start of the transmembrane and canonical intracellular domain is marked in grey. Coverage 16 %

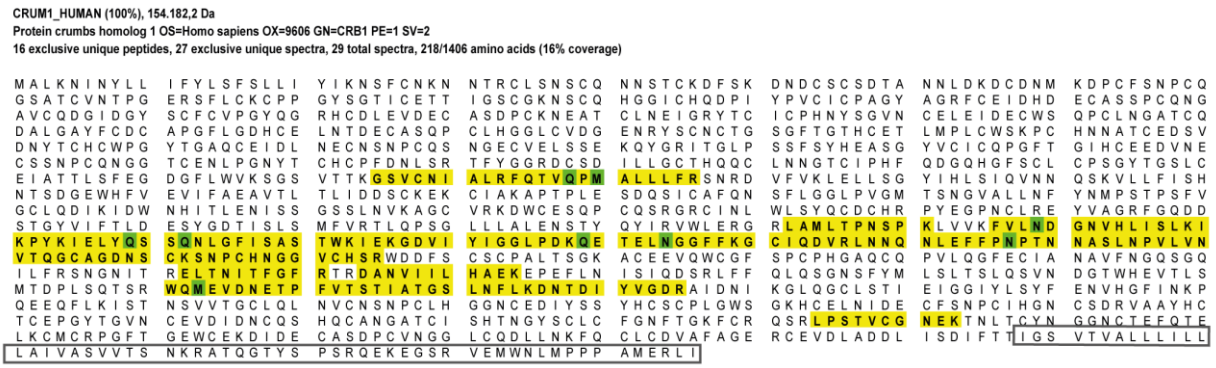

Appendix 14| Overview of the significant enriched proteins in CRB1-extracellular samples compared to GFP without incubation of porcine retina lysate Gene name are depicted together with the log_2 ratio CRB1/GFP and the –log p-value. One-sample t-test, FDR 0.05, log_2 ratio (CRB1-FLAG/GFP-FLAG) >2, n=6

Gene Name	Log_2 ratio (CRB1 extracellular /GFP)	$-log_2$ p-value	Gene Name	Log_2 ratio (CRB1 extracellular /GFP)	$-log_2$ p-value	Gene Name	Log_2 ratio (CRB1 extracellular /GFP)	$-log_2$ p-value	Gene Name	Log_2 ratio (CRB1 extracellular /GFP)	$-log_2$ p-value
CLNS1A	29.95	4.58	**CFL2**	23.10	2.06	**ROCK1**	22.13	3.57	**KEAP1**	20.85	3.57
RBM10	29.10	10.80	**ACAP2**	23.09	3.56	**RPS18**	22.12	1.41	**CAP1**	20.69	1.49
CRB1	29.08	10.44	**GID8**	23.05	3.57	**ILF2**	22.12	1.40	**IGF2BP3**	20.68	3.57
SNRPD3	27.41	9.90	**C17H20orf27**	22.94	3.57	**ARPC1B**	22.10	3.57	**PCNP**	20.63	3.57
SNRPD2	27.33	10.13	**PABPN1**	22.93	3.56	**YPEL5**	22.09	3.57	**CSRP2**	20.60	2.28
RIOK1	27.28	10.15	**E2F7**	22.92	3.57	**DDX5**	22.08	3.57	**TWF1**	20.56	2.30
STK38L	27.23	5.42	**ARPC2**	22.92	3.56	**PFDN1**	22.08	3.57	**TMEM268**	20.56	2.29
SNRPN	27.07	9.42	**PHKB**	22.92	3.57	**CDC37**	22.06	3.56	**PRPF8**	20.50	1.35
IPO8	26.83	3.57	**HDX**	22.90	3.57	**RBM17**	22.05	3.55	**GAR1**	20.48	2.29
BCLAF1	26.82	9.63	**ALYREF**	22.89	2.01	**ARMC8**	22.04	3.57	**PGD**	20.41	2.29
TET2	26.13	8.97	**RPL10**	22.88	3.57	**CCDC88C**	22.02	3.57	**PKP1**	20.33	1.74
OBI1	26.08	10.19	**TMOD3**	22.87	2.54	**SELENOF**	21.98	2.29	**GLYR1**	20.32	2.29
THRAP3	25.63	8.92	**PFKFB1**	22.86	3.57	**FABP7**	21.95	1.35	**EFTUD2**	20.29	1.58
OTUD4	25.42	7.83	**ARPC5L**	22.84	2.29	**U2SURP**	21.94	3.54	**HNRNPH3**	20.27	2.29
MOB2	25.41	11.51	**SLC4A1AP**	22.81	2.30	**WDR5**	21.91	3.57	**EIF3A**	20.24	2.06
OGT	25.28	9.35	**CLASP1**	22.80	3.56	**ARPC5**	21.91	2.29	**HDGF**	20.22	2.29
PTS	25.12	3.57	**LSM11**	22.76	3.57	**DSC1**	21.90	1.84	**MYH7B**	20.19	2.17
RRAGC	25.00	3.47	**RBM8A**	22.75	3.57	**PPP1R10**	21.90	3.57	**MATR3**	20.13	2.05
SNRPF	24.86	2.14	**ODR4**	22.74	3.57	**RANBP10**	21.90	3.56	**CCAR1**	20.05	3.53
RPS27	24.75	9.95	**MYL6**	22.71	1.37	**PSMA1**	21.87	1.36	**ANKFY1**	20.01	3.55
MRPL49	24.47	2.30	**SATB2**	22.65	3.57	**CCDC88A**	21.86	3.57	**CADM1**	19.90	1.36
ARPC4	24.47	3.91	**TAF4**	22.64	3.57	**SPTBN2**	21.83	2.30	**RBM6**	19.90	3.54
RPL23A	24.33	2.00	**SF3B6**	22.63	3.56	**CHERP**	21.77	3.55	**MYH14**	19.88	2.17
EIF4A3 DDX48	24.22	2.22	**GNGT1**	22.61	2.29	**CDC5L**	21.77	3.56	**LSM14A**	19.80	2.29
IVNS1ABP	24.16	3.57	**CAPZA1**	22.60	2.07	**SARNP**	21.68	3.56	**FIP1L1**	19.78	2.29
PROSER1	24.09	10.39	**DDX42**	22.60	2.22	**ACIN1**	21.59	3.57	**SNRNP200**	19.73	3.55
PRPF19	24.00	2.31	**TAB2**	22.48	2.29	**HYOU1**	21.58	3.55	**DDAH2**	19.54	2.29
LTBP1	23.91	8.68	**ARPC3**	22.47	2.14	**FUBP3**	21.58	2.04	**FBL**	19.43	2.30
SNRPE	23.85	2.30	**PRKCSH**	22.47	3.52	**ATP11C**	21.51	3.57	**PPM1A**	19.42	3.56
MRPL12	23.85	3.57	**MTPN**	22.43	1.34	**PNN**	21.50	3.57	**TMOD2**	19.23	2.30
SPIN3	23.83	3.57	**SF3B4**	22.43	3.56	**PRPF31**	21.45	3.56	**DDX1**	19.22	1.95
LOC100526148	23.76	3.57	**CRABP1**	22.43	3.57	**NKRF**	21.45	3.57	**DLDLAD**	19.19	2.05
UCHL1	23.76	2.07	**RGR**	22.43	1.93	**DDX39A**	21.44	2.29	**JAK2**	18.98	3.56
RPL14	23.74	2.22	**PDIA4**	22.43	2.25	**SPIN4**	21.42	3.57	**SRRT**	18.60	2.29
CAMSAP3	23.72	3.57	**RPS13**	22.43	1.43	**PRRC2A**	21.41	3.57	**EIF3D EIF3S7**	18.48	2.28
ACTR3	23.69	2.74	**SLITRK6**	22.40	3.57	**EIF3I**	21.38	2.29	**EPB41L3**	18.14	1.62
TAB3	23.69	3.56	**RPS20**	22.34	2.29	**PTMS**	21.37	3.56	**EIF4B**	9.66	2.46
RPS15A	23.64	1.36	**SCYL2**	22.33	3.57	**DDX50**	21.36	1.41	**SNRPD1**	8.64	2.46
MAP3K7	23.56	3.56	**USP15**	22.32	3.57	**MGA**	21.35	3.57	**WDR77**	8.37	5.56
RPS26	23.54	1.38	**RBM5**	22.30	3.57	**RMND5B**	21.34	3.57	**CORO1C**	7.58	2.34
RANBP9	23.54	3.57	**OAT**	22.29	1.35	**XRN2**	21.28	2.04	**ERH**	7.41	2.37
TMSB4	23.47	2.29	**SRRM2**	22.28	3.56	**PPHLN1**	21.22	3.56	**SF3B1**	7.12	1.36

SF3B2	23.44	3.56	**MRPL43**	22.27	2.29	**LUC7L**	21.19	3.54	**PPM1B**	7.08	4.08
RPL31	23.43	2.31	**TNRC6B**	22.26	3.57	**MAEA**	21.17	3.57	**SPIN1**	6.87	2.00
RPL13A	23.39	1.40	**MKLN1**	22.25	3.57	**CBR1**	21.16	2.06	**SPTAN 1**	6.34	2.70
RPL6	23.38	3.57	**CNOT1**	22.25	2.30	**HOMER1**	21.15	3.57	**STK38**	6.10	3.63
RPL15	23.36	3.57	**ARPC1A**	22.24	3.57	**PRPSAP 1**	21.09	3.54	**TAB1**	5.88	2.72
NUDT21	23.27	1.43	**WIZ**	22.24	3.57	**PURA**	21.08	3.56	**GSN**	5.34	1.36
RBMX	23.26	3.57	**HNRNPUL 1**	22.20	3.57	**MRPL47**	21.07	2.29	**PPIL4**	4.63	1.69
SNRPG	23.26	3.57	**SF3A3**	22.20	2.14	**SUCLG1**	21.01	1.32	**HNRNP L**	4.22	2.25
WDR26	23.17	3.57	**HNRNPC**	22.18	3.57	**IGF2BP2**	21.01	3.57	**DDX17**	3.47	1.51
UGGT2	23.16	2.35	**TRA2B**	22.18	2.29	**AMOT**	20.95	3.57	**ACTA1**	2.99	1.55
CPSF6	23.15	2.17	**PHF5A**	22.17	2.29	**STRBP**	20.88	2.14	**FLNA**	2.86	1.37
			MYH11	22.14	2.29	**NGLY1**	20.86	3.57			

Appendix 15| Significant enriched proteins in CRB1 extracellular isoform compared to GFP upon incubation with porcine retina lysate Gene name are shown together with the log_2 ratio CRB1extracellular /GFP and the –log p-value. One-sample t-test, FDR 0.05, log_2 ratio (CRB1 /GFP)>2, n=6

Gene Name	Log_2 ratio (CRB1 extracellular /GFP)	$-log_2$ p-value	Gene Name	Log_2 ratio (CRB1 extracellular /GFP)	$-log_2$ p-value	Gene Name	Log_2 ratio (CRB1 extracellular /GFP)	$-log_2$ p-value	Gene Name	Log_2 ratio (CRB1 extracellular /GFP)	$-log_2$ p-value
CRB1	29.48	21.78	**CPSF2**	24.27	3.57	**NFU1**	23.15	1.98	**RPL23A**	2.93	3.73
CLNS1A	29.47	2.99	**GABRB3**	24.26	3.87	**TMEM91**	23.14	2.30	**RPS9**	2.89	4.24
IPO8	28.87	19.37	**POLDIP3**	24.25	3.94	**MRPL28**	23.13	2.30	**ACTR10**	2.88	1.84
BCLAF1	28.66	4.67	**DOCK7**	24.25	19.39	**SMARCA4**	23.12	3.71	**EIF3A**	2.86	4.46
RPS28	28.37	18.27	**CCDC88A**	24.22	4.40	**ARPC1B**	23.11	2.30	**CAMK2G**	2.81	1.77
RRAGC	27.72	16.35	**PROSER1**	24.21	3.57	**TRIO**	23.09	2.11	**PIP5K1C**	2.81	8.00
OTUD4	27.65	3.05	**CYB5B**	24.20	3.48	**ARFGEF1**	23.06	1.37	**EIF3I**	2.80	4.87
UTP6	27.62	19.68	**PCYOX1**	24.18	2.01	**ASL**	23.04	1.34	**RPL27A**	2.74	1.76
RPL31	27.42	4.12	**EIF4A1**	24.16	2.00	**IGF2BP2**	23.03	3.57	**TOR1AIP2**	2.73	1.47
MOB2	27.37	2.90	**SCCPDH**	24.16	18.09	**ACBD3**	23.01	1.36	**SNRPD3**	2.73	5.06
MTHFD1L	27.36	2.47	**FXR2**	24.16	19.70	**MKLN1**	23.01	2.30	**SRSF1**	2.69	5.03
SRSF3	27.18	3.57	**ANK3**	24.15	18.30	**SRGAP3**	22.99	2.30	**RPS16**	2.68	4.43
NUDT3	27.14	2.56	**PRRC2A**	24.12	4.00	**AGAP3**	22.92	3.57	**WDR7**	2.66	4.89
RPS27	27.10	18.23	**SMU1**	24.11	2.29	**PEX5L**	22.84	1.34	**EPB41L3**	2.66	6.93
U2SURP	27.02	4.75	**GABRA1**	24.09	3.66	**WASHC1**	22.77	3.57	**EIF3S8**	2.63	5.39
MYO7A	27.00	2.30	**UBE2L3**	24.06	2.30	**OGA**	22.70	1.34	**RPS25**	2.63	1.76
FBL	26.94	3.35	**CTNND1**	24.05	2.07	**IGF2BP1**	22.69	2.16	**CDC5L**	2.61	3.57
TAB3	26.93	4.31	**YPEL5**	24.02	3.57	**ABCF2**	22.58	2.30	**VWA8**	2.60	4.57
SH3BGRL2	26.92	3.57	**KPNA4**	24.00	2.05	**DOCK4**	22.53	3.57	**FLNA**	2.59	7.54
CAMK2D	26.90	2.42	**LARP1**	23.99	3.61	**PPP1R2**	22.51	3.57	**DHX16**	2.57	7.09
RIOK1	26.86	18.82	**PRRC2C**	23.97	2.30	**PLCL2**	22.48	2.29	**RPS18**	2.57	3.63
MAP3K7	26.82	4.86	**ACIN1**	23.96	3.94	**RBM42**	22.42	2.29	**EIF3B**	2.57	6.26
THOC2	26.81	2.30	**FXR1**	23.96	3.65	**HTRA1**	22.35	3.57	**DDX42**	2.56	7.32
H1-4	26.73	2.40	**RANBP10**	23.96	17.89	**CAST**	21.81	2.02	**PPIL4**	2.53	5.97
SF3B6	26.71	4.30	**FBXO44**	23.94	18.13	**BSN**	9.98	8.03	**FAM120A**	2.52	3.54
LOC100524873	26.64	3.57	**PDE1C**	23.92	19.38	**EIF4B**	9.10	10.60	**NADK2**	2.51	1.74
SRSF7	26.48	4.03	**MRPS27**	23.91	3.65	**THRAP3**	8.59	2.52	**ROGDI**	2.47	5.15
CRX	26.44	3.57	**MACROH2A1**	23.91	3.73	**RBM10**	8.01	10.63	**CTTN**	2.47	6.21
SUMO4	26.20	3.44	**MAP7D1**	23.90	3.71	**RBM17**	7.50	2.43	**DDX23**	2.45	1.42
TET2	26.17	18.29	**CAPNS1**	23.89	2.28	**ANKFY1**	7.28	8.77	**RPS26**	2.43	1.42
SYBU	26.08	20.08	**JAKMIP1**	23.89	20.10	**WDR77**	7.05	9.54	**EIF3J**	2.43	1.71
OBI1	26.07	21.16	**TERF2**	23.88	18.71	**CHERP**	6.64	2.31	**CHD5**	2.43	4.08
MYO5B	25.97	3.96	**CAMSAP3**	23.86	18.96	**ABLIM1**	6.41	2.02	**SRSF4**	2.43	4.08
ATP5MD	25.83	17.52	**AP3M1**	23.86	1.35	**TMOD2**	6.29	8.87	**RPS7**	2.39	4.06
PFKFB2	25.82	4.06	**RUFY1**	23.86	17.39	**SBF1**	6.28	2.03	**RPS3**	2.38	5.47
IVNS1ABP	25.76	19.55	**TBC1D10B**	23.85	16.98	**STK38L**	6.17	12.37	**EIF3D**	2.37	4.70
MT-CO1	25.76	3.57	**ITSN1**	23.85	1.36	**JAK2**	5.96	8.94	**RPS2**	2.35	4.54
PLEKHB1	25.68	2.47	**PRPF6**	23.84	20.34	**FLII**	5.86	6.66	**RPS15RIG**	2.35	4.65
ZRANB2	25.65	3.87	**MARK2**	23.83	19.76	**USP15**	5.84	11.13	**RANBP9**	2.34	4.93
RAPGEF4	25.60	2.85	**DZANK1**	23.81	2.49	**CORO2B**	5.84	1.87	**CAPZA1**	2.34	1.39

MORC3	25.57	21.24	**CAVIN1**	23.80	1.36	**DBN1**	5.76	1.84	**CCT7**	2.33	5.48
RBMX	25.55	19.85	**PLA2G6**	23.80	1.36	**DNAJC13**	5.65	9.20	**RPS19**	2.32	6.39
ACAP2	25.55	21.80	**SRCIN1**	23.80	20.21	**ERMN**	5.60	8.02	**ARPC1A**	2.28	4.04
MRPL15	25.51	3.88	**RPH3A**	23.79	1.35	**PCLO**	5.46	10.84	**PPM1B**	2.26	6.89
SLAIN2	25.50	4.39	**GRIP1**	23.78	22.21	**FGG**	5.37	8.77	**RPS3A**	2.26	4.71
SEPTIN11	25.44	18.07	**WWP2**	23.78	3.57	**AP3B2**	5.35	8.67	**EIF3L**	2.24	3.77
PABPN1	25.40	3.84	**S100A10**	23.78	1.39	**SART1**	5.32	2.22	**SCYL2**	2.23	6.25
SNRPB2	25.36	2.53	**PSMB7**	23.75	2.32	**ARHGAP32**	5.27	8.10	**RPS23**	2.23	7.34
ZSCAN26	25.29	20.96	**MRPS5**	23.73	2.29	**LSM14A**	5.23	1.90	**CCT5**	2.21	5.00
LTBP1	25.25	11.92	**CAMK4**	23.72	2.15	**PLEC**	5.09	7.05	**RPSA**	2.20	4.26
L3MBTL1	25.24	2.66	**RMND5B**	23.72	20.41	**TMOD3**	5.09	7.66	**PRKCB_tv2**	2.20	4.53
POGLUT3	25.21	3.91	**CCNT2**	23.71	17.65	**TAB1**	5.00	9.67	**DNAJC8**	2.20	1.70
ARPC5L	25.16	3.56	**GRIPAP1**	23.71	2.47	**EFR3A**	4.99	2.11	**CPSF6**	2.19	4.70
PRKAR2A	25.15	2.30	**GATAD2B**	23.71	3.57	**FGB**	4.97	9.16	**RPS20**	2.19	4.82
ATG101	25.12	19.73	**PYM1**	23.69	3.56	**PPFIA2**	4.95	2.15	**HNRNPH2**	2.19	5.68
TFAM	25.09	2.42	**PPIL3**	23.69	1.33	**FGA**	4.91	8.13	**ACTA1**	2.19	5.77
SYT12	25.03	19.69	**GIT2**	23.67	2.12	**FIP1L1**	4.87	2.00	**KIF5B**	2.17	4.27
ARHGEF10	25.02	18.65	**DKC1**	23.67	17.81	**MTMR14**	4.68	4.46	**RBM39**	2.17	5.82
TTC7B	24.96	19.96	**DHX38**	23.67	18.14	**SPTBN2**	4.67	8.04	**CCT3**	2.16	4.19
TRAPPC3	24.96	2.30	**SMARCD1**	23.66	2.30	**ROCK1**	4.63	7.54	**RPS21**	2.16	4.95
MYO1C	24.95	4.53	**VAC14**	23.64	1.36	**CTBP2**	4.56	6.84	**HNRNPUL1**	2.16	3.63
ACOT9	24.92	2.66	**TAF4**	23.63	15.69	**SPIN3**	4.55	2.02	**CPT1A**	2.15	1.67
HNRNPUL2	24.91	2.48	**ARHGEF10L**	23.61	19.43	**WDR26**	4.53	5.86	**MAP1S**	2.14	4.83
TRA2B	24.90	21.03	**RAB3IP**	23.61	1.38	**LIMA1**	4.52	6.76	**TOM1L2**	2.14	4.82
ATG13	24.90	19.21	**UIMC1**	23.60	18.17	**SPIN1**	4.49	9.39	**AP3M2**	2.12	4.70
LRRFIP2	24.89	17.44	**GLMN**	23.60	1.36	**OGT**	4.39	8.47	**ACTR3**	2.12	4.49
MTMR1	24.88	4.05	**VCPIP1**	23.58	18.87	**SPINDOC**	4.27	1.46	**RPS13**	2.11	3.76
NUMA1	24.86	18.69	**RANBP3**	23.57	1.33	**AKT2**	4.26	1.74	**RPS12**	2.10	4.58
HOMER1	24.84	3.06	**RIMS1**	23.56	21.32	**SF3B4**	4.25	1.76	**SYT5**	2.09	4.00
SMNDC1	24.83	16.90	**RSBN1**	23.56	18.13	**ERH**	4.24	10.59	**CAMK2B**	2.09	4.76
LOC100526148	24.81	17.66	**GARS1**	23.55	2.27	**SPTB**	4.21	6.62	**WDR17**	2.09	4.70
SLC4A1AP	24.80	2.73	**NEDD4L**	23.51	2.08	**PRPF31**	4.10	9.53	**SFRP2**	2.07	5.95
GPATCH11	24.78	18.04	**IGBP1**	23.51	2.30	**MVP**	4.10	1.44	**RPL28**	2.07	4.44
MRPL49	24.75	2.30	**SLC1A2**	23.51	2.04	**CORO1C**	4.06	8.25	**EIF3M**	2.06	4.88
FARP1	24.74	21.32	**LLGL2**	23.48	2.36	**SRRT**	4.03	5.12	**MECP2**	2.06	1.71
RBM5	24.73	13.65	**DAB2IP**	23.47	2.30	**IQSEC3**	3.99	6.32	**H1-6**	2.06	3.85
GLYR1	24.73	17.98	**EML5**	23.46	19.79	**SNRPD1**	3.98	1.35	**YBX1**	2.05	4.13
SRRM2	24.70	19.15	**RAD23B**	23.46	3.57	**STK38**	3.92	11.41	**EEF1G**	2.04	5.12
SNRNP40	24.68	2.48	**GSK3A**	23.44	1.28	**PHF5A**	3.91	1.40	**SNRPF**	2.04	1.72
PSMB6	24.67	2.33	**TCF25**	23.43	22.27	**HNRNPH3**	3.91	1.93	**ACTBL2**	2.04	3.68
SRI	24.67	1.99	**TFR2**	23.42	2.10	**MAP1B**	3.91	7.92	**EIF3G**	2.04	5.66
HNRNPDL	24.64	3.61	**ZNFX1**	23.42	18.80	**NOP56**	3.90	1.65	**DCTN1**	2.04	5.01
EIF4E	24.61	2.33	**SYNRG**	23.42	18.57	**SF3B1**	3.78	7.18	**RPS5**	2.04	4.14
MRPS26	24.60	3.70	**CEP192**	23.41	3.57	**TNRC6B**	3.62	8.43	**RAB3GAP1**	2.03	1.70
PPP1CC	24.60	2.00	**MEPCE**	23.40	1.39	**PGAM5**	3.61	1.37	**FUS**	2.03	4.09
SRSF10	24.57	19.38	**POLR2C**	23.37	2.40	**ARPC2**	3.58	1.88	**NARS1**	2.02	4.83
RBM6	24.56	14.68	**WDR33**	23.37	19.76	**DYNLL1**	3.55	1.88	**CCT6**	2.02	4.73
IQSEC1	24.55	2.71	**EIF2S2**	23.35	2.30	**PI4KA**	3.50	5.83	**CLASP1**	2.02	5.68
GRSF1	24.54	1.37	**SIK3**	23.35	2.29	**KIAA1217**	3.46	1.89	**SARNP**	2.02	1.69
PDCL	24.53	18.56	**FN1**	23.34	18.90	**AGO2**	3.37	1.60	**EIF3H**	2.01	5.26
TAB2	24.50	16.92	**ZFR**	23.33	3.57	**DMXL2**	3.35	6.12	**RPS11**	2.00	4.75
PYCR1	24.50	20.25	**LIMCH1**	23.32	17.32	**SNRPD2**	3.32	5.65			

RBM8A	24.49	3.68	**EXOC1**	23.31	3.57	**THEM6**	3.31	1.57
HOMER2	24.49	15.71	**ODR4**	23.30	1.39	**SF3B2**	3.31	7.15
PFKFB1	24.49	17.32	**CLIP2**	23.29	2.43	**GPHN**	3.29	7.02
PSIP1	24.44	2.33	**STXBP3**	23.28	3.57	**SCAI**	3.21	8.80
SUN2	24.40	22.69	**BRCC3**	23.28	2.29	**RB1CC1**	3.21	1.31
MRPL27	24.40	19.22	**PDZD8**	23.26	2.06	**SNRPN**	3.15	4.67
ERC1	24.39	19.61	**MARK1**	23.26	22.81	**TJP2**	3.15	1.52
HNRNPL	24.38	18.39	**KCTD8**	23.25	3.57	**RPL35**	3.14	1.85
LUC7L	24.37	17.05	**CTNND2**	23.25	23.87	**SF3B3**	3.13	6.86
MRPL39	24.35	2.07	**TBC1D17**	23.24	2.30	**CCAR1**	3.11	4.71
SBF2	24.34	17.89	**MAEA**	23.23	18.32	**SV2B**	3.10	7.42
SNPH	24.33	19.55	**SACM1L**	23.23	2.27	**PURA**	3.10	4.55
TRAPPC6B	24.32	2.30	**SDHC**	23.21	1.95	**GSN**	3.08	6.22
ABI2	24.31	1.37	**MPDZ**	23.17	2.30	**FAM126B**	3.00	1.54
IDE	24.31	18.18	**RIMS2**	23.17	21.24	**DAZAP1**	2.97	7.06
GLRB	24.30	20.46	**MICOS13**	23.16	2.30	**OPLAH**	2.94	10.32
ERC2	24.27	22.01	**ARID1A**	23.15	18.32	**SPTAN1**	2.94	7.18

Appendix 16| Beta-actin levels are similar in patient and control RO Lysates of iPSC-derived RO of patient A, patient B and control were analysed by western blot analysis using antibodies against ß-actin and GAPDH.

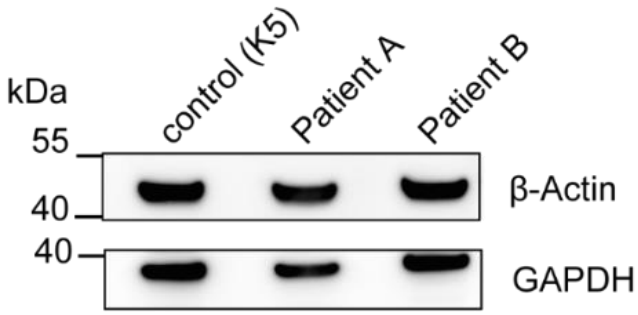

Appendix 17| Peptides located in the CRB1 extracellular domain were reduced in both patients
Graphical illustration of the CRB1 c.2834g>A;p.C948Y mutation on transcript (top panel) and protein level (middle panel). Colors represent protein domains of CRB1 with EGF (purple), laminin G (green), transmembrane (grey), FERM (yellow) and PDZ (orange). Lowe panel depicts the intensity of the different CRB1 peptides detected by mass spectrometry and data independent analysis using full-organoid lysates of control, patient A and patient B RO of 350 days of age. Peptide sequence and protein localisation are indicated. Data is depicted as mean ± SEM of three replicates.

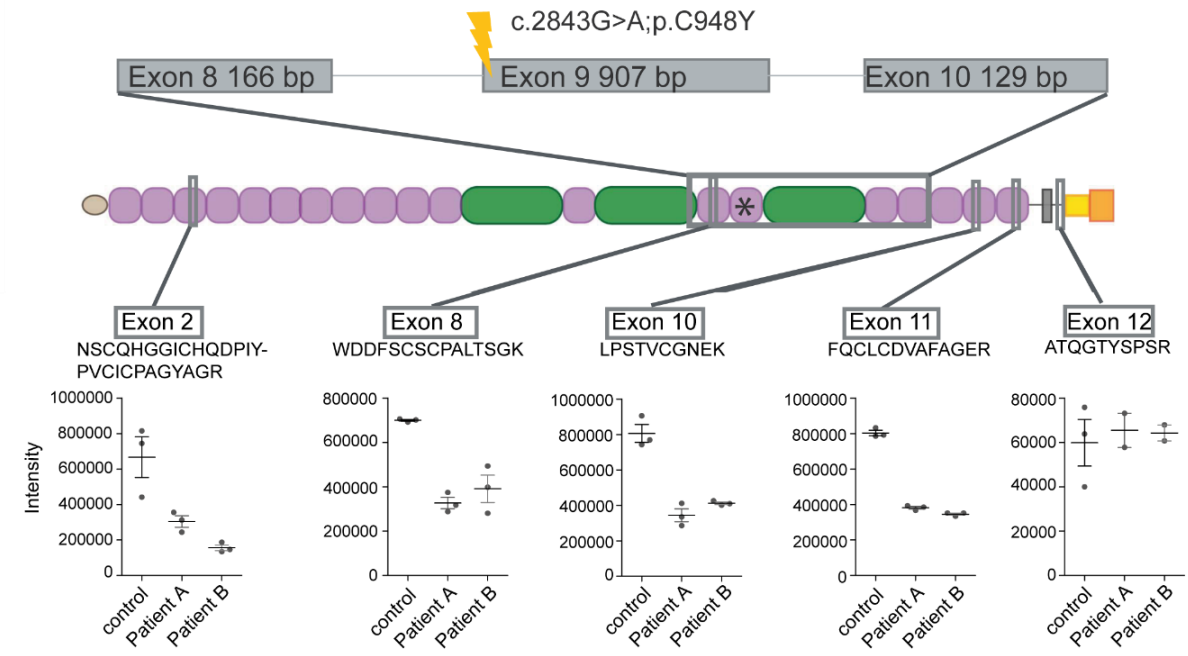

Appendix 18| Overview of the proteins that were of significant lower abundance in RO lysates of patient A and patient B. Three technical replicates of lysates of 15-16 RO were analysed by mass spectrometry and data independent analysis. Table depicts the gene name together with the log_2 ratio and the –log p-value (Two-sided t-test, FDR 0.05, S0=0.1, n=3)

Gene Name	Log_2 ratio (Patient A/K5)	Log_2 ratio (Patient B/K5)	$-log_2$ p-value (Patient A vs K5)	$-log_2$ p-value (Patient B vs K5)	Gene Name	Log_2 ratio (Patient A/K5)	Log_2 ratio (Patient B/K5)	$-log_2$ p-value (Patient A vs K5)	$-log_2$ p-value (Patient B vs K5)	Gene Name	Log_2 ratio (Patient A/K5)	Log_2 ratio (Patient B/K5)	$-log_2$ p-value (Patient A vs K5)	$-log_2$ p-value (Patient B vs K5)
NUDT4B	-0.66	-0.57	3.80	4.96	**CAP1**	-0.58	-0.49	1.90	1.99	**SLC47A2**	-0.56	-3.93	1.28	1.40
NUDT10	-0.48	-0.65	3.87	3.33	**PSMB10**	-0.68	-1.06	3.16	4.69	**TXNRD3**	-0.85	-0.66	4.01	2.20
NUDT11	-0.48	-0.65	4.06	3.61	**STAT3**	-0.38	-0.32	4.90	5.12	**HOOK3**	-0.31	-0.51	2.82	3.92
NUDT4	-0.43	-0.65	2.74	4.33	**CD200**	-0.57	-0.29	1.68	1.63	**ATCAY**	-0.44	-0.30	2.99	2.48
MED19	-0.44	-0.44	1.08	2.06	**MNDA**	-4.37	-1.62	2.40	2.57	**CCDC25**	-0.51	-0.39	1.33	1.50
SHTN1	-0.81	-0.95	5.71	5.63	**AKR1C3**	-0.68	-0.10	5.18	2.56	**PDSS2**	-2.51	-2.36	2.99	0.83
MACROD2	-0.87	-0.56	3.23	2.22	**AKR1C1**	-0.76	-0.26	5.08	3.92	**RAB43**	-5.52	-4.07	1.02	0.78
FRMD3	-1.50	-1.81	2.62	3.44	**CDKN2C**	-0.68	-0.75	2.45	1.99	**APOBEC3C**	-1.92	-1.39	2.42	1.82
TARS1	-0.08	-0.23	1.88	2.07	**PRCP**	-0.40	-0.54	4.28	4.19	**MMAA**	-1.02	-0.86	2.22	1.26
MEGF11	-0.76	-1.28	1.24	1.54	**MTHFR**	-0.57	-0.39	2.64	2.16	**SBSPON**	-0.38	-1.29	1.55	4.63
PCP4L1	-1.07	-0.53	3.37	3.13	**CRAT**	-0.41	-0.54	4.69	3.55	**SLC44A2**	-0.29	-0.24	4.11	3.85
MYO9A	-1.79	-1.02	1.80	1.07	**PPIC**	-0.61	-0.67	2.56	4.05	**CCDC28A**	-0.61	-0.59	2.99	2.54
RABGAP1	-0.20	-0.15	3.76	2.59	**MAPK8**	-0.54	-0.08	1.46	2.13	**SULF2**	-0.59	-0.82	1.96	1.92
PDLIM1	-0.60	-0.67	4.63	4.25	**MAPK10**	-0.79	-0.42	2.16	2.43	**GSPT2**	-0.18	-0.19	3.46	4.46
MYO1C	-0.74	-1.06	3.86	4.04	**MAPK9**	-1.12	-1.56	0.89	2.20	**TRIM22**	-0.27	-0.34	2.95	3.28
KCNK1	-1.02	-1.98	1.69	3.77	**HECW1**	-0.06	-0.21	2.82	1.96	**ALDH16A1**	-0.23	-0.68	2.52	4.72
APBB1	-1.28	-0.48	1.44	1.26	**ALDH1A3**	-0.60	-5.48	5.38	3.72	**UNC5B**	-0.38	-0.52	2.07	3.41
PGRMC1	-0.01	-0.48	3.91	3.05	**ZFP36L2**	-1.16	-0.73	1.13	2.19	**CPAMD8**	-0.38	-1.64	2.92	3.12
PIR	-0.90	-1.15	5.35	5.77	**LIMS1**	-0.32	-0.58	3.28	2.83	**CEND1**	-0.58	-0.25	2.65	2.65
PIK3C2B	-1.19	-0.54	1.49	0.95	**ME1**	-0.45	-0.56	5.83	4.08	**CCAR2**	-1.08	-0.57	6.48	4.48
MAN2B1	-0.74	-0.57	6.79	6.86	**SOX2**	-0.56	-0.69	1.56	4.21	**SVBP**	-0.75	-0.88	2.52	2.61
COX7A2L	-0.63	-0.47	3.23	1.63	**PITPNA**	-1.17	-0.53	3.25	3.11	**CERS5**	-3.37	-2.69	1.99	1.78
UBFD1	-0.55	-0.35	2.30	3.55	**CDC34**	-0.51	-0.15	3.67	4.04	**PARP16**	-1.59	-1.89	1.29	2.95
DYNC1I1	-0.63	-0.81	2.68	3.22	**PCYT1A**	-0.20	-0.24	2.57	1.78	**IGSF1**	-1.28	-2.26	1.10	1.68
CIT	-0.64	-0.44	1.78	2.82	**THBS3**	-2.17	-1.72	1.63	4.26	**COX18**	-0.57	-0.75	1.73	1.19
ABLIM1	-0.52	-0.47	5.37	4.29	**HINT1**	-0.36	-0.38	3.68	3.22	**ASCC1**	-0.62	-0.81	1.63	2.34
TOR1B	-0.94	-0.93	1.67	2.14	**PSEN2**	-0.28	-0.17	2.61	3.18	**DTWD2**	-0.97	-0.60	2.56	2.58
KIF3B	-0.02	-0.03	1.24	1.50	**HNMT**	-1.70	-0.39	4.71	2.95	**SUMF1**	-0.53	-0.62	1.46	2.04
NRP1	-1.14	-1.20	2.65	3.14	**PPOX**	-0.31	-0.49	2.77	3.13	**MORN4**	-1.12	-1.18	1.21	0.83
UNC13A	-0.90	-0.43	1.52	1.08	**SERPINB8**	-0.49	-0.80	2.39	3.10	**CHDH**	-0.99	-0.61	3.40	2.54
ARHGEF10	-0.46	-0.38	1.99	1.85	**PDLIM4**	-0.27	-0.46	3.66	3.46	**APPL2**	-0.68	-0.90	2.67	3.67
SYNM	-1.00	-0.75	6.15	5.85	**BCAM**	-0.45	-0.36	3.40	3.18	**MYO3A**	-0.94	-0.39	1.97	1.77
DCLK1	-0.21	-0.27	3.31	3.95	**ATP1A2**	-0.23	-0.16	5.63	6.44	**FLAD1**	-0.59	-0.39	1.11	1.95
ARPC2	-0.22	-0.29	3.17	4.60	**RAB13**	-0.04	-0.10	3.15	2.98	**VANGL1**	-0.45	-0.65	1.61	1.96
ARPC3	-0.23	-0.25	2.68	2.89	**DAP**	-0.54	-0.97	4.36	3.91	**FAM110B**	-0.42	-0.36	2.43	2.08
MID1	-0.50	-0.47	2.55	2.81	**CAV2**	-0.66	-2.44	2.32	1.62	**CIP2A**	-0.58	-1.01	4.05	5.78
IPO8	-0.63	-0.03	3.19	2.00	**USP11**	-1.84	-0.74	3.25	5.96	**NEK7**	-0.38	-0.04	3.47	2.26
IPO7	-0.62	-0.32	2.48	2.06	**AKR1D1**	-0.81	-0.46	2.37	1.72	**SMCR8**	-1.04	-1.22	0.93	1.36
TLR3	-0.89	-1.11	3.27	3.69	**AKR1C2**	-0.40	-0.24	4.33	4.62	**PPP4R1**	-0.35	-0.29	2.31	1.81
ARPC5	-0.32	-0.26	0.96	3.66	**CRIP2**	-0.51	-0.38	5.43	3.54	**CACTIN**	-0.60	-0.65	1.22	1.46
SGSM2	-4.82	-4.32	1.11	1.01	**EPHA4**	-0.65	-0.35	1.23	1.76	**CPLX3**	-1.88	-1.17	1.82	3.66

FLRT2	-0.94	-0.42	3.53	1.78	**MFAP2**	-1.57	-2.14	3.30	3.05	**MAIP1**	-0.31	-0.46	2.10	2.52
CYB5B	-0.31	-0.76	2.89	4.40	**CASP6**	-0.36	-0.36	4.86	5.05	**PALLD**	-0.37	-0.53	5.52	6.56
SEPTIN4	-0.06	-0.18	2.56	3.05	**ADK**	-0.42	-0.38	2.45	2.72	**IFT81**	-0.49	-0.25	3.11	2.19
HSPA12A	-0.93	-0.63	5.69	4.49	**LAMB2**	-0.32	-0.28	2.22	1.63	**CCT6B**	-0.02	-0.02	1.47	2.16
ADCY6	-0.77	-0.80	1.32	1.63	**ITGA1**	-0.95	-1.75	3.85	2.88	**PHYHIP**	-0.31	-0.23	3.24	2.97
DCX	-0.69	-0.55	6.33	4.96	**FXYD7**	-1.73	-1.07	5.15	4.35	**SEPTIN10**	-0.12	-0.25	2.05	2.66
AHCYL1	-0.36	-0.40	3.21	2.91	**GNG2**	-0.38	-0.42	3.34	3.76	**PXDN**	-1.41	-1.04	2.51	1.51
MGRN1	-0.33	-0.40	2.41	1.71	**S100A10**	-1.99	-2.20	3.31	3.72	**TFG**	-0.26	-0.41	3.10	4.02
KATNIP	-1.70	-0.32	3.40	1.84	**TMEM258**	-0.40	-0.90	2.76	2.78	**TNR**	-0.87	-0.54	4.62	5.04
NME2P1	-0.12	-0.26	2.53	0.80	**RPL15**	-0.30	-0.25	3.69	2.80	**APBB2**	-1.47	-1.43	1.39	2.50
PPL	-1.05	-1.55	4.99	5.33	**PCBD1**	-0.21	-0.28	2.13	2.55	**SNX21**	-0.92	-0.58	2.69	2.19
GSDME	-0.42	-0.40	4.20	2.67	**RRAS2**	-0.04	-0.43	3.22	4.03	**ZNF428**	-0.92	-0.54	5.80	4.00
SORBS3	-0.34	-0.60	1.83	1.69	**UBE2G1**	-0.40	-0.20	2.32	2.61	**SLC22A18**	-2.59	-1.80	2.12	1.36
GMDS	-0.49	-0.38	2.39	2.03	**TMSB4X**	-0.58	-0.66	3.19	3.64	**AIDA**	-0.84	-0.44	2.53	2.27
DIAPH2	-0.33	-1.33	2.45	3.71	**PPP2CB**	-0.35	-0.30	2.65	2.27	**DOCK10**	-1.22	-0.66	2.35	0.92
CUTA	-0.75	-0.94	4.91	5.98	**VSNL1**	-0.55	-0.40	2.57	2.82	**GALM**	-0.29	-0.70	2.73	4.88
PPP1R11	-0.43	-0.67	2.46	4.80	**GNAI1**	-0.22	-0.05	3.33	2.11	**PPP1R14B**	-0.31	-0.50	2.61	3.98
NOS1AP	-0.32	-0.59	1.95	1.94	**PPP2R2A**	-0.25	-0.20	2.25	1.80	**CHMP4B**	-0.49	-0.73	2.30	1.51
FLNA	-0.12	-0.50	2.73	3.24	**YBX1**	-0.32	-0.06	2.93	2.46	**TLCD1**	-1.21	-1.44	2.12	3.66
CBR3	-0.39	-1.04	4.19	3.91	**FKBP1B**	-0.61	-0.66	1.93	1.21	**FOXRED1**	-0.91	-0.48	2.49	2.97
CBR1	-0.31	-1.01	3.40	5.22	**PSPH**	-0.39	-0.56	4.54	4.23	**KCTD12**	-0.75	-0.42	3.55	3.22
CNMD	-1.85	-4.18	1.65	4.45	**KRT85**	-0.01	-0.16	1.13	1.29	**ECHDC3**	-3.28	-3.12	2.01	2.36
ATRN	-0.39	-0.26	2.89	2.49	**JAG1**	-0.64	-0.92	2.28	2.66	**SHISA4**	-3.93	-1.38	3.54	1.18
DHRS3	-1.26	-3.76	2.80	3.12	**RELN**	-0.95	-1.79	2.61	4.67	**TCEAL2**	-0.07	-0.66	2.00	1.93
C1QL1	-1.14	-0.93	3.87	2.04	**IFI35**	-1.14	-0.50	4.19	3.40	**MRPS24**	-0.65	-1.68	1.87	2.24
WFS1	-0.86	-0.88	5.64	4.83	**ABAT**	-0.21	-0.16	4.04	3.38	**SAT2**	-0.51	-0.94	2.81	5.68
TM7SF2	-0.74	-0.50	3.42	2.59	**CRB1**	-0.85	-0.88	3.53	4.46	**PHYHIPL**	-0.31	-0.23	3.09	3.04
PDE5A	-0.36	-0.39	3.97	3.36	**CDK6**	-0.62	-0.77	3.38	3.58	**SDSL**	-0.88	-0.50	3.33	3.30
LY6H	-0.41	-0.91	1.95	3.94	**CDK17**	-0.25	-0.47	1.84	1.87	**SLC41A3**	-0.72	-1.48	3.95	4.44
MTA2	-1.00	-0.24	2.18	5.12	**HSF1**	-1.13	-1.86	2.42	2.93	**ZC3HAV1L**	-0.76	-0.74	2.73	1.57
SLIT2	-1.28	-0.96	1.76	1.86	**NFKB2**	-0.28	-0.38	3.22	3.76	**PDLIM5**	-0.27	-0.38	4.44	4.98
SEC24D	-0.26	-0.41	2.80	3.00	**AMPD3**	-0.43	-0.82	3.35	4.71	**AHCYL2**	-0.28	-0.27	3.36	3.41
PLPBP	-0.32	-0.30	3.08	2.22	**ROR1**	-0.30	-0.71	2.38	1.48	**AJUBA**	-0.97	-0.46	2.52	2.40
PRSS23	-0.98	-2.36	2.36	2.30	**APLP2**	-0.14	-0.22	2.85	3.25	**THOC3**	-0.39	-0.29	2.81	2.59
GABARAP	-1.15	-0.34	2.02	3.20	**ZFP36L1**	-0.75	-1.49	4.35	2.12	**ITCH**	-0.11	-0.28	3.29	3.43
SNX4	-0.50	-0.74	2.07	1.51	**LRP1**	-0.33	-0.60	5.22	5.42	**TMEM68**	-0.39	-0.83	2.36	3.21
TRIM16	-1.82	-2.40	1.87	2.27	**CRYZ**	-1.42	-1.67	6.38	6.58	**HSPA12B**	-1.11	-0.76	3.17	3.06
PPP1R3D	-1.05	-1.43	1.75	0.97	**AHNAK**	-0.81	-1.04	7.26	7.55	**SLC2A13**	-0.91	-0.39	3.48	1.20
CPNE6	-0.67	-0.17	2.39	2.45	**FAAP100**	-0.83	-0.95	1.39	1.28	**TEFM**	-2.87	-2.30	2.59	0.89
HSPA4L	-0.20	-0.01	3.12	4.04	**SREBF2**	-2.49	-2.32	1.66	4.46	**MCCC1**	-0.31	-0.39	2.98	2.45
PTBP1	-0.14	-0.33	3.13	1.94	**NFIA**	-1.13	-0.49	2.14	1.92	**CAMKK2**	-0.67	-1.18	2.07	2.12
MAP4K4	-0.34	-0.44	2.84	2.76	**DLG1**	-0.14	-0.01	3.32	3.06	**NIBAN2**	-0.47	-0.63	3.05	3.39
PAK4	-0.32	-0.28	2.09	1.84	**PTP4A2**	-0.34	-0.01	2.20	3.12	**NELL2**	-0.78	-1.24	3.56	3.87
ALDH1A1	-0.60	-3.16	4.86	3.31	**IFIT5**	-0.25	-0.48	2.41	2.82	**PCYT2**	-0.19	-0.35	3.13	4.60
SOD1	-0.22	-0.27	4.59	4.27	**ILK**	-0.30	-0.27	2.72	2.58	**S1PR3**	-0.65	-0.67	3.08	3.61
CP	-0.46	-1.33	4.40	5.54	**SQSTM1**	-0.42	-0.96	3.76	2.67	**TSC22D3**	-0.38	-0.56	1.92	3.05
CA2	-1.00	-0.97	5.49	5.48	**PPP1R1A**	-0.68	-0.82	2.78	1.60	**S100A13**	-0.34	-0.38	3.68	3.24
ASS1	-1.14	-1.50	6.22	5.68	**EIF4EBP2**	-0.39	-0.51	1.37	3.68	**SEPTIN5**	-0.42	-0.18	4.04	3.47
SERPINA3	-0.70	-2.69	4.46	3.42	**RIPK1**	-0.78	-0.27	3.51	1.96	**MGST2**	-0.30	-0.99	2.90	4.65
AGT	-4.06	-3.85	2.49	4.54	**TUBB2A**	-0.17	-0.07	3.17	2.24	**MICU1**	-1.03	-0.93	1.07	0.97

CRYAB	-1.26	-0.43	6.09	4.20	**GIT2**	-0.27	-0.21	3.07	2.33	**MGME1**	-1.24	-0.48	1.57	1.06
TF	-1.04	-1.91	6.26	7.35	**DOC2B**	-2.63	-1.14	4.85	0.87	**ACBD6**	-0.45	-0.30	2.59	2.32
BRAF	-0.21	-0.14	0.95	4.23	**TFDP1**	-4.41	-3.69	2.74	0.93	**TXNDC17**	-0.27	-0.29	3.02	3.25
ANXA1	-0.64	-1.13	4.17	4.84	**CRMP1**	-0.07	-0.13	3.58	3.61	**PIGQ**	-0.69	-0.52	2.53	1.95
SOD2	-0.57	-0.83	4.27	3.13	**ENDOG**	-0.59	-0.37	6.37	2.77	**TRIM56**	-0.44	-0.31	2.32	1.64
THY1	-1.22	-0.25	5.57	2.84	**MDC1**	-0.55	-0.87	1.29	1.02	**TMEM175**	-0.35	-0.42	2.66	2.01
S100B	-1.85	-0.64	4.25	3.32	**KCTD2**	-0.75	-0.95	1.22	1.34	**SYT11**	-1.48	-0.71	2.10	3.44
HSPB1	-0.46	-0.62	4.33	5.03	**RFTN1**	-0.40	-0.28	3.43	2.18	**MED18**	-0.82	-0.34	2.24	1.10
SLC4A2	-0.60	-0.56	1.74	4.12	**LASP1**	-0.27	-0.29	4.01	3.90	**RAB5IF**	-0.56	-0.80	1.49	1.44
SERPINE1	-0.97	-1.61	1.38	2.43	**GPNMB**	-0.57	-4.48	4.15	1.09	**MRI1**	-0.83	-0.84	4.31	5.12
SERPING1	-0.63	-2.20	5.15	7.33	**ARHGEF6**	-0.11	-0.11	1.38	1.95	**ELOVL1**	-0.92	-0.83	4.66	4.87
CFI	-0.84	-1.73	5.60	5.57	**PEA15**	-0.28	-0.30	2.64	3.06	**CINP**	-0.49	-0.78	1.59	1.89
FGF1	-0.67	-0.36	5.88	2.96	**PGM5**	-0.73	-0.77	5.04	4.89	**ACAT2**	-0.43	-0.37	4.70	3.86
JUN	-0.17	-1.29	1.19	1.35	**QPRT**	-0.68	-1.26	3.39	5.49	**PAPPA2**	-0.54	-1.57	2.48	2.77
KRT8	-0.84	-0.15	2.71	3.92	**RPS6KA2**	-0.65	-1.05	1.42	2.25	**HDHD5**	-0.47	-0.75	1.82	2.37
GFAP	-0.61	-0.19	2.87	2.03	**CNN3**	-0.62	-0.64	2.94	3.68	**KIAA1671**	-0.58	-0.25	2.82	1.81
CALB1	-1.50	-1.57	5.80	6.02	**CNN2**	-1.44	-0.91	4.57	3.91	**FRMD8**	-0.60	-0.94	2.33	3.09
S100A6	-0.70	-0.72	4.73	4.85	**TSC22D1**	-0.13	-0.38	2.68	5.01	**CNTNAP3**	-1.34	-1.10	1.36	2.21
HEXA	-0.35	-0.49	3.83	5.01	**TOMM34**	-0.39	-0.30	2.89	5.02	**TNKS1BP1**	-0.22	-0.54	3.83	3.30
ANXA2	-0.37	-0.82	3.73	4.81	**MSMO1**	-0.61	-0.52	4.73	2.33	**TANC1**	-0.50	-0.78	3.77	3.80
CA3	-0.84	-2.07	5.55	4.42	**PKN1**	-0.53	-0.29	2.23	2.03	**KLHL4**	-1.09	-1.44	1.50	3.67
HEXB	-0.22	-0.40	3.26	4.07	**CTF1**	-0.34	-0.41	2.31	2.51	**SRR**	-0.38	-0.32	3.07	2.86
CTSL	-0.54	-0.33	3.33	2.64	**NTRK2**	-1.25	-2.47	2.83	2.82	**WWTR1**	-0.56	-1.23	1.51	3.25
APRT	-0.43	-0.66	3.69	3.46	**DBN1**	-0.19	-0.42	3.56	4.57	**HDHD2**	-0.35	-0.25	3.67	3.37
RHOA	-0.01	-0.24	3.09	3.03	**MAN2A1**	-0.89	-1.07	1.17	2.09	**MRPL18**	-0.22	-0.35	2.89	1.99
RHOB	-0.25	-0.35	3.72	3.68	**DDR2**	-1.39	-0.56	4.07	2.82	**C11orf54**	-0.28	-0.37	3.64	3.68
VIM	-0.65	-0.49	3.34	4.05	**IAH1**	-0.32	-0.37	2.84	3.61	**OSBPL5**	-0.78	-0.29	1.98	2.41
PRPH	-0.58	-0.33	4.68	3.50	**UGT3A2**	-1.08	-1.80	4.12	3.47	**SH3BGRL3**	-0.31	-0.46	4.86	5.07
INA	-0.58	-0.33	1.61	2.22	**TP53I3**	-0.50	-0.36	4.10	3.43	**SLC12A4**	-0.01	-0.01	1.68	2.15
FGF2	-0.35	-0.58	4.04	3.64	**KLHDC8B**	-3.07	-2.70	1.12	0.95	**CPVL**	-1.13	-1.57	3.75	4.49
LGALS1	-0.62	-1.37	5.33	6.23	**HSP90AA4P**	-0.06	-0.03	2.65	1.03	**C1orf198**	-0.56	-0.69	3.13	4.65
RBP1	-0.22	-0.99	3.25	5.06	**TMEM128**	-0.46	-1.07	1.34	3.62	**FZD8**	-1.46	-1.08	2.58	1.80
SPARC	-0.31	-0.57	4.14	3.32	**RILPL1**	-0.33	-0.86	2.67	3.54	**GLIPR2**	-0.50	-0.37	2.45	2.26
TPM1	-0.21	-0.44	3.21	3.92	**TCEAL5**	-0.12	-0.42	2.73	3.98	**TMEM231**	-1.24	-3.09	1.52	1.22
C1S	-1.49	-1.08	2.62	1.78	**PITRM1**	-0.57	-0.43	4.62	3.56	**ANTXR1**	-0.27	-0.55	1.67	2.42
UCHL1	-0.52	-0.21	6.43	4.69	**TOR2A**	-0.30	-0.39	1.66	3.15	**ELAC1**	-0.35	-0.47	2.78	3.78
GSTT2B	-0.33	-0.75	4.29	2.23	**SAMD4B**	-0.56	-0.47	1.73	1.39	**ADGRL3**	-0.55	-0.32	2.45	1.42
ARAF	-0.33	-0.28	2.63	3.32	**TTC38**	-0.96	-1.06	6.07	6.26	**SIAE**	-0.44	-0.58	2.92	3.68
SPP1	-0.85	-1.58	4.53	4.72	**ATAT1**	-1.12	-0.30	4.77	3.19	**SLC38A10**	-0.63	-0.62	3.71	3.24
CLU	-0.47	-1.01	4.77	5.83	**CEP170**	-0.39	-0.06	3.46	2.38	**PCDH9**	-0.56	-2.79	1.38	2.26
G6PD	-0.27	-0.25	4.00	3.95	**SLC35F1**	-0.65	-0.48	1.48	0.88	**SPON1**	-0.47	-0.31	4.76	3.65
COL11A1	-0.53	-0.87	1.70	2.89	**IDNK**	-0.65	-0.27	2.53	1.65	**MCCC2**	-0.29	-0.22	3.08	2.63
LAMP2	-0.37	-0.35	2.29	3.10	**C9orf64**	-0.89	-0.73	2.38	3.99	**GOPC**	-0.37	-0.57	2.11	2.86
VCAN	-0.80	-1.19	5.00	5.54	**CPTP**	-1.31	-1.76	2.49	2.59	**RANGRF**	-2.57	-2.81	2.12	2.07
TPT1	-0.41	-0.28	3.76	2.92	**ANKRD45**	-2.15	-2.55	1.96	3.24	**TXNRD2**	-0.46	-0.34	3.36	2.64
IRF2	-0.81	-0.68	1.20	1.18	**GKAP1**	-2.26	-2.48	2.59	2.20	**CD93**	-1.09	-0.36	4.50	3.08
ARSA	-0.47	-0.43	4.20	3.99	**YOD1**	-0.63	-0.65	1.68	2.13	**TMEM9B**	-0.76	-0.48	2.74	2.12
EZR	-0.23	-0.05	2.79	2.74	**DAB2IP**	-0.42	-0.29	3.00	2.67	**PLCB1**	-0.52	-0.20	3.69	2.58
NQO1	-0.74	-0.72	4.03	5.22	**DENND4C**	-0.46	-0.83	2.25	3.65	**COPRS**	-0.29	-0.29	3.03	3.51

GNS	-0.32	-0.18	5.25	2.72	**WASHC2A**	-0.33	-0.21	1.28	1.44	**RRAGD**	-0.12	-0.28	0.92	0.95
NQO2	-0.28	-0.48	3.11	3.66	**KCTD16**	-1.19	-0.85	2.26	1.85	**PDLIM7**	-0.56	-0.26	2.99	3.43
ITGB4	-0.35	-0.68	2.56	3.70	**ARHGAP17**	-0.52	-0.76	2.01	3.20	**MAN1C1**	-0.83	-1.23	3.81	3.16
PPP3CA	-0.33	-0.24	2.60	1.79	**POLR2M**	-0.30	-0.25	3.53	1.50	**NANS**	-0.37	-0.26	3.40	4.40
NAGA	-0.34	-0.33	3.76	3.57	**VASN**	-0.53	-0.72	2.14	3.67	**OSTC**	-0.28	-0.25	1.50	1.50
SMPD1	-0.45	-0.27	3.57	3.28	**TCEAL3**	-0.14	-0.40	1.39	2.79	**PHPT1**	-0.48	-0.59	4.04	4.20
LGALS3	-0.70	-1.09	4.36	5.37	**ACAD10**	-0.65	-0.27	2.47	2.15	**ARHGAP35**	-0.46	-0.29	3.25	3.01
ERCC2	-3.13	-1.59	2.18	1.13	**SLC25A25**	-1.77	-1.54	1.09	1.38	**CHST7**	-1.42	-0.87	1.69	1.72
NAT1	-0.61	-0.36	2.57	1.39	**TENM4**	-0.40	-0.64	3.94	3.23	**OLA1**	-0.21	-0.18	3.57	3.54
PAM	-0.63	-1.39	1.66	2.27	**REEP3**	-0.65	-0.31	3.74	3.20	**OLAH**	-2.76	-2.76	1.96	1.33
SRM	-0.38	-0.29	4.31	3.63	**CAVIN1**	-0.25	-1.56	2.21	4.31	**SEPTIN11**	-0.12	-0.41	3.59	4.55
NFKB1	-0.22	-0.55	1.94	2.88	**ERAP2**	-5.87	-2.65	4.15	5.21	**PARVA**	-0.31	-0.38	1.73	2.15
PVALB	-1.59	-0.46	3.69	1.47	**FAM117B**	-0.72	-0.22	1.64	1.31	**USP40**	-1.06	-1.22	3.55	3.12
CAST	-0.26	-0.70	1.98	5.20	**TTC37**	-0.47	-0.26	4.40	2.09	**PNPO**	-0.73	-0.21	4.95	3.27
COMT	-1.13	-2.38	5.82	6.06	**UQCC3**	-2.03	-1.38	2.22	4.67	**NECAP2**	-0.52	-0.67	4.25	3.48
GPX3	-0.52	-1.30	4.02	5.19	**C6orf89**	-3.20	-1.40	1.73	0.85	**RBM28**	-1.62	-1.27	1.49	1.09
CALB2	-1.55	-1.46	6.62	3.95	**NAPRT**	-0.27	-0.28	3.13	3.11	**MRPL16**	-0.48	-0.48	2.54	2.67
FECH	-0.26	-0.81	3.30	4.68	**KYAT3**	-0.50	-1.77	4.73	7.38	**MARCHF5**	-0.27	-0.34	2.40	2.80
CES1	-1.72	-1.29	2.46	1.72	**LIAT1**	-3.16	-1.74	2.94	1.66	**SMPD3**	-0.74	-0.42	3.91	3.85
CFL1	-0.31	-0.11	5.22	3.26	**TRIM67**	-0.38	-0.40	2.42	1.69	**ERAP1**	-0.37	-1.03	4.78	5.99
COX7B	-1.17	-0.73	2.12	3.80	**GPRIN3**	-0.49	-0.40	1.75	1.45	**GGA3**	-0.24	-0.10	3.24	2.73
EEF1B2	-0.11	-0.27	4.96	4.38	**MBOAT2**	-0.39	-0.28	2.14	2.72	**CLIC5**	-0.54	-0.91	2.40	3.69
MAOB	-0.15	-0.71	2.92	5.95	**RAPH1**	-0.66	-0.41	3.44	5.00	**GLTP**	-0.54	-0.41	2.55	1.30
YWHAB	-0.16	-0.18	2.69	1.59	**USP43**	-1.36	-0.54	3.89	1.21	**NDUFAF4**	-1.12	-2.24	2.10	1.28
MAPK1	-0.49	-0.57	4.80	5.93	**ENOSF1**	-0.79	-0.68	2.94	2.53	**ABRACL**	-0.63	-0.26	2.00	2.69
PIK3R1	-0.17	-0.19	1.72	2.30	**DGLUCY**	-0.51	-0.82	3.49	4.20	**ZNFX1**	-1.06	-0.43	2.83	2.20
EPHA2	-0.96	-1.20	3.59	2.21	**CYP2U1**	-1.22	-0.47	4.52	3.19	**RRBP1**	-0.31	-0.46	4.52	4.02
EPHB2	-1.05	-1.46	7.06	7.32	**TRMT11**	-0.35	-0.36	1.85	1.97	**KLHL14**	-1.13	-0.48	3.75	3.98
EPHB1	-1.00	-1.56	2.94	3.79	**IRF2BP2**	-0.95	-0.34	3.07	2.78	**GNG13**	-1.05	-0.44	5.05	2.35
CASP1	-1.57	-1.59	1.26	1.40	**NECAB2**	-0.82	-0.83	5.29	5.10	**GNG12**	-0.38	-0.78	2.84	4.41
PRDX6	-0.34	-0.50	3.65	4.02	**PRRT2**	-0.63	-0.25	3.34	2.28	**DKK3**	-1.27	-1.66	5.15	5.55
PEBP1	-0.40	-0.32	3.89	3.44	**MTERF4**	-1.61	-1.38	1.14	1.23	**GULP1**	-0.45	-0.45	1.55	4.85
PPIF	-0.46	-1.09	3.83	4.32	**MEGF8**	-0.46	-0.87	4.07	5.09	**CTSZ**	-0.49	-1.74	3.85	4.70
CORO1A	-0.29	-0.12	1.42	1.50	**GALNT10**	-0.54	-0.48	2.68	1.30	**RNF14**	-0.55	-0.23	2.37	1.69
STX2	-1.75	-1.95	3.52	3.08	**TRAPPC6B**	-0.42	-0.24	2.10	2.16	**CTNNAL1**	-0.58	-0.58	1.86	1.73
ABCD1	-1.01	-0.76	1.67	1.58	**MRPL52**	-0.44	-1.01	2.12	1.22	**SEC14L3**	-0.39	-0.29	3.48	2.69
SHMT1	-0.28	-0.78	3.90	4.71	**ZNF598**	-0.56	-0.27	1.59	1.51	**PCSK1N**	-1.09	-0.36	3.91	2.59
CHKA	-0.99	-0.44	3.59	1.37	**PHLDB1**	-0.39	-0.35	2.02	2.24	**ADAMTS1**	-0.99	-2.05	1.29	2.10
HPCA	-0.25	-0.19	3.68	3.68	**NAA40**	-0.70	-0.23	2.45	3.69	**DPP7**	-1.61	-0.73	6.57	5.59
EIF4A1	-0.26	-0.22	2.70	3.36	**SLC25A42**	-1.01	-0.69	1.75	1.45	**TAGLN3**	-0.34	-0.29	4.77	3.66
COL18A1	-0.32	-1.01	2.69	3.24	**LRRTM4**	-0.94	-1.56	1.44	2.99	**AK3**	-0.29	-0.66	3.16	4.56
DBNL	-0.22	-0.30	3.38	3.91	**TIMELESS**	-0.40	-1.85	4.12	0.96	**FARP1**	-0.43	-0.56	2.67	2.73
FBXO2	-0.98	-1.59	4.17	4.83	**B9D1**	-1.35	-0.57	1.18	0.90	**HSPB11**	-0.28	-0.23	3.25	2.67
JPT1	-0.23	-0.42	2.34	3.42	**SHANK2**	-2.35	-0.95	1.75	1.79	**PCDHB2**	-0.68	-0.39	3.03	1.82
TNIK	-0.20	-0.25	2.24	3.24	**THSD7A**	-0.52	-0.69	2.22	3.59	**ENTPD2**	-0.46	-0.23	1.37	1.68
ACAD8	-0.25	-0.37	3.28	2.27	**CHKB**	-0.39	-0.76	1.89	3.43	**WIF1**	-0.82	-0.59	4.08	3.98

CDV3	-0.34	-0.39	2.59	2.73	**MAN2B2**	-0.53	-0.37	4.33	3.80	**SNX9**	-0.41	-0.57	2.36	2.22
DENND2A	-1.92	-2.18	1.07	0.88	**DNAJC16**	-2.17	-2.11	1.29	2.72	**PEX16**	-2.35	-2.56	3.38	2.36
PALD1	-0.35	-0.21	2.71	2.30	**USP20**	-1.34	-0.60	1.54	1.04	**SLC25A15**	-0.71	-0.57	2.21	0.91
MRTFB	-0.55	-0.60	2.97	4.09	**GSTK1**	-0.36	-0.36	2.17	3.14	**SPCS1**	-3.70	-0.51	1.71	1.03
STRIP2	-0.25	-0.19	2.13	1.21	**CARHSP1**	-1.41	-2.44	4.52	5.29	**OAS3**	-1.53	-1.06	2.64	2.58
EPDR1	-1.33	-1.25	3.42	3.07	**TDRKH**	-0.59	-0.25	1.59	2.15	**ROBO1**	-0.65	-0.75	1.02	1.51
NENF	-0.28	-0.38	3.44	3.53	**CIAO2B**	-0.81	-0.88	1.25	1.22	**NUMBL**	-0.17	-0.22	2.35	1.27
NDRG2	-0.59	-0.32	4.23	3.53	**TLN1**	-0.41	-0.65	5.85	7.54	**GSN**	-0,07	-0,57	1.87	5.38

Appendix 19| Proteins that were significantly increased in lysates of both patient A and patient B RO compared to control Three technical replicates of lysates of 15-16 RO were analysed by mass spectrometry and data independent analysis. Table depicts the gene name together with the log_2 ratio and the –log p-value (Two-sided t-test, FDR 0.05, S0=0.1, n=3)

Gene Name	Log_2 ratio (Patient A/K5)	Log_2 ratio (Patient B/K5)	$-log_2$ p-value (Patient A vs K5)	$-log_2$ p-value (Patient B vs K5)	Gene Name	Log_2 ratio (Patient A/K5)	Log_2 ratio (Patient B/K5)	$-log_2$ p-value (Patient A vs K5)	$-log_2$ p-value (Patient B vs K5)	Gene Name	Log_2 ratio (Patient A/K5)	Log_2 ratio (Patient B/K5)	$-log_2$ p-value (Patient A vs K5)	$-log_2$ p-value (Patient B vs K5)
ZNF593OS	0.92	0.56	3.07	1.96	**NSF**	0.17	0.21	3.69	3.58	**ORMDL3**	0.44	0.43	2.25	2.52
NBDY	0.43	0.39	2.57	2.17	**CDKN1B**	0.27	0.31	2.21	2.48	**NUP93**	0.26	0.56	2.54	3.82
ARHGAP10	1.10	0.46	3.45	1.63	**NEDD4**	0.53	0.56	2.70	2.35	**ARHGAP24**	3.25	2.65	1.28	1.69
FAM234B	2.04	2.13	2.85	3.00	**PIP4K2A**	0.14	0.57	2.76	4.14	**TMEM256**	0.58	0.50	1.39	1.76
DENND11	0.91	1.39	1.14	1.45	**SOX9**	0.61	0.48	1.70	3.73	**GPD1L**	0.77	0.57	4.40	5.29
PCARE	0.94	1.36	2.37	2.96	**GCLC**	0.45	0.30	4.43	2.93	**CADM2**	0.71	0.83	5.09	5.42
FBLL1	0.48	0.72	3.12	2.53	**CD151**	0.28	0.32	2.29	2.02	**STAG2**	0.30	0.41	2.08	2.01
ARHGAP42	0.59	0.77	1.74	1.97	**DHPS**	0.49	0.36	2.77	1.74	**FSTL5**	0.70	0.66	4.73	4.59
DISP2	0.87	0.96	1.75	1.50	**AARS1**	0.27	0.23	4.98	4.20	**PAQR4**	0.46	0.53	2.70	2.72
HMGB1	0.50	0.40	2.91	3.01	**NUP153**	0.26	0.27	2.46	2.55	**WDTC1**	0.45	0.62	1.67	2.01
WASH2P	1.15	1.34	2.30	2.37	**RGS3**	0.67	1.25	1.18	2.42	**MINDY1**	0.26	0.23	1.70	1.88
HAX1	0.32	0.48	2.00	2.51	**SULT1A1**	0.28	0.70	2.19	2.89	**ARL6IP6**	0.77	0.50	2.16	3.05
AP4M1	1.29	2.06	1.67	2.34	**CPT1A**	0.26	0.24	4.60	4.00	**RNF148**	2.14	1.97	3.20	3.17
TULP1	0.41	0.52	3.39	3.83	**RAB28**	0.28	0.54	2.72	3.85	**UBR7**	0.39	0.39	2.27	2.27
TUB	0.48	0.59	2.82	2.99	**PDE6C**	0.39	0.91	2.66	2.83	**ZNF513**	0.18	0.64	1.92	1.41
MATN2	1.08	0.61	3.97	1.72	**UBE2D1**	0.08	0.33	1.82	1.92	**GDPD1**	0.56	0.44	4.38	4.20
FOXN3	0.34	0.33	2.10	1.77	**CLCN3**	0.03	0.18	3.25	4.09	**C19orf47**	3.10	3.22	1.84	1.41
EML1	0.55	0.80	4.95	5.78	**NUP98**	0.69	0.66	3.46	3.89	**LRRC57**	0.73	0.92	4.68	5.92
MANBA	0.89	0.52	3.66	2.21	**SLC16A1**	1.19	0.82	6.10	5.49	**PCYOX1L**	0.42	0.30	2.76	1.75
KPNA3	0.21	0.29	3.71	2.48	**BCAT1**	1.41	0.52	4.43	3.01	**RDH13**	0.53	0.34	2.74	2.29
FAAH	0.25	0.30	3.56	3.81	**SLC12A2**	0.41	0.33	2.41	2.12	**AQP11**	0.78	0.94	2.19	2.41
PITPNM1	0.36	0.33	4.69	4.25	**CASP7**	0.81	0.79	2.67	2.84	**KCT2**	0.88	0.58	2.39	1.27
NOP56	0.57	0.79	5.13	4.09	**CDH11**	0.21	0.25	1.98	1.64	**NFATC2IP**	0.85	1.18	2.14	2.50
PEX7	0.51	0.67	1.94	2.07	**SNU13**	0.41	0.50	2.90	3.50	**TNRC6A**	0.97	0.44	2.25	1.27
C2CD2L	0.49	0.40	2.83	2.39	**CTBP2**	0.20	0.43	3.32	4.56	**SLC17A7**	0.45	0.43	2.51	2.61
ARHGAP33	0.20	0.39	2.24	3.07	**TMEM50B**	0.47	0.57	2.77	3.07	**FBXO22**	0.47	0.60	3.50	3.98
GNGT2	0.32	0.48	3.40	2.43	**RP1**	0.80	1.47	1.87	3.05	**DOCK8**	0.49	0.43	1.95	2.51
GNGT1	0.28	0.50	3.49	4.10	**STX17**	0.47	0.34	3.20	2.59	**USP32**	0.40	0.67	3.24	2.17
DVL2	0.54	0.94	2.05	2.83	**JAM2**	0.47	0.54	3.16	3.73	**NUP37**	0.64	1.05	2.57	3.52
SLC9A3R1	0.29	0.40	3.43	4.81	**NUP107**	0.74	0.93	3.39	3.52	**ENGASE**	0.34	0.51	2.66	3.46
RASGRF2	0.27	0.51	1.84	2.79	**SESN3**	1.66	2.31	2.69	3.14	**NBEA**	0.27	0.27	3.08	2.64
LIN7A	0.19	0.36	3.50	2.96	**SESN1**	0.47	0.51	1.77	3.25	**RASSF8**	1.22	1.55	3.14	4.52
ABCC4	0.58	0.57	3.57	4.51	**SNAP25**	0.75	0.69	5.89	5.93	**SPATA20**	0.58	1.00	2.87	3.72
CAPN5	0.55	0.48	3.60	3.51	**STXBP1**	0.57	0.49	4.80	4.47	**ZCRB1**	3.00	1.95	1.70	1.14
RNF113A	0.42	0.43	2.92	2.88	**TSPAN5**	1.63	1.43	1.11	1.01	**FAM174A**	4.11	3.89	1.98	1.79
CRX	0.36	1.01	4.15	6.43	**SNRPD1**	0.28	0.43	3.01	5.09	**WDR20**	0.55	0.43	2.68	2.97
SART1	0.37	0.36	3.02	4.51	**SNRPD2**	0.29	0.46	2.59	3.22	**MARCHF1**	0.71	0.68	2.81	2.75
FIBP	0.39	0.58	1.95	2.11	**H4-16**	0.33	0.46	3.25	3.71	**SLC2A12**	1.94	1.95	0.97	0.96

PROM1	0.52	0.20	4.15	2.36	**SUPT4H1**	0.30	0.32	2.80	2.71	**DMXL2**	0.30	0.26	3.25	3.12
EPB41L2	0.69	0.65	4.93	4.55	**SELENOW**	0.56	0.53	2.15	1.55	**NUP210**	0.44	0.46	3.33	3.71
EPB41	0.68	0.85	2.07	1.77	**TUBA4A**	0.14	0.18	2.89	2.81	**PNISR**	0.26	0.38	1.58	1.64
EPB41L1	0.36	0.80	2.98	3.20	**DLG1**	0.15	0.16	2.17	2.46	**ABHD5**	0.88	0.73	2.72	2.19
DNPH1	0.48	0.23	3.72	3.37	**SRPK1**	0.27	0.29	3.14	2.70	**NUP133**	0.34	0.89	1.66	3.05
SYNGR1	0.35	0.44	2.79	2.95	**ABCA4**	1.61	1.38	4.58	4.31	**CHAC2**	1.73	2.09	1.53	1.74
GTPBP6	0.63	0.54	1.61	1.57	**GSTO1**	1.28	1.15	5.21	4.95	**SNRNP27**	0.72	0.77	2.20	2.32
ZBTB14	0.59	0.58	2.11	2.23	**ARG2**	0.67	0.68	2.79	3.03	**MADD**	0.39	0.85	2.87	4.28
ORC5	1.57	1.87	1.59	2.99	**MAP1A**	0.19	0.26	4.80	5.58	**DNAJC9**	0.37	0.53	2.73	3.05
PDE6D	0.26	0.39	3.35	3.65	**SSBP2**	0.07	0.27	2.41	3.15	**AHCTF1**	0.72	0.75	3.31	3.36
RAD21	0.38	0.33	3.43	3.74	**HMGN5**	0.70	0.73	4.49	4.89	**PIEZO1**	1.03	0.64	1.53	1.08
LZTS3	0.64	0.79	1.61	1.45	**PPP2R2B**	0.19	0.59	1.35	2.34	**FAM3C**	0.55	0.32	3.71	1.75
MCM3AP	0.71	1.41	1.76	2.91	**SORD**	0.42	0.41	5.19	4.60	**H1-10**	0.57	0.23	5.91	3.08
PICALM	0.12	0.31	2.66	3.44	**PRCD**	0.35	0.35	1.88	1.86	**SNX19**	0.50	0.82	2.80	2.87
RAD1	1.82	1.95	1.20	1.46	**SPTBN1**	0.14	0.44	4.19	4.33	**PHF3**	1.32	0.99	1.75	0.98
EIF1B	0.21	0.31	2.10	4.76	**SRSF2**	0.43	0.52	2.09	2.55	**NUP205**	0.67	0.74	3.09	3.13
TIMM17B	0.36	0.36	2.46	3.27	**ANK2**	0.14	0.12	4.62	5.55	**ANP32B**	0.23	0.33	3.45	4.48
DNAJC6	0.43	0.77	2.60	3.69	**NAAA**	2.23	2.32	1.11	1.17	**HTRA1**	0.90	0.25	4.55	2.75
DNAJB6	1.09	1.84	4.81	2.72	**BDH1**	0.62	0.43	3.20	3.21	**DPF3**	0.51	0.78	2.25	4.42
PTP4A3	0.22	0.44	2.33	2.94	**NUCB1**	0.20	0.18	3.45	3.28	**RPGR**	0.67	0.56	5.78	4.17
SF3B1	0.23	0.42	2.64	3.54	**GUCY2D**	1.11	0.88	4.35	3.96	**TANK**	0.92	0.45	1.44	1.00
LYPLA1	0.41	0.39	3.81	3.87	**PPARD**	1.46	1.02	2.39	2.11	**STMN2**	0.23	0.51	3.48	2.64
SURF6	0.47	0.43	2.94	1.81	**ROM1**	0.58	1.04	2.51	3.79	**OSBP2**	0.26	0.14	2.22	1.87
IDH1	0.46	0.42	4.82	4.40	**REL**	0.35	0.32	1.91	2.05	**TMEM230**	0.36	0.40	2.10	1.27
SMNDC1	0.48	0.60	2.97	3.07	**EML5**	1.69	1.43	1.15	1.31	**C18orf25**	0.34	0.77	2.04	3.51
CPD	0.29	0.28	2.26	1.72	**PPAT**	0.29	0.38	2.86	2.62	**LENG9**	0.75	1.69	1.93	2.86
RGS20	0.51	0.84	1.61	2.28	**KHDRBS1**	0.25	0.30	2.94	4.89	**PYCR2**	1.29	0.00	3.89	1.19
SLC22A5	2.31	2.46	4.25	4.77	**BCL2L1**	0.68	1.36	2.66	3.82	**DCPS**	0.44	0.40	4.21	4.15
B3GAT3	1.03	0.33	4.91	2.51	**GOLGA2**	0.29	0.19	3.31	2.36	**FLYWCH2**	0.37	0.35	2.81	2.25
NFASC	0.49	0.51	5.64	5.68	**MGAT3**	0.30	0.33	2.11	2.74	**SLC25A36**	3.00	3.25	1.08	0.94
UFL1	0.35	0.37	4.95	4.54	**GALNT2**	0.34	0.25	3.97	3.07	**SLC25A33**	2.05	2.01	0.86	1.01
NDUFB4	0.25	0.21	3.31	3.06	**NUP160**	0.53	0.60	3.15	3.06	**YIPF6**	0.75	1.02	2.43	1.96
UNC5C	1.76	1.60	2.16	1.54	**LMAN2**	0.69	0.44	5.43	5.59	**RNF31**	1.27	1.19	1.06	1.00
RTN3	0.35	0.21	1.85	2.42	**ANK3**	0.24	0.21	3.31	3.29	**MMAB**	0.85	0.51	3.11	1.55
VAPA	0.32	0.01	3.97	3.05	**BNIP3**	1.89	1.03	2.96	0.93	**WDR89**	0.55	0.49	1.55	1.38
PIGN	0.92	0.56	1.88	1.22	**CSTF3**	0.30	0.38	3.53	2.77	**DPH3**	0.40	0.70	1.96	2.21
ADGRL2	0.21	0.19	2.87	2.17	**PAK1**	0.32	0.12	4.25	2.71	**FAM89A**	1.98	1.92	1.85	1.68
SFT2D2	0.47	0.42	2.79	1.81	**PRDX4**	0.11	0.27	2.95	4.04	**C16orf74**	0.82	0.58	4.27	3.12
ATP6V1G2	0.29	0.30	2.42	3.33	**CBX3**	0.27	0.31	5.06	3.98	**APIP**	0.46	0.62	2.77	2.98
CEP43	0.77	0.75	3.09	2.64	**STX3**	1.00	0.86	6.03	4.92	**REEP6**	0.29	0.28	3.12	2.57
RAB3D	0.27	0.23	2.66	1.07	**PDCL**	0.07	0.58	2.10	2.47	**DDRGK1**	0.44	0.38	2.64	2.30
LSM8	0.20	0.25	2.95	3.11	**MAB21L1**	0.48	0.82	3.22	4.35	**NARS2**	0.41	0.37	2.26	2.47
WIZ	0.40	1.01	1.57	3.36	**XRCC4**	0.30	0.35	3.15	3.37	**NSL1**	0.76	0.81	2.93	2.81
NUDT14	0.36	0.44	1.94	2.10	**TCOF1**	0.41	0.37	2.88	2.84	**CDK5RAP3**	0.31	0.27	2.99	2.25
DDAH2	0.44	0.53	5.35	3.23	**SF3B2**	0.22	0.43	3.69	5.37	**CDHR1**	0.68	1.28	3.64	4.26
OLFM2	0.59	0.39	3.06	2.17	**CAMK2B**	0.19	0.20	3.93	3.40	**CLMN**	0.50	0.55	1.82	1.96
ACTL6A	0.22	0.44	2.77	2.84	**SNW1**	0.40	0.95	2.42	3.44	**ZNF512B**	0.84	0.64	2.24	1.70
PNP	0.27	0.57	4.53	4.55	**IQGAP2**	0.25	0.03	4.13	4.64	**NSMCE3**	0.66	0.88	1.54	2.13
HPRT1	0.41	0.42	4.07	4.21	**KRR1**	0.46	0.66	1.27	1.98	**ZMAT2**	1.65	1.82	1.81	2.96
AK1	0.48	0.74	4.39	4.43	**THOC5**	0.96	0.60	1.64	1.39	**CFAP418**	0.42	0.56	2.64	2.63
IGHG1	3.42	2.41	3.06	2.65	**SPTAN1**	0.26	0.33	4.13	4.01	**TRPM7**	0.89	0.26	1.95	1.15

HLA-B	0.79	0.44	3.44	3.73	**BLMH**	0.24	0.27	3.87	3.36	**PANX1**	1.52	1.25	1.58	1.36
OPN1SW	3.23	2.88	5.66	5.02	**CNGB1**	0.87	0.90	2.88	3.95	**PASK**	0.40	0.78	2.30	3.52
HMGN1	0.61	0.60	4.22	4.25	**RAB33A**	0.46	0.11	1.25	1.34	**INTS14**	0.42	0.61	1.26	1.51
SLC25A4	0.23	0.05	3.73	2.74	**MPP2**	0.20	0.46	3.28	4.35	**NMNAT3**	0.94	0.55	2.33	1.44
HMGN2	0.12	0.53	2.47	4.80	**DPYSL3**	0.28	0.61	3.36	3.97	**SORT1**	0.34	0.27	2.45	2.74
PRKCB	0.01	0.02	3.70	2.30	**MAP7**	0.40	0.37	2.80	2.70	**SEPHS2**	0.40	0.48	2.07	2.38
GLA	1.58	1.42	6.44	4.87	**FLOT2**	0.27	0.26	3.08	3.02	**PIP5K1A**	0.26	0.34	2.73	2.23
PTMA	0.33	0.58	3.17	4.29	**PLS1**	0.44	0.23	3.58	3.16	**DMAC2L**	0.57	0.76	1.46	2.78
CDK1	0.43	0.53	2.64	3.45	**SMC1A**	0.32	0.27	3.05	2.94	**SLC29A1**	1.11	0.69	3.61	2.95
TPM1	0.35	0.14	2.43	4.21	**DIP2A**	0.47	0.28	4.35	3.94	**BAG1**	0.20	0.46	3.60	3.91
ITGAV	0.37	0.22	4.60	3.14	**MVP**	1.67	1.82	6.09	6.57	**ATF6B**	2.14	2.19	1.45	1.72
DBI	0.34	0.73	2.67	3.88	**CRYM**	2.80	2.68	7.41	6.89	**AKAP9**	0.23	0.55	2.13	3.27
ACYP1	0.43	0.46	3.83	3.47	**NUMA1**	0.52	0.36	4.59	3.75	**DPYSL5**	0.28	0.31	4.74	4.26
TUBB	0.02	0.17	2.90	2.52	**NTM**	0.30	0.35	4.05	2.59	**BCL7B**	0.02	0.34	1.71	2.52
RHO	4.37	0.53	4.12	1.07	**GAPVD1**	0.22	0.28	2.87	3.34	**NUDT12**	0.37	0.41	2.41	2.75
ASNS	0.35	0.72	2.51	4.16	**POLD3**	0.41	0.52	2.09	1.54	**SGIP1**	0.38	0.50	2.57	3.67
SYP	0.69	0.76	3.35	3.52	**BRD3**	0.33	0.66	2.28	3.12	**GORASP1**	0.16	0.12	2.98	3.00
SNRPB2	0.20	0.38	3.33	2.78	**RHEB**	0.31	0.39	4.76	5.07	**PLCD4**	0.28	0.38	3.03	3.35
ENO2	0.41	0.41	3.48	2.60	**SF3B4**	0.32	0.42	1.68	1.82	**CPPED1**	0.60	0.45	5.02	4.49
SNRPC	0.37	0.44	3.82	4.09	**SF3A1**	0.20	0.36	3.02	4.24	**RTBDN**	2.09	1.37	3.28	1.35
GSTM1	0.15	0.03	2.05	1.46	**SS18**	1.79	2.34	1.05	1.41	**LRRC1**	0.26	0.22	3.27	2.38
ANXA4	0.94	0.59	7.31	5.33	**NPTX1**	0.75	0.76	2.37	2.38	**ABHD14A**	1.19	2.09	1.22	2.10
HNRNPA1	0.18	0.34	2.35	3.09	**VAMP3**	0.16	0.12	2.03	1.71	**DUSP23**	0.86	0.90	3.54	3.41
SNRPA1	0.48	0.51	3.94	3.26	**USF2**	0.00	0.80	2.46	3.71	**ALG8**	0.40	1.00	3.13	4.32
ALDOC	0.54	0.49	4.85	4.72	**ATP6AP1**	0.20	0.23	3.69	2.26	**NUP85**	0.47	0.55	3.17	3.45
C4B_2	1.89	0.03	3.82	3.93	**VPS72**	0.75	3.51	1.70	1.14	**HIRIP3**	0.69	0.71	2.53	2.61
H2AC12	0.62	0.05	3.31	1.07	**PCK2**	0.46	0.33	3.90	2.91	**SFXN3**	0.63	0.50	4.83	3.81
HLA-C	0.55	0.44	3.40	4.68	**TPD52L1**	0.38	0.32	1.78	1.70	**RBM24**	0.71	1.05	1.11	1.44
H1-2	0.23	0.40	4.54	4.77	**IMPG1**	0.48	0.66	4.33	5.07	**TM2D2**	1.96	1.71	2.38	1.47
SAG	0.34	1.08	4.57	5.66	**ARHGAP44**	1.52	1.69	2.90	3.73	**BBS2**	0.21	0.62	3.20	4.95
ARRB1	0.29	1.07	2.17	4.49	**KNOP1**	1.71	1.86	1.02	1.09	**PACSIN1**	0.30	0.50	4.10	4.14
PTPRF	0.44	0.43	2.90	2.86	**PDS5A**	0.35	0.53	4.16	4.27	**ITPA**	0.37	0.44	4.20	3.98
PRKAR1A	0.26	0.33	4.14	5.49	**ZNF423**	1.45	1.66	1.31	1.52	**PECR**	2.14	2.18	1.89	1.73
HSPA2	0.22	0.30	2.35	2.52	**PWWP3A**	1.84	0.72	1.21	0.99	**CADM1**	0.80	0.60	5.05	3.72
ACADM	1.31	1.35	6.48	5.23	**GFOD2**	0.47	0.47	3.03	3.23	**GTPBP4**	0.84	1.04	2.11	3.01
GNAT1	0.40	0.63	5.27	5.42	**LRIT3**	1.50	0.88	1.57	1.17	**IMPG2**	0.67	0.68	6.00	6.07
PC	0.27	0.20	3.08	2.31	**ARL13B**	0.69	0.86	1.70	1.89	**UCK1**	0.22	0.30	2.70	3.73
PRPS2	0.18	0.08	2.26	4.45	**ALDH1L2**	0.49	0.36	3.56	3.67	**PKIB**	0.17	0.16	1.87	3.14
TPR	0.30	0.24	2.76	2.29	**CERKL**	3.12	2.79	1.74	1.58	**CCSER1**	0.56	0.69	2.21	2.42
MYL4	1.35	0.48	3.90	2.04	**NADK2**	0.68	0.44	3.71	2.61	**ACTR6**	1.23	1.26	1.70	2.08
IFITM1	2.56	0.99	1.92	1.01	**PDCD4**	0.37	0.28	3.96	2.94	**TMEM168**	0.31	0.42	2.49	2.52
PRKAR2A	0.32	0.41	3.12	3.46	**ORMDL2**	1.08	1.19	1.24	1.36	**SIL1**	1.07	0.41	3.10	1.39
GLUL	0.23	0.55	2.97	6.29	**COBLL1**	0.44	0.62	3.67	4.15	**TXNIP**	1.67	1.89	1.76	1.93
B4GALT1	3.85	3.44	2.05	0.94	**TMEM97**	0.82	1.02	2.08	1.73	**TPK1**	0.41	0.41	2.88	2.65
ACADS	1.67	1.10	3.93	3.39	**ZNF326**	0.44	0.38	2.43	2.35	**MFSD1**	3.09	3.43	2.36	2.55
CREB1	0.37	0.44	2.43	2.71	**IGSF11**	0.88	0.60	4.00	2.57	**DNAJC5**	0.24	0.31	2.70	3.49
H1-3	4.32	5.11	1.70	2.34	**KIAA2026**	0.54	0.93	1.89	3.09	**DSN1**	0.59	0.78	1.82	2.04
MGMT	1.03	0.34	3.03	1.51	**PPM1H**	0.27	0.43	4.68	3.01	**ZNF768**	0.13	0.26	3.60	2.73
PDE6A	0.34	0.60	4.03	4.06	**NHLRC3**	0.68	0.44	3.63	2.70	**CCDC134**	0.64	0.53	4.49	2.77

CPE	0.27	0.78	2.63	4.59	**WDR44**	0.30	0.31	4.54	3.20	**TMEM38A**	0.83	0.48	3.33	1.93
STMN1	0.24	0.52	2.67	2.73	**TMEM201**	0.36	0.42	1.73	2.08	**LDAH**	0.81	0.51	5.52	5.01
PRKACA	0.41	0.42	3.99	3.37	**C1orf167**	4.95	5.32	4.95	5.29	**SH2D4A**	1.51	2.40	1.63	2.41
ARF4	0.03	0.15	2.55	2.17	**NUP188**	0.46	0.67	1.94	4.28	**GORASP2**	0.30	0.36	3.13	3.71
PDE6G	0.29	0.64	2.76	3.94	**HYI**	0.47	0.38	3.96	4.17	**QTRT2**	0.44	0.56	2.78	4.24
POLR2C	0.24	0.38	2.41	3.22	**MPP7**	0.57	0.38	3.24	3.39	**COPS7B**	0.27	0.25	2.21	2.29
RAB3B	0.56	0.47	4.10	3.18	**TMEM63B**	0.50	0.62	2.05	1.62	**CERS4**	0.38	0.41	2.59	2.51
MSH3	0.73	0.93	3.67	4.85	**TMTC3**	0.45	0.18	1.45	1.95	**LIN7B**	0.47	0.51	1.77	1.63
GUCY2C	1.11	0.88	5.77	4.57	**DDI2**	0.49	0.55	3.46	3.15	**XPO5**	0.21	0.43	2.55	3.23
M6PR	0.73	0.48	4.43	3.67	**DDI1**	0.49	0.55	0.89	0.91	**SCPEP1**	1.65	1.48	2.31	2.27
NT5E	0.53	0.50	2.47	2.52	**LRCH1**	0.35	0.49	1.68	2.27	**NMRAL1**	2.79	3.70	1.60	2.08
CD9	0.75	0.38	4.19	2.95	**LYPLAL1**	0.77	0.34	3.95	1.97	**VEZT**	0.52	0.37	1.96	1.91
FBL	0.34	0.70	2.39	4.97	**BSPRY**	0.51	0.43	1.64	1.67	**NCOA5**	0.38	0.55	3.30	3.00
PRKACB	0.40	0.44	3.33	3.82	**EGFLAM**	0.89	0.86	5.65	4.40	**ANKH**	0.76	1.35	1.60	2.44
GIGYF2	0.03	0.45	2.41	2.80	**FMN1**	0.64	0.93	3.59	3.99	**ZDBF2**	1.09	0.58	3.28	2.20
WARS1	0.21	0.24	3.74	3.70	**BRAWNIN**	1.90	2.88	1.98	2.45	**EPB41L5**	0.32	0.36	3.65	3.39
PRPH2	0.49	0.85	3.00	4.66	**ANKRD40**	0.76	0.46	1.54	1.26	**JPH1**	1.84	1.33	1.01	0.98
TNC	0.87	1.07	5.54	6.61	**UHRF1BP1**	0.81	0.38	3.35	2.58	**CABP5**	0.90	0.94	3.16	2.62
CDK2	0.48	0.43	2.56	2.41	**ZNF787**	0.26	0.40	2.26	2.05	**NGRN**	1.59	1.66	1.36	1.71
NFYB	0.75	0.80	1.55	2.07	**SDE2**	0.34	0.33	1.47	1.61	**GPR108**	1.10	0.68	3.69	2.93
DNMT1	0.22	0.22	3.26	2.85	**SLC18B1**	3.24	2.69	1.48	1.25	**LUC7L**	0.28	0.40	2.62	3.22
HMGB2	0.50	0.40	4.73	3.75	**SLC25A24**	0.69	0.21	5.08	2.98	**TRIM36**	0.48	0.35	3.92	4.05
COL8A1	1.47	1.08	2.13	1.57	**RINT1**	0.90	0.57	2.40	1.30	**RTN4**	0.36	0.22	3.89	2.94
CD82	0.97	0.90	3.10	3.19	**ZCCHC8**	0.41	0.25	2.22	1.57	**RPRD1B**	0.26	0.28	2.35	2.42
GSTM2	0.35	0.21	3.46	2.67	**LLGL2**	0.55	0.61	3.22	3.58	**MIEF1**	0.86	0.68	2.48	1.70
TPP2	0.98	1.39	7.83	7.84	**BLOC1S2**	0.41	0.50	2.08	1.77	**BIRC6**	0.33	0.44	2.47	2.33
EPHA3	1.08	1.23	0.95	0.94	**SMARCD2**	0.32	0.68	1.81	1.75	**DDX21**	0.68	0.61	2.36	2.23
MPG	0.32	0.36	1.59	1.84	**RANBP10**	0.29	0.47	1.74	2.53	**ASAH2**	0.44	0.45	2.26	1.76
DDT	0.30	0.41	2.89	3.33	**DSTYK**	2.53	2.83	1.87	1.70	**SLC17A5**	0.75	0.64	1.94	1.65
GSTT1	0.67	0.25	4.11	3.95	**CCDC149**	1.88	1.24	2.11	0.98	**FBXO6**	4.62	4.56	5.26	2.43
SERPINB1	1.57	1.52	5.79	4.87	**MOB3C**	0.26	0.19	1.04	1.83	**UBQLN1**	0.07	0.02	2.83	3.28
CHRNB4	0.88	2.05	1.90	3.36	**HECW1**	1.54	0.98	0.96	1.42	**RAB6B**	0.27	0.09	5.28	2.74
PRKAR2B	0.35	0.46	3.30	3.71	**SV2B**	0.37	0.40	4.13	4.38	**MDN1**	0.42	0.71	3.27	3.04
L1CAM	0.70	0.45	5.19	3.72	**BZW1**	0.12	0.49	2.97	2.58	**LIN7C**	0.11	0.15	2.44	3.84
CCKBR	1.51	1.29	3.54	3.22	**MON1B**	0.43	0.57	1.89	2.83	**INTS10**	0.54	0.87	1.99	2.47
CHRNA3	0.34	1.18	2.30	4.47	**NDUFAF7**	0.38	0.45	1.94	2.93	**TMEM38B**	0.39	0.57	1.93	2.74
CTH	1.19	0.87	6.26	5.77	**LPCAT2**	0.67	0.47	5.77	5.03	**AIG1**	0.81	0.57	3.08	2.79
ACSL1	0.54	0.52	3.67	3.30	**RAB11FIP2**	1.21	1.05	2.14	1.94	**BSDC1**	0.45	0.28	4.84	3.23
EPHX2	0.73	0.44	5.56	4.78	**DYM**	0.40	0.35	2.44	1.80	**TRMT1**	0.47	0.68	2.40	3.00
RCVRN	0.45	0.80	4.91	5.13	**NEGR1**	0.22	0.39	2.60	4.62	**CLDND1**	1.05	1.09	2.21	1.42
MYH10	0.46	0.01	1.50	1.55	**GPR155**	1.39	1.02	1.74	1.33	**AIPL1**	0.34	1.64	3.62	6.53
MYH11	0.32	0.07	3.17	3.77	**CACNA2D4**	1.11	1.05	2.92	2.63	**PALS2**	0.51	0.49	2.78	2.00
BSG	1.11	0.63	6.13	5.06	**RD3**	0.69	1.01	4.90	5.35	**IGSF9**	1.01	0.83	1.31	1.16
DEK	0.25	0.47	4.21	3.97	**RAI1**	1.35	0.99	1.67	1.04	**CGN**	0.30	0.37	4.01	3.42
ATP7B	1.30	1.41	1.12	0.94	**CPLX4**	0.77	0.50	3.00	2.34	**RBM27**	0.31	0.44	2.67	2.25
PPM1A	0.18	0.23	3.17	3.35	**NPM2**	2.54	3.21	2.94	3.44	**LRIT1**	0.58	1.24	2.64	3.57
KRT2	0.65	1.55	1.18	1.26	**SETD3**	0.34	0.47	2.70	3.60	**OPTC**	0.32	0.38	2.24	2.98
PDE6B	0.25	0.95	3.00	5.73	**TTC7B**	0.32	0.63	2.03	3.18	**CFDP1**	0.50	0.44	3.20	3.38
ATP6V1E1	0.21	0.28	3.24	3.91	**METTL3**	0.34	0.40	2.16	3.29	**LRWD1**	0.27	0.72	3.07	3.94

ARR3	0.57	0.30	4.40	3.06	**TLK1**	0.60	0.44	2.03	1.20	**CGGBP1**	0.22	0.21	3.23	2.41
TALDO1	0.57	0.53	4.30	3.92	**VPS36**	0.51	0.50	4.14	3.30	**SUN2**	0.26	0.38	1.71	2.15
ANP32A	0.28	0.37	4.22	4.26	**PPFIBP1**	0.61	1.08	2.67	3.69	**SHPK**	0.33	0.36	3.69	3.92
PBX2	0.43	0.40	3.15	3.29	**GLB1L2**	0.38	0.49	1.66	2.23	**AMACR**	0.58	0.42	2.81	3.99
PBX3	0.43	0.40	1.48	1.61	**DCUN1D3**	0.28	0.56	1.94	2.76	**POLG2**	0.92	0.61	1.65	1.20
ETV3	1.21	0.61	1.79	1.10	**CCAR1**	0.25	0.38	4.22	5.36	**SLC12A6**	0.73	0.65	1.99	1.72
TMPO	0.58	0.25	2.11	3.02	**AMOTL1**	1.81	2.88	0.95	0.99	**SLC12A4**	0.48	0.40	1.68	1.45
MTREX	0.28	0.21	1.80	2.28	**HACE1**	0.29	0.63	2.10	3.50	**XPO7**	0.30	0.23	5.26	3.39
MCAM	0.63	0.43	3.99	3.42	**WDR17**	0.32	0.28	1.80	1.40	**TRMT6**	0.32	0.59	2.07	3.25
MSH2	0.33	0.47	2.83	3.45	**ABCA7**	0.99	0.69	5.26	3.33	**PTBP2**	0.19	0.44	2.20	3.38
TSFM	0.55	0.74	4.44	3.46	**CLYBL**	0.71	0.39	2.40	1.57	**CROT**	0.26	0.25	3.00	2.31
PHKA1	0.97	0.60	2.06	2.30	**MIER1**	0.58	0.49	2.88	2.25	**PARP4**	1.01	1.02	2.71	2.75
TESMIN	1.58	1.08	2.23	1.39	**CA5B**	1.34	1.80	1.38	1.78	**RCOR1**	0.46	0.80	1.44	1.90
ATP6V1D	0.27	0.41	2.38	2.78	**MAST1**	0.30	0.29	1.88	2.70	**DNPEP**	0.73	1.09	3.78	4.48
SRPRB	0.61	0.23	6.47	3.13	**EPB41L3**	0.67	0.85	5.61	8.07	**ZMYND8**	0.33	1.13	1.96	3.67
CLIC4	0.25	0.32	3.35	3.46	**MAP3K2**	1.93	0.09	1.24	2.28	**MYO5B**	0.43	0.34	3.49	3.08
DYNC1LI1	0.23	0.18	2.75	3.74	**WBP11**	0.25	0.60	3.49	4.39	**CA14**	0.63	0.33	5.29	4.22
AK5	0.43	0.71	2.60	2.34	**NOP58**	0.46	0.59	4.12	4.60	**PLA2G4C**	0.63	0.34	3.44	2.53
DDX49	1.52	1.39	2.89	2.86	**RNF11**	1.23	0.97	1.51	1.26	**WASF3**	0.49	0.33	4.00	4.03
FAM169A	0.30	0.31	3.39	3.34	**NOC2L**	0.87	0.96	1.60	2.28	**CORO2B**	0.31	0.34	3.78	4.22
SMC3	0.30	0.54	3.93	4.61	**C2CD2**	0.55	0.55	1.90	2.88					
PIN4	0.49	0.57	3.61	4.80	**DCAF1**	0.45	0.28	2.76	2.51					

Appendix 20| Components of signalling pathways including WNT, NOTCH and HIF1 are significantly different between patient A and patient B RO KEGG pathway analysis was performed using ShinyGO to identify significantly enriched pathways among proteins of higher abundance in **(A)** patient A and **(B)** patient B iPSC-derived RO. Top 50 significantly enriched pathways are depicted (FDR=0.05)

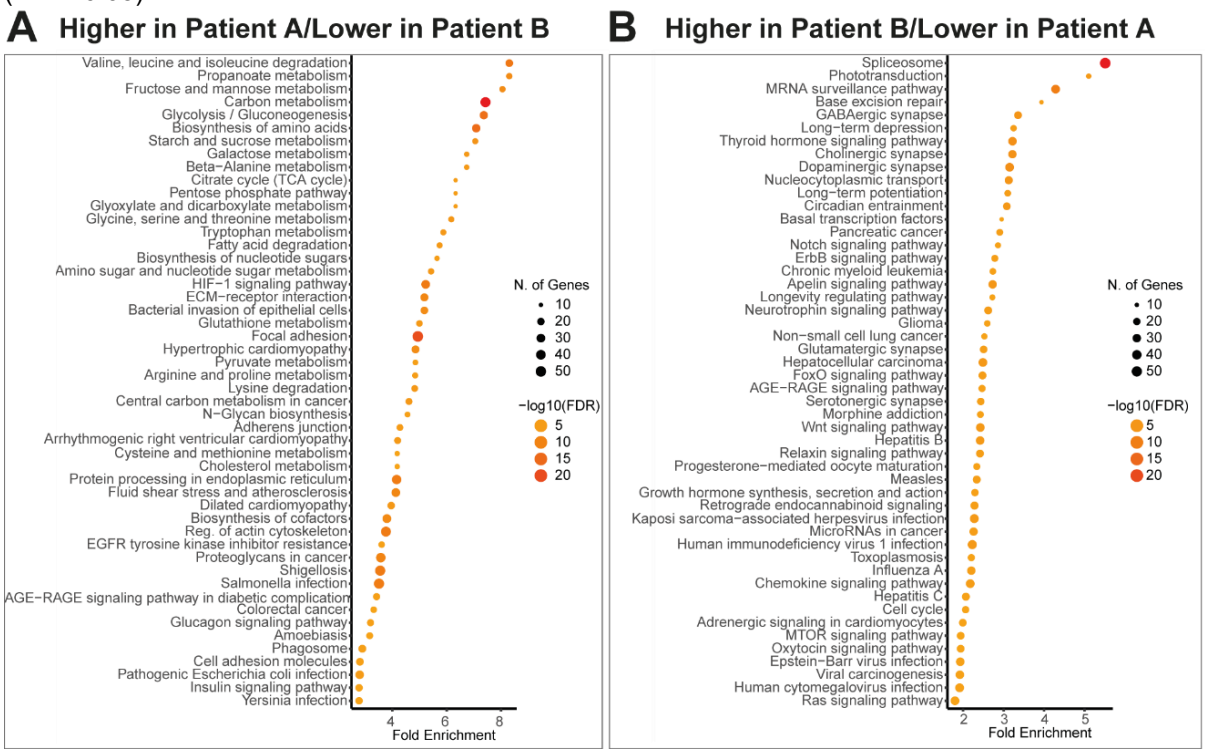

Appendix 21| Overview of the significantly different proteins between RO of patient A and patient B Table depicts gene name together with the log_2 ratio (Patient A/K5) and (Patient B/K5) as well as the corresponding $–log_2$ p-values. Two-sided t-test, FDR 0.05, S0=0.1, n=3

Gene	Log_2 ratio (Patient A/K5)	Log_2 ratio (Patient B/K5)	$-log_2$ p-value (Patient A vs K5)	$-log_2$ p-value (Patient B vs K5)	Gene	Log_2 ratio (Patient A/K5)	Log_2 ratio (Patient B/K5)	$-log_2$ p-value (Patient A vs K5)	$-log_2$ p-value (Patient B vs K5)	Gene	Log_2 ratio (Patient A/K5)	Log_2 ratio (Patient B/K5)	$-log_2$ p-value (Patient A vs K5)	$-log_2$ p-value (Patient B vs K5)
ABCA7	0.99	0.69	5.26	3.33	**GNGT1**	0.28	0.50	3.49	4.10	**PLCB4**	-0.72	-0.01	2.39	0.16
ABL2	-0.14	0.26	1.20	2.01	**GNGT2**	0.32	0.48	3.40	2.43	**PLCE1**	-1.40	-0.34	2.84	1.00
ACADVL	-0.09	-0.42	1.99	4.68	**GPC6**	-0.15	-0.56	0.03	1.16	**PLCG1**	-0.08	-0.47	0.24	3.75
ACTA1	0.13	-0.59	0.84	2.21	**GRK7**	-0.04	0.50	0.15	2.72	**PLEKHB1**	-0.73	0.57	0.77	1.65
ACTN1	-0.10	-0.30	2.86	4.06	**GUCA1A**	-0.18	0.58	0.46	2.67	**PLS1**	0.44	0.19	2.19	0.07
AIPL1	0.34	1.64	3.62	6.53	**GUCA1B**	-0.49	0.54	0.70	2.03	**PML**	-0.58	0.18	1.51	0.88
AKT1	-0.52	0.03	3.70	0.13	**GUSB**	0.97	-0.20	5.03	2.15	**PPFIA2**	-0.09	0.55	2.27	0.88
AKT2	-0.14	0.00	3.40	1.17	**GYG1**	0.05	-0.49	1.01	3.79	**PPP2R5C**	0.20	0.62	0.74	0.46
ALDOA	0.13	-0.35	0.24	3.66	**HDAC1**	-0.25	0.44	0.75	2.27	**PRICKLE2**	-0.30	0.16	2.53	1.32
ALDOC	0.54	0.49	4.85	4.72	**HDAC2**	-0.24	0.35	1.70	2.87	**PRKACB**	0.40	0.44	3.33	3.82
APC	-0.60	-0.18	1.25	0.15	**HK1**	0.21	-0.05	3.79	1.33	**PRKCA**	0.03	0.07	0.68	0.35
APOB	0.73	-0.15	3.03	0.49	**HK2**	0.13	-0.26	3.74	1.49	**PRKCB**	0.01	0.02	3.70	2.30
ARL6	-0.08	0.94	0.12	3.68	**HKDC1**	0.24	-0.04	3.07	4.74	**PRMT6**	-0.35	0.29	2.02	1.68
ATM	0.18	0.37	2.24	4.11	**HSP90AA1**	-0.03	-0.09	0.50	0.92	**PRRT2**	-0.63	-0.25	3.34	2.28
ATP13A2	0.54	0.01	1.78	0.06	**HSP90AB1**	-0.20	-0.31	1.55	0.60	**PSAP**	0.32	0.08	3.60	2.28
BAG3	0.07	-0.72	1.44	5.13	**HSP90B1**	0.33	-0.21	5.06	3.50	**PSEN2**	-0.28	-0.17	2.61	3.18
BANP	-0.71	0.99	0.30	1.77	**HSPA5**	0.31	0.07	3.89	1.46	**PXN**	0.39	0.05	3.98	0.27
BAX	0.02	-0.32	0.01	2.49	**HSPA6**	0.18	-0.15	2.65	1.37	**RASA4**	-1.08	0.55	4.79	4.60
BBS1	0.05	0.40	0.87	3.71	**HSPA9**	0.44	0.41	3.70	0.44	**RASAL2**	-0.08	0.23	0.68	2.49
BBS2	0.21	0.62	3.20	4.95	**HSPB8**	0.37	-0.05	3.54	0.74	**RASGRF2**	0.27	0.51	1.84	2.79
BBS5	0.03	0.68	0.03	2.98	**HSPD1**	0.21	-0.24	3.62	3.86	**RBBP4**	-0.20	0.31	3.36	2.71
BBS7	0.04	0.48	0.75	3.28	**HSPE1**	0.22	-0.28	3.46	3.23	**RCVRN**	0.45	0.80	4.91	5.13
BBS9	0.05	0.42	0.16	3.04	**IDUA**	0.17	-0.82	2.51	3.63	**RELA**	-0.08	-0.41	0.54	3.21
BCL2	0.44	-0.14	2.16	0.93	**IFT122**	-0.62	0.30	1.80	1.68	**RFC4**	0.30	0.63	1.50	2.73
BCL2L1	0.68	1.36	2.66	3.82	**IFT140**	-0.40	0.28	5.47	3.14	**RGR**	-0.01	0.83	0.26	3.14
BRAF	-0.21	-0.14	0.95	4.23	**IFT172**	-0.81	0.09	2.07	0.49	**RICTOR**	-0.47	-0.04	2.77	0.14
BRSK1	-0.23	0.34	0.18	0.37	**IFT22**	-0.31	0.37	1.80	1.59	**RIMS2**	0.23	0.55	0.47	1.51
CADPS	-0.40	-0.09	3.58	1.21	**IFT27**	-0.31	-0.06	3.79	0.89	**RNF34**	-0.98	0.07	1.81	0.23
CALR	0.23	-0.35	3.22	2.96	**IFT43**	0.03	0.42	0.31	2.10	**ROM1**	0.58	1.04	2.51	3.79
CAMK2A	-0.28	0.10	1.79	2.74	**IFT57**	-0.50	0.19	1.71	0.84	**ROR1**	-0.30	-0.71	2.38	1.48
CAMK2B	0.19	0.20	3.93	3.40	**IFT80**	-0.71	-0.09	1.46	1.10	**RP1**	0.80	1.47	1.87	3.05
CAMK2G	0.02	0.16	0.75	2.35	**IFT81**	-0.49	-0.25	3.11	2.19	**RPA1**	0.00	0.22	0.18	2.67
CCND1	0.13	1.08	0.09	1.65	**IFT88**	-0.41	0.17	2.71	0.99	**RPH3A**	-0.98	-0.32	1.60	0.64
CD44	0.03	0.28	0.24	3.27	**IGF1R**	0.58	0.26	2.45	1.29	**RPL23**	-0.27	-0.04	3.57	0.17
CDHR1	0.68	1.28	3.64	4.26	**IKBKB**	-0.58	0.15	2.06	1.18	**RPS6KB1**	0.67	-0.12	1.09	1.48
CDK1	0.26	0.49	1.26	1.40	**INS**	0.78	-1.09	5.46	3.89	**RPS6KB2**	1.96	0.80	0.53	1.24

CDK5	-0.37	0.26	4.77	3.81	**JMY**	-0.36	0.45	0.76	1.52	**RRM2B**	-0.28	0.08	2.26	2.93
CHD3	-0.51	0.57	0.18	1.73	**KAT2B**	0.08	1.35	0.00	3.98	**RRS1**	-3.52	0.57	1.36	0.20
CHD4	-0.35	0.61	2.01	3.78	**KDM1A**	-0.20	0.43	1.16	3.21	**RS1**	-0.04	0.31	2.23	3.35
CHD8	0.00	2.63	2.48	0.61	**KRAS**	-0.23	-0.07	2.39	1.34	**SEPTIN11**	-0.12	-0.25	0.03	2.06
CHID1	0.02	-0.26	0.51	2.13	**KSR1**	-0.11	0.49	1.70	4.53	**SEPTIN5**	-0.42	-0.18	4.04	3.47
CHRNA3	0.34	1.18	2.30	4.47	**LDHB**	-0.05	-0.23	0.58	2.59	**SERPINH1**	0.14	-0.32	3.88	3.88
CHUK	-0.72	-0.18	2.17	0.08	**LIMA1**	0.40	0.06	1.72	0.42	**SFRP2**	-0.57	0.10	2.52	1.91
CLGN	0.03	-0.43	0.87	4.16	**LIN7A**	0.19	0.36	3.50	2.96	**SGSH**	0.60	-0.26	3.27	1.34
COMP	1.09	-0.29	3.37	0.28	**LIN7B**	0.47	0.51	1.77	1.63	**SHC1**	0.29	-1.14	0.33	1.34
CPLX2	-0.66	-0.09	2.78	0.75	**LIN7C**	0.11	0.15	2.44	3.84	**SIRT1**	0.02	0.29	0.08	2.90
CREBBP	0.03	0.32	0.50	1.07	**LUM**	1.90	0.28	4.35	0.80	**SLC32A1**	-0.70	-0.01	2.87	0.37
CSNK2A1	-0.22	0.10	2.04	0.92	**MAML2**	0.20	0.58	0.98	2.44	**SMAD3**	-0.06	0.11	0.94	1.85
CSNK2A2	-0.26	0.08	2.96	1.36	**MANBA**	0.89	0.52	3.66	2.21	**SNAP47**	0.18	0.84	0.75	2.65
CTBP1	0.20	0.51	2.37	2.75	**MANF**	0.33	-0.19	4.75	2.87	**SNCA**	-0.21	0.74	3.21	0.87
CTBP2	0.20	0.43	3.32	4.56	**MAPK1**	-0.49	-0.57	4.80	5.93	**SNCG**	-1.24	-0.20	2.84	0.57
CTH	1.19	0.87	6.26	5.77	**MAPK10**	-0.79	-0.42	2.16	2.43	**SNW1**	0.40	0.95	2.42	3.44
CTNND2	-0.01	0.03	0.58	0.98	**MAPK14**	-0.52	0.51	2.41	2.75	**SORBS1**	0.12	-0.58	1.68	3.06
CXXC4	-0.02	0.52	0.38	1.56	**MAPK8**	-0.54	-0.08	1.46	2.13	**SRPRA**	0.24	-0.09	1.88	0.35
DDX5	0.06	0.15	0.86	3.23	**MBD3**	-0.90	0.43	1.05	0.81	**SRPRB**	0.61	0.23	6.47	3.13
DNAJB1	0.12	-0.02	3.70	0.34	**MBTPS1**	-0.29	-1.01	0.72	3.18	**STK4**	0.20	0.47	0.19	1.83
DNAJB11	0.40	-0.03	4.75	1.18	**MEF2C**	0.13	0.37	2.11	5.53	**STX1B**	-0.68	-0.03	3.84	0.51
DNAJC3	0.33	0.00	2.55	0.12	**METAP2**	-0.49	0.07	3.61	2.94	**STXBP5**	0.09	0.37	0.29	1.31
DTX3	-0.79	0.73	3.15	4.22	**MLST8**	-0.03	0.29	0.30	1.58	**SUPT16H**	-0.91	0.81	1.17	2.60
DVL1	1.95	2.63	0.89	1.86	**MRE11**	-0.22	0.24	1.75	2.11	**SYN1**	-0.61	0.03	3.36	0.77
DVL2	2.68	3.43	1.02	0.31	**MTA2**	-1.00	-0.24	2.18	5.12	**SYN2**	-0.61	0.03	2.10	0.63
EGF	0.84	0.15	2.01	0.95	**MTOR**	0.03	0.26	0.71	3.85	**SYN3**	-0.53	-0.19	3.06	1.53
EGFR	0.09	-0.37	1.31	1.88	**MYDGF**	0.14	-0.32	2.63	2.60	**SYNJ1**	0.07	0.23	0.66	0.01
EGLN1	0.05	-0.24	0.31	2.06	**MYH10**	0.32	0.07	0.27	1.38	**SYT1**	0.02	0.32	0.35	2.09
EHD1	0.19	0.27	1.13	1.70	**MYH14**	0.32	-0.05	5.68	0.87	**SYT11**	-1.48	-0.71	2.10	3.44
EHD3	0.16	0.03	0.76	0.28	**MYH9**	0.20	-0.27	4.90	3.76	**SYT2**	0.26	0.44	0.82	2.25
EHMT1	-0.41	0.66	0.91	2.23	**NAGLU**	-0.19	-0.66	1.28	3.50	**TAF5**	-0.59	0.56	2.14	2.51
EIF4EBP1	0.28	-0.49	1.19	1.92	**NAPB**	-0.05	0.17	1.79	4.43	**TAF9B**	-0.55	0.23	1.68	1.32
ENO1	0.09	-0.46	2.60	4.08	**NBN**	-0.35	0.02	1.86	0.64	**TBK1**	-0.28	0.15	2.47	0.99
ENO2	0.41	0.41	3.48	2.60	**NCS1**	-0.64	-0.15	2.77	1.07	**TBL1X**	-0.28	0.43	0.91	0.62
EP300	-0.69	-0.09	0.95	0.11	**NFKB1**	-0.22	-0.55	1.94	2.88	**TBL1XR1**	-0.33	0.37	1.86	1.67
ERBB2	-0.04	-0.54	2.80	1.10	**NGFR**	-0.37	-0.09	3.51	0.65	**TBL1Y**	-0.21	0.51	0.22	0.86
ERO1A	0.78	-0.28	5.31	2.14	**NMT2**	-0.31	0.00	0.31	1.80	**TBP**	0.42	3.43	0.52	3.99
ERP44	0.21	-0.01	3.51	0.08	**NPM1**	-0.29	0.22	3.26	2.24	**TFRC**	0.03	-0.81	0.80	4.48
FAF2	0.00	-0.25	0.27	4.45	**NR2E3**	-1.81	1.56	2.96	6.70	**THBS1**	0.92	-0.66	2.53	2.05
FGF1	-0.67	-0.36	5.88	2.96	**NRXN1**	-0.73	-0.34	1.84	0.21	**THBS4**	1.28	-0.22	3.05	0.68
FHL3	-0.16	-0.72	0.74	3.38	**NRXN2**	-0.94	-0.01	0.93	0.14	**TLN1**	-0.41	-0.65	5.85	7.54
FHOD1	-0.06	-0.33	0.39	1.27	**PAK4**	-0.32	-0.28	2.09	1.84	**TP53RK**	0.12	0.29	1.69	3.25
FLNA	-0.12	-0.50	2.73	3.24	**PDC**	-0.02	0.57	1.98	5.29	**TPM1**	-0.07	-0.70	0.62	1.84
FLNB	-0.12	-0.50	0.60	6.35	**PDE6A**	0.34	0.60	4.03	4.06	**TPM3**	0.49	0.28	2.15	2.16
FMR1	-0.04	0.27	0.36	1.29	**PDE6B**	0.25	0.95	3.00	5.73	**TPM4**	-0.09	-0.79	0.55	3.45
GAA	-0.01	-0.35	0.44	3.59	**PDE6C**	0.39	0.91	2.66	2.83	**TRIM24**	-0.68	0.25	3.05	2.27
GAD2	-0.84	0.44	2.52	1.68	**PDE6G**	0.29	0.64	2.76	3.94	**TRIP6**	-0.21	-0.42	1.20	3.28
GALC	-0.19	-0.69	2.50	4.14	**PDGFRB**	0.13	-0.02	1.06	1.23	**TTC21B**	-0.27	0.31	2.19	2.20
GAPDH	0.28	-0.09	3.98	2.16	**PDIA5**	0.54	0.08	3.14	0.94	**TTC30A**	-0.60	0.52	2.42	2.69
GC	1.07	-0.19	5.48	3.03	**PDIA6**	0.36	-0.25	4.28	3.48	**TTC5**	-0.08	0.46	0.47	2.16
GFPT1	0.37	0.00	2.53	0.11	**PDK1**	0.59	-0.15	3.03	1.06	**TTC8**	0.27	0.69	1.14	3.44

GIPC1	-0.37	0.17	2.00	1.50	**PDLIM2**	-0.24	-0.89	0.04	1.53	**TXNDC5**	0.16	-0.24	2.25	3.52
GLB1	0.10	-0.07	3.71	1.62	**PDLIM3**	0.22	-0.32	2.66	2.23	**UNC119**	-0.18	0.66	1.35	3.70
GNA11	0.10	0.18	1.86	2.68	**PDLIM4**	-0.27	-0.46	3.66	3.46	**UNC13A**	-0.90	-0.43	1.52	1.08
GNAT1	0.40	0.63	5.27	5.42	**PFKL**	0.17	-0.31	3.65	2.52	**USP7**	-0.17	0.24	3.97	4.67
GNAT2	-0.13	0.37	2.21	2.57	**PFKM**	0.22	-0.25	3.55	2.50	**VAPB**	-0.01	-0.16	4.36	0.11
GNB1	0.02	0.29	0.02	2.30	**PFKP**	0.51	-0.36	5.09	4.03	**VCAN**	-0.80	-1.19	5.00	5.54
GNB2	-0.02	0.18	3.15	5.02	**PGK1**	0.55	-0.19	4.60	3.14	**WDR35**	-0.30	0.26	1.74	1.93
GNB3	0.00	0.21	2.98	3.20	**PHLPP2**	-0.32	0.39	1.63	0.70	**WIF1**	-0.82	-0.59	4.08	3.98
GNB5	-0.73	0.09	2.47	1.15	**PIP4K2A**	0.14	0.57	2.76	4.14	**WIPI1**	-0.48	-1.06	1.22	2.06
GNG13	-1.05	-0.44	5.05	2.35	**PIP5K1C**	0.04	0.32	1.18	3.19	**ZNF385A**	-0.17	0.73	1.97	3.79
GNG3	-0.59	0.03	3.08	0.04	**PLA2G6**	-0.49	0.46	1.47	1.89					
GNG7	0.13	0.43	2.08	4.49	**PLCB1**	-0.52	-0.20	3.69	2.58					

Appendix 22| WGS confirmed causal homozygous CRB1 variant in both patients
Read alignment of WGS of patient A and patient B against the human reference genome (GRCh38) visualised using the Integrative Genomics Viewer. Figure depicts the location chr1:197434706-197434706 and confirms homozygous G>A mutation at location chr1:197434706 in both patients, which was annotated as the causal variant according to the diagnostic pipeline. Mismatch due to variant is marked in green. The homozygous variant is annotated as missense and splice region variant.

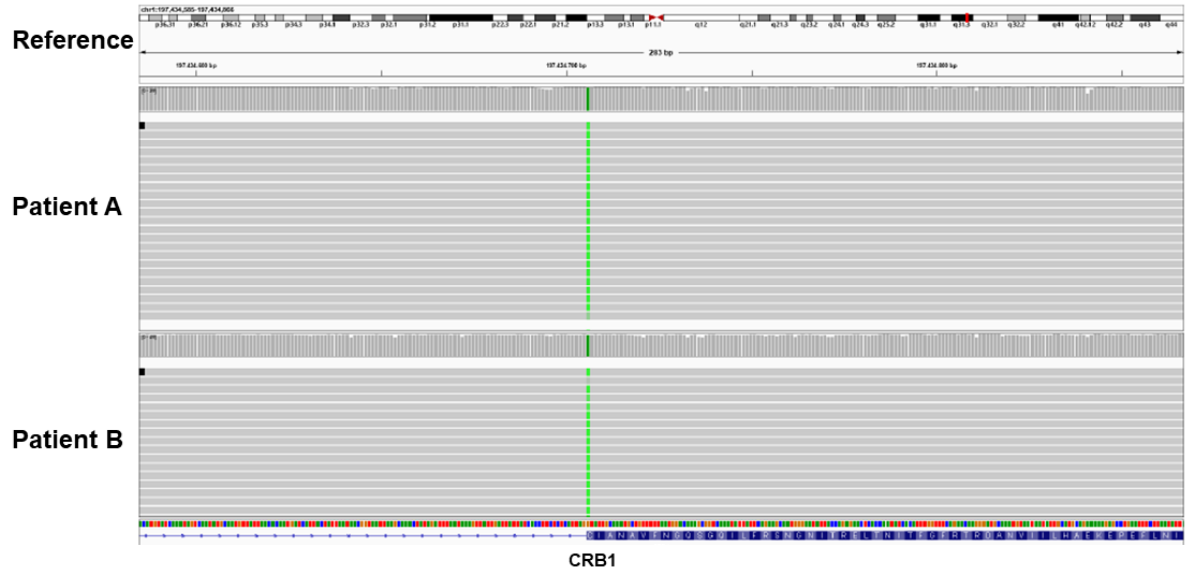

.

Appendix 23| Potential harmful canidates identified by WGS WGS was performed to identify variants that might contribute to the severer phenotype observed in patient A. Variants were selected based on an allele frequency below 0.1 %, potential impact on protein (missense, splice, framshift or stop variants), potential impact on gene expression (3'UTR, 5'UTR, upstream or downstream variants).

chr	start	ref	obs	Patient A	Patient B	gene	Variant	Disease association
5	112842451	C	T	het	wt	**APC**	missense	Colorectal cancer, Brain tumor-polyposis syndrome 2, Desmoid disease, Adenoma, Hepatoblastoma, Gastric cancer, Gastric adenocarcinoma, Gardner syndrome, Adenomatous polyposis coli
17	38512545	C	T	het	wt	**ARHGAP23**	downstream	
19	19054287	A	G	het	wt	**ARMC6**	missense	
11	108271294	A	G	het	wt	**ATM**	missense	Hereditary cancer-predisposing syndrome
6	16327690	C	A	het	wt	**ATXN1**	missense	Spinocerebellar ataxia 1
18	63321768	A	-	het	wt	**BCL2**	upstream	Leukemia/lymphoma
18	63321771	AC	-	het	wt	**BCL2**	upstream	Leukemia/lymphoma
17	66830950	C	T	het	wt	**CACNG5**	upstream	
4	15502479	A	C	het	wt	**CC2D2A**	missense	Meckel syndrome 6, Joubert syndrome 9
2	55285997	G	A	het	wt	**CCDC88A**	upstream	PEHO syndrome-like
2	55285999	G	A	het	wt	**CCDC88A**	upstream	PEHO syndrome-like
18	61333465	A	G	het	wt	**CDH20**	5'UTR	
18	61556184	C	T	het	wt	**CDH20**	downstream	
10	71815192	G	A	het	wt	**CDH23**	missense	Usher syndrome, type 1D, Gaucher disease
11	126065050	A	G	het	wt	**CDON**	upstream	Holoprosencephaly 11
11	126065066	A	G	het	wt	**CDON**	upstream	Holoprosencephaly 11
2	168517514	-	TAATTA	het	wt	**CERS6**	intron	
2	168517515	-	TT	het	wt	**CERS6**	intron	
2	168574370	-	TGTGTGTG	het	wt	**CERS6**	intron	
2	168604391	GTG	-	het	wt	**CERS6**	intron	
2	168604395	G	-	het	wt	**CERS6**	intron	
2	168633162	-	TT	het	wt	**CERS6**	intron	
2	168688828	G	A	het	wt	**CERS6**	intron	
18	11851696	C	A	het	wt	**CHMP1B**	missense	Dystonia 25
16	4419721	G	C	het	wt	**CORO7**	upstream	
20	504473	G	T	het	wt	**CSNK2A1**	intron,3'UTR	Okur-Chung neurodevelopmental syndrome
4	104491490	A	C	het	wt	**CXXC4**	missense	
4	107949437	C	T	het	wt	**CYP2U1**	missense	Spastic paraplegia 56
8	64593234	TGTGT	-	het	wt	**CYP7B1**	3'UTR	Spastic paraplegia 5A
8	64593240	T	-	het	wt	**CYP7B1**	3'UTR	Spastic paraplegia 5A
2	229366978	C	T	het	wt	**DNER**	missense	
5	147408765	G	A	het	wt	**DPYSL3**	missense	
20	46394526	C	T	het	wt	**ELMO2**	5'UTR	Vascular malformation
9	93565146	ATACA	-	het	wt	**FAM120A**	3'UTR	
4	186706708	C	G	het	wt	**FAT1**	missense	
5	141652796	G	C	het	wt	**FCHSD1**	upstream	
7	33011116	T	G	het	wt	**FKBP9**	downstream	Anemia
7	100676196	G	A	het	wt	**GNB2**	5'UTR,intron	Neurodevelopmental disorder with hypotonia and dysmorphic facies
2	156432144	T	G	het	wt	**GPD2**	upstream	Type 2 diabetes mellitus
5	176597502	C	T	het	wt	**GPRIN1**	missense	
14	77333306	G	T	het	wt	**GSTZ1**	downstream	Maleylacetoacetate isomerase deficiency
17	45149855	C	T	het	wt	**HEXIM1**	missense	
9	125234607	-	ATAC	het	wt	**HSPA5**	downstream	
11	66254662	C	A	het	wt	**KLC2**	upstream	Spastic paraplegia, optic atrophy, and neuropathy
11	18391342	G	A	het	wt	**LDHA**	upstream	Glycogen storage disease XI
19	39315249	G	A	het	wt	**LRFN1**	missense	
1	36178169	A	C	het	wt	**MAP7D1**	missense	
11	45909305	C	T	het	wt	**MAPK8IP1**	upstream	Diabetes mellitus, noninsulin-dependent
4	2931921	C	T	het	wt	**MFSD10**	missense	Hypertension
10	72551288	G	C	het	wt	**MICU1**	missense	Myopathy with extrapyramidal signs
5	141371769	G	C	het	wt	**PCDHGA3**	missense	
8	18029283	G	C	het	wt	**PCM1**	downstream	
18	62716721	C	G	het	wt	**PHLPP1**	missense	
6	36856585	C	T	het	wt	**PPIL1**	splice_donor	Pontocerebellar hypoplasia
16	29813278	C	T	het	wt	**PRRT2**	missense	Paroxysmal kinesigenic dyskinesia
7	137223308	-	A	het	wt	**PTN**	downstream	

11	48130501	C	T	het	wt	**PTPRJ**	missense	Colon cancer
2	65130606	C	G	het	wt	**RAB1A**	upstream	
15	89225800	-	AAATA	het	wt	**RLBP1**	upstream	Bothnia retinal dystrophy
1	25797242	G	A	het	wt	**SELENON**	upstream	Myopathy
11	111598678	T	C	het	wt	**SIK2**	upstream	
19	38119400	T	A	het	wt	**SIPA1L3**	missense	
20	4854778	C	T	het	wt	**SLC23A2**	3'UTR	
20	38720610	GGTGTGT	A	het	wt	**SLC32A1**	upstream	
5	123001433	T	C	het	wt	**SNX24**	missense	
4	38014729	G	C	het	wt	**TBC1D1**	missense	
6	37316811	G	A	het	wt	**TBC1D22B**	missense	
16	1510376	G	T	het	wt	**TELO2**	3'UTR	You-Hoover-Fong syndrome
2	229921982	T	G	het	wt	**TRIP12**	5'UTR	Intellectual developmental disorder
10	69448273	A	G	het	wt	**TSPAN15**	upstream	
5	160066252	C	T	het	wt	**TTC1**	downstream	
5	160066252	C	T	het	wt	**TTC1**	downstream	
5	160065005	G	-	het	wt	**TTC1**	frameshift	
15	70668580	C	G	het	wt	**UACA**	missense	
16	77982432	A	C	het	wt	**VAT1L**	downstream	

Appendix 24| Potential protective modifiers WGS was performed to identify variants that might protect patient B from a severe phenotype. Variants were selected based on an allele frequency below 0.1 %, potential impact on protein (missense, splice, framshift or stop variants), potential impact on gene expression (3'UTR, 5'UTR, upstream or downstream variants).

chr	start	ref	obs	Patient A	Patient B	gene	Variant	Disease
19	38645139	A	T	wt	het	**ACTN4**	upstream	Glomerulosclerosis
5	7827204	A	G	wt	het	**ADCY2**	3'UTR	
8	140527549	C	G	wt	het	**AGO2**	3'UTR	Lessel-Kreienkamp syndrome
3	186620776	G	A	wt	het	**AHSG**	missense	Alopecia-intellectual disability syndrome 1
15	85655787	G	A	wt	het	**AKAP13**	missense	
1	243850198	C	T	wt	het	**AKT3**	5'UTR	Megalencephaly-polymicrogyria-polydactyly-hydrocephalus syndrome 2
2	231377515	G	A	wt	het	**ARMC9**	downstream	Joubert syndrome 30
8	61668261	C	T	wt	het	**ASPH**	missense	Traboulsi syndrome
19	48953877	T	C	wt	het	**BAX**	upstream	Colorectal cancer
7	81948104	G	T	wt	het	**CACNA2D1**	3'UTR	
7	134933740	C	A	wt	het	**CALD1**	missense	
17	40138121	A	T	wt	het	**CASC3**	upstream	
10	59787478	A	C	wt	het	**CCDC6**	downstream	
14	99604091	T	G	wt	het	**CCDC85C**	5'UTR	
17	73280410	C	T	wt	het	**CDC42EP4**	downstream	
3	126416330	G	C	wt	het	**CFAP100**	missense	
3	354762	C	A	wt	het	**CHL1**	missense	
3	149176410	G	C	wt	het	**CP**	missense	Hermansky-Pudlak syndrome 3
9	123351196	G	T	wt	het	**CRB2**	upstream	Focal segmental glomerulosclerosis 9
2	219275536	C	G	wt	het	**DNAJB2**	upstream	Spinal muscular atrophy
14	73701944	-	A	wt	het	**DNAL1**	3'UTR	Ciliary dyskinesia
14	72771817	C	T	wt	het	**DPF3**	missense	
19	7957463	T	G	wt	het	**ELAVL1**	upstream	
4	139057356	G	A	wt	het	**ELF2**	3'UTR	
11	33774515	A	G	wt	het	**FBXO3**	5'UTR	
19	7688226	-	TTTG	wt	het	**FCER2,TRAPPC5**	downstream	
19	7688232	-	G	wt	het	**FCER2,TRAPPC5**	downstream	
7	43541235	G	T	wt	het	**HECW1**	missense	
7	43541242	TACA	-	wt	het	**HECW1**	frameshift	
4	8868162	C	A	wt	het	**HMX1**	missense	Oculoauricular syndrome
11	119042073	T	G	wt	het	**HYOU1**	upstream	Immunodeficiency 59 and hypoglycemia
2	216672556	C	T	wt	het	**IGFBP5**	3'UTR	
13	110725933	T	C	wt	het	**ING1**	downstream	Squamous cell carcinoma
10	30011438	C	T	wt	het	**JCAD**	downstream	
1	202719535	A	C	wt	het	**KDM5B**	downstream	Intellectual developmental disorder
11	66261715	C	T	wt	het	**KLC2**	5'UTR	Spastic paraplegia, optic atrophy, and neuropathy
8	142782578	G	-	wt	het	**LYNX1**	upstream	
15	23610811	A	T	wt	het	**MKRN3**	3'UTR	Precocious puberty
17	62623876	C	T	wt	het	**MRC2**	upstream	
20	47634056	A	G	wt	het	**NCOA3**	missense	
15	87866444	T	C	wt	het	**NTRK3**	3'UTR	
10	34815315	G	A	wt	het	**PARD3**	5'UTR	
2	178463091	A	G	wt	het	**PJVK**	downstream	Deafness
11	73646286	G	T	wt	het	**PLEKHB1**	5'UTR	
9	131515503	C	T	wt	het	**POMT1**	missense	Muscular dystrophy-dystroglycanopathy
19	45375626	C	A	wt	het	**PPP1R13L**	downstream	
7	100434432	G	A	wt	het	**PPP1R35**	downstream	
1	56708464	A	G	wt	het	**PRKAA2**	3'UTR	
6	43162077	A	T	wt	het	**PTK7**	downstream	
11	48160049	T	G	wt	het	**PTPRJ**	missense	Colon cancer

2	73080007	G	-	wt	het	**RAB11FIP5**	frameshift	
10	47346224	G	A	wt	het	**RBP3**	upstream	RP 66
14	67699083	T	G	wt	het	**RDH11,RDH12**	upstream	LCA 13
14	67699209	C	T	wt	het	**RDH11,RDH12**	upstream	LCA 13
2	174398443	G	T	wt	het	**SCRN3**	splice_donor	
4	89837063	G	A	wt	het	**SNCA**	5'UTR	Dementia
19	40502838	C	T	wt	het	**SPTBN4**	missense	Neurodevelopmental disorder with hypotonia, neuropathy, and deafness
9	97483101	A	G	wt	het	**TDRD7**	missense	Cataract
9	100320392	G	A	wt	het	**TEX10**	missense	
11	60928869	C	T	wt	het	**TMEM132A**	missense	
8	144432346	G	C	wt	het	**TONSL**	missense	Spondyloepimetaphyseal dysplasia
18	31946066	G	T	wt	het	**TRAPPC8**	upstream	
7	100874220	A	T	wt	het	**TRIP6,SRRT**	upstream	
7	100874220	A	T	wt	het	**TRIP6,SRRT**	upstream	
7	2666201	T	-	wt	het	**TTYH3**	downstream	
15	91006419	T	C	wt	het	**VPS33B**	missense	Arthrogryposis, renal dysfunction, and cholestasis 1
3	185024358	A	G	wt	het	**VPS8**	missense	
8	1956772	G	A	wt	het	**ARHGEF10**	missense	Slowed nerve conduction velocity
17	28713840	C	T	wt	het	**RAB34**	downstream	
19	543116	T	G	wt	het	**GZMM**	upstream	

Appendix 25| Peptides detected for CRB2 in lysates of patient and control RO analysed by mass spectrometry (A) Illustration of the CRB2 protein domains. Colors depict different domains. **(B)** Intensity of the peptides detected in the replicates of full-proteome lysates of iPSC-derived RO of patient A, patient B and control. Not all peptides were detected in all samples. Data is depicted as mean ± SEM.

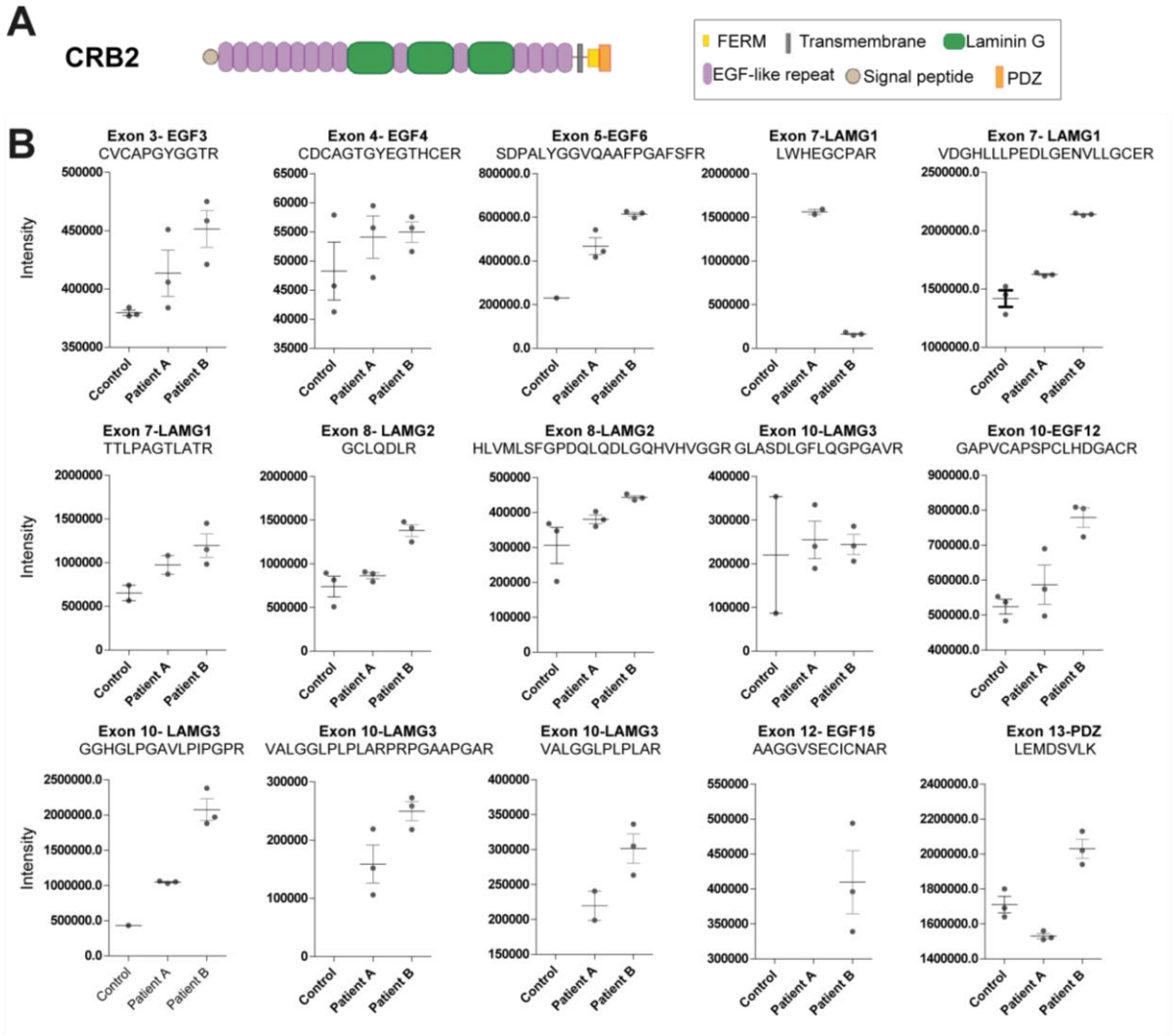

Appendix 26| Overview of the proteins that were significantly higher abundant in CRB2-FLAG samples compared to GFP-FLAG after SDS wash but without incubation of porcine retina lysate Table presents the genes together with the log_2 ratio and the $–log_2$ p-value (One-sample t-test, FDR 0.05, log_2 ratio (CRB3-FLAG/GFP-FLAG) >2, n=6) [1]

Gene	Log_2 ratio (CRB2/ GFP)	$-log_2$ p-value	Gene	Log_2 ratio (CRB 2/GF P)	$-log_2$ p-value	Gene	Log_2 ratio (CRB 2/GF P)	$-log_2$ p-value
CRB2	32.40	5.83	**MRPL48**	22.97	14.21	**LIN7C**	21.66	3.54
OBI1	25.53	2.90	**E2F7**	22.89	19.31	**CCDC88A**	21.52	16.63
SDF2L1	25.34	16.76	**RPS7**	22.89	3.67	**ODR4**	21.50	2.29
GNGT1	25.27	2.18	**NDUFB11**	22.87	2.29	**TXNDC5**	21.49	3.56
MRPL43	25.05	17.20	**PIP4P1**	22.79	17.28	**EMC1**	21.36	2.29
BCLAF1	25.00	2.83	**ZNF471**	22.78	13.79	**SLC9A3R1**	21.27	2.02
FKBP10	24.95	19.80	**SPTBN2**	22.72	3.82	**GMFG**	21.25	2.29
MRPL49	24.81	3.99	**DNAJC3**	22.70	17.49	**TTC17**	21.24	16.54
MRPL13	24.69	3.87	**MANF**	22.66	16.23	**TNRC6B**	21.22	16.55
MAGT1	24.56	19.15	**NGLY1**	22.58	17.97	**SLIT2**	21.18	15.51
ZNF768	24.55	13.76	**PPHLN1**	22.54	3.57	**AP1B1**	21.10	2.28
CISD3	24.51	18.97	**PLOD3**	22.50	3.76	**LAMC1**	21.07	17.20
MRPL15	24.50	16.13	**SF3B2**	22.49	4.14	**MAP3K7**	21.07	12.31
TFRC	24.50	15.11	**RPS27L**	22.44	2.13	**DSC1**	20.87	2.29
MRPL46	24.49	14.79	**FBXO3**	22.42	16.22	**USP15**	20.61	19.15
SUMO4	24.49	2.33	**SNRPG**	22.40	2.29	**CKAP5**	20.53	2.06
TRAF7	24.45	19.00	**IGF2R**	22.39	2.30	**CCDC88C**	20.45	2.30
IVNS1ABP	24.41	15.47	**TAB1**	22.39	4.44	**TMOD3**	20.45	2.55
MRPL24	24.32	3.96	**ADAMTS1**	22.39	3.57	**RBM17**	20.18	3.56
H2AZ2	24.29	2.29	**DDX5**	22.32	2.32	**DNAJC10**	20.07	15.03
THRAP3	24.24	4.57	**TM9SF2**	22.31	3.57	**ANKFY1**	19.85	4.14
SELENOF	24.24	16.66	**CLGN**	22.31	18.08	**TYK2**	19.47	4.14
MRPL27	24.20	3.57	**PPIL1**	22.31	14.82	**U2SURP**	18.03	2.29
MRPL2	24.16	2.29	**PROSER1**	22.30	3.57	**NT5C2**	17.40	3.54
MRPL32	24.03	15.34	**NCLN**	22.26	3.57	**UGGT2**	9.08	2.92
LMAN1	23.96	2.85	**CSRP2**	22.21	14.79	**EIF4B**	6.64	2.10
MRPL39	23.93	17.04	**COLGALT1**	22.20	19.64	**SNRPN**	5.58	2.27
MRPL28	23.82	15.71	**TMEM19**	22.19	2.40	**SNRPD2**	5.11	1.90
RPS15 RIG	23.78	3.57	**PRPF31**	22.18	2.45	**SNRPD3**	4.58	7.36
H1-4	23.77	2.30	**CNN2**	22.16	2.09	**ERH**	4.58	8.17
MRPL11	23.77	3.57	**SPIN3**	22.15	2.29	**WDR77**	4.49	6.06
PTS	23.70	3.57	**DDX6**	22.09	3.56	**MOB2**	4.29	1.97
PSMB6	23.69	3.76	**DDR2**	22.05	3.57	**CANX**	4.13	6.44
SDF2	23.65	4.02	**PSMD12**	22.05	2.13	**DNAJB11**	3.69	8.53
TET2	23.62	18.76	**P4HA1**	22.04	18.21	**MRPL47**	3.58	1.99
GLYR1	23.57	2.30	**PTDSS1**	22.01	2.30	**PDIA4**	3.54	1.91
OTUD4	23.57	12.45	**LMAN2L**	21.98	3.57	**MRPL9**	3.42	1.96
PSMA3	23.50	3.65	**PHF5A**	21.95	2.29	**RPL23**	3.42	7.16
RPL34	23.39	2.22	**SF3B4**	21.93	2.29	**SPIN1**	3.24	6.31
RPS20	23.34	15.91	**INHBE**	21.92	16.96	**MRPL1**	3.20	1.90
MRPL16	23.28	17.50	**ITGAV**	21.90	2.63	**STK38L**	2.96	3.94
LOC100626015	23.18	17.50	**LTBP1**	21.82	16.24	**PSPC1**	2.81	6.80
STT3B	23.14	16.37	**GLG1**	21.75	4.06	**HSPA5**	2.39	7.90
SPCS3	23.13	15.91	**WDR26**	21.73	17.50	**PPM1B**	2.38	5.37
CEP76	23.11	15.64	**HMGB2**	21.71	2.29	**PRMT1**	2.21	5.11
P3H1	23.07	2.30	**EMILIN3**	21.71	3.57	**RPN1**	2.21	2.96
TAF6L	23.05	18.85	**NOTCH2**	21.70	16.15	**STK38**	2.13	5.00
IPO8	23.02	18.63	**CAPNS1**	21.70	2.29			
PSMB1	22.99	14.91	**ERLEC1**	21.70	15.22			

Appendix 27| CRB2 retinal interactome Table depicts significantly enriched proteins in CRB2-FLAG samples compared to GFP upon incubation with porcine retina lysates analysed by mass spectrometry. Table presents the gene name, the log_2 ratio and the $–log_2$ p-value (One-sample t-test, FDR 0.05, log_2 ratio (CRB2-FLAG/GFP-FLAG) >2, n=6). [1]

Gene	Log_2 ratio (CRB2/ GFP)	$-log_2$ p-value	Gene	Log_2 ratio (CRB2/ GFP)	$-log_2$ p-value	Gene	Log_2 ratio (CRB2/GFP)	$-log_2$ p-value
ARHGAP21	30.11	3.57	**RBM5**	23.50	18.66	**SNRPD1**	3.68	7.13
CLNS1A	28.12	2.89	**ERGIC1**	23.50	2.38	**TMOD3**	3.64	8.17
GLYR1	26.73	2.73	**ITGB1**	23.50	2.39	**RPLP1**	3.60	1.88
RIOK1	26.31	17.76	**SCAI**	23.47	2.12	**SF3B1**	3.50	7.05
TRAF7	26.20	19.52	**PRPS2**	23.47	3.57	**TAB1**	3.49	8.00
MRPL43	26.02	1.53	**CBX1**	23.47	1.35	**ERH**	3.48	7.92
FBXO44	25.90	4.30	**RDH11**	23.47	16.54	**LSM14A**	3.32	1.59
FLII	25.90	3.81	**IVD**	23.44	1.38	**TMOD2**	3.25	8.60
TMX1	25.88	3.57	**SNPH**	23.38	18.50	**RPL23**	3.23	7.19
FKBP10	25.83	17.06	**PIP4P2**	23.36	3.57	**FGG**	3.22	4.69
SDF2L1	25.80	16.38	**TJP2**	23.36	2.44	**FGA**	3.20	5.12
RPL8	25.79	3.57	**SGTB**	23.32	2.12	**MOB2**	3.20	8.58
MRPL13	25.64	3.90	**HOMER1**	23.31	3.57	**ZSCAN26**	3.19	1.57
MRPL27	25.59	3.92	**LIMA1**	23.29	2.40	**FGB**	3.17	5.08
MRPL3	25.59	17.65	**SMNDC1**	23.25	3.73	**STK38L**	3.15	8.07
MTRES1	25.56	2.55	**PLOD3**	23.25	3.67	**SPIN1**	3.14	8.48
IVNS1ABP	25.51	16.59	**TMEM11**	23.24	3.57	**CCAR1**	3.12	5.07
CISD3	25.50	17.96	**PSMB7**	23.21	2.30	**CRYBB3**	3.09	1.25
MRPL15	25.46	3.84	**DDX19B**	23.21	2.29	**ROGDI**	3.07	6.11
OBI1	25.41	16.30	**EPN3**	23.17	2.03	**SKP1**	3.07	5.69
SNRPG	25.41	17.72	**TBCB 1**	23.15	2.46	**ERMN**	3.07	7.12
SF3B4	25.41	3.57	**GOLGA2**	23.15	3.53	**ABLIM1**	3.06	5.41
MRPL47	25.34	2.80	**POLDIP3**	23.15	2.09	**AP3B2**	3.00	10.72
CRB1	25.32	17.71	**RBM6**	23.14	15.55	**DNAJB11**	2.99	6.23
MRPL1	25.16	3.94	**PTDSS1**	23.12	2.69	**ACOT9**	2.92	1.82
ZNF768	25.13	14.20	**SLC15A2**	23.09	1.35	**SNRPD2**	2.88	5.90
RPS15 RIG	25.08	3.72	**SBF2**	23.08	2.75	**EPB41**	2.87	6.29
MRPL39	25.05	2.52	**CEP76**	23.06	2.29	**ARPC1A**	2.86	4.25
SLC4A1AP	25.02	2.63	**LTBP1**	23.01	2.30	**TYK2**	2.86	7.57
CHERP	24.95	14.49	**SLC30A9**	22.99	2.30	**MRPL49**	2.83	1.24
PHF5A	24.95	4.06	**HGS**	22.97	3.54	**SF3B2**	2.83	6.44
MRPL46	24.94	16.10	**TTC7B**	22.97	2.16	**GSN**	2.83	6.35
DCTN3	24.90	19.55	**SLC6A9**	22.93	1.37	**LOC100626015**	2.82	4.33
ICA	24.88	2.29	**SNRNP40**	22.91	2.30	**SRRT**	2.82	4.76
RBM17	24.84	4.64	**GMPR2**	22.91	1.37	**MTMR14**	2.80	7.03
SLC38A3	24.75	2.39	**HNRNPUL1**	22.89	1.37	**SCFD1**	2.73	1.78
ARPC2	24.73	3.57	**ERLEC1**	22.89	19.34	**SPINDOC**	2.71	6.87
OTUD4	24.72	15.78	**CPPED1**	22.88	1.37	**DAZAP1**	2.65	5.71
MRPL32	24.62	16.65	**ARMC10**	22.88	1.37	**PRMT8**	2.64	1.77
TET2	24.62	17.56	**CPE**	22.86	3.57	**MRPL12**	2.64	6.55
SRSF7	24.62	16.51	**MESD**	22.83	2.36	**MPI**	2.58	1.72
MRPL28	24.61	3.85	**GABARAPL2**	22.81	3.57	**PRPSAP1**	2.55	4.82
U2SURP	24.55	3.10	**GUCA1A**	22.80	1.41	**WDR7**	2.53	5.59
TRAPPC3	24.46	16.70	**CAPRIN1**	22.76	1.39	**PRPF31**	2.53	7.81
MGST1	24.40	3.66	**TM9SF3**	22.74	19.51	**EFR3A**	2.52	1.49
MRPL16	24.36	2.67	**L2HGDH**	22.74	3.60	**RPS20**	2.51	4.07
CAPNS1	24.34	3.83	**GCDH**	22.73	1.39	**PGAM5**	2.49	8.86
LYPLA1	24.31	2.33	**TBL1XR1**	22.71	2.30	**SF3B6**	2.49	5.95
RPL29	24.31	3.57	**MPP5**	22.68	2.30	**CLASP1**	2.49	4.90
LMAN2L	24.31	3.57	**PHKB**	22.65	2.31	**PLEC**	2.47	6.99
TXNDC5	24.26	4.31	**BZW2**	22.61	3.70	**SEC61A1**	2.45	1.80
SLC24A1	24.24	2.34	**KPNA3**	22.61	2.30	**SPTBN2**	2.45	6.86
MT-CO1	24.21	2.29	**PDAP1**	22.59	1.32	**ROCK1**	2.44	1.47
MRPL48	24.21	4.03	**SEC31A**	22.58	3.48	**STK38**	2.44	6.38
PSMB2	24.16	1.41	**PTPRD**	22.57	2.30	**FBXO3**	2.42	1.45
ARID1A	24.12	18.15	**GUCY1A1**	22.51	2.30	**SV2B**	2.41	6.02
FYCO1	24.09	1.38	**APLP2**	22.49	18.97	**FHL1**	2.39	1.72
HNRNPH2	24.07	1.40	**CHMP5**	22.49	2.29	**ISCU**	2.38	1.68
MRPL14	24.06	2.20	**INHBE**	22.44	2.30	**C2CD2L**	2.38	4.16
MORC3	24.04	19.07	**RAB3GAP1**	22.44	1.45	**EEF1D**	2.37	4.60
MTMR1	24.04	2.57	**MYO1C**	22.42	3.57	**EIF3C**	2.33	3.84
TAB3	24.03	16.77	**EPB41L5**	22.35	1.37	**CORO1C**	2.33	4.09
PTS	24.03	2.30	**MVP**	22.33	2.16	**AP3D1**	2.32	4.07
PFKFB1	24.03	2.30	**PNPLA6**	22.31	1.36	**EPB41L3**	2.32	6.15
TPT1	24.01	3.56	**PRRC2A**	22.31	2.30	**SNRPD3**	2.30	4.59
PDCD6	23.99	18.48	**DHX38**	22.23	2.30	**SDF2**	2.29	5.48
IPO8	23.96	18.42	**DKC1**	22.21	2.30	**TUBG1**	2.29	1.72
CAV1	23.93	16.84	**EMILIN3**	22.14	3.57	**CORO1B**	2.27	1.67

EIF3H	23.91	2.10	**DNAJC12**	21.95	2.29	**FUS**	2.26	3.58
CLCC1	23.91	2.14	**PTPN23**	21.71	1.32	**ARMC8**	2.25	1.44
POGLUT3	23.88	2.72	**CAST**	21.06	3.49	**VARS1**	2.25	5.46
NOP56	23.86	2.55	**CRB2**	16.81	8.95	**LIN7C**	2.22	3.16
PPIL1	23.85	20.30	**DNAJC10**	8.13	2.42	**VWA8**	2.22	1.44
ZRANB2	23.84	16.47	**BCLAF1**	7.34	2.49	**MYO5A**	2.20	4.58
CCDC88A	23.82	4.30	**RB1CC1**	7.15	2.05	**HSPA5**	2.20	6.18
GMFG	23.81	16.29	**THRAP3**	6.50	7.99	**SF3B3**	2.19	6.52
NUFIP2	23.77	3.85	**DNAJC13**	5.68	1.98	**HTATSF1**	2.19	4.21
ARHGEF10	23.77	18.52	**SELENOF**	5.61	1.75	**OPLAH**	2.19	5.14
ZNF471	23.76	10.97	**MAP3K7**	5.57	2.03	**EEF1B**	2.19	5.29
GRIA4	23.74	3.57	**UGGT2**	5.48	6.21	**EIF3A**	2.18	4.54
WDR26	23.72	4.02	**RBM10**	5.22	7.45	**PI4KA**	2.18	5.03
GID8	23.72	1.48	**EIF4B**	5.03	6.95	**DMXL2**	2.17	5.03
PRPSAP2	23.72	16.44	**ANKFY1**	4.88	6.98	**TJP1**	2.15	1.72
DNAJC3	23.71	17.40	**CORO2B**	4.83	2.03	**THEM6**	2.15	6.64
DEK	23.71	3.57	**MRPL17**	4.77	2.06	**AP3M2**	2.13	5.52
MOGS	23.70	2.09	**WDR77**	4.66	8.41	**ARL8A**	2.13	1.64
EIF3K	23.69	2.52	**TFRC**	4.51	1.63	**FAM126B**	2.13	1.75
SPIN3	23.69	1.51	**NT5C2**	4.49	8.07	**NCLN**	2.09	1.69
NGLY1	23.65	19.30	**FBXO2**	4.39	7.38	**PRMT1**	2.09	5.34
SIRT2	23.64	2.09	**UTP6**	4.20	2.07	**RPS21**	2.09	4.58
ATG13	23.63	20.51	**USP15**	4.06	6.35	**LMAN2**	2.08	5.15
LYPLA2	23.61	3.83	**FBL**	3.97	1.42	**EEF1G**	2.08	5.19
MTA2	23.60	2.42	**CLGN**	3.93	7.31	**HIBCH**	2.07	1.71
TARDBP	23.58	3.69	**MRPL9**	3.91	1.97	**RPS16**	2.06	5.22
ACTR10	23.57	2.46	**OGT**	3.87	6.03	**PSPC1**	2.06	4.74
FARP1	23.53	18.81	**CANX**	3.85	7.37	**CCT6**	2.04	4.99
COPS5	23.52	2.09	**SLAIN2**	3.85	1.95	**SNRNP70**	2.03	3.04
SART1	23.51	2.72	**MRPL44**	3.75	1.98	**ACTR2**	2.03	4.62
SUMF2	23.51	2.30	**AKT2**	3.68	5.95	**NADK2**	2.02	1.74
MYO6	2.02	4.54	**SPTB**	2.01	5.09	**MAP1B**	2.01	5.64
RPS27A	2.01	1.33						

Appendix 28| Specific peptides detected for CRB1 and CRB2 by mass spectrometry Alignment of CRB1 protein sequence of *H.sapiens* (bottom strand) and *S.scrofa* (top strand). Specific peptides identified are highlighted in green. [1]

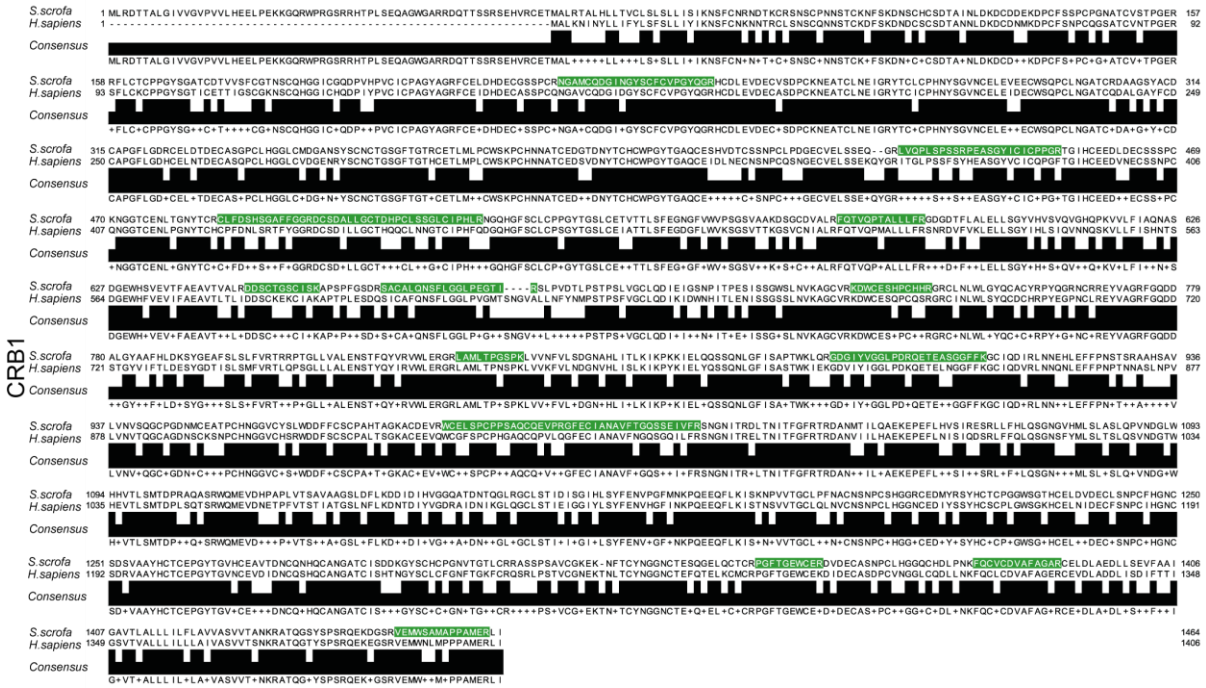

Appendix 29| Peptides selected for monoclonal antibody presentation Alignment of porcine and human **(A)** CRB2 and **(B)** CRB1 together with the consensus sequence. Selected peptide antigens are circled in orange

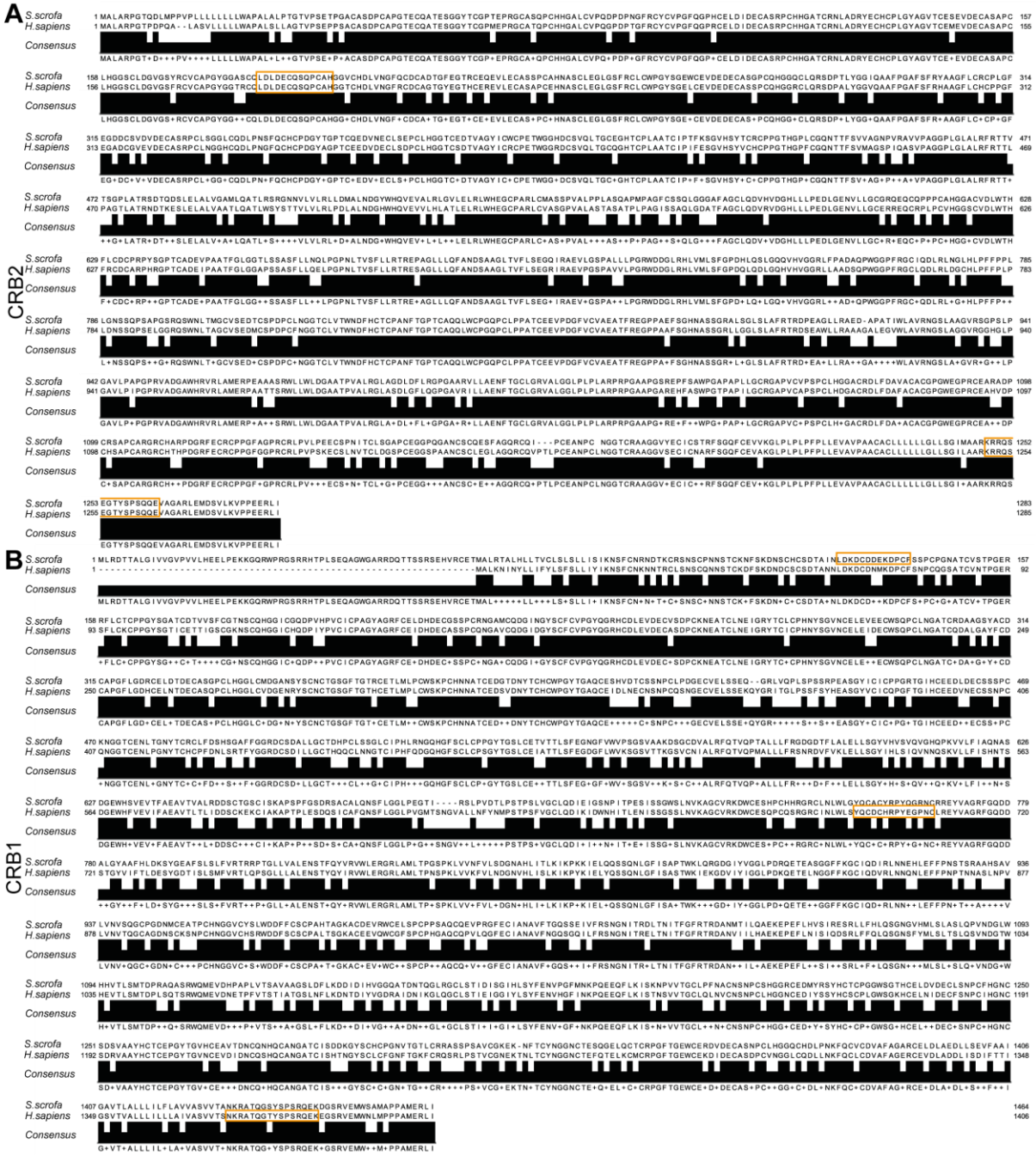

Appendix 30| First screening of supernatant hybridomas reveals positive clones against human and porcine CRB Supernatant of different hybridomas clones generated upon immunization of rat and mouse with the selected peptide antigens against CRB1 and CRB2, were screened for detection of human and porcine CRB1 by western blot analysis or immunofluorescence microscopy. Nt= not tested; WB=Western Blot; IF=immunofluorescence

Name	Clone	IgG subclass	Species	WB Human CRB	WB Porcine retina	IF human RO	IF porcine retina	IF human retina
CRB1B	15F11	IgG2c	Rat	No	No	nt	nt	nt
CRB1B	21D11	IgG2c	Rat	No	No	nt	nt	nt
CRB1B	8B2	IgG2c	Rat	No	No	nt	nt	nt
CRB1B	16C7	IgG2c	Rat	No	No	nt	nt	nt
CRB1B	16F4	IgG2c	Rat	No	No	nt	nt	nt
CRB1B	7E8	IgG2c	Rat	No	No	nt	nt	nt
CRB1B	23G4	IgG2c	Rat	No	No	nt	nt	nt
CRB1B	23G8	IgG2c	Rat	No	No	nt	nt	nt
CRB1B	6B10	IgG2c	Rat	No	No	nt	nt	nt
CRB1B	6A9	IgG2c	Rat	No	No	nt	nt	nt
CRB1B	13B4	IgG2c	Rat	No	No	nt	nt	nt
CRB1B	7H9	IgG2c	Rat	No	No	nt	nt	nt
CRB1B	5D10	IgG2c	Rat	No	No	nt	nt	nt
CRB1B	8E1	IgG2c	Rat	No	No	nt	nt	nt
CRB1B	6E9	IgG2c	Rat	No	No	nt	nt	nt
CRB1B	14C10	IgG2c	Rat	No	No	nt	nt	nt
CRB1B	15H4	IgG2c	Rat	No	No	nt	nt	nt
CRB1B	23A12	IgG2a	Rat	No	No	nt	nt	nt
CRB1B	13C5	IgG2a	Rat	No	No	nt	nt	nt
CRB1B	7B1	IgG2a	Rat	No	No	nt	nt	nt
CRB1B	5A1	IgG2a	Rat	No	No	nt	nt	nt
CRB1B	21E11	IgG1	Rat	No	No	nt	nt	nt
CRB1B	17C11	IgG2a	Rat	No	No	nt	nt	nt
CRB1B	18E5	IgG2a	Rat	No	No	nt	nt	nt
CRB1B	17E2	IgG2a	Rat	No	No	nt	nt	nt
CRB1B	23G11	IgG2a	Rat	No	No	nt	nt	nt
CRB1B	24C10	IgG2a	Rat	No	No	nt	nt	nt
CRB1B	17D1	IgG1/2a	Rat	No	No	nt	nt	nt
CRB1B	22F5	IgG1/2a	Rat	No	No	nt	nt	nt
CRB1B	24H5	IgG1	Rat	No	No	nt	nt	nt
CRB1B	20A10	IgG1	Rat	No	No	nt	nt	nt
CRB2B	13G5	IgG2a	Rat	No	No	nt	nt	nt
CRB2B	13H5	IgG2a	Rat	No	No	nt	nt	nt
CRB2B	8F8	IgG2a	Rat	No	No	nt	nt	nt
CRB2B	10A5	IgG2a	Rat	No	No	nt	nt	nt
CRB2B	**15A7**	**IgG2a**	**Rat**	**Yes**	**No**	**nt**	**nt**	**nt**
CRB2B	2E6	IgG2a	Rat	No	No	nt	nt	nt
CRB2B	23C5	IgG2a	Rat	No	No	nt	nt	nt
CRB2B	13B12	IgG2a	Rat	No	No	nt	nt	nt
CRB2B	14B11	IgG2a	Rat	No	No	nt	nt	nt
CRB2B	8A12	IgG2a	Rat	No	No	nt	nt	nt
CRB2B	8H1	IgG2a	Rat	No	No	nt	nt	nt
CRB2B	14H6	IgG2a	Rat	No	No	nt	nt	nt
CRB2B	9A2	IgG2a	Rat	No	No	nt	nt	nt
CRB2B	24B10	IgG2a	Rat	No	No	nt	nt	nt
CRB2B	23G11	IgG2a	Rat	No	No	nt	nt	nt
CRB2B	14G5	IgG2a	Rat	No	No	nt	nt	nt
CRB2B	14F11	IgG2a	Rat	No	No	nt	nt	nt
CRB2B	23D4	IgG2a	Rat	No	No	nt	nt	nt
CRB2B	16G11	IgG2a	Rat	No	No	nt	nt	nt
CRB2B	20B4	IgG2a	Rat	No	No	nt	nt	nt
CRB2B	22A12	IgG2a	Rat	No	No	nt	nt	nt
CRB2B	8H4	IgG2a	Rat	No	No	nt	nt	nt
CRB2B	21B5	IgG2a	Rat	No	No	nt	nt	nt
CRB2B	23B6	IgG2a	Rat	No	No	nt	nt	nt
CRB2B	16D6	IgG2a	Rat	No	No	nt	nt	nt
CRB2B	13B10	IgG2a	Rat	No	No	nt	nt	nt
CRB2B	22E12	IgG2a	Rat	No	No	nt	nt	nt
CRB2B	**4H2**	**IgG2a**	**Rat**	**yes**	**No**	**No**	**No**	**No**
CRB2B	**6C4**	**IgG2a**	**Rat**	**yes**	**No**	**Yes**	**No**	**No**
CRB2B	**5F2**	**IgG2a**	**Rat**	**Yes**	**No**	**No**	**No**	**No**
CRB2B	6C5	IgG2a	Rat	No	No	nt	nt	nt
CRB2B	6D4	IgG2a	Rat	No	No	nt	nt	nt
CRB2B	7B6	IgG2a	Rat	No	No	nt	nt	nt
CRB2B	6H3	IgG2a	Rat	No	No	nt	nt	nt
CRB2B	**15D2**	**IgG2a**	**Rat**	**yes**	**No**	**No**	**No**	**No**
CRB2B	7H3	IgG2a	Rat	No	No	nt	nt	nt
CRB2B	5H3	IgG2a	Rat	No	No	nt	nt	nt

CRB2B	24B11	IgG2a	Rat	No	No	nt	nt	nt
CRB2B	7C5	IgG2a	Rat	No	No	nt	nt	nt
CRB2B	12D1	IgG2a	Rat	No	No	nt	nt	nt
CRB1C	22C1	IgG1	Rat	No	No	nt	nt	nt
CRB1C	15E10	IgG2c	Rat	No	No	nt	nt	nt
CRB1C	12E8	IgG2a	Rat	No	No	nt	nt	nt
CRB1C	22C2	IgG2b	Rat	No	No	nt	nt	nt
CRB1C	26F9	IgG2a	Mouse	No	No	nt	nt	nt
CRB1C	25D11	IgG2a	Mouse	No	No	nt	nt	nt
CRB1C	26F8	IgG1	Mouse	No	No	nt	nt	nt
CRB1C	26G11	IgG2b	Mouse	No	No	nt	nt	nt
CRB1C	25D5	IgG1	Mouse	No	No	nt	nt	nt
CRB1C	**25G2**	**IgG3**	**Mouse**	**Yes**	**Yes**	**Yes**	**Yes**	**No**
CRB1C	26D9	IgG3	Mouse	No	No	nt	nt	nt
CRB1C	25F6	IgG3	Mouse	No	No	nt	nt	nt
CRB1C	26B6	IgG3	Rat	No	No	nt	nt	nt
CRB1A	25E19	IgG3	mouse	No	No	nt	nt	nt
CRB1A	25C10	IgG3	mouse	No	No	nt	nt	nt
CRB1B	26A10	IgG1	mouse	No	No	nt	nt	nt
CRB1B	26E2	IgG1	mouse	No	No	nt	nt	nt
CRB1B	25G8	IgG1	mouse	No	No	nt	nt	nt
CRB1B	26C6	IgG1	mouse	No	No	nt	nt	nt
CRB1B	25C7	IgG1	mouse	No	No	nt	nt	nt
CRB1B	25G4	IgG1	mouse	No	No	nt	nt	nt
CRB1B	26D4	IgG1	mouse	No	No	nt	nt	nt
CRB1B	26A9	IgG1	mouse	No	No	nt	nt	nt
CRB1B	25G3	IgG1	mouse	No	No	nt	nt	nt
CRB1B	26D1	IgG1	mouse	No	No	nt	nt	nt
CRB1B	26E1	IgG2a	mouse	No	No	nt	nt	nt
CRB1B	25G4	IgG2a	mouse	No	No	nt	nt	nt
CRB1B	25F10	IgG2a	mouse	No	No	nt	nt	nt
CRB1B	**27A5**	**IgG2b**	**mouse**	**Yes**	**Yes**	**Yes**	**Yes**	**No**
CRB1B	25B12	IgG2b	mouse	No	No	nt	nt	nt
CRB1B	26H3	IgG3	mouse	No	No	nt	nt	nt
CRB1B	25B5	IgG3	mouse	No	No	nt	nt	nt
CRB1B	26G6	IgG3	mouse	No	No	nt	nt	nt
CRB1B	25D3	IgG3	mouse	No	No	nt	nt	nt
CRB1B	28H7	IgG3	mouse	No	No	nt	nt	nt
CRB1B	25B11	IgG3	mouse	No	No	nt	nt	nt
CRB1B	25G11	IgG3	mouse	No	No	nt	nt	nt
CRB1B	26E12	IgG3	mouse	No	No	nt	nt	nt
CRB1B	25E9	IgG2a IgG2b	mouse	No	No	nt	nt	nt
CRB1B	26E11	IgG3 IgG2b	mouse	No	No	nt	nt	nt

Appendix 31| CRB1B 27A5 and CRB1C25G2 maintain ability to recognise CRB1 upon re-cloning
Western blot analysis of CRB1B 27A5 and CRB1C25G2 prior (initial supernatant) and after re-cloning (after re-cloning) using HEK293T cell lysates overexpressing human canonical CRB1.